Multisource Forest Inventory : a Generic and Flexible Tool for Forest Resource Estimation and Mapping at a Fine Scale

Ankit Sagar

A Dissertation Presented to

The **UNIVERSITY OF LORRAINE**

*Ecole Doctorale Sciences et Ingénierie des Ressources Naturelles (**SIReNa**)*

*Laboratoire d'Inventaire Forestier (**LIF**)*

Presented and Publicly Defended by

Ankit SAGAR

On September 21, 2023

In Partial Fulfilment of the Requirements for the Degree of

Doctor of Philosophy (*PhD*)

Speciality: Biologie et écologie des forêts et des agrosystèmes

Multisource Forest Inventory: a Generic and Flexible Tool for Forest Resource Estimation and Mapping at a Fine Scale

Members of the Jury:

Supervisor:	**Cédric Vega**	Senior Researcher IGN, ENSG, LIF, Nancy, France
Co-supervisor:	**Jean-Pierre Renaud**	Researcher ONF RDI, Nancy, France
Reviewers:	**Sylvie Durrieu**	ICPEF INRAE, Montpellier, France
	Philippe Lejeune	Professor University of Liège, Belgium
Examiners:	**Laurent Saint-André** (President of Jury)	Senior Researcher INRAE, Champenoux, France
	Claudine Richter	Head, RDI Department ONF, Fontainebleau, France

Foreword

This PhD was conducted at the Laboratoire d'Inventaire Forestier (LIF) - Institut National de l'Information Géographique et Forestière (IGN) and the Université de Lorraine in Nancy, France. The PhD was funded by the French National Research Agency (ANR) through the French PIA programs “Lorraine Université d’Excellence” (Project Impact DeepSurf: Reference ANR-15-IDEX-04-LUE) and “Laboratoire d'Excellence ARBRE” (Reference ANR-11-LABX-0002-01).

I humbly and affectionately dedicate this work to my family.

Thank you for your unconditional and everlasting support and love.

Acknowledgments

Only slowly did I begin to realize that it's done: I am a PhD now! Years of hard work towards a successful defence have never felt better! I would like to thank all the people who contributed in their particular way to the achievement of this doctoral thesis.

First and foremost, I would like to express my deepest gratitude to my thesis supervisor, **Cédric Vega**, and co-supervisor, **Jean-Pierre Renaud**, for entrusting me with this opportunity and providing their invaluable help, advice, and continuous guidance over the past three years. This PhD study is replete with numerous discussions with both of them, which enabled me to bring this work to its successful completion. Their advice and opinions have significantly contributed not only to the work on this dissertation but also taught me qualities such as perseverance, discipline, adherence to established plans, attention to detail, critical thinking, and a commitment to achieving high-quality results. Without their patience, enthusiasm, professionalism, and unwavering support, this dissertation would have been entirely different. They were always available to help solve any problems, and I could not have asked for better supervisors. I hope to emulate their integrity, work ethic, and passion in my future research career.

I would like to express my sincere gratitude to **Sylvie Durrieu** and **Philippe Lejeune** for accepting to review my PhD thesis. I am also grateful to **Laurent Saint-André** and **Claudine Richter** for agreeing to be examiners on my thesis committee. Additionally, I would like to thank the members of my thesis monitoring committee, **Milena Planells**, **Guillaume Chauvet**, and **Yves Jolivet**, for their valuable advice, insightful proposals, and constructive remarks.

I would like to extend my special thanks to **Olivier Bouriaud** and my lab director, **Jean-Daniel Bontemps**, for their continuous help and support from the beginning to the end of my PhD thesis. Additionally, I would like to express my gratitude to **Christian Piedallu** for his invaluable suggestions and providing me with crucial data, which greatly facilitated the progress of my work.

I would like to thank the French PIA project '*Lorraine Université d'Excellence'*, with reference to *ANR-15-IDEX-04-LUE*, for providing financial assistance through the project *Impact DeepSurf* and the *Labex ARBRE* (*ANR-11-LABX-0002-01*) for allowing me to pursue my PhD thesis in France.

I owe a big thanks to all my colleagues who also grew to be good friends over time. Thank you, Nikola Besic, Lionel Hertzog, Dương Ho Kim Trinh, Helene Secherre, Minna Pulkkinen, Lina Jarboui, Timothee Audinot, Clementine Ols and Baptiste Kerfriden for sharing your knowledge and skills with me and countless funny moments over a cup of coffee. I have to thank all my friends from India who always pushed me to achieve more.

But my greatest love and deepest gratitude go to my mother, **Suman Gupta**, and father, **Manindra Kumar Gupta -** my greatest fans and unwavering believers in me! You do not always approve of what I do, but you always support me, patiently listening to my tears of both sadness and happiness.

Thank you for raising me into what I am today, this dissertation is your achievement as well! I also thank my brother, **Sumeet Sagar**, and sister-in-law, **Komal Sagar**, for their love and everlasting support.

Of course, this list is not exhaustive, and I thank all those who know me and made me feel like I exist...

Abstract

The French National Forest Inventory (NFI) is a statistical survey designed to produce estimates of forest attributes at national down to regional scales. Below these scales, the estimation domain is sparsely sampled, resulting in poor estimation precision. Such a decrease in precision prevents forest managers and stakeholders from using NFI estimates to develop forest management strategies and inform decision-making processes over small functional-management scales. In order to support these activities, NFI precision has to be improved at such scales.

Over the past few decades, it has been shown that combining NFI data with spatially continuous auxiliary data (e.g. remote sensing data, thematic maps) can significantly improve estimation precision beyond regional scales. This combination is often referred to as Multisource National Forest Inventory (MSNFI). Hence, the first objective of this thesis was to develop a methodology within the context of MSNFI, for improving the Small Area Estimation (SAE) precision of forest attributes at municipality level and provide estimates in small impacted areas of bark beetle outbreaks. The second objective of the thesis aimed to provide high resolution prediction maps on the quantity and location of the forest attributes within an inferential framework. Based on these objectives, four studies were conducted in four chapters.

In Chapter I, auxiliary data obtained from forest maps, Landsat images, and Digital Aerial Photogrammetry (DAP) were combined with NFI data to develop a flexible multi-scale model-assisted approach for SAE of Growing Stock Volume (GSV) and Basal Area (BA) at the municipality or group of municipalities' level in Sologne and Orléans forest located in Centre of France. The scaling framework was controlled by a minimum number of NFI plots per computation domain and a maximum error threshold. When the target estimation error was set to 10%, the approach yielded 23 estimated grouped domains (out of 157 municipalities), with an average estimation error below 7.7% for both forest attributes. However, when the targeted error threshold was relaxed to 50%, a larger number of smaller domains (80 domains) were obtained for both attributes, but with a higher average error of 15.1%. The results demonstrated that the approach not only provided estimates for the entire area of interest but also provided users with the flexibility to improve the precision of the estimates while maintaining a balanced spatial scale.

In Chapter II, a convex hull method was used to identify the proportion of extrapolated predictions (predictions outside the calibration domain) in model-based map products. The study utilized a combination of Airborne Laser Scanning (ALS) and Management Forest Inventory (MFI) data over the Mouterhouse forest, located in the North-Eastern part of France. The study also compares the impact of various sampling efforts on model precision and extrapolation levels. The result showed that the model precision stabilized quickly with small sampling effort (~1 plot/100ha), but the extrapolation level remained high. Extrapolation level stabilised at higher sampling intensity (~1 plot/20ha). The method serves as a valuable tool for building accuracy maps corresponding to the

predictions falling inside or outside of the calibration domain. Additionally, it enables the identification of areas that requires additional sampling effort to improve model accuracy.

In Chapter III, a model-based approach and k-nearest neighbours (kNN) models were used to produce pixel-wise estimates complemented with prediction and reliability maps of GSV, BA and Volume Increment (VI). The reliability map was computed using precision and accuracy maps. The accuracy map was produced using the methodology from the Chapter II. This study was carried out in Sologne and Orléans forest. The auxiliary data included a forest map, Landsat 8 images and 3D point cloud data from ALS and DAP. The result showed that a minimum of 84% of the predictions were highly reliable. The performance of both ALS and DAP were similar, offering the possibility of utilizing cost-effective and frequently updated DAP for monitoring purposes. The high resolution outputs were significant for forest management and decision making purposes.

In Chapter IV, a model-based approach was used for SAE of GSV and BA impacted by bark-beetle outbreak in the Vosges forests located in North-Eastern France. The study utilized the anomaly map derived from the ForDead method that uses time-series analysis of Sentinel 2 data for spruce and fir dominated stands only. Forest attributes within the estimation domains were predicted using the method developed in Chapter III, utilizing ALS and Sentinel 2 as the main sources of auxiliary data. Two models were evaluated: a general model covering the entire area and a specific model for spruce and fir. The result showed that the outbreaks impacted 1,139 ha of spruce and fir dominated stands between 2021 and 2022. The corresponding estimates of GSV were 494,213 m^3 (± 2.2%) with the general model and 505,401 m^3 (± 2.7%) with the specific model. On average, the impacted GSV was 67 m^3/ha higher than the population mean, indicating that mature stands were primarily impacted. Future research is needed to address the uncertainties associated with surface detection and their integration in resource estimations.

Keywords: multisource forest inventory, statistical inference, small area estimation, remote sensing, 3D point cloud, forest disturbances.

Résumé

L'inventaire forestier national (IFN) a pour mission d'évaluer en continue les ressources forestières et de leurs évolutions. La méthode comporte deux phases statistiques et s'appuie sur une grille de sondage systématique à 1 km de résolution, divisée en 10 fractions annuelles. La première phase vise à estimer la surface forestière et consiste en une photo-interprétation d'un échantillon de 100 000 points tirés au hasard dans la fraction annuelle de la grille de sondage. La seconde phase consiste en la réalisation d'inventaire sur le terrain, afin d'évaluer les ressources. Elle repose sur un échantillon d'environ 6 500 points tirés des points classé en forêt lors de la première phase. La combinaison des deux phases permet d'estimer des moyennes, des totaux et leurs variances associées. Le plan de sondage est dimensionné pour produire des estimations jusqu'aux échelles régionales et contribuer à l'élaboration de la politique forestière et à l'évaluation de son impact. Avec le développement de la bioéconomie, l'enjeu porte aujourd'hui sur la production d'informations à l'échelle des territoires où se déclinent les plans régionaux de la forêt et du bois et les schémas régionaux biomasse, et où s'opère la structuration de la filière forêt-bois. Cela inclut à la fois la production de cartes et d'estimations sur des petits domaines géographiques.

Les méthodes d'inventaire forestier multisource permettent d'améliorer la précision des estimations de l'IFN à ces échelles opérationnelles. Elles reposent sur la combinaison des données échantillonnées sur le terrain, précises sur la plan thématique (i.e. on mesure ce que l'on estime) mais ponctuelles et à faible densité spatiale, avec des données auxiliaires peu précises sur le plan thématique (i.e. elles produisent une information corrélée avec ce que l'on estime), mais continues dans l'espace et à haute, voire très haute résolution spatiales, grâce à des méthodes statistiques appropriées. Cette combinaison permet d'obtenir des estimations précises à des échelles plus fines à coût marginal.

L'établissement de ces méthodes en France pose de nombreuses difficultés. Les forêts françaises sont parmi les plus diversifiées d'Europe, du fait des gradients climatiques et environnementaux présents sur le territoire, et des pratiques de gestion. Cette diversité nécessite d'adapter la méthode aux propriétés des territoires, impactant son niveau de généricité et les gains de précision. Des résultats préliminaires en forêt feuillue de plaine ont montré que les données de structure issues du Lidar et de la photogrammétrie numériques étaient parmi les données auxiliaires les plus corrélées aux principaux attributs forestiers d'intérêt, comme le volume ou la surface terrière, les données optiques à moyenne résolution spatiales (~ 30 m) ne permettant pas d'améliorer les estimations sur le territoire de l'étude.

Partant de ce constant, l'objectif de la thèse est de contribuer au développement d'une méthode d'inventaire forestier multisource adaptées au contexte forestier français. Les recherches s'appuient sur les bases de données de l'IFN ainsi que sur les données de télédétection disponibles à l'IGN (notamment carte forestière, images satellites haute résolution, données 3D laser et photos, topographie à haute résolution), en priorité sur un site forestier feuillu de plaine (Sologne, ~7500 km^2)

et un territoire à enjeux en zone de montagne (Vosges, ~ 3600 km^2). Elles mobilisent également les cartes prédictives environnementales à haute-résolution spatiale produites par l'UMR Silva (portail SILVAE et bases de données Digitalis). Les objectifs spécifiques sont :

- de développer des méthodes flexibles d'estimation de petits domaines permettant d'adapter la taille du domaine et la procédure d'estimation à l'objectif de précision recherché. Cet objectif inclut des approches inférentielles assistées d'un modèle, proche du cadre d'estimation de l'IFN, qui nécessitent un certain nombre de points dans le domaine d'estimation ; mais aussi des approches basées sur des modèles, plus sensibles aux spécifications du modèle et sensibles aux biais, mais qui offrent une plus grande flexibilité de prédiction à des résolutions plus fines.

- de développer des méthodes de cartographie d'attributs forestiers permettant de spatialiser les erreurs de prédiction et la fiabilité du modèle. Comme certaines méthodes de modélisation comme les k-plus proches voisins ou les forêts aléatoire, fréquemment utilisées dans les inventaires forestiers multisource en raison de leur capacité à prédire plusieurs attributs forestiers à partir d'un unique modèle, sont incapables d'extrapoler, une attention particulière a porté sur la définition et la spatialisation du domaine de validité des modèles.

- d'évaluer la capacité de ces méthodes à estimer la quantité de ressources impactée par des stress biotiques tel que les attaques de scolytes, qui causent d'importants ravages, notamment dans les Vosges sur les peuplements de conifères.

Ces objectifs ont été abordés dans quatre articles, qui constituent les quatre principaux chapitres de la thèse :

- Le chapitre un présente une méthode multi-échelle d'estimation de petits domaines basée sur des estimateurs assistés d'un modèle. L'échelle cible est celle de la commune ou de la communauté de commune.

- Le chapitre deux présente une méthode pour déterminer le domaine de validité des modèles en utilisant des enveloppes convexes dans l'espace des variables auxiliaires.

- Le chapitre trois généralise la méthode des enveloppes convexes pour la production de cartes de prédictions assorties d'indices de fiabilités de ces prédictions.

- Le chapitre quatre propose une méthode d'estimation de petits domaines basées sur un modèle permettant d'estimer dans des domaines géographiques dépourvus de point terrain, avec pour application, les ressources impactées par les scolytes dans les Vosges.

Au Chapitre I, nous introduisons un algorithme de changement d'échelle générant les plus petits groupes de domaines possibles qui répondent aux exigences de densité d'échantillonnage et l'erreur d'estimation prescrites par l'utilisateur. L'algorithme partitionne l'espace de manière récursive divisant la population des domaines en deux groupes tant que les conditions de précision prescrites ne sont pas remplies. L'algorithme a été testé sur deux attributs forestiers majeurs (à savoir le matériel sur pied et la surface terrière) dans une superficie de 7 500 km^2 dominés par les forêts de feuillus du centre de la France. Les domaines d'estimation comprenaient 157 municipalités. Les données auxiliaires ont été dérivées d'une carte forestière, de modèles photogrammétriques (DAP) et d'images Landsat. Un cadre assisté par modèle a été utilisée pour l'estimation Le cadre de mise à l'échelle était contrôlé par un nombre minimal de placettes de terrain par domaine de calcul (minimum de 3 placettes par domaine) et un seuil d'erreur maximal (de 10 à 50%). Lorsque l'erreur d'estimation cible est fixée à 10%, l'approche produit 23 domaines estimés (regroupés sur 157 communes), avec une erreur d'estimation moyenne inférieure à 7,7% pour les deux attributs forestiers considérés. Cependant, lorsque le seuil d'erreur cible est assoupli à 50%, un plus grand nombre de domaines plus petits (80 domaines) sont obtenus, mais avec une erreur moyenne plus élevée de 15,1%. Parmi ces domaines, 65 % étaient constitués de communes individuelles. Pour des fins de comparaison, l'estimation a également été réalisée à l'échelle des communes. Sur les 157 communes étudiées, seules 93 avaient été échantillonnées avec un minimum de 3 placettes et, par conséquent, estimées. Des valeurs manquantes ont été générées pour les 64 communes restantes. Des erreurs moyennes de 15,9% et 15,6% ont été obtenues pour le matériel sur pied et la surface terrière, respectivement, mais des erreurs d'estimation supérieures à 50% ont été obtenues pour certaines communes. L'algorithme fournit un cadre d'estimation flexible pour l'estimation sur petits domaines. Ses principaux avantages s'appuient sur sa capacité à produire des estimations basées sur un seuil de précision présélectionné et à produire des résultats sur toute la zone d'intérêt, en évitant les zones sans aucune estimation. L'algorithme pourrait également être utilisé sur tout type de couches de polygones (pas seulement administratives), à condition que le plan d'échantillonnage sur le terrain permettre l'estimation. Cela fait de l'algorithme proposé un outil pratique notamment pour les décideurs et les gestionnaires forestiers.

Au Chapitre II, une méthode d'enveloppe convexe a été utilisée pour identifier le domaine de validité des modèles ainsi que la proportion de prédictions extrapolées (prédictions en dehors du domaine de calibration) dans les produits cartographiques basés sur ces modèles. L'étude a utilisé une combinaison de données de LIDAR aéroporté (ALS) et d'Inventaire Forestier de Gestion (IFG) dans la forêt de Mouterhouse, située dans le nord-est de la France. L'étude compare également l'impact de différents efforts d'échantillonnage sur la précision du modèle et leurs impacts sur les niveaux d'extrapolation et de fiabilité des prédictions. Cela a été fait en sous-échantillonnant de manière itérative un ensemble de 487 placettes systématiques de l'IFG en utilisant des sous-grilles imbriquées permettant de diviser l'échantillon par deux à chaque niveau. L'analyse a été réalisée pour tous les échantillons alternatifs et évaluée par rapport à 56 placettes de validation indépendantes. Les résultats ont montré que la proportion de pixels extrapolés diminuait considérablement avec l'augmentation de

l’effort d’échantillonnage. Il atteint un plateau (environ 20 % d'extrapolation) avec une intensité d'échantillonnage d'environ 250 placettes de calibration. Cela contraste avec les résultats sur l’erreur quadratique moyenne (RMSE) des modèles, qui atteint un plateau avec un échantillonnage de beaucoup plus faible intensité. Ce résultat souligne le fait qu’avec un faible effort d’échantillonnage, le risque d’extrapolation reste élevé, même avec un RMSE relativement faible. Pour tous les attributs examinés (c.-à-d. la densité du peuplement, la surface terrière et le diamètre quadratique moyen) Les estimations se sont généralement révélées biaisées pour les placettes de validation extrapolées. La méthode permet d’identifier facilement les pixels situés hors domaine de calibration, ce qui en fait un outil intéressant pour évaluer la transférabilité des modèles pour une zone d’intérêt. Cela peut également servir à comparer des modèles « concurrents » lors d’une phase de sélection de variables pour l’élaboration d’un modèle. Du point de vue de la calibration, cette méthode peut également servir a posteriori pour évaluer des zones (dans l’espace auxiliaire) qui méritent des efforts d’échantillonnage supplémentaires pour améliorer la fiabilité des modèles.

Au Chapitre III, nous abordons le problème de la fiabilité des prédictions des modèles en utilisant une approche originale s'appuyant sur un cadre d'inférence basé sur un modèle et des modèles basés sur les k plus proches voisins (kNN) pour produire des estimations par pixel et évaluer de la qualité des prédictions associées. Cette approche tire parti des propriétés de rééchantillonnage d'un estimateur et la combine avec l’approche développée au Chapitre II (i.e. enveloppes convexes), pour mesurer respectivement la précision et l'exactitude des prédictions par pixels. Cette étude a été réalisée dans les forêts de Sologne et Orléans. Les données auxiliaires comprenaient une carte forestière, des images Landsat 8 et des données de nuages de points 3D provenant d’ALS et de DAP. Les modèles kNN ont été construits indépendamment pour les deux sources de données 3D. Les deux modèles sélectionnés comprenaient 5 variables auxiliaires et ont été générés en utilisant les 5 plus proches voisins ainsi qu’une mesure de distance basée sur une approche canonique des voisins les plus similaires (MSN). Les modèles ont montré une erreur quadratique moyenne relative allant de 35,7 % (pour la surface terrière en utilisant DAP) en calibration à 63,4 % (pour le matériel sur pied en utilisant ALS) en validation. Les résultats ont montré qu'au moins 84 % des prédictions étaient fiables. La quantité d'extrapolation variait de 4,3 % (DAP) à 6,3 % (ALS). Une relation a été trouvée entre l'extrapolation et la distance kNN, ouvrant de nouvelles perspectives pour corriger les erreurs d'extrapolation. Les performances de l'ALS et de la DAP étaient similaires, offrant la possibilité d'utiliser des données DAP, plus fréquemment mise à jour, représentant ainsi un plus grand potentiel pour des fins de surveillance des forêts. La méthode proposée a fourni des estimations cohérentes des attributs forestiers ainsi que les cartes associées. Elle a également fourni des informations spatialement explicites sur la précision des prédictions de pixels, soulignant leur exactitude et fiabilité. La méthode a donc produit des sorties à haute résolution, importantes tant pour la prise de décisions que pour la gestion forestière.

Au Chapitre IV, un cadre d'inférence basé sur un modèle a été utilisée pour l'estimation du volume de bois sur pied et de la surface terrière impactés par une épidémie de scolytes dans les forêts des Vosges, situées dans le nord-est de la France. L'étude a utilisé une carte d'anomalies (produite par la méthode ForDead) qui utilise une analyse de séries temporelles des données Sentinel 2 sur les peuplements dominés par l'épicéa et le sapin. Les attributs forestiers dans les domaines d'estimation ont été prédits à l'aide de la méthode développée au Chapitre III, utilisant l'ALS et Sentinel 2 comme principales sources de données auxiliaires. Deux modèles ont été évalués : un modèle général couvrant l'ensemble de la zone et un modèle spécifique pour l'épicéa et le sapin. Les résultats ont montré que les épidémies ont impacté 1 139 hectares de peuplements dominés par l'épicéa et le sapin entre 2021 et 2022. Les estimations correspondantes du matériel sur pied étaient de 494 213 m^3 (± 2,2 %) avec le modèle général et de 505 401 m^3 (± 2,7 %) avec le modèle spécifique. En moyenne, le matériel sur pied impacté était de 67 m^3/ha plus élevé que la moyenne de la population (377 m^3/ha), indiquant que les peuplements matures étaient principalement touchés. Des recherches futures sont nécessaires pour aborder les incertitudes associées à la détection de surface et leur intégration dans les estimations des ressources. Le renouvellement régulier des modèles 3D par des moyens photogrammétriques pourrait permettre de renouveler la carte forestière tous les 3 ans en France, ouvrant des possibilités pour surveiller la dynamique des ressources impactées par diverses perturbations.

Nous avons développé une approche de cartographie des ressources forestières à haute résolution permettant de produire des indicateurs de fiabilité au niveau des pixels. Des approches SAE ont également été utilisées avec succès pour permettre l'estimation dans différents types de domaines en utilisant des estimateurs assistés par des modèles ou basés sur des modèles, selon les cas spécifiques.

Alors que la recherche présentée dans cette thèse s'est principalement concentrée sur des variables d'état et des quantités agrégées, des développements supplémentaires sont cependant nécessaires pour traiter les problèmes d'estimation liés aux variables de flux (par exemple, l'accroissement en volume du stock sur pied). L'estimation des variables de flux pose des défis car elle nécessite une intégration temporelle des variables auxiliaires, qui peuvent être hétérogènes dans le temps. Une amélioration possible pour ces variables est attendue, grâce au développement de séries temporelles harmonisées de bases de données de télédétection, ainsi qu'à la disponibilité croissante de modèles 3D dérivés de l'ALS et de la DAP. Ces séries temporelles pourraient fournir des données auxiliaires en corrélation avec les flux mesurés sur le terrain, permettant un gain de précision significatif pour leurs estimations dans des petits domaines. Le programme LiDAR HD (2020-2025) à l'échelle nationale permettra de générer un MNT à haute résolution sur l'ensemble du territoire. Cela facilitera la mise en œuvre de modèles numériques de hauteur (MNH) photogrammétriques peu coûteux et régulièrement mis à jour à des fins de surveillance.

Dans certains pays où l'acquisition de données DAP ou même ALS est limitée, la question de l'applicabilité des méthodes d'IMS à la couverture d'un paysage à grande échelle ou pour les situations où le régime de perturbation des forêts est répandu reste entière. Dans de tels cas, une alternative aux

données DAP ou ALS conventionnelles pourrait consister en l'utilisation de données de télédétection provenant de plates-formes spatiales. Par exemple, l'intégration de données 3D provenant du capteur LiDAR de la NASA, nommé Global Ecosystem Dynamics Investigation (GEDI) avec d'autres données de télédétection spatialement continues pour générer des cartes des ressources forestières. Cependant, la détection et la caractérisation des perturbations sous la couverture nuageuse constituent un défi important pour les données optiques spatiales. Par ailleurs, des capteurs radar spatiaux pénétrant les nuages, tels que Sentinel-1 ou ALOS PALSAR, pourraient également être intégrés à GEDI pour générer des modèles, permettant ainsi une estimation plus précise des ressources forestières.

Les travaux menés dans cette thèse ont donc permis de mettre en évidence toute l'importance des approches d'IMS pour estimer différents attributs forestiers à des résolutions fines, ainsi que certaines pistes qu'il reste à explorer pour améliorer la méthode.

Mots clés: inventaire forestier multisource, statistiques inferencielles, estimation de petits domaines, télédétection, nuages de points 3D, perturbations forestières.

Table of Contents

Scientific contributions

Articles published/submitted in peer-reviewed international journals

I. Vega, C., Renaud, J.P., **Sagar, A.**, Bouriaud, O., 2021. A new small area estimation algorithm to balance between statistical precision and scale. International Journal of Applied Earth Observation and Geoinformation 97, 102303. https://doi.org/10.1016/j.jag.2021.102303.

II. Renaud, J.P., **Sagar, A.**, Barbillon, P., Bouriaud, O., Deleuze, C. and Vega, C., 2022. Characterizing the calibration domain of remote sensing models using convex hulls. International Journal of Applied Earth Observation and Geoinformation, 112, p.102939. https://doi.org/10.1016/j.jag.2022.102939.

III. **Sagar, A.**, Vega, C., Bouriaud, O., Piedallu, C., Renaud, J.P., 2022. Multisource forest inventories: a new model-based approach using k-NN to reconcile forest attributes statistics and map products. ISPRS Journal of Photogrammetry and Remote Sensing, 192. https://doi.org/10.1016/j.isprsjprs.2022.08.016.

IV. **Sagar, A.**, Vega, C., Bouriaud, O., Renaud, J.P., 2023. Forest resource predictive maps: a bridge for small area estimation of forest disturbance areas. Manuscript submitted.

Conference paper published

I. **Sagar, A.**, Véga, C., Piédallu, C., Bouriaud, O., Renaud, J.P. (2021). High Resolution Mapping of Forest Resources and Prediction Uncertainty using Multisource Inventory Approach. In Proceedings of the SilviLaser Conference 2021 (pp. 219–221). https://doi.org/10.34726/wim.1986.

II. Renaud, J.P., **Sagar, A.**, Barbillon, P., Bouriaud, O., Deleuze, C., Véga, C. (2021). Convex hull: Another Perspective about Model Predictions and Map Derivatives from Remote Sensing Data. In Proceedings of the SilviLaser Conference 2021 (pp. 71–73). https://doi.org/10.34726/wim.1919.

Oral Presentations

I. **Sagar, A.**, Vega, C., Renaud, J.P., Downscaling NFI estimates to small areas. September 21, 2020, 29th IGN research day, Nancy, France.

II. **Sagar, A.**, Renaud, J.P., Vega, C., Small area estimation methods for the National Forest Inventory. October 20, 2020, DEEPSURF conference: Forests and carbon storage, Nancy, France.

III. **Sagar, A.**, Vega, C., Renaud, J.P., High resolution mapping of forest resources using Multisource Inventory approach: a comparison between airborne LiDAR and aerial photogrammetry. March 26, 2021, SIReNa seminar, Nancy, France.

IV. **Sagar, A.**, Vega, C., Bouriaud, O., Piedallu, C., Renaud, J.P., High resolution mapping of forest resources and prediction uncertainty using Multisource Inventory approach. September 27 to 29, 2021, SilviLaser conference, Vienna, Austria.

V. **Sagar, A.**, Vega, C., Bouriaud, O., Piedallu, C., Renaud, J.P., High resolution mapping of forest resources and prediction uncertainty using Multisource Inventory approach. October 27 to 29, 2021, INCA conference, Chandigarh, India.

VI. **Sagar, A.**, Vega, C., Renaud, J.P., Bouriaud, O., Piédallu, C., Forest resources estimation and mapping of dieback affected forest in Vosges mountainous region. September 7 to 8, 2022, DEEPSURF conference: Forests and carbon storage, Nancy, France.

VII. **Sagar, A.**, Renaud, J.P., Vega, C., Multisource Forest Inventory flexible tool for forest information and decision making. March 30, 2023, 32nd IGN research day, Paris, France. Available at https://www.youtube.com/watch?v=Bf9c6398v94.

List of figures

List of tables

List of abbreviations

FAO	Food and Agricultural Organization
Mha	Million hectares
UNCCD	United Nations Convention to Combat Desertification
ERTS	Earth Resources Technology Satellite
SPOT	Satellite pour l'Observation de la Terre
AVHRR	Advanced Very High Resolution Radiometer
MODIS	Moderate Resolution Imaging Spectroradiometer
NFI	National Forest Inventory
GSV	Growing stock volume
UNFCCC	United Nations Framework Convention on Climate Change
MCPFE	Ministerial Conference on the Protection of Forests in Europe
ENFIN	European National Forest Inventory Network
COST Action	European Cooperation in Science and Technology
IPCC	Intergovernmental Panel on Climate Change
IGN	Institut national de l'information géographique et forestière
CBH	Circumference at breast height
BA	Basal area
FMI	Forest Management Inventory
ONF	Office National des Forêts
MSNFI	Multisource National Forest Inventory
DBH	Diameter at breast height
Radar	Radio detection and ranging
ALOS	Advanced Land Observing Satellite
PALSAR	Phased Array type L-band Synthetic Aperture Radar
InSAR	Interferometric Synthetic Aperture Radar
RADARSAT	Radar Satellite
LiDAR	Light Detection and Ranging
DAP	Digital aerial photogrammetry
GIS	Geographic information system
GLAS	Geoscience Laser Altimeter System
ICESat	Ice, Cloud, and Land Elevation Satellite
GEDI	Global Ecosystem Dynamics Investigation
OLS	Ordinary least squares
PLS	Partial least squares
SUR	Seemingly unrelated regression
GWR	Geographic weighted regression

kNN	k-nearest neighbors
SRS	Simple random sampling
GREG	Generalised regression estimator
AGB	Aboveground biomass
SAE	Small area estimation
DOI	Domains of interest
ALS	Airborne laser scanning
VI	Growing stock volume increment
DSM	Digital surface model
SIFT	Scale-invariant-feature transform
DTM	Digital terrain model
CHM	Canopy height model
BIC	Bayesian information criterion
RMSE	Root mean squared error
BSP	Binary space partitioning
SAETree	Small area estimation Tree structure
RE	Relative efficiency
AOI	Area of interest
ABA	Area-based approach
SAR	Synthetic Aperture Radar
GPS	Global Positioning System
EPSG	European Petroleum Survey Group
AGL	Above ground level
ME	Mean error
TE	Total error
CV	Coefficient of variation
DAFOR	Département d’analyse des forêts et des haies
RF	Random forest
CNN	Convolutional neural network
RNN	Recurrent neural network

Introduction

1. Forests - a sustainable asset

Forests, as we know them today, are viewed, defined, and assessed differently by different groups and individuals for different purposes. From a long time, forests have been seen as a land with a diverse ecosystem that serves as a home to a variety of wildlife, provides feed for livestock (Arroyo-Rodríguez et al., 2020), offers a reserve of timber, fuel wood, resin, and other wood and non-wood forest products (Ramage et al., 2017), and supports the livelihoods of rural communities (FAO, 2020; Santoro et al., 2020). Nowadays, contemporary users such as forest managers and policymakers have turned their attention to the influences that the forest exerts for the benefit of the environment, in the balance of cycles of nature. As forests are sensitive to the role that stands of trees can play with respect to soil protection and land stability, the control they exert over water quality, regulation and flow (Rodrigues et al., 2021), the influence that the tree formations have on the climate, rain, and wind, not to mention the carbon fixation in the atmosphere to combat the forecasted global warming trends (Chambers et al., 2001). All of these functions of forests are critical to the health and well-being of the planet and its inhabitants.

With modern expectations defined, and many functions of the forest better recognised, it is important to protect, maintain, and monitor forests to ensure that these vital resources are sustained for future generations. To accomplish this, it is crucial to have a clear and common definition of forests, which will serve as the foundation for the sustainable utilization and management of forest resources worldwide. However, defining what constitutes a forest is a complex task, as forests are not uniform throughout the globe because their structure and composition vary greatly depending on the geographical location, soil composition, temperature, precipitation patterns, and human activities. The definition of a forest is also influenced by the perspective of the person defining it. For example, people living in boreal forests of Europe or North America might define forests based on dominant coniferous tree species and cold climate adaptations, while those in tropical forests of Asia or Africa may emphasize the rich biodiversity and complex ecological relationships. Similarly, an economist will define forest differently than a conservationist (Achard, 2009). Currently, there are over 800 different definitions of forests in use across the world, with some countries using several definitions at the same time (Lund, 2018). But, the most widely accepted and used definition of forests is the one developed by the United Nations Food and Agricultural Organization (FAO), which defines forests as *"land spanning more than 0.5 hectares with trees higher than 5 meters and a canopy cover of more than 10 percent, or trees able to reach these thresholds in situ"* (FAO, 2010).

1.1. Forest distribution - surface and stocks

According to the definition of FAO, today there are approximately 4 billion hectares of forests globally, covering over 31% of the total land area. These forests are spread across different types of biomes, with tropical forests making up the largest portion (46%) of the global forest area, followed by

boreal forests (27%), temperate forests (16%), and subtropical forests (11%) (Figure 1; FAO, 2020). Meanwhile, Europe's forests make up 6% of the global forest area. This amounts to 227 million hectares (Mha) of forests, which cover 35% of Europe's landmass. The forest coverage in Europe varies from country to country, with most countries having 35% to 45% of their national territory covered by forests. Northern European countries, such as Finland and Sweden, have the highest forest coverage, with a staggering 75% and 69% of their total land area being covered by forests, respectively. The extensive forest coverage in these countries is largely dominated by coniferous species, which also accounts for 46% of Europe's forests. On the other hand, broadleaved species make up 37% of Europe's forest cover and are primarily found in South-West Europe. The remaining forests are a mixture of both coniferous and broadleaved species, primarily located in Central-West Europe (FAO, 2020; Forest Europe, 2020).

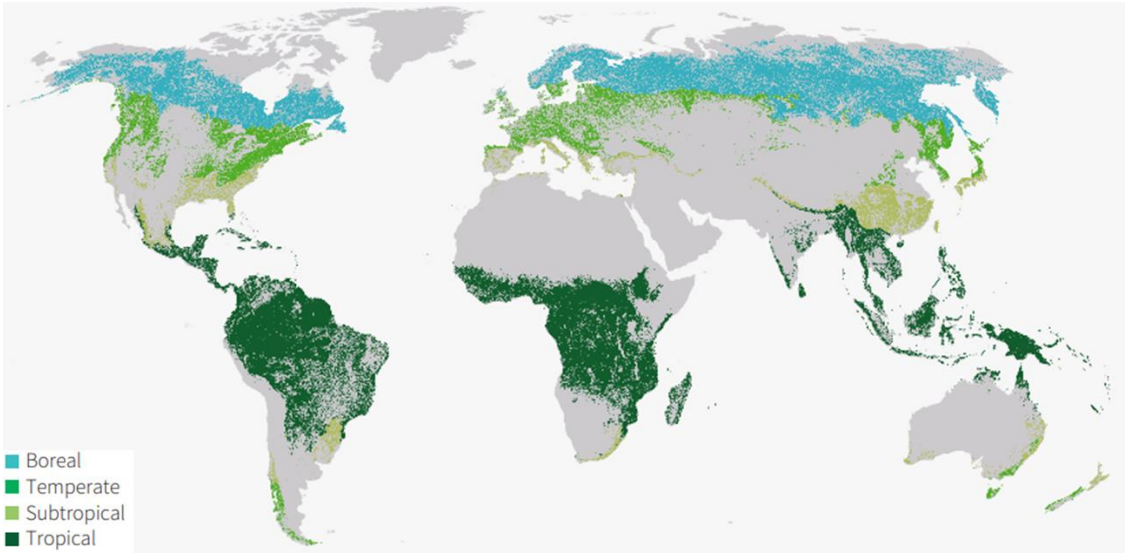

Figure 1. *Distribution of global forest area. Adapted from FAO (2020).*

Between 1990 and 2020, the global growing stock of trees decreased marginally from 560 billion m^3 to 557 billion m^3, mainly due to decline in forest area. Conversely, there has been an overall increase in growing stock per unit area (Figure 2), rising from 132 m^3/ha in 1990 to 137 m^3/ha in 2020 (FAO, 2020). This increase is observed in all parts of the world, with significant growth observed in East Asia and Europe. The growth in East Asia can be attributed to major reforestation programs implemented in recent decades. In contrast, in Europe, the transition from agricultural land to forest land (Barbier et al., 2010) and the widespread use of forest management practices has been instrumental in promoting forest growth. As a result, over the past three decades, the European growing stock has increased by 14%, and it is currently estimated to be 35 billion m^3. The average area-related growing stock in Europe amounts to 169 m^3/ha, ranging from 60 m^3/ha in South-West Europe to 255 m^3/ha in Central-East Europe (Forest Europe, 2020).

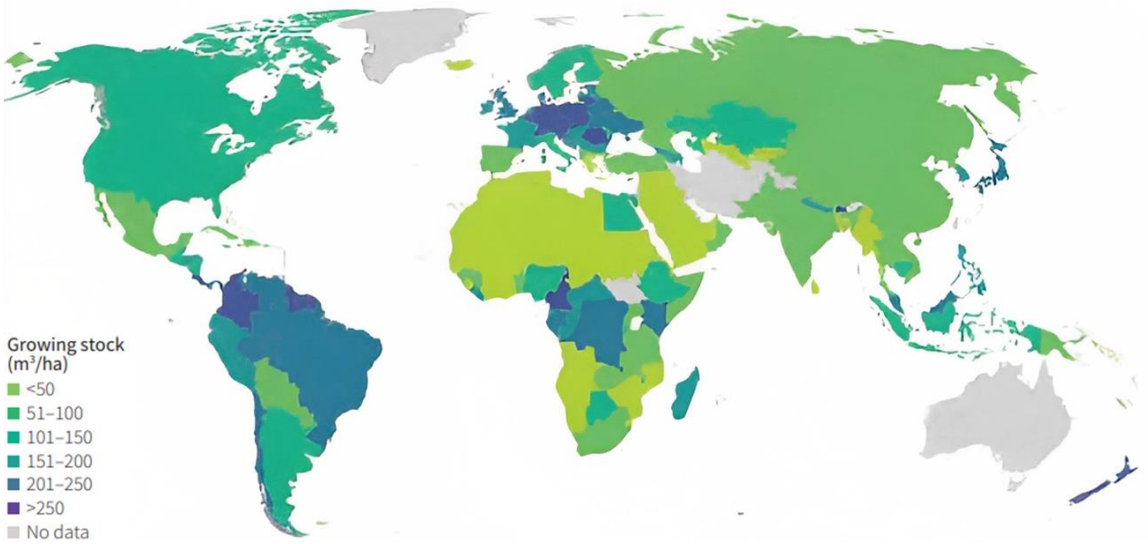

Figure 2. *Distribution of forest growing stock per unit area, by country. Adapted from FAO (2020).*

1.2. Forest dynamics

Forest dynamics refer to the underlying biological and physical forces that shape and change the four main demographic processes of forests establishment, dispersal, growth, and mortality across a range of spatial and temporal scales (Petit and Hampe, 2006). These forces are mainly driven by two fundamental elements which are forest disturbance and forest succession (Frelich, 2016). Forest disturbances are events that disrupt or alter the natural ecological processes within forest ecosystems, leading to changes in the forest's structure and composition. These disturbances can include a range of natural events such as landslides, windstorms, flood, volcanic eruptions, wildfires, droughts, and insect outbreaks (Seidl et al., 2017). The extent and severity of these disturbances can range from small-scale localized impacts to large-scale landscape-level changes. Importantly, not all disturbances are harmful to forest ecosystems, as many natural disturbances can actually create opportunities for new growth and succession (Binelli et al., 2008). These disturbances alter environmental factors such as soil chemistry, sunlight, temperature and humidity that allow different species to flourish where they might have previously struggled, i.e. forest succession (Finegan, 1984). The disturbance affected area goes into the process of succession over many years and host many different species during this time (Yamamoto, 2000). For instance, the boreal forest in North America has adapted to periodic wildfires, which help in maintaining and rotating various species that rely on open habitats and nutrient cycling that may result from fires (Christensen, 2014). The 1988 natural-caused fire in Yellowstone National Park burned a substantial proportion of forests, and the area is initiated by a natural process of forest succession. Pioneer species, such as aspen, willow, and other deciduous trees, were the first to colonize the burned area, followed by coniferous trees like lodgepole pine and white spruce. Over time, the forest began to recover, becoming more diverse in terms of species composition and age structure (Romme et al., 2011).

- **Current drivers of forest dynamics**

Both elements (forest disturbance and forest succession) of forest dynamics are interconnected processes that can influence the long-term development of forest ecosystems. However, recent increases in natural disturbance events, driven by ongoing climate change, have significantly disrupted forest dynamics processes and affected forest composition, productivity, and distribution worldwide (Canelles et al., 2021). The ongoing rise in global temperature and changes in precipitation patterns have led to a more frequent range of effects, including severe drought events, increased susceptibility to insect outbreaks, and more frequent occurrences of wildfires events (Jentsch and Beierkuhnlein, 2008). As a consequence, these events pose challenges for forest ecosystem, as they disrupt growth and increase mortality rates of trees. For example, during the 2010 drought in the Amazon rainforest, a substantial proportion of trees were impacted, with many experiencing reduced growth rates or mortality (Lewis et al., 2011). The ongoing drought conditions have also ignited severe dieback activities in western United States, with some forests experiencing more than 70% tree mortality (Vose et al., 2016). According to UNCCD (2022), there has been a 29% increase in drought events worldwide since 2000. Similarly, the frequency of wildfire events has also increased in recent years, resulting in nearly twice as many occurrences and an additional 3 Mha of forest loss annually compared to what was seen before 2001 (FAO, 2020). Moreover, the impact of climate change on the intensity and severity of windstorms has also increased over the last few decades, with an accelerated increase observed since 1990 (Senf and Seidl, 2020). The exceptional storms of 1999 in Europe, Martin and Lothar, serve as a prime example of the destructive effects storms can have on forests. These storms caused damage to 180 million m^3 of wood, and also led to insect outbreaks that persisted long after the storms had passed (Schelhaas et al., 2003).

1.3. Need to monitor forests

The ongoing degradation of forests, primarily due to climate change-induced disturbances, is not only causing a persistent decline in the quality and quantity of forest resources, but also leaves a significant impact on the ecosystem services provided by them. According to Myers (1996) *"the accelerating decline of many of the world's forests represents one of the greatest problems and opportunities facing the global community"*. This sparked an extensive debate about the most effective ways to manage their future. A crucial aspect of this debate is the need for accurate information about the status of forests, especially information on where and how they change over time. This information is needed across a range of spatial, spectral and temporal scales, which needs to be accurate and thorough, detailed yet global, current yet permanent, and can continuously monitors the forest mantle, forms, content, nature, health and vitality (Cohen et al., 2001). Remote sensing can aid in this process by providing valuable data and insights about changes in the forest ecosystem across these scales (Franklin, 2001).

- **Remote sensing in forestry**

The term remote sensing was first coined in 1960, which refers to the " *noncontact recording of Earth's information from the ultraviolet, visible, infrared, and microwave regions of the electromagnetic spectrum by means of instruments such as cameras, scanners, lasers, linear arrays, and/or area arrays located on ground, air or space platforms"* (Jensen, 2007). Although remote sensing had been in use since the 1850s, when photographs were first taken from hot air balloons and kites, many of its early applications were for military purposes (Colwell, 1964). Over the past century, the application of remote sensing technology has greatly evolved, with forestry being one of the early sectors to adopt it after the military sector (Koch, 2015). In the 1950s, colour infrared photography was used first in forestry for differentiating vegetation types, while aerial photographs providing 3D information were used to estimate forest resources (Nyyssönen, 1955). However, these early estimation techniques were limited to local areas and lacked a global perspective. Space photography gained prominence in the late 1960s with the Gemini and Apollo missions, and in 1972, photographs from the Skylab space station were used to construct land-use maps. Also in the same year, the first Earth Resources Technology Satellite (ERTS-1), which was later renamed as Landsat 1, was launched. This marked the beginning of the evolution of spaceborne remote sensing methods in forests, leading to the development of numerous satellites (e.g. SPOT, AVHRR, and MODIS) with improved capabilities. These satellites were primarily used for making maps of forest type, cover and area (McRoberts et al., 2010a).

Since the early 1980s, satellite images from multiple time periods have been used for detecting and mapping changes in forests associated with deforestation, forest recovery and natural disturbances such as fire and windstorms. Data from AVHRR sensor was among the first to be analysed for inter-annual spectral changes in forests (Hansen and DeFries, 2004; Lambin and Strahlers, 1994), and to relate these changes to climatic variations (Eastman and Fulk, 1993). Lately, data from the SPOT (Fraser et al., 2003) and MODIS (Langner et al., 2007) sensors were also used to map large-scale forest land cover changes. However, the low spatial resolution of these sensors makes it challenging to accurately map changes at the level of forest management units, which are usually managed at finer, smaller scales (Hayes et al., 2008). For instance, MODIS can accurately detect forest harvest changes larger than 50 ha, but those smaller than 20 ha cannot be detected (Jin and Sader, 2005). Detailed mapping of forest changes at such scales is only possible through the use of high spatial resolution sensors, such as QuickBird and IKONOS (Clark et al., 2004). But the data from these sensors are not explicitly intended for forest monitoring purposes due to their high cost and lack of systematic, routine collection. The freely available data from Landsat series of satellites has been the primary source of data for monitoring forests, as they have been systematically acquiring images covering most of the Earth's surface for nearly 50 years at a resolution suitable for forest management practises (Cohen and Goward, 2004).

Access to accurate and reliable data is crucial for making informed decisions in forestry, particularly when it comes to estimating forest resources. While remote sensing technologies have revolutionized forest mapping (e.g. land use land cover, forest type maps), relying solely on these methods for forest resource estimation may not provide a complete picture of forests. There are limitations to the information that remote sensing can provide, such as the inability to distinguish between different species, age classes, diameter classes, or tree height. These limitations can be overcome by complementing remote sensing data with information from field surveys, such as data from National Forest Inventory (NFI) programs.

2. NFI - history and objectives

National Forest Inventories (NFIs) are a long-standing, comprehensive forest assessment programs established in many countries to provide accurate information about the amount and the state of forests. NFIs are based on systematic field surveys, typically conducted on statistical samples consisting of field plots, used primarily to collect detailed information about the country's forest resources (Tomppo et al., 2010). This valuable information is then used by policymakers, government agencies, forest managers, researchers, and other stakeholders for a variety of purposes, such as developing policies related to forestry, managing forests, planning and conservation efforts (McRoberts et al., 2010b).

The history of forest inventories dates back to the late 15th century, when intensive use of forest resources led to timber shortages, prompting timber users to develop strategies for forest planning around cities and mines (Gabler and Schadauer, 2007). These early strategies were primarily based on visual inspections and basic measurement techniques, which were used to collect forest information on crude estimates of growing stock volume (GSV) and forest area. The first inventories were often local and conducted by timber users and companies, mainly for assessing the availability of timber resources. However, it soon became obvious that such localized information could not be easily used to compile national-level forest information for formulating national forest policies; thus, NFIs were initiated (Vidal et al., 2016b). Since then, forest information has been collected and compiled through user-driven NFIs in many countries (Robert et al., 2010). But these NFIs were not systematic and were driven by the needs of the end users, rather than by a comprehensive inventory plan.

It was not until late 1910s, the first systematic NFI based on statistical sampling methods was started in Nordic countries, with Norway implementing the first NFI in 1919 (Tomter, 2016), followed by Finland in 1921 (Korhonen, 2016) and Sweden in 1923 (Fridman and Westerlund, 2016). The primary reason for the establishment of NFIs in Nordic countries was the over-exploitation of forest resources. The NFIs were established to provide accurate forest resource information for efficient forest management and forest industry investment planning purposes (Robert et al., 2010). Although, assessing the productivity of forests and the potential for taxation of forest income was one of the factors that prompted the initiation of the Finnish NFI (Korhonen, 2016). In all these countries, the inventory was conducted on numerous sample plots which were strategically placed throughout the country to not only collect information about forest area and GSV, but also size, age, species structures of forest within each sample plots. The information from all these plots was then aggregated at national level for developing national forest policies. Since then these inventories became a crucial part of national forest planning, and were gradually adopted by at least 40 countries accounting for more than 50% of the Earth's forested area (McRoberts et al., 2010b).

The establishment of NFI in many other countries like USA and UK was motivated by the fear of over-exploitation of forest resources, while in countries like Austria, Germany, and Poland it was

initiated during the Second World War reconstruction phase (Breidenbach et al., 2021; Vidal et al., 2016b). Concerns regarding the state of forest in the face of climate change were a major trigger for initiating new NFIs, particularly in developing countries like Peru and Ecuador (Segura et al., 2016). Over time, due to these concerns, NFIs have evolved to provide information for a much broader range of issues, such as forest health status and damage, carbon pools, biodiversity and land use changes (Breidenbach et al., 2021). Currently, statistical sample-based NFI are conducted in most of the European countries (29 countries; Brus et al., 2019) to not only support national level forest policies, but also to report at international conventions, such as FAO, United Nations Framework Convention on Climate Change (UNFCCC), Ministerial Conference on the Protection of Forests in Europe (MCPFE), Montreal Process, European National Forest Inventory Network (ENFIN), European Cooperation in Science and Technology (COST Action) and Intergovernmental Panel on Climate Change (IPCC) to support international forest-related policy and decision-making (Vidal et al., 2016a). At the global level, NFIs are still lacking in many countries - especially in developed countries - although new NFIs are being initiated from time to time (Zeng et al., 2015).

2.1. French NFI - history and objectives

The French NFI was initiated in 1958 as a department of the French ministry in charge of the forests, with the aim of assessing the state of forests in France after the Second World War. This assessment was crucial for evaluating the potential for sustainable timber harvesting. In 1994, the NFI was transformed into a public institution, and in 2012, it merged with the National Geographic Institute (IGN) to form the *"Institut national de l'information géographique et forestière"* (in short still IGN) (Hervé, 2016).

Before 2004, the NFI was covering one administrative unit called *"département"* at a time. During that period, there were 96 départements in France. Each département was densely sampled with NFI plots, and approximately 8 départements were inventoried annually. The entire country was covered for the first time in 1980 and again in 1990, taking almost a decade to update the NFI database. This pace of inventory allows for a much precise estimate of the country's forest resources, but also highlights the need for regular updates to keep the data current. By the time the data were outdated for estimation in those départements that were inventoried more than 5 years ago. The NFI changed its methodology in 2004 in response to the need for timely assessment of the impact of major disturbance events, particularly after the storms of 1999 (Hervé, 2016; Vidal et al., 2007).

- **Sampling methods**

The new sampling strategy is designed to cover the entire French metropolitan territory on an annual basis. It is based on a systematic 1 km^2 unit grid (Figure 3.a), which is divided into two 5-year samples. Both 5-year samples are further divided into five systematic sub-samples, with one sub-

sample being inventoried each year (Figure 3.b). The sample plots are revisited after five years to evaluate the stand growth, tree mortality or the amount of harvested wood. To optimize the logistics between the first and second visit, the annual sub-samples from the first 5-year sample are juxtaposed with the annual sub-samples from the second 5-year sample (Figure 3.b) (Hervé, 2016).

The new method is based on a two-phase stratified sampling design. Each year, ~80,000 sample points on the corresponding year's grid are examined on high-resolution aerial photographs (BD ORTHO®; 0.5 m spatial resolution) in the first phase to determine the land use and land cover type. The sample points are randomly selected inside the 1 km^2 unit grid. In the second phase, stratified sub-sample points are selected from the first phase sample points. This stratification is based on land cover type, i.e. for forested areas, field measurements are conducted on ~6,500 sample plots (Figure 3.c) (Vidal et al., 2016b).

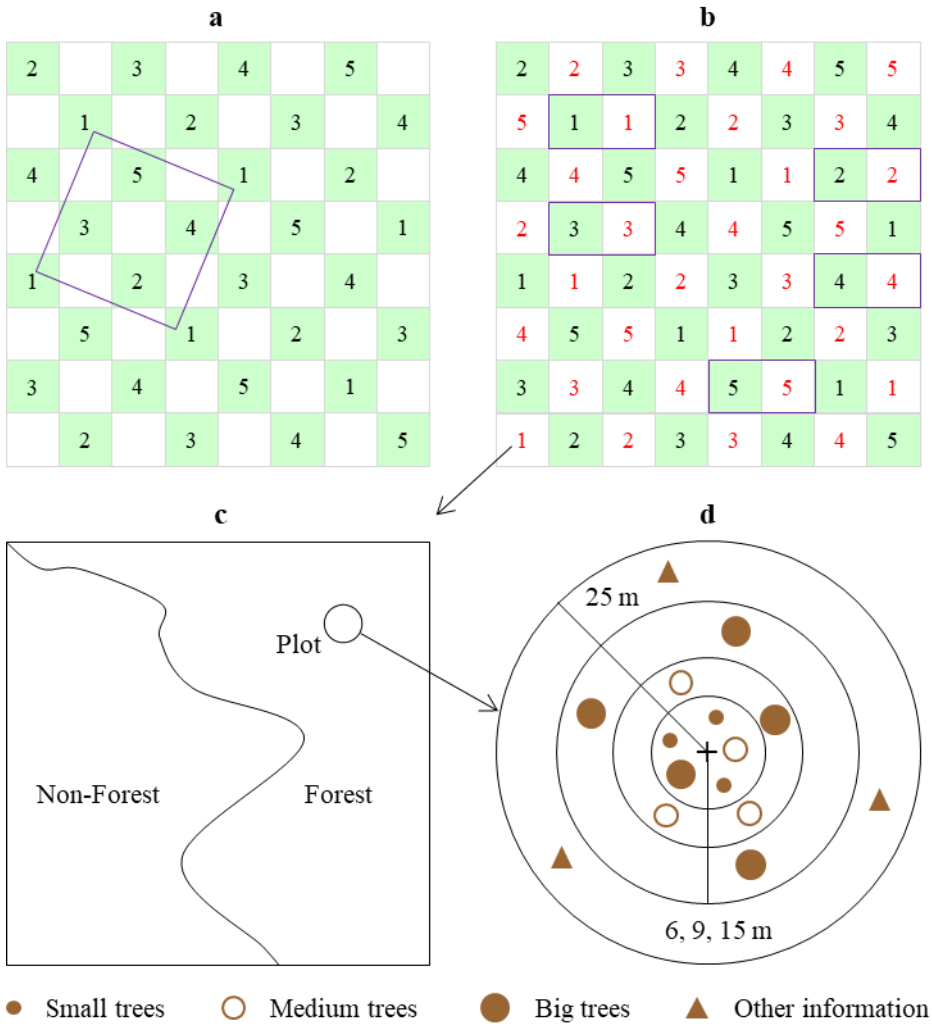

Figure 3. *An overview of the current sampling method used in French NFI: (a) Each square cell represent 1 km^2. Text in black represents year number from the first 5-year sample; (b) Text in red represents year number from the second 5-year sample. The plots from the first cycle are revisited after 5 year; (c) Location of the plot in 1 km^2 cell; (d) NFI field information collected from 4 concentric circular plots.*

Field information is collected within four concentric circular plots of radii 6, 9, 15, and 25 m (Figure 3.d). Tree measurements are limited to the first three concentric plots, with tree larger than 23.5, 70.5 or 117.5 cm at circumference at breast height (CBH at 1.3m) are measured on 6, 9 and 15 m radius plots, respectively. The larger plot of 25 m radius is used to assess stand and crown description, as well as soil information (Robert et al., 2010).

2.2. Limitation of NFI

Today, the sampling design of NFI in France and many other countries is primarily aimed to meet national requirements. The data provided by NFI is mainly used to produce precise and reliable estimates of forest attributes of interest, such as GSV and basal area (BA), at the national or even regional scales (Figure 4.a) (Kangas et al., 2019; Magnussen et al., 2018; Sagar et al., 2021). These estimates are then used for various purposes from developing national or regional level forest policies to sustainable forest planning. For example, in Canada, NFI data has been used to develop national policies related to carbon sequestration, biodiversity conservation, and sustainable forest management (Stinson et al., 2016). Similarly, in Sweden, regional-level estimates of forest resources produced using NFI data are used to develop forest management plans that ensure the sustainable use of the forest resources (Fridman and Westerlund, 2016).

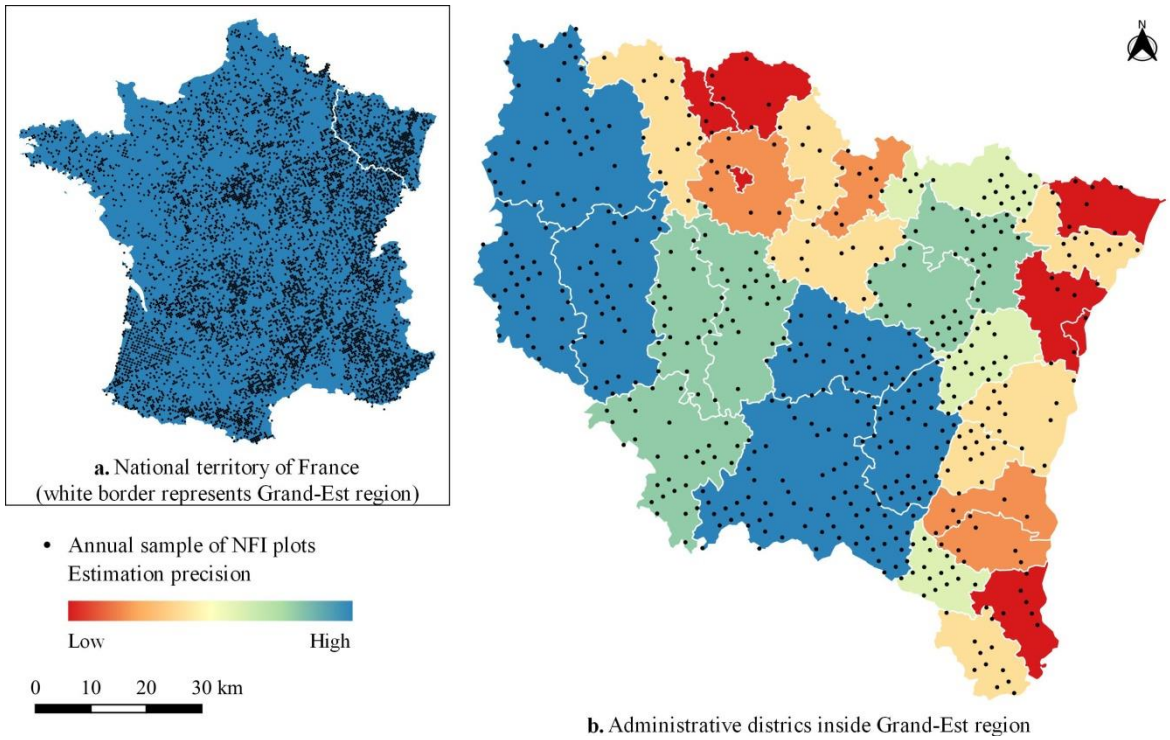

Figure 4. *Illustration of the impact of the sample size on the estimation precision related to different estimation domains: (a) At national or regional level – the NFI sample size is large enough to provide precise estimates; (b) At district level – the number of NFI plots can vary greatly, from high to low or even none in some domains, resulting in imprecise estimates.*

Over the past few decades, there has been an increased interest towards the evaluation of forest ecosystem services, together with a surge in the bio-economy, the demand for precise information on forest resources requires timely and more localized estimates than before (Kangas et al., 2018; Næsset et al., 2011). The utility of NFI data would greatly increase if there were simpler ways of achieving this precise and localized estimate of forest attributes at sub-regional domains, such as municipalities, districts and other forest management units (Tomppo et al., 2008b). At such domains, the NFI sampling intensity, i.e. the ratio of the sample size to the population size, remains roughly the same as national or regional scales, but the sample size decreases significantly leading to imprecise estimates (Figure 4.b) (Fortin, 2020). One possible solution to improve the estimation precision in such localized domains is to increase the NFI sample size. However, field measurements are typically expensive, time-consuming, and resource-intensive tasks. Moreover, a common issue in every NFI is the inability to obtain field measurements in certain situations. Factors such as dangerous terrain or denied access can prevent fieldwork (Magnussen et al., 2018).

In situations where extensive fieldwork is not feasible, alternative approaches such as post-stratification can be used to improve estimation precision. Post-stratification is widely used in operational NFIs in several countries, including Netherlands, France, Slovakia, Switzerland, Sweden, and USA (Barrett et al., 2016). This technique allows for a more detailed characterization of the forest population by dividing it into meaningful strata based on factors such as species composition, forest types, forest height distribution, or ecological regions. By sampling proportionally within each stratum, the NFI can account for variations in forest attributes and ensure that estimates accurately reflect the characteristics of different forest components (Pulkkinen et al., 2018). It has been shown that post-stratification can improve estimation precision at larger geographical scales, such as national or regional scales (Fridman et al., 2014; Haakana et al., 2020, 2019; McRoberts et al., 2005). However, a drawback of post-stratification in forest inventory, particularly for smaller areas, is the lack of control over sample size allocation within strata. Since sampling units are assigned to strata after data collection, the sample sizes within each stratum cannot be predetermined or controlled. Consequently, this variability in sample sizes may result in inadequate samples within certain strata, potentially compromising the precision of the final estimates (Haakana et al., 2020; McRoberts, 2010).

Several countries, such as Canada, Norway, and Finland, conduct inventories of their forest resources at the forest management level, known as Forest Management Inventories (FMIs). The use of FMIs in these countries has enabled a paradigm shift from imprecise estimates of forest attributes to highly precise estimates at smaller localized domains (Maltamo et al., 2009). This level of precision is achieved primarily through a more detailed and intensive sampling design than that of traditional NFIs (Koivuniemi and Korhonen, 2006). However, FMIs are often conducted using different methods, which can make it challenging to compare and aggregate results across different forest properties or regions. Furthermore, FMIs measures a narrower range of parameters than NFIs, focusing only on the forest resources that are most relevant to the specific management objectives of the area being

inventoried. The FMIs are usually carried out by private institutions, agencies, and individual forest landowners or managers, and are often focused on specific areas, such as production forests, for timely planning and harvesting of timber resources (Kangas et al., 2018). One example of such management inventory is conducted by the Office National des Forêts (ONF) in France, where they intensively manage forest resources in certain départements of the country to meet the timber production needs. Overall, while both NFI and FMI serve important roles in forest planning and management, they differ in their scope and scale, with FMI providing more detailed information at a local scale, and NFI providing a broader perspective across a larger geographic area (Maltamo et al., 2021). FMIs can be expensive as NFI but are spatially limited to some forest management units and therefore may not provide a comprehensive overview of the country's forest resources (Gillis, 2001). Thus, there is a need for methods that can downscale forest resource estimates at smaller localized domains with improved precision at the landscape level, without significantly increasing inventory costs.

3. MSNFI - history and objectives

The need for comprehensive, cost-effective, timely, and improved forest statistics, such as population estimates of means and totals of forest attributes of interest, at a local scale has contributed towards the introduction and ongoing methodological development of Multisource National Forest Inventory (MSNFI) approaches. The approach combines NFI field plot data with auxiliary data (e.g. remote sensing data, thematic maps) using statistical techniques (Figure 5; Tomppo et al., 2008; Tuominen et al., 2020). The inclusion of auxiliary data fills up the gap in providing continuous spatial forest information at the landscape level, which was not previously possible using NFI data alone (Barrett et al., 2016). According to McRoberts and Tomppo, (2007), integrating auxiliary data with NFI data can: *(i)* provide a less expensive and faster way to estimate forest attributes of interest, *(ii)* increase the estimation precision for larger areas (such as national or regional level), and *(iii)* provide estimates with acceptable precision for smaller areas (such as municipalities, communes, or forest districts). This combination not only improves the NFI estimates of forest attributes in areas with few to no NFI field plots (as shown in Figure 4.b) but also produces wall-to-wall maps of corresponding forest attributes of interest (Saarela et al., 2020; Sagar et al., 2021). These maps, when reconciled with forest statistics, have the potential to provide detailed spatial information about the amount and location of the forest resources. The resource maps can assist forest managers and stakeholders in forestry-related decision-making process (Hauglin et al., 2021).

The history of MSNFI dates back to the 1980s when satellite-based remote sensing images became widely available. During that period, Finnish researchers came up with a methodology of combining NFI data of Finland with optical satellite images, for obtaining reliable estimates of forest attributes such as GSV, mean tree height, mean tree diameter at breast height (DBH), and tree density, at smaller domains such as municipalities, which was previously not possible using field inventory data alone (Danson, 1987; Poso et al., 1984; Tomppo, 1988). After the first operative results obtained in 1990 (Tomppo, 1990), the development of MSNFI methods in Finland picked up pace. Additional auxiliary datasets, such as digital map data of various types, including basic forest map data and soil map data, were incorporated with the aim of providing improved estimates of forest attributes in the form of statistics and thematic maps at national, provincial, and municipal levels without significantly increasing the inventory costs (Tomppo, 2006; Tomppo et al., 2008a; Tomppo and Halme, 2004). In Finland, MSNFI forest resources maps for the entire country are produced every two years (Mäkisara et al., 2022).

Since the successful implementation of MSNFI approaches in Finland, somewhat similar methods to the Finnish MSNFI, utilizing NFI data and auxiliary data, have been developed and tested in several other countries like Norway (Gjertsen et al., 1999), Sweden (Reese et al., 2002), USA (McRoberts et al., 2002), China (Tomppo et al., 2001), Brazil (Vibrans et al., 2013), Austria (Koukal et al., 2007), Italy (Chirici et al., 2020; Maselli et al., 2005), New Zealand (Tomppo et al., 1999), Ireland

(McInerney et al., 2018) and France (Irulappa-Pillai-Vijayakumar et al., 2019). All these MSNFIs share a common principle, with different methodology adopted to estimate various kind of forest attributes at different estimation domains.

3.1. System component

MSNFI requires four system components, as shown in Figure 5: *(i)* NFI field plot data; *(ii)* auxiliary data; *(iii)* modelling framework; *(iv)* inference framework. The description of NFI field plot data can be found in the previous Section 2, while the remaining components will be discussed in subsequent sections.

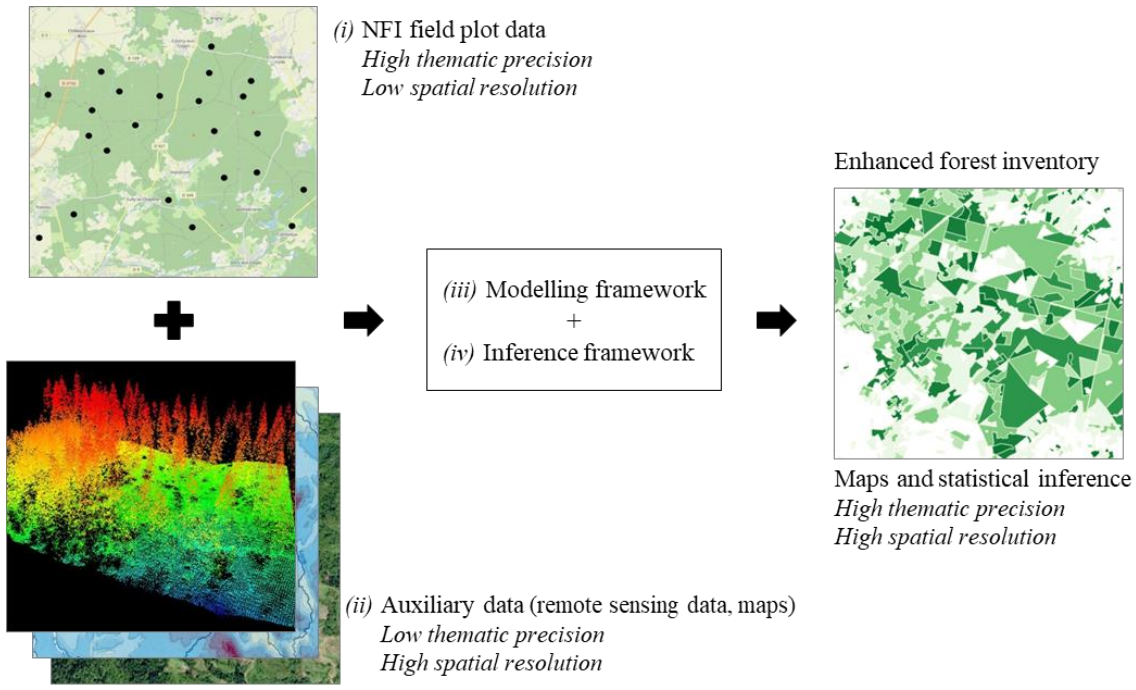

Figure 5. *Illustration of working principle of MSNFI with its four system components: (i) NFI field plot data; (ii) auxiliary data; (iii) modelling framework; (iv) inference framework.*

3.1.1. Auxiliary data

Over the past few decades, auxiliary data from remote sensing technologies has been the principal focus of attention in estimation of forest attributes of interest. According to the FAO (2010), *"Remote sensing data enable consistent information to be collected globally, which can be analysed in the same way for different points in time to derive better estimates of forest resources. Remote sensing does not replace the need for good field data but combining both provides better results than either method alone"*. The FAO has now fully integrated the remote sensing component in the assessment of global forest resources. Several types of remote sensing data are available, including optical satellite data with low, medium and high spatial resolution, such as AVHRR, MODIS, Landsat, Sentinel-2,

QuickBird, and IKONOS (Hansen et al., 2008; Tomppo et al., 2008a), satellite-borne radio detection and ranging (radar) data from ALOS PALSAR, Sentinel-1, InSAR, and RADARSAT (Næsset et al., 2011), and 3D point cloud data from Light Detection and Ranging (LiDAR) and digital aerial photogrammetry (DAP) (Breidenbach and Astrup, 2012; Næsset, 2002a; Næsset et al., 2013). The selection of any of these data sources depends upon various factor, as stated by Barrett et al. (2016) and Zolkos et al. (2013). According to them, the selected data should be *(i)* relevant to the forest attributes of interest, *(ii)* available at low cost, *(iii)* regularly updated, and *(iv)* exhaustive over the territory.

Optical remote sensing satellites capture images of the Earth's surface in the visible and infrared (0.4 - 15.0 μm) range of the electromagnetic spectrum. These images usually cover vast land surfaces and provide crucial information about forest extent and composition (Wulder, 1998). Additionally, most of the optical satellite images are freely available, making them an essential component in MSNFI cost reduction. However, the availability of optical imagery may be impeded by haze, cloud cover, and cloud shadow (Cohen et al., 1996), while the derived vegetation indices tends to saturate in mid biomass (~130 Mg/ha) (Zhao et al., 2016). Upon reviewing various optical satellite-based remote sensing data for estimating major forest attributes such as GSV, mean tree height, tree density, and BA, Barrett et al. (2016) reveal that medium resolution satellite (spatial resolution between 10 and 30 m) are the most often used satellite systems, with the Landsat series of satellites used in most NFIs (13 NFIs out of 48). The Landsat program is the longest-running optical Earth imaging program in history with a vast database of images covering much of the Earth's surface that are freely accessible in a standardized, high-quality, pre-processed format (McRoberts et al., 2010a). The Landsat-8 satellite captures a large scenic coverage of 185 km x 180 km per image and acquires 740 scenes per day, offering nine spectral bands with a spatial resolution of 30 meters and a temporal resolution of 16 days (Weng et al., 2014). This spatial resolution is well-suited to the plot diameter of many NFIs, making Landsat data a popular choice. The Landsat images in combination with NFI plot data have been the focus of many studies in the estimation of major forest attributes such as GSV, BA, tree height, and tree density (Chirici et al., 2008; Gjertsen et al., 1999; Irulappa-Pillai-Vijayakumar et al., 2019; McInerney et al., 2018; Vibrans et al., 2013).

Several inventory-related information defining the forest structure, such as forest density, volume, and height distribution, cannot be directly derived from optical remote sensing imagery. Breidenbach and Astrup (2012) have emphasized the importance of forest structure information as an auxiliary variable for estimating major forest attributes. The cloud-penetrating capability of spaceborne radar sensors has been investigated to compute forest structural properties and estimate several forest attributes of interest (Duncanson et al., 2020; Hajnsek et al., 2009; Silva et al., 2021). However, the complexity of processing radar data poses a challenge, and estimates obtained in complex canopies and mountainous areas are found to be less accurate (Boyd and Danson, 2005; Duncanson et al., 2020). 3D point cloud data obtained from DAP, and more specifically from LiDAR, have proven to be

the most crucial auxiliary sources of data for characterizing forest canopy information and accurately estimating major forest attributes (Durrieu et al., 2015; Gobakken et al., 2012; Næsset et al., 2011; White et al., 2013; Zolkos et al., 2013). However, the acquisition and processing of LiDAR data can be expensive compared to other types of auxiliary data, making it impractical to obtain and renew continuous coverage over a large geographical areas (Næsset et al., 2011). One possible solution is to share the cost of acquisition among multiple forest agencies and stakeholders working on various applications, such as road and harvest planning and design, erosion and hydrological modelling, geographic information system (GIS) analysis, and detailed land planning (Chirici et al., 2020; Reutebuch et al., 2005). Another possibility is to use spaceborne LiDAR sensors, such as the Geoscience Laser Altimeter System (GLAS), Ice, Cloud, and Land Elevation Satellite (ICESat), and Global Ecosystem Dynamics Investigation (GEDI), which provide vegetation height information across the globe at relatively low cost. However, these sensors provide low density discontinuous footprints rather than continuous data (Guerra-Hernández and Pascual, 2021). Additionally, due to their high power consumption, most of these sensors have been or will be decommissioned after a few years of service (Silva et al., 2021). Owing to their large availability, low cost, and fast renewal in many countries, DAP can be considered as an efficient 3D data source in forest monitoring (Rahlf et al., 2017).

3.1.2. Modelling framework

When auxiliary data are available, NFIs can take advantage of these new sources of information for increasing the estimation precision of forest attributes of interest at a finer spatial scale. Predictive models that relate forest attributes to these auxiliary data can be used to achieve this. In context of MSNFI, the predictive models developed for the prediction and mapping of forest attributes of interest are mainly divided into two categories: *(i)* parametric models, and *(ii)* non-parametric models (Hill et al., 2014).

3.1.2.1. Parametric models

Parametric models assume that the data from a population's sample can be modelled by a probability distribution, such as a Gaussian or Poisson distribution. These models rely on a fixed set of parameters to predict the elements of the population (McRoberts et al., 2010a). Many parametric models, such as discriminant analysis (McRoberts, 2009) and regression analysis (Hudak et al., 2006; Woods et al., 2011) are common in the forestry literature. Among these, regression models based on NFI and auxiliary data have traditionally been the most widely implemented method for predicting forest attributes (Brosofske et al., 2014). For instance, Hudak et al. (2006) used multiple linear regression models for prediction and mapping of tree density and BA in temperate coniferous forests, while LeMaire et al. (2011) used stepwise multiple linear regression model for predicting stand volume and stand dominant height in Brazilian rainforest. Muukkonen and Heiskanen (2005) used

regression model for predicting volume, age, and overstory biomass in boreal forest of Finland. Additionally, many studies that have integrated LiDAR with NFI have used regression models to predict various forest attributes of interest, such as GSV, biomass, BA, density, and tree height (Næsset, 2007; Nilsson, 1997; Woods et al., 2011).

Different methods can be used to estimate the parameters of regression models, including ordinary least squares (OLS), maximum likelihood, partial least squares (PLS), seemingly unrelated regression (SUR), and mixed-effect models (Næsset, 2007, 2002b; Packalén et al., 2011). These models usually assume a linear relationship between the response variable (e.g., forest attribute) and the predictor variables (e.g., auxiliary variables). However, it is important to note that the linear relationship assumed by the model may not always hold true in complex forest systems (Kangas et al., 2016). Hence, these assumptions need to be tested and accounted for normality, homogeneity of variance, and noncollinearity of predictors. One should know *(i)* what these assumptions are; *(ii)* how to test them, and *(iii)* what to do if they are violated (Hudak et al., 2006). A well-specified regression model is parsimonious and easy to interpret (Woods et al., 2011). Furthermore, if the model accurately describes the population of interest and is unbiased, it has the ability to make predictions beyond the range of the sample data used to construct the model, i.e. in extrapolation (White et al., 2017). However, extrapolation always exposes the user to potentially unreliable predictions, especially when the modelled attribute is following a non-linear relationship outside the calibration domain.

Parametric models are often univariate, meaning that they are specific to one response variable, and do not consider the correlations between several other forest attributes of interest. This could lead to bias when using predictions of multiple forest attributes together to obtain specific indicators (e.g., using predicted basal areas and heights to estimate volumes). To avoid this problem, several response variables can be predicted together using methods such as PLS or SUR. With these methods, the natural variation between the forest attributes is preserved (Breidenbach et al., 2010; Moeur and Stage, 1995). Moreover, all these models do not consider the spatial dependence of the data, which may lead to biased estimates. A potential solution is to use a geographic weighted regression (GWR) model, which adapts a global regression model to a specific region, incorporating a weighting function to capture the spatial variations and associations between the response and the predictor variables (Gagliasso et al., 2014). One study by Chirici et al. (2020) showed that the GWR produced more accurate estimates of GSV than conventional regression models.

3.1.2.2. Non-parametric models

Prediction models that do not necessarily require any assumptions about the underlying distribution of the data are characterized as non-parametric models (Altman, 1992; Chirici et al., 2008). They can easily capture the non-linear dependencies of the auxiliary variables used to model forest attributes. Such models can be particularly useful when the relationship between the response

and the predictor variables is complex, which is often the case with remote sensing data that have nonlinear relationships (Nilson and Peterson, 1994). Non-parametric models offer several advantages, including the ability to predict multiple forest attributes simultaneously in a single multivariate model while retaining the relationships between predicted attributes. Secondly, a well specified non-parametric model can preserve the entire range of variation that was present in the original data and avoid any unrealistic predictions, i.e., extrapolation (Moeur and Stage, 1995). These advantages make non-parametric models more attractive and broadly applicable in MSNFI than corresponding parametric models (Fan, 2000). One common type of non-parametric model is the random forest model, which is an ensemble of decision trees that account for the complex hierarchical structure of the data and includes random effects that capture variability in the data (Breiman, 2001). While estimating forest attributes in a Spanish temperate forest, Esteban et al. (2019) found that the random forest model appropriately described the relationship between the NFI-measured biomass and volume per unit area, and remotely sensed data obtained from airborne LiDAR and Landsat images. Cosenza et al. (2021) compared the performance of random forest model with regression model for estimating GSV in boreal forests of Finland. They found that the random forest model performed better than the regression model, and suggested that random forest is a robust approach for practical applications in forest inventory.

Another non-parametric model widely used in MSNFI is the *k*-nearest neighbors (kNN) model, which effectively estimates and maps forest attributes of interest using NFI and remote sensing data (McRoberts et al., 2010a). The model works by matching observations from a reference set that have both response and predictor variables to the target units that only have predictor variables. To predict the target units, the model identifies the *k*-nearest observations from the reference set by calculating a distance measure based on the predictor variables. When $k = 1$, the response variable values of the nearest reference observation are directly substituted to make the prediction. When $k > 1$, the response variable values of the *k*-nearest reference observations are weighted averaged by distance to make the prediction (Queinnec et al., 2021). The performance of kNN depends upon the particularity of auxiliary variables, number of nearest neighbour (*k*) and selection of distance metric (McRoberts et al., 2017). Popular choice for distance metric include Mahalanobis distance, Euclidean distance, weighted Euclidean distance, and metric based on canonical correlation analysis (Moeur and Stage, 1995). The optimal value of *k* is a trade-off between accuracy and variance (Irulappa-Pillai-Vijayakumar et al., 2019). A large *k* value (>3 to 10) generally improves the prediction accuracy (McRoberts et al., 2015a). However, an optimal configuration for kNN model probably does not exist in general terms but has to be sought empirically on the basis of available data and of the local aims of the estimation.

According to Chirici et al. (2008), kNN models are accurate enough to support local forest planning activities. While Tomppo (2006) demonstrated that kNN predictions may exhibit bias when covering several vegetation zones with different tree species compositions in a large area of interest. Conversely, Deo et al. (2011) found that the pixel-level accuracy of forest attribute estimation with

kNN was low compared to larger estimation domains. This finding was also supported by Reese et al. (2002), who reported that the kNN model error was five times lower for 100 ha aggregation than at the pixel level. It is important to note that both studies utilized spaceborne remote sensing images and kNN parameters of nearest neighbour as 1. For $k \neq 1$, much smaller model error has been obtained for smaller estimation domains (Chirici et al., 2016). Furthermore, changes in imaging conditions within the area of satellite image can modify the covariance structure between the field data and the image data. Biases can be mitigated by restricting the areas corresponding to the vegetation structure and imaging conditions of the pixel in question. In a study comparing the performance of random forest with kNN model for estimating GSV and BA, McInerney and Nieuwenhuis (2009) found that kNN outperformed random forest in terms of model error and mean deviations of corresponding forest attributes. Beaudoin et al. (2014) used the kNN model to produce continuous maps of 127 forest attributes to support regional policy and management issues in Canada. The kNN model is operationally applied in many national or local forest inventories in Finland, Sweden, Norway, Austria, China, the USA, Germany, New Zealand, and Ireland (McInerney et al., 2018; McRoberts et al., 2010a).

3.1.3. Inference framework

In order to achieve accurate and reliable estimates of forest attributes, it is crucial to select an appropriate and rigorous inference framework. Such a framework can be used to make statistical inferences for the assessment of population parameters, including total, mean, and variance, of the forest attributes within their respective estimation domains. These domains could be anything, from larger areas (such as national or regional level) up to smaller areas (such as municipality, canton, or pixel level). Various inference framework utilizing NFI and auxiliary data for the estimation of forest attributes are available. But the selection of the appropriate inference framework should always be based on the requirement of the end-users. Figure 6 provides an overview of the working principles of four inference frameworks, namely: *(i)* design-based inference (without models), *(ii)* model-assisted inference, *(iii)* model-based inference (without probability sampling), *(iv)* and hybrid inference.

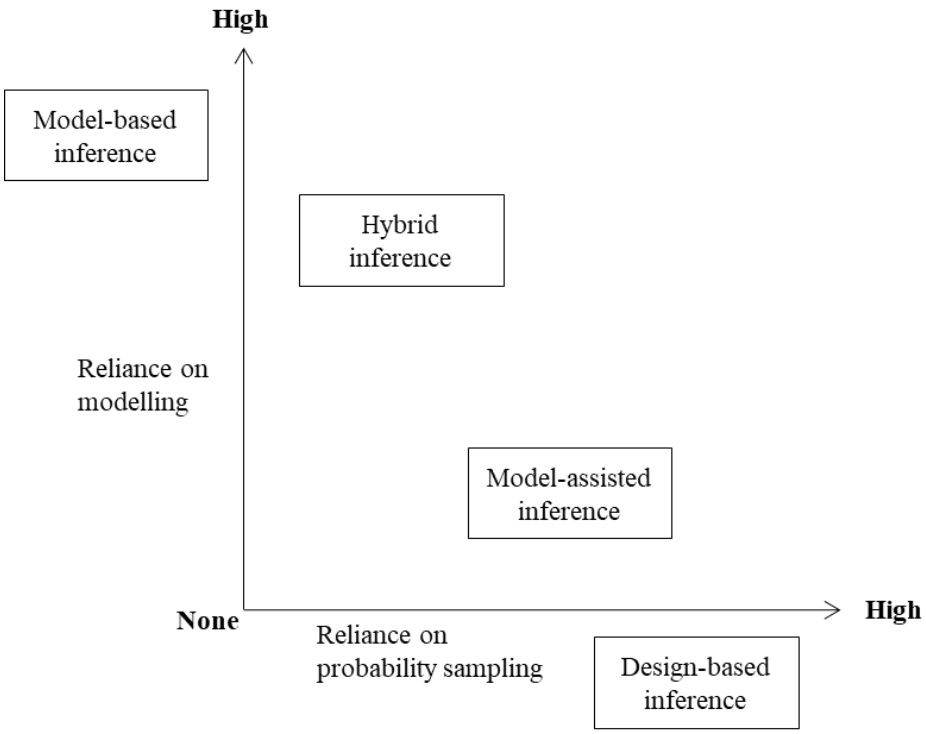

Figure 6. *An overview of the extent to which different inference framework rely on the model and probability sampling (Ståhl et al., 2016).*

3.1.3.1. Basics of various inference frameworks and their application in forest inventory

This section provides a detailed introduction to the four inference paradigms and their respective applications in the context of forest inventory. In section 3.1.3.2, an overview of the advantages and disadvantages of each method is presented.

3.1.3.1.1. Design-based inference

Design-based inference has a long history in statistics, with its early origins dating back to the Neyman's, work in 1934, where he emphasized on the independency of this inference framework from any assumptions regarding the structure and distribution of the population units. Instead, design-based inference depends on the distribution of all possible estimates that are consistent with the sampling design (Neyman, 1934). However, by the time Neyman's paper was published, design-based inference were already serving as a basis for infering population parameters in context of survey sampling in the Nordic countries (Gregoire, 1998). The term probability-based inference is often used interchangeably with design-based inference, because the properties of estimators related with this inference framework are not solely determined by the sampling design, but also by a probability-based sampling mechanism that determines the probability of selection of population units into the sample (Hansen et al., 1983).

Design-based inference typically assumes a finite population of elements, where one or more fixed target quantities (e.g., response variables or forest attributes of interest) are associated with those elements. Normally, the objective is to estimate some fixed population parameters of those target quantities. In order to estimate these unknown but fixed parameters, a probability based sample is randomly drawn from the population using an appropriate sampling design in such a way that every element has a non-zero probability of being selected in the sample. Estimators are then derived according to the sampling design (McRoberts et al., 2010a). A typical design-based estimator, Horvitz-Thompson estimator (Horvitz and Thompson, 1952) can be applied with any probability sampling design for which the inclusion probabilities are known for the sampled units. The estimator then assigns weights to each sampled unit based on these inclusion probabilities (Särndal et al., 1992). Upon using this estimator, the estimate of population total (Eq.1) and its variance (Eq.2) are computed as:

$$\hat{\tau}_{db} = \sum_{i \in s} \frac{y_i}{\pi_i} \qquad (\textbf{\textit{Eq.1}})$$

$$var(\hat{\tau}_{db}) = \sum_{i \in U} \sum_{j \in U} (\pi_{ij} - \pi_i \pi_j) \frac{y_i}{\pi_i} \frac{y_j}{\pi_j} \qquad (\textbf{\textit{Eq.2}})$$

where, subscript *'db'* refers to design-based, y_i is the variable of interest (or response variable) for the *i:th* sampled element, π_i is the inclusion probability of that element, s is the sample, and π_{ij} is the joint probability of inclusion for unit i and j in set U.

Official statistical surveys, including sample-based national forest inventories in many countries uses design-based method as the standard mode of inference (Tomppo et al., 2010). Several design-based estimators, such as Horvitz-Thompson and simple random sampling (SRS) estimator, were typically used for estimating forest attributes of interest from national up to regional level. SRS can be seen as a special case of the Horvitz-Thompson estimator, where all sampled units are assigned equal weights. Breidenbach and Astrup (2012) utilized the SRS estimator to estimate forest biomass using Norwegian NFI data, while Hill et al. (2018) used SRS estimator to estimate multiple forest attributes in the western part of Germany. The main strength of all design-based approaches relies on the objective assessment of the uncertainty of the estimator, provided that the sample is large enough to approximate a normal distribution.

3.1.3.1.2. Model-assisted inference

When auxiliary data are available, the performance of estimators within a design-based framework can be improved. Once NFI data have been acquired, a model-assisted approach can be used in the estimation stage (Särndal et al., 1992). This approach is commonly used in forest inventories, particularly in those that rely on auxiliary data to downscale estimates in smaller domains or to increase the precision of design-based estimates (Saarela et al., 2015a). In a model-assisted approach,

the design-based properties of the sample are preserved (design-unbiasedness), and the model is often referred to as a "*working model*". For linear working models, the estimators are often called as generalised regression estimator (GREG) or generalised difference estimator (Breidt and Opsomer, 2017; Wojcik et al., 2022). The design-unbiasedness implies that these estimators are unbiased regardless of the accuracy of the assigned model (i.e., the working model does not need to fit perfectly) (Ekström and Nilsson, 2021). The general form of model-assisted estimator (Ståhl et al., 2016) for estimating the population total (Eq.3) and variance (Eq.4) can be expressed as:

$$\hat{t}_{ma} = \sum_{i \in U} \hat{y}_i + \sum_{i \in s} \frac{(y_i - \hat{y}_i)}{\pi_i} \quad \textbf{(Eq.3)}$$

$$var(\hat{t}_{ma}) = \sum_{i \in U} \sum_{j \in U} (\pi_{ij} - \pi_i \pi_j) \left(\frac{(y_i - \hat{y}_i)}{\pi_i} \frac{(y_j - \hat{y}_j)}{\pi_j} \right) \quad \textbf{(Eq.4)}$$

where, subscript *'ma'* refers to model assisted. The first part of Eq.3 is a sum of model estimates of each element within the population, while the second part refers to the Horvitz-Thompson estimator (Eq.1) of the model's residuals. The estimator is thus composed of a first crude estimates that is corrected using a correction term (mean error), resulting in an asymptotically unbiased estimate. For the variance, Eq.4 is similar to Eq.2, except that in the former equation, residuals are used instead of the measured values (y). This result in a smaller variance for the model-assisted estimator compared to the one obtained from NFI data alone (Eq.2). The Swiss and Italian NFI provide a prime example of this, by utilizing model-assisted regression estimators to improve the precision of design-based estimates at national and regional scales (Brassel and Lischke, 2001; Fattorini et al., 2006).

Boudreau et al. (2008) conducted a study in Quebec, Canada, where they initially established a simple linear regression model to capture the relationship between NFI and auxiliary data from Landsat-7 and spaceborne GLAS 3D point cloud data. Later, they used a model-assisted regression estimator to estimate the forest aboveground biomass (AGB). Remarkably, despite utilizing spaceborne 3D data sensors, their reported average biomass per hectare was found to be within 4% of an independent estimate developed for the North American boreal forest by Botkin and Simpson (1990). Following the approach taken by Boudreau et al. (2008), Andersen et al. (2009) also used a model-assisted regression estimator to estimate forest biomass over the western Kenai Peninsula of Alaska, using systematic strip samples of high-density LiDAR data and NFI plots located within the LiDAR strips. In contrast, while working in the boreal forest of Kuortane, Finland, Saarela et al. (2015) found that the use of full coverage Landsat data improved the precision of the model-assisted estimates of biomass compared to the use of LiDAR strip data. Furthermore, they also demonstrated the precision gains with model-assisted estimators compared to SRS. A study by Gregoire et al. (2011) in Hedmark County, Norway, found that SRS was overestimating AGB. This sparked a series of investigations in which model-assisted methods were widely employed to estimate forest attributes over large areas using field sample data and LiDAR data.

Opsomer et al. (2007) used a model-assisted approach to estimate various forest attributes in the western USA using NFI and Landsat data. Baffetta et al. (2009) also used a similar combination of data to estimate timber volume in Italy. In another study, Irulappa-Pillai-Vijayakumar et al. (2019) utilized kNN models along with a model-assisted estimator to estimate several forest attributes in Central France. In their study they explored different combinations of auxiliary data to improve the estimation precision. The findings from the study showed that incorporating 3D data resulted in improved estimation precision (relative efficiency: RE = 1.9) compared to relying solely on Landsat data (RE = 0.9). Moreover, when all auxiliary data were combined, the relative efficiency further increased (RE = 2.1) for state variables (i.e. GSV, BA). However, for flux variables like VI, the improvement was not significant, emphasizing the importance of including time series of 3D data to capture growth-related information.

3.1.3.1.3. Model-based inference

Ever since Matérn (1960) introduced his paper on model-based inference in context of forest surveys, a debate has ensued about the possibility of replacing classical design-based inference with model-based inference (Gregoire, 1998). However, the assumptions that form the basis of model-based inference are considerably different from those of design-based.

First, the observation made for a population unit is a random variable whose value is regarded as a realization from a distribution of possible values. This differs from design-based inference, where the observed value is treated as fixed, not random. Therefore, in the model-based approach, the observed reality is considered as a random realization of a superpopulation, and model-based inference is also sometimes referred to as superpopulation inference (Graubardand and Korn, 2002). Secondly, the basis of a model-based inference is the model itself, not the probabilistic characteristics of the sample collected. It is worth noting that samples deliberately non-probabilistic (purposefully selected) may produce entirely valid model-based inference, given that the model is correctly specified. Thirdly, in design-based inference, randomization occurs through the random selection of population units for inclusion in the sample, whereas in model-based inference, randomization occurs through the random realizations from the distributions of the target/response variable for each population unit (McRoberts et al., 2010a).

For instance, with model-based inference, a linear model (Eq.5) is fitted to the sample data.

$$y_i = f(X_i\,;\,\beta) + \varepsilon_i \qquad \textbf{(Eq.5)}$$

where, X_i corresponds to the auxiliary variable for the i_{th} population unit, β is the vector of parameters that are to be estimated, and ε_i is the random residuals. The model prediction, $f(X_i\,;\,\hat{\beta})$, for the ith population unit gives an estimate of the possible values for the unit; i.e. $\hat{\mu}_i = f(X_i\,;\,\hat{\beta})$. The model-based estimators for the population parameter of mean (Eq.6) and variance (Eq.7) are:

$$\hat{\mu}_{mb} = \frac{1}{N}\sum_{i=1}^{N}\hat{\mu}_i \quad \textbf{(Eq.6)}$$

$$var_{(\hat{\mu}_{mb})} = \frac{1}{N^2}\sum_{i=1}^{N}\sum_{j=1}^{N} C\hat{o}v(\hat{\mu}_i, \hat{\mu}_j) \quad \textbf{(Eq.7)}$$

where, subscript *'mb'* refers to model-based, and N to the population size. The covariance associated with each population unit, denoted by $C\hat{o}v(\hat{\mu}_i, \hat{\mu}_j)$, varies depending on the prediction models used for its calculation. Linear models and other parametric models can be used to derive estimates of covariance, while in non-parametric models like kNN, more complex covariance structures are observed (McRoberts et al., 2007). For such non-parametric models, an emperical variance estimation is often used via bootstrap resampling techniques for variance estimation (Efron and Tibshirani, 1994). McRoberts et al. (2023, 2011) presented a model-based bootstrap methods for non-parametric kNN models in estimating the population mean (Eq.8) and variance (Eq.9). These are computed as follow:

$$\hat{\mu}_{mb\_boot} = \frac{1}{n_{boot}}\sum_{b=1}^{n_{boot}}\hat{\mu}_{boot}^{b} \quad \textbf{(Eq.8)}$$

$$var\left(\hat{\mu}_{mb\_boot}\right) = \frac{1}{n_{boot}-1}\sum_{b=1}^{n_{boot}}\left(\hat{\mu}_{boot}^{b} - \hat{\mu}_{mb\_boot}\right)^2 \quad \textbf{(Eq.9)}$$

where, subscript *'mb_boot'* refers to bootstrap model-based, $\hat{\mu}_{boot}^{b}$ is the mean of the boot b, and n_{boot} is the number of bootstrap sample.

Many studies have applied model-based inference for estimating forest attributes. For example, McRoberts et al. (2007) combined a kNN model with a model-based approach to estimate population parameters of volume, basal area, and tree density in small areas. Their findings showed that the kNN model-based approach contributes in alleviating the problem of inadequate sample sizes for small areas. Additionally, several other authors have also used kNN model-based approach to estimate various forest attributes of interest (Beaudoin et al., 2014; Breidenbach et al., 2010; Chirici et al., 2012; McRoberts et al., 2011).

The main strengths of model-based approaches are certainly their efficiency, i.e., their capacity to produce predictions in areas with no field measurements, and their ability to produce maps, provided that the models are correctly specified and potential bias is acceptable. Consequently, a large number of studies utilize model-based approaches to map forest attributes of interest over large areas. For example, Baccini et al. (2008) combined MODIS and GLAS data with forest inventory data to map AGB over tropical forests in Africa. Asner et al. (2012) utilized a model-based approach to map aboveground carbon stocks using field plots and airborne LiDAR data in Peruvian Amazon forests. Helmer et al. (2010) have used a model-based approach combining field plot data and time series of Landsat images to map multiple forests attributes of interest.

3.1.3.1.4. Hybrid inference

Independent variables, such as auxiliary data are needed for the standard application of model-based inference. However, it may not be feasible to collect such data for all units in the population before conducting a forest survey, or it can be expensive. In such cases, one can acquire a probability sample of auxiliary data and use it to estimate the population mean or total of the auxiliary variable through a combination of design-based and model-based inferences (McRoberts et al., 2016). Thus, this combination of design-based properties of the auxiliary data implemented in the first phase followed by an application of model-based inference in the second phase is termed as hybrid inference. This terminology was first introduced by Corona et al. (2014). However, Ståhl et al. (2016) reported that prior to the work of Corona et al. (2014), the design-based component of this inference framework had not been fully recognized in previous studies, resulting in the use of different terminology such as model-based inference, pseudo-synthetic estimator (Mandallaz, 2013), and model-dependent inference (Gobakken et al., 2012). All of these studies follow a common approach where the expected value of an estimator is assessed based on both the model and the design. In the same manner, a conditioning approach is used to obtain the variance of the estimator, which usually consists of two components: one related to the sampling error and another related to the model error (Fortin et al., 2018). The general form of hybrid estimator (Ståhl et al., 2016) for estimating the population total (Eq.10) of a linear model (Eq.5) can be expressed as:

$$E(\hat{\tau}^*) = \sum_{i \in s} \frac{X_i \hat{\beta}}{\pi_i} = \pi' X \hat{\beta} \qquad \textbf{(Eq.10)}$$

where, the symbol s represents a sample of auxiliary data, π_i denotes the probability of including population element i into the auxiliary data sample, π is an n-length column vector of $(1/\pi_i)$ values, and X refers to a $n \times p$ matrix of sampled auxiliary data. The model parameters are estimated from a sample that is assumed to be independent from the sample of auxiliary data.

While computing the variance (Eq.11) of the estimator from Eq.10, it is important to note that the component $\pi' X$ of the estimator refer to a $1 \times p$ matrix of design-based estimator of population totals of auxiliary data. This matrix is denoted as $\hat{\tau}_x$ in Eq.11, and multiplied by matrix of estimated model parameter, i.e. $\hat{\tau}_{x_J}.\hat{\beta}_J$. In each term the two components are independent, but the estimators of the auxiliary variable totals as well as the estimators of the parameters are typically correlated. Thus, the variance due to sample and model is:

$$var(E[\hat{\tau}^*]) = var\left(\hat{\tau}_x \hat{\beta}\right) = \beta' cov(\hat{\tau}_x)\beta + \tau_x cov\left(\hat{\beta}\right)\tau_x' + Tr\left(cov(\hat{\tau}_x)cov\left(\hat{\beta}\right)\right) \qquad \textbf{(Eq.11)}$$

where, $cov(\hat{\tau}_x)$ is the covariance matrix of the estimators of the auxiliary variable totals and $cov\left(\hat{\beta}\right)$ is the covariance matrix of the model parameter estimators. The Tr-operator is the trace, i.e., the sum of the diagonal entries in the matrix.

The findings from the brief literature review are summarized in Figure 7.

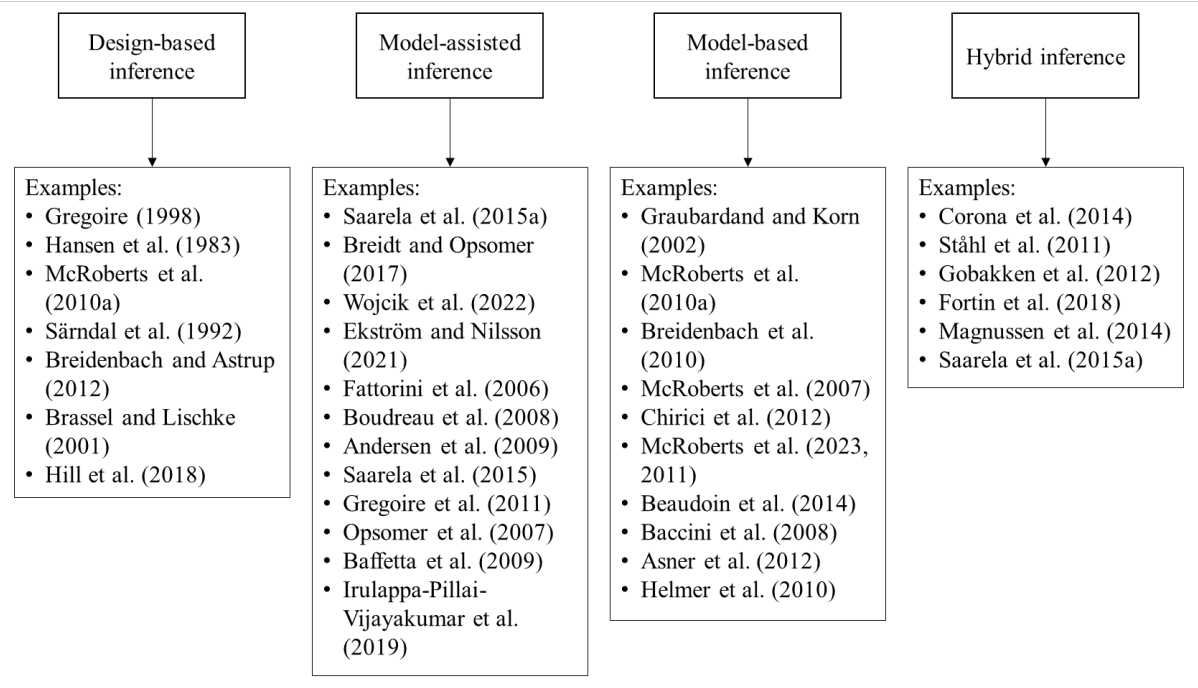

Figure 7. *Overview of studies on design-based, model-assisted, model-based and hybrid inference.*

3.1.3.2. Advantage and disadvantage of various inference frameworks

Design-based inference is the most commonly used and standard mode of inference in many NFIs due to its statistical soundness. However, with the increasing availability of various types of auxiliary data, particularly remote sensing data, the popularity of other inference frameworks such as model-assisted and model-based frameworks is growing. It is then essential to rigorously utilize these statistical approaches (Gregoire et al., 2016). On the other hand, hybrid inference methods have not yet gained widespread attention as they are relatively new and less well-established compared to other inference frameworks.

Design-based estimators are typically design-unbiased which is based on the sampling design used, meaning that the statistical expectation of the estimator, $\hat{\mu}$, across all possible samples obtained with the sampling design is an unbiased estimate of the population parameter, i.e. $E(\hat{\mu}) = \mu$ (Gregoire, 1998). However, due to the random selection of samples in the design-based approach, the resulting estimator produces estimates that are considered as random variables and can differ depending on which population elements are included in the sample. Also, the low sample size may produce large confidence intervals. Therefore, a specific and small sample may yield an estimate that deviates significantly from the true value of the population parameter (McRoberts et al., 2010a).

On the other hand, model-assisted estimator leverages information from the observations of population units in the sample to lower the variance of population parameter estimate. Here inference

is determined by the sampling design, while a model is used as a driver to enhance the precision of the estimates. Even if the model used is not the "*true*" model, the results are not biased (Haakana et al., 2019; McRoberts et al., 2010a; Särndal et al., 1992). Empirical evidence from Ene et al. (2012) and Saarela et al. (2015) suggests that if the model used is extremely poor, there is a possibility that the model-assisted estimator may have higher variance than the estimation based solely on NFI field plots. However, it should be noted that a well-specified model has the potential to substantially improve the precision of a model-assisted estimator compared to a strictly design-based estimator.

If well-specified models are available, Lohr (1999), Magnussen (2015), and McRoberts et al. (2015) suggest that model-based estimators provides a competitive alternative to model-assisted estimators. This approach offers certain advantages, as it does not rely on a probability sample from the target area. Collection of such samples may not always be feasible due to restricted access to private land, remote areas, or dangerous terrain. In addition, if a probability sample has been selected and used for model development, then model-based and model-assisted estimations could typically yield similar values of the population total. However, the complete reliance of model-based inference on the model can have significant impact on the precision of the inference if the model is mis specified (Hansen et al., 1983).

An advantage of hybrid inference is its straightforward approach when wall-to-wall auxiliary data are not available or expensive to acquire. This approach can account for both sampling and model errors, and can produce more precise estimates than the design-based methods (Fortin et al., 2018). According to Corona et al. (2014) and Ståhl et al. (2016), for precise estimation, the approach requires a well-defined sampling design and a valid statistical model. Furthermore, variance estimation can also be computationally intensive. Hybrid inference has only been used in a limited number of forest inventories, particularly in temperate and boreal forests. McRoberts et al. (2016) stated that reducing the variance of the hybrid estimator remains a challenging task in tropical inventories with a large number of species.

In addition, it's worth noting that there are other advantages and disadvantages specific to small area estimation and forest resource mapping. These will be discussed in detail in the next section 3.1.3.2.1 and section 3.1.3.2.2. Figure 8 illustrates the respective roles of NFI and auxiliary data within an inferential framework for generating outputs at various scales.

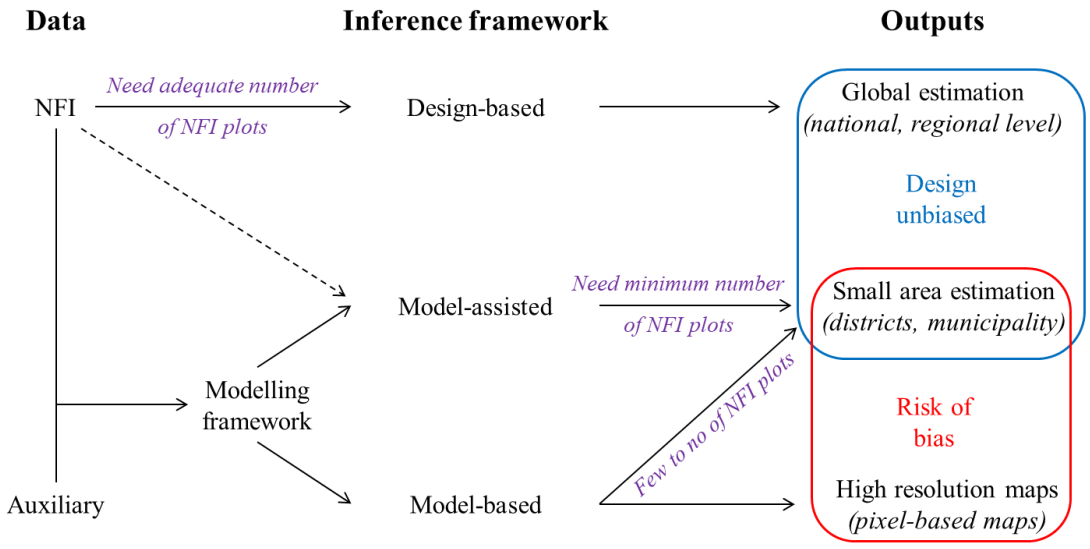

Figure 8. *Illustration of the working principle of inference framework using NFI and auxiliary data to generate outputs at various scales.*

3.1.3.2.1 Small area estimation

Since the earliest adoption of statistical methods in forest inventories, their frequency and sophistication have steadily increased, with the overall aim of providing high-quality information on forest resources to inform decision-making (Dettmann et al., 2022). One ongoing trend involves using data collected from large-scale NFIs to produce improved and precise estimates of forest attributes for areas smaller than the inventories were actually designed to address, without significantly increasing the inventory costs (Magnussen et al., 2014). A "*small area*" in this case refers to an estimation domain that has limited or insufficient field plots to meet the required precision needs for estimation based solely on field plots. This could be any geographical area, temporal domain, or demographic group that is a subset of a larger area from which NFI sample data were collected. In such areas, design-based estimators do not provide sufficient precision because the estimators are constrained by the NFI sample size, which is typically low beyond regional scales (as shown in Figure 4) (Rao and Molina, 2015).

A commonly asked question is how to leverage NFI data to produce precise estimates in small areas with low or inadequate NFI sample plots. One means of answering this question is through the use of small area estimation (SAE) techniques, which aim to improve the estimation precision for population subsets known as small domains of interest (DOI) (Dettmann et al., 2022). It should be noted that these small DOI do not always refer to a particular geographical scale of inference but rather to situations where few, if any, NFI sample plots are available for estimation (Rao and Molina, 2015).

SAE techniques improve precision by "*borrowing strength*" through the use of NFI and auxiliary data external to the DOI to increase the effective sample size when constructing models. This "*external strength*" reduces the estimation uncertainty, and offers an efficient and cost-effective option for estimation in smaller DOI without increasing the NFI sampling intensity (Magnussen et al., 2014). While the utilization of SAE has grown across multiple disciplines, its application in forest inventory has begun to emerge in published literature over the past several decades (Breidenbach et al., 2010; Goerndt et al., 2011). SAE technique have been applied to improve the precision of NFI-derived estimates (Breidenbach and Astrup, 2012), in forest stand inventories (Ver Planck et al., 2018), and commercial landowner inventories (Coulston et al., 2021).

The "*borrowing*" process in SAE is orchestrated by a model to obtain a measure of estimation precision (Bell et al., 2022). Several small area estimators utilizing NFI plot and auxiliary data are available, but the selection of an appropriate estimator should be based on NFI plot distribution over the DOI (Frescino et al., 2022). Given a reasonable number of NFI plots available in the DOI, it is possible to use a model-assisted estimator to compute both the population mean and variance (Kangas et al., 2019). For instance, Astrup et al. (2019) used a model-assisted estimator to produce better local information by generating municipal level forest statistics in Norway. Hill et al. (2018) also employed model-assisted estimators for timber volume estimation at forest district and sub-district levels in the German state of Rhineland-Palatinate. However, in cases where the DOI is smaller and contains few or no NFI plots, model-based estimators are capable of producing estimates. Kangas et al. (2019) have stated that as the scale of DOI decreases the pressure to use model-based approach increases. As a result, the model-based approach has become an appealing and widely adopted method in SAE (Haakana et al., 2020). Usually, model-assisted estimators were used on the scale of municipalities or larger areas, while model based approach were used on the scale of pixels and forest stands (Breidenbach and Astrup, 2012; Guldin, 2021). Chen et al. (2016) have used model-based estimator for pixel level estimation of forest biomass in north-eastern Minnesota, USA. Similarly, Chirici et al. (2020) have used model-based approach for pixel level estimation of GSV in central Italy.

3.1.3.2.2 Forest resource mapping

Contemporary users of NFI data often require more than statistical charts and tables – they want forest resource maps. These maps are useful for perspective management practices, as they provide an attractive and credible way to accurately pinpoint the amount and location of forest resources instead of relying solely on statistical tables (Chojnacky et al., 2006). Over the past few decades, there has been a significant increase in the construction, distribution, and use of forest resource maps. McRoberts et al. (2010) attributed this phenomenon to three factors: *(i)* the availability of various remote sensing data products in usable formats at feasible costs, *(ii)* access to fast personal computers, and *(iii)* the widespread availability of efficient data-processing algorithms and supporting computer software.

Significant efforts have been made in northern Europe to develop wall-to-wall mapping techniques for forest attributes. Tomppo (1990) applied the kNN technique to produce localized estimates and maps based on Finnish NFI and optical remote sensing data. The method exhibits great potential for mapping continuous variables such as GSV, forest cover type, and BA. Tomppo also incorporated this method on an operational basis in Finland to produce forest resource maps at every two years. Barrett et al. (2016), in their review of operational NFIs across 48 countries, found that 30 countries construct forest resource map products by combining their NFI data with remote sensing data. These NFIs produce maps for forest type (57%), forest cover (57%), GSV (20%), biomass (15%), and forest species type (28%). Maps of stem density, age, mean diameter, forest productivity, BA, and fertility are constructed by less than 10% of the NFI.

The resulting forest resource map products are often disconnected from an inferential framework (Saarela et al., 2020). The utility of map products would be greatly enhanced if they formed a suitable basis for inferring values of parameters that describe the population depicted by those maps. However, connecting inferences to map products involves complexities that are not straightforward. For instance, when addressing map uncertainty, design-based methods are not appropriate for map-based inference because they do not account for the uncertainty of predictions. Instead, ad-hoc methods are used, which do not accurately consider the uncertainty of the estimator involved (Ståhl et al., 2016). Recently, methods have been proposed to map estimation uncertainties, and these maps have been included in a model-based inferential framework (Esteban et al., 2019; Saarela et al., 2020, 2018). For example, Esteban et al. (2019) presented an uncertainty map through bootstrapping, while Saarela et al. (2020) used model residual error to produce this map. These maps, along with corresponding uncertainties, are fundamental for forest planning and management.

4. Research objectives

The MSNFI methods have recently been introduced and tested in France. The first research project to use MSNFI (IFM-GT, Ademe, 2016-19; *www.inventaire-forestier.ign.fr*; Irulappa-Pillai-Vijayakumar et al., 2019) aimed at improving the precision of design-based estimates of several forest attributes, such as GSV, BA, and production volume, through a model-assisted approach. The method was demonstrated over the lowland forests of Sologne and Orléans in France. The auxiliary data considered included a forest map, satellite-based optical remote sensing images from Landsat 8, and 3D variables derived from photogrammetric canopy height models.

The results were promising, but the deployment of the approach at an operational level requires additional research. The performance of the method needs to be tested in various topographical and forest conditions, and auxiliary data relevant to these conditions should be considered. It is for example the case with topographical information (i.e. elevation, slope) in mountainous areas. The same applies to remote sensing data. While the method was initially tested with 30 m Landsat data, it would be interesting to explore the potential benefits of higher resolution products such as Sentinel-2, as well as the usefulness of time-series data. Another key issue to consider is the scale of analysis. While the method has been tested at a large scale, its potential for small area estimation needs to be demonstrated across a range of domain sizes and structures. Finally while estimation approaches mostly rely on aggregated values, the question of computing reliability of underlying maps at pixel level is of particular importance. This would offer increased flexibility in terms of methods and applications.

Following this, the main objective of this thesis is to demonstrate to which scale MSNFI approaches could be applied with model-assisted estimations, and for which precision? Another objective is to support models underlying MSNFI approaches with reliability assessment at pixel level to provide more robustness and flexibility in model-based estimations. Based on these objectives the thesis is divided into four Chapters. Chapter I – III has been published in the peer-reviewed international journals, while Chapter IV is the author's version of the submitted manuscript. The specific objectives of the different Chapters were to:

Chapter I: develop a flexible model-assisted estimation framework to optimise the size of SAE domains according to criteria of minimum sample size and maximum error.

Chapter II: propose a method to identify extrapolation in predictive models of forest attributes and to demonstrate how sampling intensity impact extrapolation level.

Chapter III: provide high resolution prediction and associated prediction reliability maps of forest attributes within an inferential framework.

Chapter IV: adapt the method developed in Chapter III for SAE of forest resources impacted by bark beetle outbreak.

Chapter I: A new small area estimation algorithm to balance between statistical precision and scale

Authors: Cédric Vega[1, *], Jean-Pierre Renaud[1, 2], Ankit Sagar[1, 3], Olivier Bouriaud[1]

[1]Laboratoire d'Inventaire Forestier, Université de Lorraine, ENSG, IGN, INRA, *Nancy, France*

[2]Office National des Forêts, Pôle Recherche Développement Innovation, *Villers-les-Nancy, France*

[3]Université de Lorraine, faculté des Sciences et Technologies - Campus Aiguillettes, UMR Silva, *Nancy, France*

[*]corresponding author

The article has been published in the International Journal of Applied Earth Observations and Geoinformation. It is available at the following DOI: https://doi.org/10.1016/j.jag.2021.102303.

Authors' contributions

Cédric Vega (CV) and Jean-Pierre Renaud (JPR) conceived and design the work. CV and JPR contributed to data acquisition and processing. CV, JPR, Ankit Sagar and Olivier Bouriaud contributed to interpretation of the results. All authors contributed to drafting the work and have approved the submitted version.

Abstract

Combining national forest inventory (NFI) data with auxiliary information allows downscaling and improving the precision of NFI estimates for small domains, where normally too few field plots are available to produce reliable estimates. In most situations, small domains represent administrative units that could greatly vary in size and forested area. In small and poorly sampled domains, the precision of estimates often drop below expected standards.

To tackle this issue, we introduce a downscaling algorithm generating the smallest possible groups of domains satisfying prescribed sampling density and estimation error. The binary space partitioning algorithm recursively divides the population of domains in two groups while the prescribed precision conditions are fulfilled.

The algorithm was tested on two major forest attributes (i.e. growing stock and basal area) in an area of 7,500 km^2 dominated by hardwood forests in the centre of France. The estimation domains consisted in 157 municipalities. The field data included 819 NFI plots surveyed during a 5 years period. The auxiliary data consisted in 48 metrics derived from a forest map, photogrammetric models and Landsat images. A model-assisted framework was used for estimation. For each forest attribute, the best model was selected using a best-subset approach using a Bayesian Information Criteria. The retained models explained 58 % and 41 % of the observed variance for the growing stocks and basal areas respectively. The performance of the algorithm was evaluated using a minimum of 3 NFI points per domain and estimation errors varying from 10 to 50 %.

For a target estimation error set to 10 %, the algorithm led to a limited number of estimation domains (< 23 for both attributes) of large size (~ 15,000 ha) having an average estimation error lower than 7.7 % for both attributes. Relaxing the targeted error threshold to 50 % led to a larger amount of smaller domains (80 domains of 4,176 ha in average) for both attributes, and maximum estimation errors reaching 42.8 %. Among those domains 65 % consisted in single municipalities. For the sake of comparison, the estimation was also conducted at the scale of municipalities. Out of the 157 municipalities studied, only 93 were sampled with at least 3 NFI points and therefore estimated. Missing values were generated for the remaining 64 municipalities. Average errors of 15.9 % and 15.6 % were obtained for growing stock and basal area respectively, but estimation errors greater than 50 % were obtained for some municipalities.

The algorithm provides a flexible estimation framework for small area estimation. The key advantages of the approach are relying on its capacity to produce estimations based on a preselected precision threshold and to produce results over the whole area of interest, avoiding areas without any estimates. The algorithm could also be used on any kind of polygon layers (not only administrative ones), provided that the field sampling design enable estimation. This makes the proposed algorithm a convenient tool notably for decision makers and forest managers.

Keywords: national forest inventory, small area estimation, downscaling algorithm, photogrammetry, aerial photographs, Landsat.

1. Introduction

National Forest Inventories (NFIs) are designed to produce estimates and associated confidence intervals of forest attributes over scales ranging from the national down to the regional levels (Kangas et al., 2019). Below those scales, the properties of the estimation domains (i.e. a computation area) are too sparsely sampled and the precision of estimates decreases (Coelho and Pereira, 2011). In most countries, this decrease in precision prevents from using NFI estimates to support decision-making at the scale of functional territories, at which management strategies are applied.

Precision improvements can be achieved through the combined use of NFI data with auxiliary information correlated with the forest attributes of interest. Such a combination has a long tradition in forest inventories, with the use of aerial photographs in two-phase sampling designs for improving estimation of both forest area and attributes. With the development and the diversification of auxiliary data sources, mainly driven by remote sensing technologies, such data combination approaches have been grouped under the term of multisource national forest inventory (MSNFI) (Tomppo et al., 2008b).

The development of 3D remote sensing, especially airborne laser scanning (Kangas et al., 2018; Nilsson et al., 2017) and digital photogrammetry (Irulappa-Pillai-Vijayakumar et al., 2019; Vega and St-onge, 2008), contributed to enhance precision gains, due to their high correlation with the forest attributes of interest when used as auxiliary variables (Hill et al., 2018). Such precision gains allow to downscale estimates of key forest attributes to small domains for which the sample size is normally too small to provide reliable estimates based solely on field plots (Tomppo et al., 2008b; Vandendijck et al., 2016). Those small domains often correspond to administrative areas such as municipalities (Breidenbach and Astrup, 2012; Tomppo et al., 2008b), or management units (Magnussen and Breidenbach, 2017; Mauro et al., 2017).

Several estimation approaches have been used in MSNFI. Some authors have applied model-assisted, others model-based approaches, to compute estimates at plot or stand levels (Mauro et al., 2017; McRoberts et al., 2013; Rao and Molina, 2015). Each method has its pros and cons and the selection of an inference framework is dictated by the sampling design and the plot distribution over the areas of interest. In design-based approaches, inference relies on the sampling design and estimators are unbiased by construction (Ene et al., 2016; Ståhl et al., 2016). However, the performance of design-based approaches depends on the sampling effort over the area of interest (Breidenbach et al., 2010; Haakana et al., 2020; McRoberts et al., 2013). For some specific domains, field sample size might therefore be too small and the uncertainty too large to meet the precision requirements. In such cases, as well as in areas of interest without any field plots, model-based approaches represent alternatives (Magnussen, 2015; Vandendijck et al., 2016). Those so-called indirect estimators (Rao and Molina, 2015) take advantage of sample plots and auxiliary data available outside of the area of interest. This makes model-based approaches appealing for management

inventories with limited sample plots (Kangas et al., 2018; Næsset, 2004). Although various methods have been developed to build estimates (Datta and Rao, 2009), the performance of model-based estimations still amply depends on model specifications (Kangas et al., 2016; Knaub, 2017; Magnussen, 2015). In complex managed forests, models often exhibits saturation or heteroscedasticity problems (Chirici et al., 2020; Frank et al., 2020; Saarela et al., 2020) which could be associated to the limitations of auxiliary data to capture the whole dynamic of field attributes or their increased variability induced by management practices, among others. In such cases, if the sampling design and target scales are relevant, the model-assisted inference is an appealing estimation framework owing to the theoretical unbiasedness of the estimators (Chen et al., 2016; Magnussen et al., 2014).

Another MSNFI aspect that could be considered as a significant constraint in some situations is its dependence on administrative boundaries (Magnussen et al., 2014). Administrative domains can be heterogeneous in size and forest coverage. These variations may lead to improperly reduce sample size in some area of interest, and yield inappropriate small area estimations (Magnussen et al., 2014; Vandendijck et al., 2016). Breidenbach and Astrup (2012) and Hill et al. (2018) reported a significant amount of domains not estimated due to the lack of field plots. For the same reasons, Tomppo et al. (2008) restricted their estimates to groups of municipalities in some areas. Thus, definition and generation of optimal estimation domains is an important matter with direct consequences on prediction availability over some areas. Their availability depends on the sampling rate, the forest heterogeneity, the inference framework and the user needs. The later could vary greatly within the stakeholder sphere, from landscape scale for decision makers to forest stands for local managers.

In this context, this paper intended to analyse the balance between spatial scale and estimation precision under a model-assisted framework. We proposed a flexible algorithm designed to build up estimation domains, here corresponding to municipalities or groups of municipalities, with areas as small as possible given a targeted precision level (i.e. maximum error allowed in a given domain). The method relies on polygon layers as a support for a top-down binary space partitioning approach to generate a flexible multiscale small area data structure.

2. Material and methods

2.1. Study site

The study site covers the Sologne and Orléans area, in the Centre of France (Figure 9). It represents a territory of 7,335 km^2, forested at 48 % (3,600 km^2). The forests spread over 157 municipalities. The forest area at the municipality level ranges from 11 to 8,495 ha, hence creating a heterogeneous context for small area estimation.

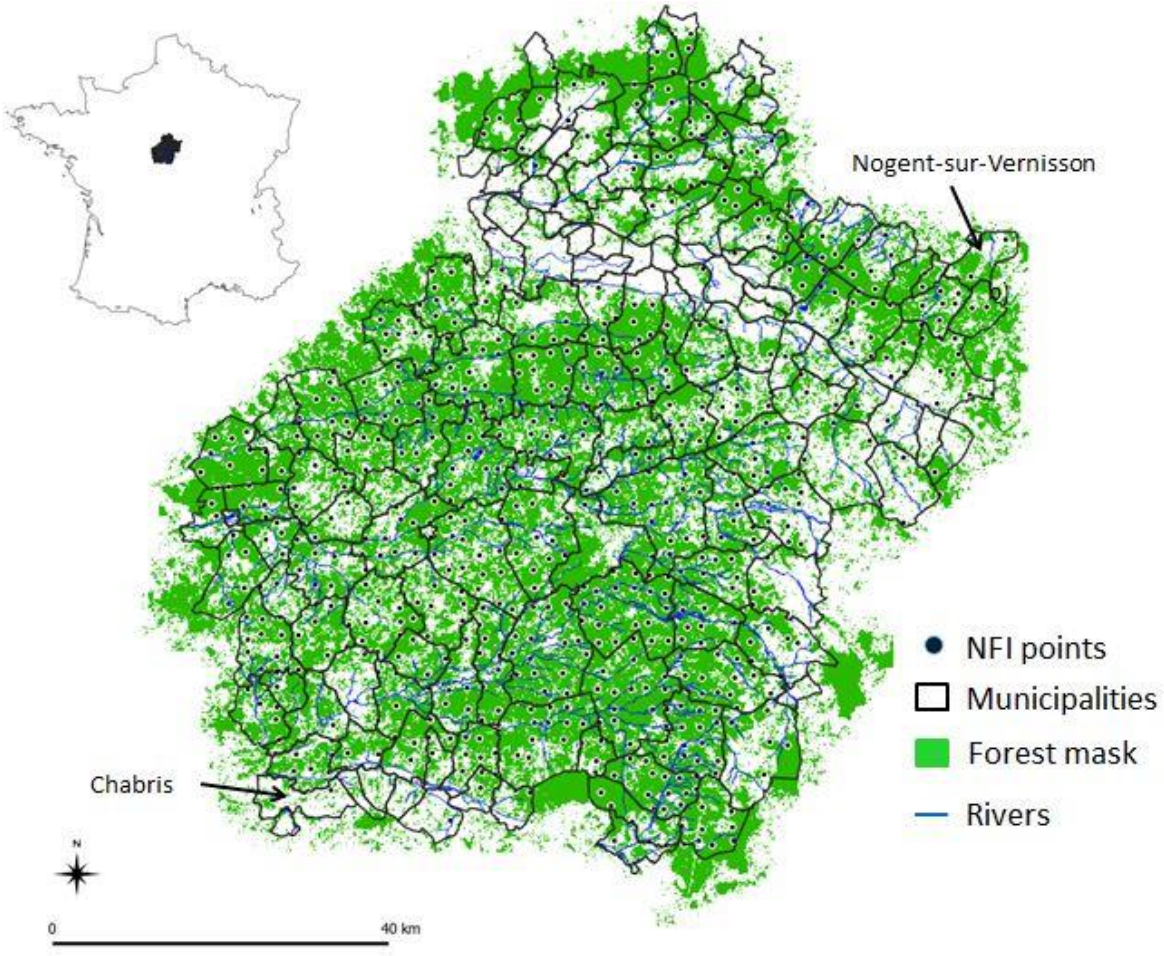

Figure 9. *Localization of the study area, showing the forest mask and the NFI plots along with the municipality outlines.*

The area is influenced by a degraded oceanic climate, with mean annual temperatures of 10.9°C and mean annual precipitations of 731 mm. The slowly undulating relief ranges from 70 m to 180 m elevations, and supports soils made of sand and clay. The forests are representative of oak-dominated French broadleaved forests (Jarret, 2004). Broadleaved species account for 75.3 % of the area and are dominated by oaks (i.e. *Quercus robur* L. and *Quercus petraea* Mill.). Coniferous stands represent 15.5 % of the forest area and are mainly composed of maritime pines (*Pinus pinaster* Ait.) and Scots pines (*Pinus sylvestris* L.). The remaining forest area is covered by mixed stands consisting mostly of

oaks and Scots pine. Forest structure is mainly and markedly influenced by ownership through management strategies. The Southern part of the study site is dominated by private forests (90 %) with various intensities of management. The Northern part includes the largest French state forest, which covers around 346 km^2 and is intensely managed.

2.2. NFI data

Since 2005, the French NFI is continuous over time and space, covering the whole metropolitan territory each year with independent samples. The two-phase sampling scheme relies on a systematic grid having a 1 km resolution. Each year, one-tenth of the grid (~80,000 points) is photo-interpreted on infrared aerial photographs (0.5 m resolution) for land use and land cover, which build the first-phase sample. The second phase sample is drawn from the first phase with sampling rates depending on land cover types. For forested areas, around 6,500 points are surveyed every year country-wise.

In this study, data from 819 NFI plots acquired between 2010 and 2014 were considered. Such a 5 years interval allows the computation of consolidated estimates and is used routinely for the official French NFI statistics. The last inventory year corresponded to the acquisition time for the majority of the auxiliary data. Details of the NFI sampling scheme, field measurements and estimation methods are provided in Hervé et al. (2014) and Robert et al. (2009). For the purpose of this study, growing stock volume and basal area were considered as response variables (Table 1). Those variables were selected owing to their importance in forestry, but the method could be applied to any other forest attribute provided a correlation exists with the auxiliary data.

Table 1. *Mean, minimum, maximum and standard deviation of growing stock and basal area from the 819 field plots surveyed.*

Response variables	Mean	Min	Max	SD
Growing stock ($m^3.ha^{-1}$)	152.14	0.69	721.21	107.26
Basal area ($m^2.ha^{-1}$)	20.14	0.40	62.69	11.32

2.3. Auxiliary data sources and processing

The auxiliary data consisted in 1) the forest map (BDForêt® v2) of the French National Institute of Geographic and Forest Information (IGN), 2) a canopy height model derived from digital aerial photographs (DAP), and 3) Landsat images. Various metrics were extracted from the auxiliary data, at a 30 m spatial resolution. Such a resolution matches the pixel size of Landsat images and the diameter of the field plots in which dendrometric measurements are made.

The BD Forêt® V2 is a vector map generated through the photo-interpretation of near-infrared aerial photographs. The map provides information about vegetation structure and composition following a national nomenclature, for forest patches of at least 0.5 ha in size. The map over the region of interest was generated using aerial images acquired in 2008. For the purpose of this study, the map information was summarized into 3 forest types (FT): pure hardwood, pure conifers and mixed stands. Each cell of the auxiliary grid was assigned the value of the FT map at the centre of the cell. Only the cells completely included in the FT map were considered for the analysis (Särndal et al., 1978).

The DAP Digital Surface Models (DSM) were generated using aerial images acquired in 2013 (July 06 to 12) and 2014 (May 18 to July 16) using an IGN camera (sensor V28T, 14,650 x 10,700 pixels of 6.8 µm each) mounted with a 125 mm Zeiss lens. The acquisition was done at 6,400 m above ground level, leading to an image resolution of 0.35 m at ground level. The image overlap was 60 % along track and 25 % across track, allowing photogrammetric processing. Images were oriented by IGN's production services. The photogrammetric reconstruction was done using Micmac open source photogrammetric software (Rupnik et al., 2017). The dense image matching strategy relies on a Per-Images Matching approach in image geometry and a 'Scale-Invariant-Feature Transform' (SIFT) detector (Lowe, 2004). The 3D point cloud resulting from the dense matching was converted into a 1 m digital surface model (DSM) using the maximum elevation per pixels. A canopy height model (CHM) was then produced by subtracting to the DSM, a digital terrain model (DTM) generated at the same resolution using airborne laser scanning data acquired in 2014. Multiple metrics were derived from the CHM (see Irulappa-Pillai-Vijayakumar et al., 2019) for each cell of the 30 m grid. Those included standard height descriptive statistics such as percentiles 0 to 100 by 10 (p0, p10, …, p100), percentiles 95 and 99 (p95, p99), mean (hmean), standard deviation (hstd), variance (hvar), and median absolute deviation (hmad). These metrics were completed with attributes describing the canopy structure, namely : mean inner canopy volume (Vi), mean outer canopy volume (Vo, defined as the volume comprised between the CHM and hmax), mean inner canopy volume above a given threshold value (Th) fixed here at 5 m (Vci), mean outer canopy volume above Th (Vco, complement of Vci to the maximum height), mean inner canopy volume below Th (Vgi) and its complement (Vgo), gap ration (Ga) defined as the proportion of plot area below Th, and rumple area (Ra) defined as the ratio of the CHM surface to the plot surface (see (Véga et al. (2016) for more details).

Four level 2A Landsat images were collected from Theia platform (*https://theia-landsat.cnes.fr*). The images were acquired on September 8, 2014. The processing level 2A includes atmospheric corrections, cloud detection and orthorectification (Hagolle et al., 2015). The following auxiliary variables were considered: 7 raw reflectance bands, brightness (Br), greenness (Gr), wetness (We) (Baig et al., 2014), normalized difference vegetation index (NDVI), Green NDVI (GNDVI), Enhance Vegetation Index (EVI), Specific Leaf Area Vegetation Index (SLAVI), Soil Adjusted Vegetation Index (SAVI), Modified Soil Adjusted Vegetation Index (MSAVI), simple ratio (SR), Normalized Difference Moisture Index (NDMI) and Normalized Difference Water Index (NDWI) (Barati et al.,

2011). The values corresponding to the centre of the 30 m grid cells were assigned to each cell. Metrics computational details are provided in Irulappa-Pillai-Vijayakumar et al. (2019).

2.4. Estimation framework

The relationship between growing stock, basal area and the auxiliary variables was investigated using multiple linear models. A best subset approach with a Bayesian information criterion (BIC) was applied to identify the optimal model for each forest attribute. The performance of the selected models was evaluated using a 10 fold cross validation approach and summarized with the cross-validated coefficient of determination (R^2), the cross-validated root mean squared error (RMSE) and the relative RMSE (RMSE%). The RMSE was computed as follow:

$$RMSE = \sqrt{\frac{\sum_{i=1}^{n}(y_i - \hat{y}_i)^2}{n}} \quad \textbf{(Eq.12)}$$

where n is the number of field plots, y_i the field observed values and $\hat{y}_i$ the predicted ones.

The small domain estimation procedure relied on the small area estimator for exhaustive auxiliary information provided in Mandallaz, (2013, equations 20 and 21). The mean and variance estimators are defined as follow:

$$\hat{Y}_{g.small} = \frac{1}{n_{1,g}}\sum \widehat{Y_1}(x) + \frac{1}{n_{2,g}}\sum (Y_2(x) - \widehat{Y_2}(x)) \quad \textbf{(Eq.13)}$$

$$\hat{\mathrm{V}}\mathrm{ar}(\hat{Y}_{g.small}) = \frac{1}{n_{1,g}(n_{1,g}-1)}\sum_{1,g}(\widehat{Y_1}(x) - \bar{\hat{Y}}_{1,g})^2 + \frac{1}{n_{2,g}(n_{2,g}-1)}\sum_{2,g}(\widehat{R_2}(x) - \bar{\hat{R}}_{2,g})^2 \quad \textbf{(Eq.14)}$$

where $Y_i(x)$ are the observed values (with i = 1 for auxiliary data and i = 2 for NFI data), $\widehat{Y_1}(x)$ the predicted ones, $\widehat{R_2}(x)$ the residual in small area g, $\bar{\hat{R}}_{2,g}$ the mean residual over g, $n_{1,g}$ and $n_{2,g}$ the number of pixels of auxiliary data and NFI plots in g respectively. The estimation error ($E_{\%}$) is defined as the ratio of the standard deviation and the mean:

$$E_{\%} = \frac{\sqrt{\widehat{Var}(\hat{y}_{g.small})}}{\hat{y}_{g.small}} * 100 \quad \textbf{(Eq.15)}$$

These estimators are implemented in the R package forestinventory (Hill et al., 2021).

2.5. Multiscale estimation framework

A top-down binary space partitioning (BSP) was used to downscale the estimates from the whole set of municipalities up to individual municipalities. It recursively divides the set municipalities into two equally-sized sets, thus generating a Small Area Estimation Tree structure (SAETree). At each

iteration, the division is performed on the direction perpendicular to the major axis of the bounding box either in x or y dimension in order to minimize the perimeter to surface ratio (Figure 10). The mean ($\hat{Y}_{g.small}$, Eq.13), variance ($\hat{\mathrm{V}}\mathrm{ar}\left(\hat{Y}_{g.small}\right)$, Eq.14) and error value ($E_{\%}$, Eq.15) are re-evaluated for each newly created domain pair. The division process iterates until either a user defined error threshold ($E_{m\%}$) for one of the two children domain or the minimum number of NFI plots per domain is reached ($i.e. E_{\%} > E_{m\%}$) (Figure 11). In both cases the parent domain of the SAETree is selected.

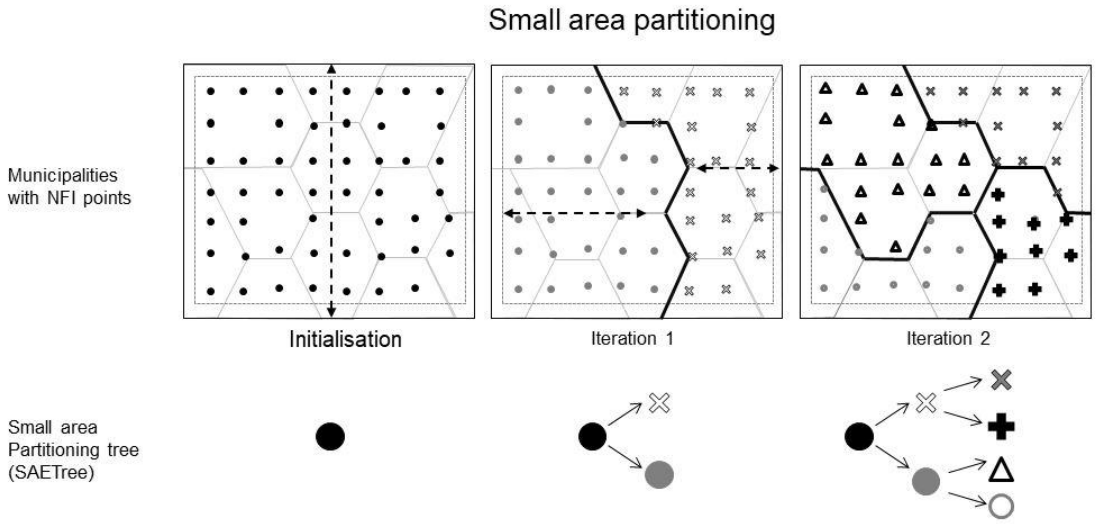

Figure 10. *Principle of binary space partitioning of municipalities.*

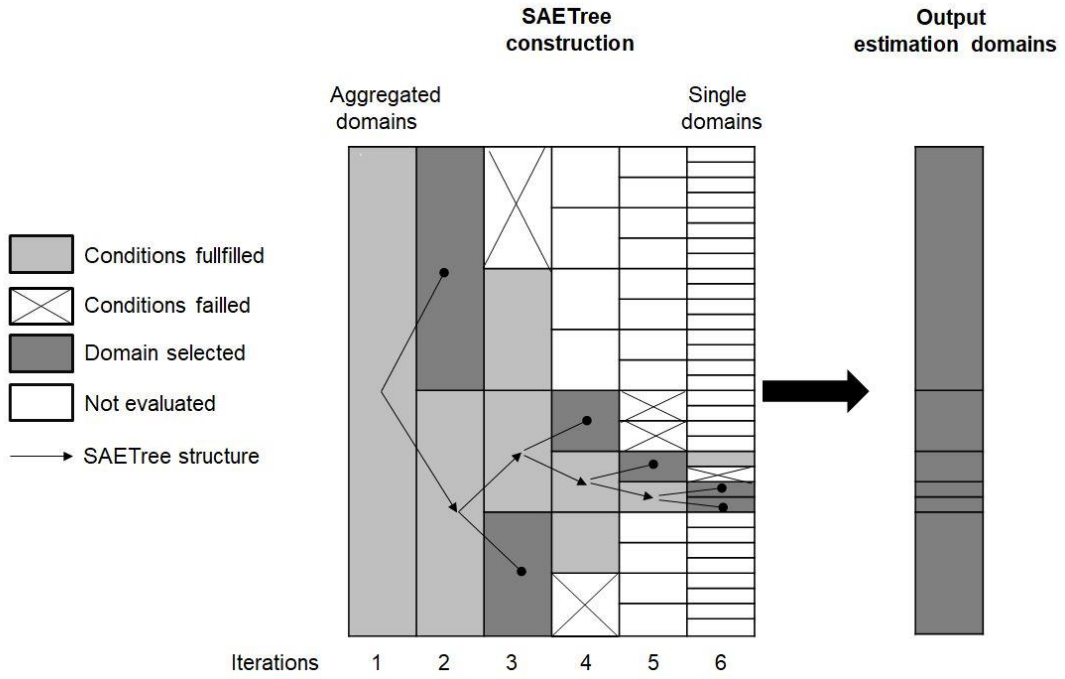

Figure 11. *Schematical representation of the small area estimation tree construction (SAETree) for the estimation domain optimisation. The vertical bars illustrate the partition of the domain through the iterations (binary split at each iteration). The colour code and arrows provide an example of an output tree structure.*

3. Results

The growing stock and the basal area were modelled as a function of the auxiliary data. Table 2 shows the models selected for the two surveyed forest attributes. The model for growing stock included the forest type, 3 CHM-based distribution variables (p60, hmad and hvar), a canopy roughness index (Ra), and a measure of the amount of vegetation (SR). The model explained 58 % of the field observed variation in growing stock. The 10-fold cross validated model RMSE was 69.4 $m^3.ha^{-1}$, corresponding to 43.5 % of the field observed stock. The model for basal area explained 41 % of the field observed variance, and had a cross-validated RMSE of 8.9 $m^2.ha^{-1}$ (42.4 %). The model shared 5 predictor variables with the growing stock model (FT, p60, hmad, Ra, SR) and hvar is replaced with 2 volume metrics describing the gap structure (Vgi and Vgo). Both models showed residual heteroscedasticity (*i.e.* increased residuals for high field attributes levels) which could not be alleviated by neither variable transformations nor interaction terms (Figure 12).

Table 2. *Predictor variables and 10-fold cross validated R2, RMSE and RMSE% for growing stock volume and basal area.*

Response variables	Predictor variables	R2	RMSE	RMSE%
Growing stock ($m^3.ha^{-1}$)	FT, p60, hmad, hvar, Ra, SR	0.58	69.4	43.5
Basal area ($m^2.ha^{-1}$)	FT, p60, hmad, Ra, SR, Vgi, Vgo	0.41	8.9	42.4

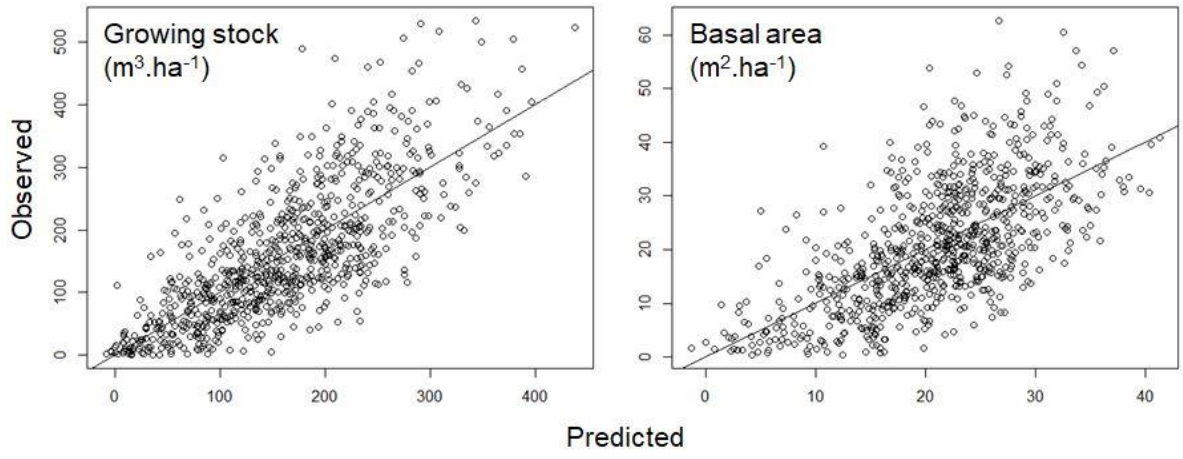

Figure 12. *Observed versus predicted values for growing stock volume (left) and basal area (right).*

Table 3 and Figure 13 illustrate the estimation means and errors achieved at the municipality levels and the corresponding estimation errors. Over the 157 municipalities of the study region, only 90 had at least 3 NFI points and were estimated. Those 90 municipalities represent 78.9 % of the study region. The mean growing stock is estimated at 155 $m^3.ha^{-1}$ with an average error of 15.9 % ranging from 2.8 % to 51.4 %. Compared to a simple random sampling estimation based on the field data

alone (results not reported), the relative efficiency (RE) of the model-assisted estimations, defined as the ratio of estimated variances achieved a value of 4.7. Similarly, the mean basal area is estimated at 20.4 $m^2.ha^{-1}$ with an average error of 15.6 % ranging from 4.7 to 50.8 %. The relative efficiency of the estimation reached 2.83. Spatially, most of the municipalities that could not be estimated are found along the Loire river basin in the Northern part of the area, as well as in the South-Eastern part. Estimation means revealed the heterogeneity of the area, despite the Northern and the South-Eastern areas exhibit higher values than the central part, which is more agricultural. Overall, the error patterns appeared correlated to the municipality area, the lowest errors being found in municipalities having a greater forested area and a higher number of NFI points.

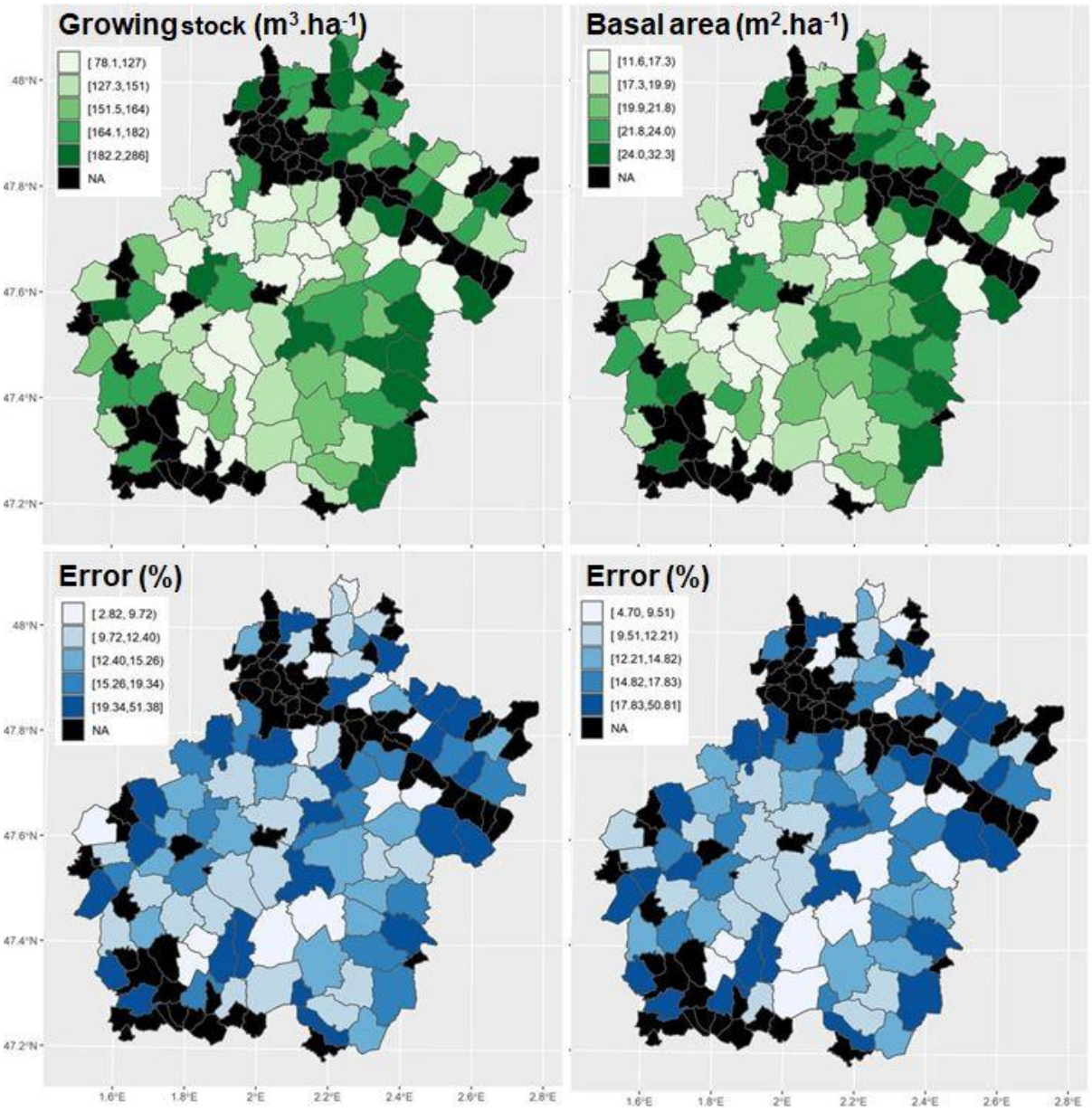

Figure 13. *Estimation mean and corresponding mean error at the scale of municipality for the growing stock and basal area. Similar colour classes have been used for Figure 13, Figure 14, and Figure 15.*

Table 3. *Model-assisted estimates and error at the scale of municipalities. RE stands for the relative efficiency, ratio of the variance of estimates obtained without and with auxiliary data. Out of the 157 municipalities, only 90 had at least 3 NFI points and were estimated. Average municipality area is 5035.9 ± 2129.5 ha. Average NFI point per municipality is 7.1 ± 3.9. Numbers in parenthesis are standard deviations.*

Attribute	Mean estimate	Mean error (%)	Error range (%)	RE
Growing stock ($m^3.ha^{-1}$)	155 (35.3)	15.9 (7.4)	2.8-51.4	4.7(6)
Basal area ($m^2.ha^{-1}$)	20.4 (4.0)	15.6 (7.1)	4.7-50.8	2.83(3.7)

The results of the multiscale approach are presented Table 4, Figure 14, and Figure 15. For the two forest attributes surveyed, relaxing the accepted error ($E_{m\%}$) translated into an increase in the number of domains, along with an increase in mean estimation error ($E_{\%}$), and a decrease in the average number of NFI plots per domain. For growing stock, the number of domains ranged from 20 to 80. This corresponded to domain varying from 16705 ± 8673 ha ($E_{m\%}$ = 10) to 4176 ± 2319 ha ($E_{m\%}$ = 50) in area. The mean growing stock ranged from 153.5 ± 21.1 $m^3.ha^{-1}$ at $E_{m\%}$ = 10 to 159.9 ± 36.1 $m^3.ha^{-1}$ at $E_{m\%}$ = 20. Despite the relaxing of $E_{m\%}$ the increases in average error remained moderated varying from 7.5 % at $E_{m\%}$ = 10 to 15.1 at $E_{m\%}$ = 50. This behaviour is further illustrated by the relative efficiency which stabilized after 30 % $E_{m\%}$ with an average value of 3.7. Similar results were obtained for basal area. The number of domains varied from 23 to 80, which corresponded to average domain area of 14527 ± 8557 ha and 4176 ± 2319 ha respectively. The mean estimated basal area ranged from 20.1 ± 2.2 $m^2.ha^{-1}$ ($E_{m\%}$ = 10) to 20.8 ± 3.8 $m^2.ha^{-1}$ ($E_{m\%}$ = 30). The corresponding mean domain error is minimum at $E_{m\%}$ = 10 with a value of 7.7 ± 1.4 % and maximum at $E_{m\%}$ = 50, with a value of 14.6 ± 5.7 %. The relative efficiency was stable over the scales, reaching a maximum value of 2.7. For both forest attributes, the estimation stabilized with errors greater than 30 %.

Figure 14 and Figure 15 provide insights into the spatial characteristics of estimation means and corresponding estimation errors for $E_{m\%}$ values of 10 and 50 %. For both forest attributes, a low $E_{m\%}$ results in a small number of large domains having similar errors. Such a constraining error condition provide a broad description of the resource, highlighting contrasted differences in forest attributes such as the ones differencing the high values in the north-western area from the low ones found in the central part. Increasing $E_{m\%}$ provided a more detailed representation of the distribution of forest resources, at the cost of a higher variability of error locally, and for the whole area.

Table 4. *Optimised small area estimation means, for different error thresholds ranging from 10 to 50 %. Numbers in parenthesis are standard deviations.*

Attribute	$E_{m\%}$	Number of domains	Area (ha)	NFI plots	Estimate	Error $E_{(\%)}$	Max Error (%)	RE
Growing stock ($m^3.ha^{-1}$)	10	20	16705(8673)	35.1(16.6)	153.5(21.1)	7.5(1.0)	9.5	2.8(0.8)
	20	61	5477(4107)	11.5(8.2)	159.9(36.1)	13.7(3.9)	19.9	3.7(4.4)
	30	78	4283(2325)	9.0(5.0)	159.1(37.1)	14.6(4.6)	26.0	3.7(4.1)
	40	79	4229(2341)	8.9(5.1)	159.5(37.1)	14.7(4.9)	31.8	3.7(4.1)
	50	80	4176(2319)	8.8(5.0)	159.6(36.9)	15.1(5.8)	42.5	3.7(4.1)
Basal area ($m^2.ha^{-1}$)	10	23	14527(8557)	30.1(16.1)	20.1(2.2)	7.7(1.4)	10.0	2.7(3.8)
	20	67	4987(3139)	10.5(6.6)	20.8(3.7)	13.0(3.5)	19.5	2.5(2.9)
	30	77	4339(2332)	9.1(5.1)	20.7(3.8)	14.0(4.4)	24.3	2.7(3.5)
	40	80	4176(2319)	8.8(5.0)	20.7(3.8)	14.6(5.7)	38.3	2.7(3.4)
	50	80	4176(2319)	8.8(5.0)	20.7(3.8)	14.6(5.7)	38.3	2.7(3.4)

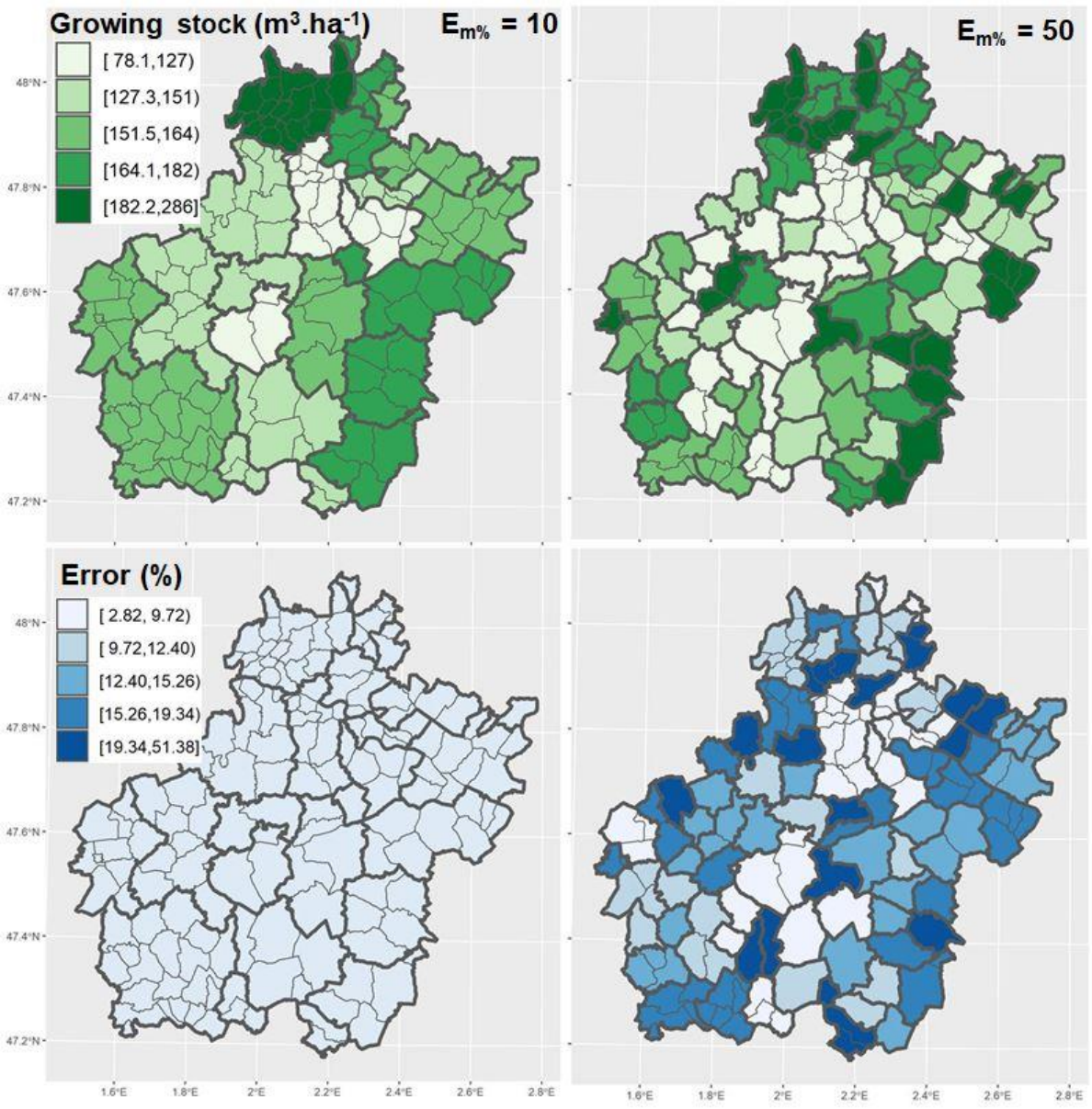

Figure 14. *Multiscale mean growing volume and associated errors generated using maximum errors ($E_{m\%}$) of 10 and 50 %. The tick lines represent the computed domains while the thin ones show the municipality outlines. Similar colour classes have been used for Figure 13, Figure 14, and Figure 15.*

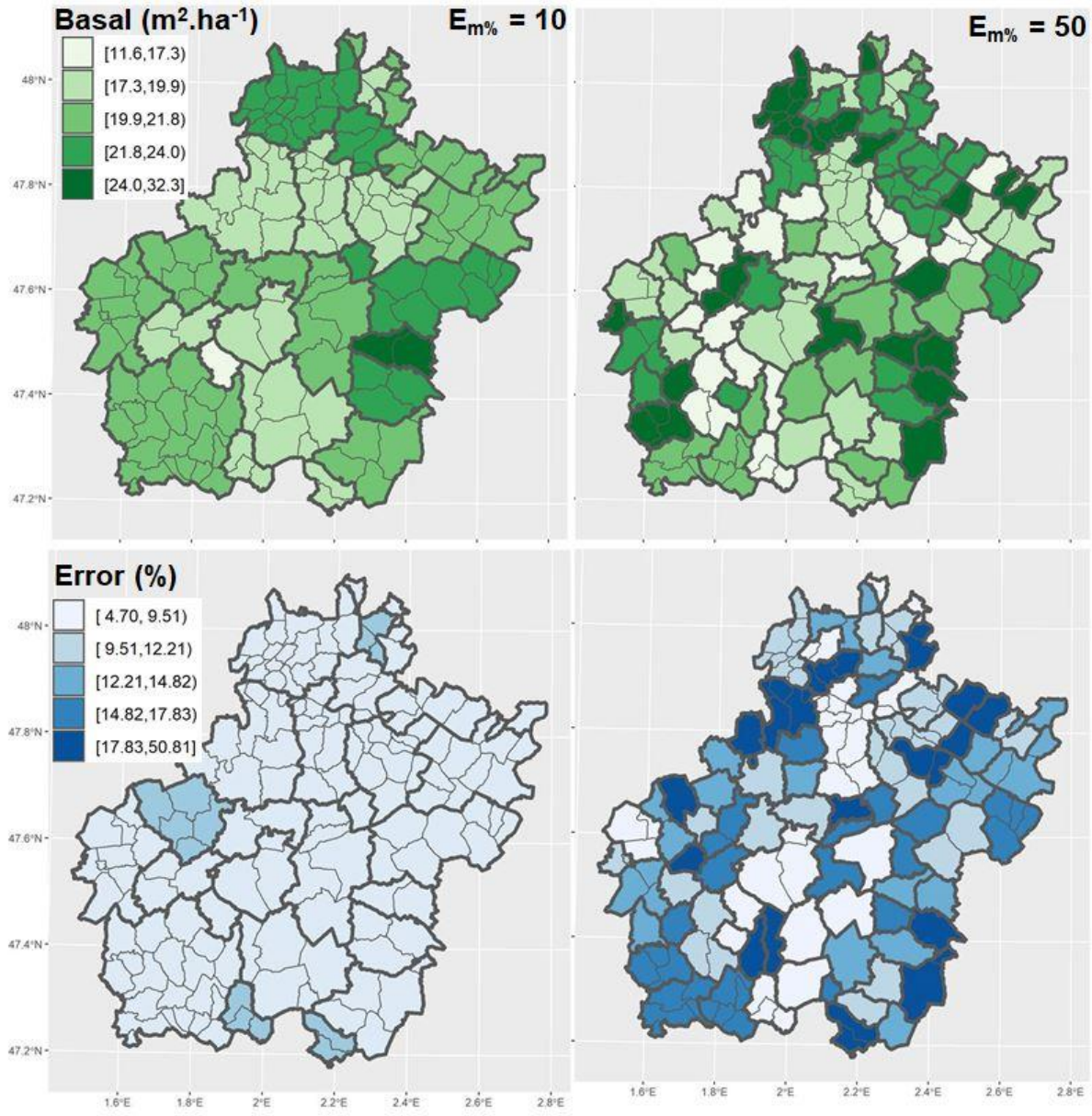

Figure 15. *Multiscale mean basal area and associated errors generated using maximum errors ($E_{m\%}$) of 10 and 50 %. The tick lines represent the computed domains while the thin ones show the municipality outlines. Similar colour classes have been used for Figure 13, Figure 14, and Figure 15.*

4. Discussion

Small area estimation approaches applied to NFI data usually rely on the spatial limits of administrative units such as forest districts or municipalities (Magnussen et al., 2017). In the model assisted framework, estimation is only possible if the amount of field inventory plots allows it. Such a limit often prevents from providing estimates at fine scales (Hill et al., 2018). In areas characterized by heterogeneous and fragmented forests or in areas with limited forest coverage, the number of NFI points is thus critical for estimation. In such situations, the use of administrative units for small area estimations becomes sub-optimal and the question of grouping municipalities becomes central (Tomppo et al., 2008b). The need to ventilate attributes, for example by species or diameter classes, further emphasizes the importance of adjusting the computation domains to the local conditions. The proposed algorithm provides a flexible framework to adapt small area domains to the user needs, according to a targeted estimation error. The downscaling framework thus enables users to balance between precision and spatial scale, and to optimize the rendering of attributes of interest, with respect to the performance of the underlying algorithm.

The models used in the present study exhibit saturation for growing volume above 300 $m^3.ha^{-1}$, as well as heteroscedasticity of the model residuals. Such issues have been reported in various studies (Breidenbach et al., 2018; Breidenbach and Astrup, 2012; Chirici et al., 2020; Frank et al., 2020; Saarela et al., 2015b). Heterogeneity in forest attributes resulting from stand history and disturbances (Sheil and Bongers, 2020) as well as the incapacity of the auxiliary data to describe this variability could explain these results (Ni-Meister et al., 2010). In this study, photogrammetric models derived from aerial photographs were used to assess canopy structure and related properties. On the one hand, such models benefit from large spatial coverage and frequent renewal, making them attractive for updating estimates and monitoring forest dynamics (Vega and St-onge, 2008). Height growth estimation from diachronic models also showed potential for improving estimation of flux variables such as growing stock increment (Irulappa-Pillai-Vijayakumar et al., 2019). On the other hand, the quality of photogrammetric models depends on the acquisition conditions and matching algorithms (Remondino et al., 2014). The usual widespread design of aerial surveys (*i.e.* 60 %-30 % image overlap along and between flight lines respectively; 25-50 cm image resolution at the ground level) often fails to render fine scale canopy structures such as canopy gaps between crowns (White et al., 2013). Also, the incapacity of photogrammetric models to describe the sub-canopy structure, limits their capability to capture the variability in forest structures as compared to lidar data (Drake et al., 2002) and results in a partial description of forest structures. The problem of heteroscedasticity reveals possible model misspecification issues and was considered in various studies. Methods proposed to address this issue include variable transformations (Hill et al., 2018), the use of mixed-models adapted to heteroscedastic residuals (Hou et al., 2017; Saarela et al., 2015b), or the use of a variance model (Frank et al., 2020). Frank et al. (2020) advocated that heteroscedasticity could not be alleviated from models of some forest attributes. Possible improvements could be achieved by using adequate

auxiliary data. Indeed, lidar derived metrics were not found to saturate at high biomass levels (Véga et al., 2015) and seem to capture greater details in the forest structure variability (White et al., 2013). Times series of both photogrammetric (Irulappa-Pillai-Vijayakumar et al., 2019) and satellite data (Morin et al., 2019) also have the potential to provide additional information about stand trajectories or structures that could improve prediction of attributes related to fluxes for example.

The analysis of the domains estimated with various targeted error levels provides insights into forest structure at the scale of territory. Figure 13, Figure 14, Figure 15 show that the algorithm enables to render the spatial complexity of the forest attributes at various spatial scales. For example, greater growing stock and basal area values were found in the Northern and South-Eastern part of the study area. Those areas correspond to pure deciduous or pine forests which are state forests that are generally more intensely managed and with higher growing stock levels. By contrast, the central and Western parts are dominated by open forests and humid areas and exhibited lower attribute values with either greater domain sizes or estimation errors. Surprisingly, the number of domain generated saturate with $E_{m\%}$ greater than 20. This indicates that that the heterogeneity in forest within municipalities strongly penalized the downscaling process. Furthermore, a close look at Figure 14, Figure 15 reveals that estimation at the municipality level is reached for a large number of municipalities (65%), such as the large forested municipalities located in the South-Eastern part of the study area. Conversely, municipalities having a low forest area and a limited number of NFI points (*i.e.* black municipalities in Figure 13) prevented the division process of the algorithm independently from $E_{m\%}$.

Compared with the results obtained for single municipalities, which left some municipalities without any estimation, the proposed multiscale approach succeeded in providing estimations for the entire region of interest with a higher precision and preserved the capacity to produce estimates at the municipality level in densely forested areas, wherever $E_{m\%}$ allows such estimations. Being able to fix $E_{m\%}$ to a given level is attractive for official statistics or decision makers who require estimates with a high degree of precision. At the management level or for forest prospection, the greater spatial resolution generated by increasing $E_{m\%}$, could be privileged for orienting local management strategies. The possibility of grouping together municipalities having a limited number of NFI points due to low forest coverage or highly fragmented forests could be considered by some as having a limited interest. However, those areas are also currently experiencing an increase in forested area and stocks due to the forest expansion associated with agricultural land abandonment (Mather et al., 1999). This forest expansion is at the origin of new resources for wood production which are currently not taken into account by stakeholders, while representing a growing amount of forest area and stock (Denardou et al., 2017). With the increase in NFI points expected following the expansion in forest areas, the algorithm will allow to provide strategic information about the localisation and characteristics of those new resources thus enhancing the capabilities of forest stakeholders to take them into account in management strategies.

The proposed downscaling approach remains naive by construction and is probably not optimal, since a fixed binary division factor is applied at each step of the SAETree. Indeed, if one out of the two child nodes does not pass the error threshold, the estimation will remain at the parent node. Improved spatial resolution might be obtained using an aggregation approach (Gómez et al., 2009). Aggregative approaches also provide the opportunity to aggregate neighbours with respect to either their spatial or attribute properties, making the approach attractive. That said, the SAETree approach allow comparisons between scales and attributes, making for example pair-wise division simpler and more efficient than aggregative approaches that might conduct to different domain shapes with respect to the aggregation criteria used or the auxiliary variable considered.

In the method developed here, NFI plots are required to produce estimates of forest attributes. This requirement is a major limitation for domains in which the number of NFI plots is insufficient. In such situations, domain aggregations are unavoidable in a model-assisted approach. If finer scales are nevertheless required, the remaining option would be to use a model-based approach (Ene et al., 2016; Magnussen, 2015; Saarela et al., 2015b). Such approaches could be privileged for reaching management units or for small area estimation in a context of environmental crises such as forest fire (Moisen et al., 2004) or biotic damages (*e.g.* insect outbreaks). In such situations therefore, careful attention must be paid to model specifications (Ståhl et al., 2016).

5. Conclusions

In response to the need of adapting computation domains to spatial properties of administrative units, the proposed algorithm enables partitioning a study area into smaller domains, where sample size and area are adaptively tuned according to a selected error level. Thus, it creates a partitioning of domains, down to the smallest possible size, depending on the error threshold fixed by users.

The downscaling potential of the algorithm depends on the statistical strength between field attributes and auxiliary variables, but also on the spatial heterogeneity of the forests. While different partitions are obtained based on the targeted error threshold and the forest attributes considered, estimations remain spatially consistent owing to the hierarchical structure of the SAEtree. It thus offers the possibility to balance between estimation error and domain size. At the largest scales, generated by relaxing the error threshold, the limiting factor to obtain estimates remains the amount of field plots in the domain, which is a well-known constrain affecting model-assisted estimation approaches.

As the proposed approach rely simply on an iterative division of space, it could be applied to polygon or point (*i.e.* through an appropriate tessellation of space) layers, independently from administrative boundaries. Therefore, it can be adapted to reflect forest heterogeneity, making partitions more relevant either geographically or ecologically, as needed.

While the estimation scales required by stakeholders are often vague, especially in terms of optimum domain size, the proposed algorithm constitutes an appealing approach for flexible and user controlled precision.

Acknowledgements

We deeply acknowledge Claire Bastick and François Morneau (IGN) for their support with NFI data, Gregoire Maillet and Ana-Maria Rosu (IGN) for their assistance with the photogrammetric workflow, and Dinesh Babu Irulappa-Pillai-Vijayakumar for his contribution to the ADEME project.

Funding

This research was funded by The French Environmental Management Agency (ADEME), grant number 16-60-C0007. The methods and algorithms for processing photogrammetric data were supported by DIABOLO project from the European Union's Horizon 2020 research and innovation program under grant agreement No 633464, as well as CHM-ERA project from the French National Research Agency (ANR) as part of the "Investissements d'Avenir" program (ANR-11-LABX-0002-01, Lab of Excellence ARBRE). Ankit Sagar received the financial support of the French PIA project "Lorraine Université d'Excellence", reference ANR-15-IDEX-04-LUE, through the project Impact DeepSurf.

Chapter II: Characterizing the calibration domain of remote sensing models using convex hulls

Authors: Jean-Pierre Renaud[1, 2, *], Ankit Sagar[2, 3], Pierre Barbillon[4], Oliver Bouriaud[5, 2], Christine Deleuze[1], Cédric Vega[2]

[1]Office National des Forêts, Département RDI, *France*

[2]Institut National de l'Information Géographique et Forestière (IGN), Laboratoire d'Inventaire Forestier (LIF), *Nancy, France*

[3]UMR Silva, Université de Lorraine, faculté des Sciences et Technologies Campus Aiguillettes, *Nancy, France*

[4]UMR MIA-Paris, Université Paris-Saclay, AgroParisTech, INRAE, *Paris Cedex 05, France*

[5]Ștefan cel Mare University of Suceava, *Suceava, Romania*

[*]corresponding author

The article has been published in the International Journal of Applied Earth Observations and Geoinformation. It is available at the following DOI: https://doi.org/10.1016/j.jag.2022.102939.

Authors' contributions

Jean-Pierre Renaud (JPR) conceived and design the work. JPR and Cédric Vega (CV) contributed to data acquisition. JPR and Ankit Sagar (AS) developed the R-code for data processing and convex hull computation. JPR, AS, CV and Olivier Bouriaud were responsible for interpreting the results. All authors contributed to drafting the work and have approved the submitted version.

Abstract

The ever-increasing availability of remote sensing data allows production of forest attributes maps, which are usually made using model-based approaches. These map products are sensitive to various bias sources, including model extrapolation. To identify, over a case study forest, the proportion of extrapolated predictions, we used a convex hull method applied to the auxiliary data space of an airborne laser scanning (ALS) flight. The impact of different sampling efforts was also evaluated. This was done by iteratively thinning a set of 487 systematic plots using nested sub-grids allowing to divide the sample by two at each level. The analysis were conducted for all alternative samples and evaluated against 56 independent validation plots. Residuals of the extrapolated validation plots were computed and examined as a function of their distance to the model calibration domain. Extrapolation was also characterized for the pixels of the area of interest (AOI) to upscale at population level. Results showed that the proportion of extrapolated pixels greatly reduced with an increasing sampling effort. It reached a plateau (ca. 20% extrapolation) with a sampling intensity of ca. 250-calibration plots. This contrasts with results on model's root mean squared error (RMSE), which reached a plateau at a much lower sampling intensity. This result emphasizes the fact that with a low sampling effort, extrapolation risk remains high, even at a relatively low RMSE. For all attributes examined (*i.e.*, stand density, basal area, and quadratic mean diameter) estimations were generally found to be biased for validation plots that were extrapolated. The method allows an easy identification of map pixels that are out of the calibration domain, making it an interesting tool to evaluate model transferability over an area of interest (AOI). It could also serve to compare "*competing*" models at a variable selection phase. From a model calibration perspective, it could serve *a posteriori*, to evaluate areas (in the auxiliary space) that merit further sampling efforts to improve model reliability.

Keywords: calibration domain, model-based maps, model transferability, extrapolation bias, airborne laser scanning, sampling effort.

1. Introduction

The ever-increasing availability of remote sensing data facilitates the production of forest attributes maps, which are usually made using model-dependant approaches (e.g., Coops et al., 2021; Magnussen et al., 2016; McRoberts et al., 2010; Saarela et al., 2015; Ståhl et al., 2016). In such approaches, auxiliary variables are linked to forest attributes through field calibration samples that are used to build models. These calibration samples do not necessarily need to follow a rigorous sampling design, and their purposive selection can sometimes be performed to meet cost effectiveness criteria. According to Magnussen (2015), in simple situations, model-dependant approaches are credible alternatives to the design-based ones usually followed by national forest inventories. Globally, estimates might be considered unbiased when a sufficiently large sample is used for model calibration (Magnussen, 2015) and when the model is used within its validity domain. However, locally, for small domains or for conditions not encountered during calibration (i.e., pixels out of the calibration auxiliary space), there is no evidence that model predictions would be reliable or unbiased (Hsu et al., 2020; Magnussen et al., 2016). Even though this crucial role played by the calibration sample is recognised by many authors (e.g., Bouvier et al., 2019; Frazer et al., 2011; Mesgaran et al., 2014; Meyer and Pebesma, 2021; Saarela et al., 2015), reliability maps of forest attributes are infrequent and, to paraphrase McRoberts (2011), such maps with predictions out of the models' validity domain have a non-negligible risk of being potentially unreliable and rather "*pretty pictures*".

To minimise model's prediction errors, different strategies have been proposed to efficiently distribute field samples in the auxiliary space of the remote sensing data (Grafström et al., 2014; Hawbaker et al., 2009; Maltamo et al., 2011; Pesonen et al., 2009; van Aardt et al., 2006). Some authors have proposed to stratify the ALS data to spread the sampling effort over the whole auxiliary space (Frazer et al., 2011; Hawbaker et al., 2009). Maltamo et al. (2011) also compared different plot selection strategies to optimise precision. Nevertheless, to the best of our knowledge, none have tried to identify the validity domain of models used to predict forest attributes or to identify extrapolated predictions on the resulting maps. Owing to the simplicity of the method (Barber et al., 1996), one motivation of this study was therefore to use convex hulls as a tool for evaluating the quality and the validity domain of models used over an AOI.

Characterizing the validity domain of a regression model is not a new problem, and not restricted to the remote sensing community (Bouchet et al., 2020; Brooks et al., 1988; Conn et al., 2015; Cook, 1977; Ebert et al., 2014; Mesgaran et al., 2014; Meyer and Pebesma, 2021). In ecology for example, models used outside their calibration range produce frequently unreliable predictions of species distribution for example (Conn et al., 2015). Even though there is no universal definition of extrapolation, some authors have proposed algorithms based on statistical properties of the auxiliary space, such as Cook's or Mahalanobis distances, or dissimilarity indexes to identify extrapolation situations (Bouchet et al., 2020; Conn et al., 2015; Cook, 1977; Mesgaran et al., 2014; Meyer and

Pebesma, 2021), while others have used different forms of convex or concave hulls (Brooks et al., 1988; Conn et al., 2015; Ebert et al., 2014).

In their best practices guide of ALS approaches in forestry, White et al. (2013) illustrated that convex hull could be used to show uncovered forest structures by an ALS model. They showed that an inefficient calibration sample could leave a large part of the model predictions out of the calibration domain. Such a situation is prone to errors, as model transferability could be questioned outside the range of the sampled conditions (Brooks et al., 1988; Conn et al., 2015). Another important aspect about extrapolated predictions is their distance to the calibration data, since a remote prediction is expected to be more prone to bias than one located just beside the calibration domain.

As extrapolated predictions over an AOI are rarely reported in the remote sensing literature and considering that they may produce biased estimates, and locally erroneous maps, a first objective of this study was to use convex hulls to evaluate the proportion of an AOI auxiliary space covered by a model and characterize the residual error associated to the extrapolated predictions. The proportion of extrapolated pixels over the AOI was used as an indicator of model representativity. A secondary objective was to evaluate how sampling intensities affects the degree of extrapolation and how extrapolation distance influence prediction errors.

2. Data and methods

The study area is based on an ALS flight performed in February 2019 in North-eastern France, which covers a forested area of 18,646 ha, with a mean pulse emission density of 16 points per m². Within this area, a set of 487 systematic field plots were carried out in the Mouterhouse forest (5,324 ha) during the winter of 2019-2020 (Figure 16). The Mouterhouse forest consisted of broadleaved, mixed, and coniferous stands (respectively 43%, 23% and 34% on an area basis) that were considered as representative of the whole ALS area. The main species are Scots pine (*Pinus sylvestris*), sessile oak (*Quercus petraea*), beech (*Fagus sylvatica*), Douglas fir (*Pseudotsuga menziesii*) and Norway spruce (*Picea abies*). Diameter (starting at 17.5 cm) and tree species were measured in these calibration plots of 15-meter radius spaced at every ~300 meter, on a systematic grid. An independent set of 56 plots, located in the same forest area was used as a validation data set.

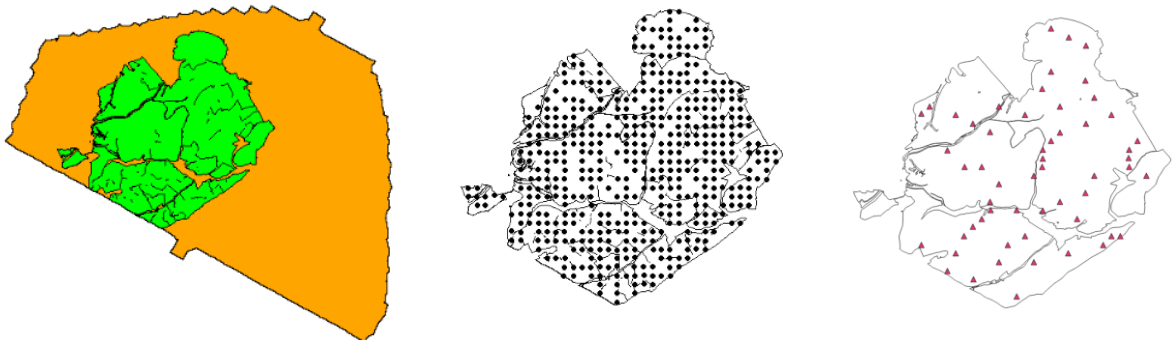

Figure 16. *The ALS flight area in orange, with the Mouterhouse forest in green (left) and for illustration, its initial 487 systematic (middle) and 56 validation (right) plots.*

To evaluate the effect of different sampling efforts, the systematic plot grid was thinned by half several times to obtain coarser grids, down to a minimum of 8 remaining plots, sequentially producing systematic subsamples (Figure 17). The process follows the approach in used by the French National Forest Inventory and described in Vidal et al. (2007). It consists of a system of nested sub-grids allowing to divide the sample by two at each level. As indicated in Vidal et al. (2007) such an approach preserves the properties of the systematic sample at every grid levels. Furthermore, multiple subsamples of the sampling intensity were used at each thinning iteration, using alternative plot samples of the same grid resolution as replicates (i.e., for example the green and blue dots of the first iteration in Figure 17). These replicates allowed to obtain estimates of attributes variability at each grid resolution (i.e., for each level of sampling intensity). As the number of candidate replicates grow exponentially at each iteration, a maximum of 40 replicates were used at lower grid resolutions for computational ease. When all replicates of a given grid resolution had not exactly the sample number of plots due to the spatial configuration of the forest, each replicate was trimmed to the minimal value found for that given resolution by randomly removing exceeding plots. This approach was retained

since the initial sampling design was systematic and allowed a more even spatial repartition of the sampling effort. As a result, more precise estimates were then available at coarser grid resolution, resulting from the larger number of replicates for these lower sampling efforts.

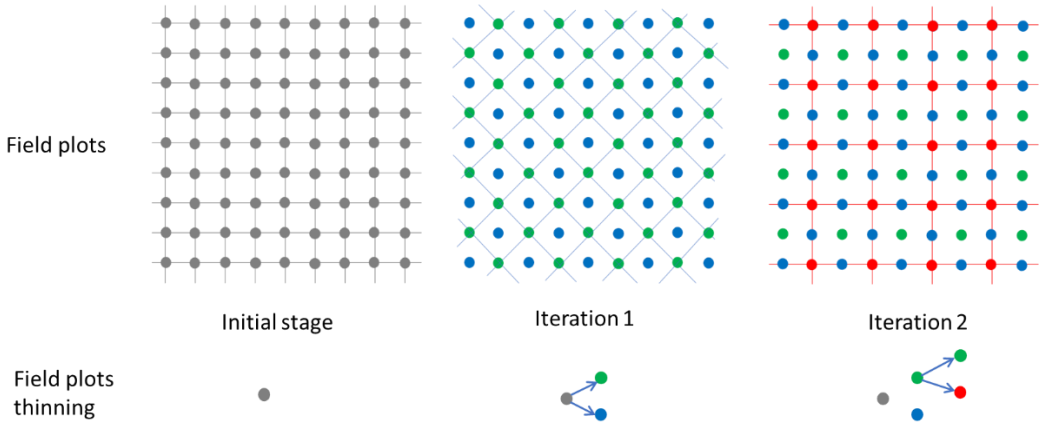

Figure 17. *Illustration of the thinning process from the initial dense grid (left) to the second thinning iteration (right). Field pots are symbolised by dots. At each iteration, every second plot is removed, yielding a thinned grid. At each iteration, all plots of the same spatial resolution were used as replicates of the same sampling effort (e.g., 2 replicates at iteration 1: green and blue dots).*

As shown in Figure 16, no field plots were available for 71% of the ALS acquisition area (the orange section). This situation offers the opportunity to examine the impact of model application outside of its "spatial" calibration area. Standard area-based ALS metrics (ABA) were computed using the R package lidR (Roussel and Auty, 2021). Metric computation was performed over the field plots, as well as over a raster grid of 30 m resolution for the whole ALS area. A simple working linear regression model (Bouvier et al., 2015; Magnussen et al., 2012) was adjusted to estimate basal area (G), quadratic mean diameter (Dg) and tree density per hectare (N) separately. The retained working model parameters (Eq.16) included 3 independent variables: mean (Hmean), and standard deviation (Hsd) of all ALS pulse heights and the average slope (Slope) of the pixels (or of the field plots), computed from the digital terrain model (DTM) using the R package terra (Hijmans, 2021). The working model is as follow:

$$(\mathrm{N}, \mathrm{G}, \mathrm{Dg}) \sim \beta_1 \, \mathrm{H_{mean}} + \beta_2 \, \mathrm{H_{SD}} + \beta_3 \, \mathrm{Slope} + \varepsilon \qquad (\textbf{\textit{Eq.16}})$$

where β_i are model parameters obtained for each dependant variables separately (N, G, Dg).

Models' performance was evaluated using root mean square error (RMSE; Eq.17) computed from the validation samples, as:

$$RMSE = \sqrt{\frac{\sum_{i=1}^{n} (y_i - \hat{y}_i)^2}{n}} \qquad (\textbf{\textit{Eq.17}})$$

where n is the number of validation field plots, y_i the observed values of field attributes and $\hat{y}_i$ the predicted values. RMSE was further divided by the validation attribute mean to obtain a relative RMSE.

Using the calibration auxiliary space of the model independent variables, convex hulls were computed for all field calibration configurations associated to the different sampling efforts compared. The "geometry" package (Habel et al., 2019) was used to build convex hulls around the the auxiliary space of the calibration domains. The volume of the convex hull was also extracted from the scaled auxiliary space. Then, validation plots or pixels of the AOI were classified as being located inside or outside the hulls using the "inhull" function of the same package. For the Mouterhouse forest, as well as for the extended ALS area, the proportions of extrapolated pixels were computed. The yaImpute R package (Crookston and Finley, 2008), was then used to obtain their Euclidian distances (using scaled X variables) to the nearest calibration plot. The same operation was performed for the validation plots which were also used to compute residuals from the models' predictions (Eq.18):

$$residual_i = (y_i - \hat{y}_i) \qquad \textbf{(Eq.18)}$$

where, y_i is the observed value, $\hat{y}_i$ is predicted value. Means and standard deviations of all these indicators were obtained for each level of sampling intensity by aggregating replicates and were reported in the relevant figures.

3. Results

A conventional way to evaluate the quality of a model adjustment is to examine its validation RMSE. In this study, based on the results of decreasing sampling intensities, it appeared that the relative mean RMSEs tended to reach a plateau when ca. 50 calibration plots were used to build models, regardless of the forest attributes examined (Figure 18.a). This plateau represented relative RMSE values of ca. 18%, 27% and 42% for Dg, G and N respectively. In absolute values, it represented a mean RMSE of 5.9 cm for Dg, 6.5 m²/ha for G and 117 stems/ha for N.

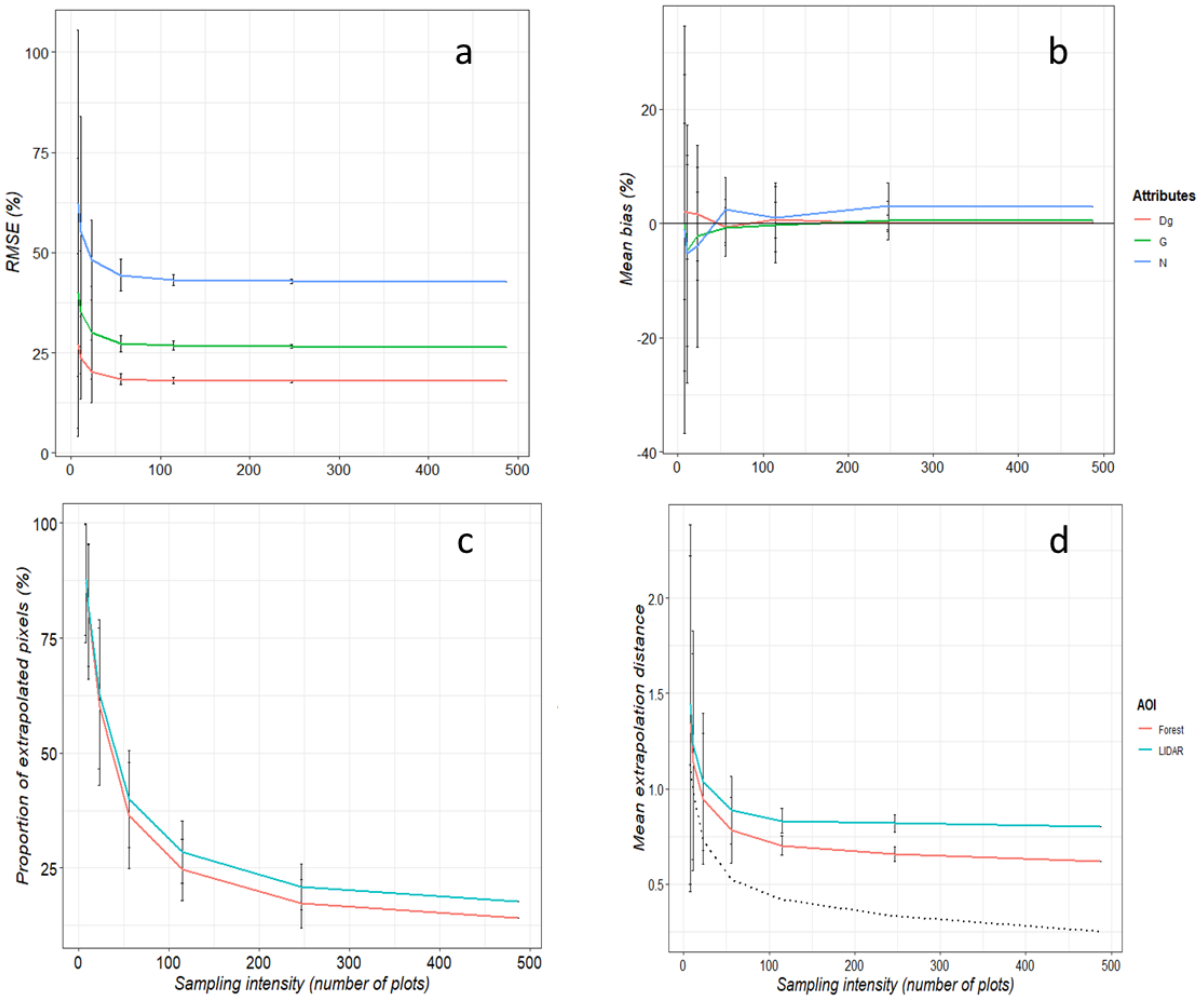

Figure 18. *Impact of sampling intensities on: (a) the relative root means squared errors (RMSE in %) of validation plots for the different forest attributes examined; (b) the mean relative bias (in %); (c) the mean proportion of pixels located outside the calibration hull for each AOI (whole Lidar area or the Moutherhouse forest only); and (d) the mean scaled extrapolation distances for each AOI. (The dashed line is the mean interpolation distance for the calibration plots). In all graphs, error bars represent 2 standard deviations of the replicated sampling intensities.*

Mean bias per sampling intensity is shown in Figure 18.b. While for all forest attributes examined no bias was globally observed, a large variability was nevertheless present at small sampling

intensities. It showed that in such a situation (e.g., with less than 25 plots to calibrate a model) it was possible to obtain a bias larger than 10% for a given replicate (Figure 18.b).

As opposed to RMSE, the mean proportion of extrapolated pixels remained relatively high at low sampling intensities (Figure 18.c). For example, with less than 100 calibration plots, more than 25% of the pixels over the Mouterhouse forest, or 29% over the whole Lidar area were located outside the auxiliary space defined by the calibration hulls. Only minor differences in proportion of extrapolated pixels between the two AOI examined were observed, slightly more extrapolated pixels (ca. 3%) were observed within the extended AOI, as opposed to the Mouterhouse forest area. With the full calibration dataset (487 plots) the proportion of extrapolated pixels was less than 18% (Figure 18.c).

When the sampling effort decreases, a larger number of pixels were found outside the calibration hull and their distances to the nearest calibration plots (in the auxiliary space) tended to increase. For example, with a sampling effort of 487 calibration plots, the mean extrapolation distances observed were respectively 0.6 and 0.8 for the Mouterhouse forest or the extended area respectively, while it was almost twice, i.e., 1.2, when less than 20 plots were used for calibration (Figure 18.d). Greater extrapolation distances to the calibration domain were also consistently observed for the extended lidar area as compared to the Mouterhouse forest, as shown in Figure 18.d. The mean interpolation distance (i.e., distance among the auxiliary space of the calibration plots) was also shown in Figure 18.d (the dashed line). This mean interpolation distance (of the calibration plots) was low (0.3) for the largest sampling effort (487 plots) but increased with at reduced sampling intensities. When less than 50 plots were used to calibrate models, the mean interpolation distance tended to be larger than 0.5 (Figure 18.d).

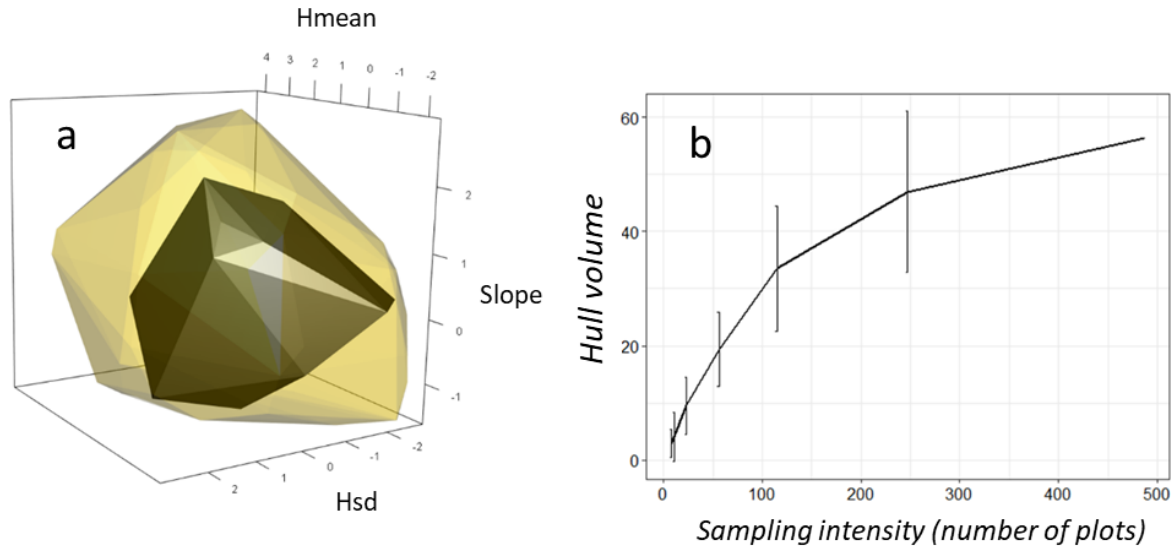

Figure 19. *3D representation of the convex hull (a) obtained from the model's auxiliary space using 487 (yellow) and 23 calibration plots (black) and (b) the effect of sampling effort on the convex hull volumes. (As all variables are scaled, the hull volume is unit less).*

The explored variability of the auxiliary space was also presented in terms of convex hulls volumes (Figure 19). Figure 19.a presents envelops of the auxiliary space for two sampling intensities: 487 plots (in yellow) and 23 plots (in black). An obvious shrinkage of the volume of the calibration domain was associated to the reduction of the sampling intensity. To illustrate more completely this phenomenon, the volumes of the convex hulls were presented as a function of the sampling intensity in Figure 19.b. From that figure, it appeared that below a sampling effort of 247 plots, a large reduction in the hull volumes was observed. The convex hull volumes were also computed (data not shown) for the pixel's population of the Mouterhouse forest and the extended lidar area. It yielded volumes 2.5 and 2.9 times larger than the convex hull volume obtained with the full set of calibration plots (487 plots). This result suggested that a large part (>60%) of the convex hull volumes of the AOI was not included within the volume of the calibration domain.

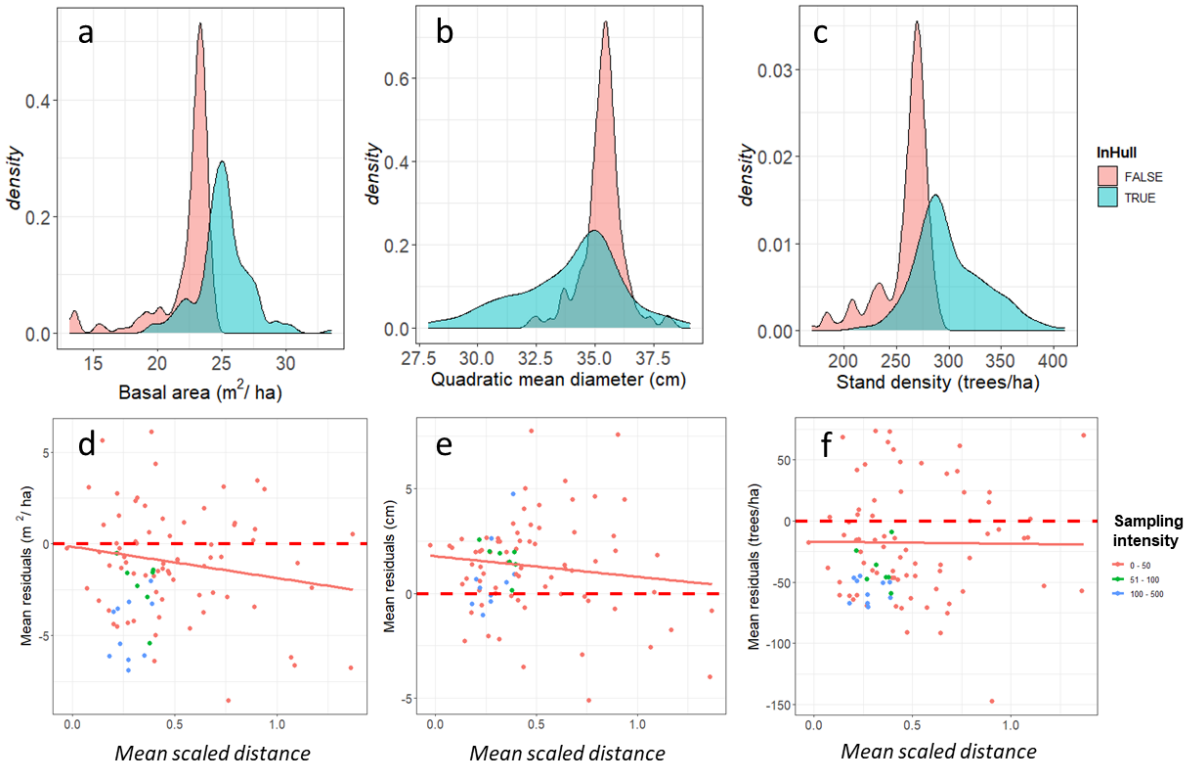

Figure 20. *Distribution of forest attributes of the mean values of the validation plots grouped as inside (InHull = TRUE) or outside (InHull = FALSE) the calibration domain, aggregated over all replicates of sampling intensities (a-c). Mean residuals of the extrapolated plots (d-f, InHull = FALSE) are also given according to their mean distances to the calibration domain. The solid lines in plates d to f represented the regression line. Legend corresponds to classes of sampling intensities. (Attributes are basal area (a, d), quadratic mean diameter (b, e), and tree density per hectare (c, f).*

For each replicate of the sampling grid resolutions, validation plots were classified as being inside or outside the calibration domain, based on their auxiliary space. The forest attributes observed in each group were aggregated, and their distribution compared (Figure 20.a-c). Results showed, for G and N,

that the validation plots located outside of the hulls (InHull = FALSE) were more frequently at the lower end of the distributions compared to interpolated ones (InHull = TRUE) (Figure 20a and c). For quadratic mean diameter, both distributions were overlapping (Figure 20.b). This translated, for basal area and stand density, into a clear tendency for an underestimation bias associated with an increase in extrapolation distances (Figure 20.d and f). For quadratic mean diameters, a trend toward reduced residuals with increasing extrapolation distance was also observed. Clearly from Figure 20 (d-f), even for large sampling efforts (green and blue points), the extrapolated plots were globally underestimated for G and N and overestimated for Dg. This result underlined the importance of minimising extrapolation in model predictions and suggested a contribution of the extrapolation distance to bias.

4. Discussion

Our results are emphasizing the interest of convex hulls to identify model predictions that are made outside their calibration range not only for producing potentially more reliable maps, but also to ascertain forest attribute predictions. Even though it is well-known that unreliable predictions may results from such situations (Brooks et al., 1988), the proportion of extrapolated predictions are rarely reported in the remote sensing community involved in forest modelling. In most studies, the main model quality indicators reported are often the RMSE and coefficient of determination (R^2). However, as underlined by Persson and Ståhl (2020), the use of RMSE has shortcomings, since it represents only a limited facet of the error structure. In a simulation study, Kangas et al. (2016) also showed that RMSE can significantly underestimate the real model uncertainty. Our results showed that RMSE tended to reach a plateau, at sampling intensities where the proportion of extrapolated pixels was not yet stabilized. This result is not due to a curse of dimensionality problem (Sagar et al., 2021) since we purposefully used a simple working model (Bouvier et al., 2015; Magnussen et al., 2012). At low sampling intensities the calibration domain tended to have a reduced convex hull volume (Figure 19), and the proportion of extrapolated pixels tended clearly to increase. Distances of extrapolated pixels to the calibration domain also tended to increase at low sampling intensities (Figure 18). This shrinkage of the model's auxiliary space is problematic, since one would expect the calibration domain to cover as much as possible the ranges of the target population to produce reliable predictions (Stage and Crookston, 2007). This is particularly critical for models that cannot extrapolate due to their nature (e.g., non-parametric models such as k-NN or random Forest) or for non-linear relationships of forest attributes over a wider range of the predictors space (Corona et al., 2014; Magnussen et al., 2010; Stage and Crookston, 2007). In heterogeneous forests, a low sampling intensity is thus synonymous of a restricted calibration domain and of a potentially low model transferability to unsampled areas (Mesgaran et al., 2014; Meyer and Pebesma, 2021; White et al., 2013), especially when empirical models are used.

Of course, the extrapolation problem mentioned above is particularly important in a model-based perspective, or when maps are directly produced from model predictions. Forest managers receiving such maps containing locally extrapolated predictions should be warned, and pixels out of the model's validity domain should be identified as potentially unreliable. However, in a design-based perspective, an estimator frequently used is the generalized regression estimator (GREG). For internal models, GREG is considered as approximately unbiased, regardless of how well the model fits the relationship between the inventory and auxiliary data (Corona et al., 2014; Gregoire, 1998; Lehtonen et al., 2003; Ståhl et al., 2016; Wojcik et al., 2022). This absence of bias is nevertheless associated with an adequate sample size and the assumption that residuals obtained from the calibration data are representative of the whole population. These conditions thus permit to correct model misspecification (Lehtonen et al., 2003; Särndal et al., 1992). However, for operational forest management, concerns are frequently associated with small domains where only few, or even no calibration data are available

to correct model errors. In GREG, two terms are used: the mean (or total) of model predictions for each pixel of the AOI, and a Horvitz-Thompson estimator of the residuals computed over the calibration plots (Corona et al., 2014; Gregoire, 1998; Särndal et al., 1992; Ståhl et al., 2016; Wojcik et al., 2022). In Moutherhouse, predictions that were extrapolated had frequently non-null mean residuals. They concerned mainly young stands with low G and a low number of tallied stems, as shown in Figure 20, but also occurred in mature plots still having low G and N, but large Dg suggesting that they resulted from thinning operations. Extrapolated predictions were mainly underestimated for G and N and overestimated for Dg (Figure 20d-f). Even though it is out of the scope of this study, an evaluation of the impact of extrapolations on GREG's estimation of small domains would certainly be worth further investigations.

We used an initial sampling effort of *ca*. 1 field plots per 8 ha (487 plots). At this intensity, less than 18 % of the pixels from the AOI were found to be outside of the calibration domain. However, this proportion raised drastically when the sampling grid was thinned to a density of 1 plot every 33 ha or more (<115 calibration plots over the AOI). A similar pattern was nevertheless not observed for RMSE, that reached a plateau at a sampling intensity of *ca*. 1 field plot per 70 ha (50 plots) (Figure 18). When the sampling grid contained less than 50 calibration plots, the proportion of extrapolated pixels exceed 35 % and mean predictions of extrapolated pixels were biased (Figure 20). Interestingly, a sampling intensity of 1 field plot per 70 ha (50 plots) is also the sample size that allow G to be estimated with a precision of 5% based on the field sample plots alone (Kangas and Maltamo, 2006).

In a Wisconsin forest, (Hawbaker et al., 2009) used a much lower sampling intensity (one plot per 700 ha) but stratified their training plots using the ALS predictor space. With this approach, they extended their calibration domain and obtained more accurate results, as compared to a simple random sampling design. This improvement was thus directly related to a better representativity of their calibration domain. In a Norwegian forest, Maltamo et al. (2011) also observed that stratifying field plots based on ALS data improved relative RMSE by 5 to 10%. That improvement was nevertheless dependant on sampling intensities. With a large sampling effort (at least 1 plot per 340 ha), all sampling designs tested had similar RMSE (Maltamo et al., 2011). We conjecture that the convergence in RMSE past a given sampling intensity is related to the proportions of extrapolated pixels in these studies, which unfortunately were not quantified or reported. Spatially systematic samples have favourable properties because they are spatially balanced (Stevens, 1997; Stevens and Olsen, 2004), thus avoiding sampling voids over an AOI (Christianson and Kaufman, 2016; Meyer and Pebesma, 2021). In our case study, a systematic sampling design was used. This sample could be considered as efficient in obtaining a calibration sample covering all aspects of the AOI. But it seems that under a sampling effort of 1 field plot per 70 ha (50 plots), a large amount of the AOI's auxiliary space is left uncovered. This could be related to the heterogeneity or the aggregation structure of the forest. Indeed, spatial regularity, or spatial structures can strongly reduce the efficiency of a systematic

sample (Stevens and Olsen, 2004), as some aggregated forest structures may be missed bellow a given sampling resolution.

More advanced sampling methods can be implemented to reduce extrapolation. For instance, a sampling based on the cube method could be tested (Grafström et al., 2014). This method aims to improve the spread of the probabilistic samples in the space of some auxiliary variables and could be used to sample from the space of the dependent variables used for model construction. Even though the impact of extrapolation on the prediction's bias hasn't been fully studied or established (Magnussen et al., 2010), it is probable that the informative spreading of the sample could enable to reduce extrapolation situations.

Several authors have shown that NFI data are efficient to train ALS models (Hollaus et al., 2007; Maltamo et al., 2009; Vega et al., 2021). In France, the NFI plot density, over a 5-year period, represents an average sampling effort of 1 plot per 570 ha (Hervé, 2016). This intensity over the Moutherhouse forest appears to be low and would probably have led to a large proportion of extrapolated pixels. The use of convex hull in such contexts, could contribute to improved model reliability through identification of area of the predictor space requiring complementary sampling effort or to identify potentially unreliable predictions areas in maps, made for decision-makers or forest managers (Sagar et al., 2021). Certainly, problems associated to low sampling efforts could be more easily diagnosed using the proposed convex hull approach. A drawback though of the method is its large computational requirements in high dimensionalities, that restricts its use to the comparison of parsimonious models. Nevertheless, the question of model transferability at different scales remains a question beyond the scope on the present study.

With an increased sampling intensity, mean extrapolation distances tended to be reduced. Meyer and Pebesma (2021) used such a distance-based criterion to estimate prediction's reliability in random Forest models. They used the mean calibration distance of their auxiliary space (i.e., interpolation distances) to build an index of potentially spurious predictions. From Figure 20, such a tendency of larger biases with increasing extrapolation distances can be observed, but the relationship is noisy. From a calibration perspective though, a clear impact of the sampling intensities is observed on the mean interpolation distances (Figure 18), reflecting a denser calibration auxiliary space with larger sampling efforts.

Convex hull could also serve at a model selection stage. Comparing convex hull volumes of competing models with the ones of the AOI could serve as indicators of models' extrapolation potential. The lowest the hull volume ratio, the lowest the extrapolation risk. In addition to the volume ratio, the extrapolation distance could serve as an indicator of outliers. Models with extrapolation distance largely above their interpolation counterpart should be considered with care. The impact of models' predictions out of their validity domain on maps is certainly an aspect that worth further investigation and this study is a first step toward the use of this interesting tool.

5. Conclusions

This study presented the use of convex hulls as a multivariate tool allowing to identify model's calibration domains and their transferability over an AOI. It showed that the achieved RMSE can hide extrapolation issues, with risks of local bias. Our results also suggest that addressing the extrapolation issue requires a higher sampling intensity than the one considered for achieving a given RMSE target. The use of convex hulls allows to produce maps with identified predictions that are made outside model's calibration domains. From an operational forest management point of view, knowing where predictions are out of there validity domain could represent a valuable outcome of this approach. Convex hulls could also help to compare "competing" models at a variable selection phase, provided that a limited number of variables are constituting the auxiliary space, due to the large computational requirement of the convex hull method in high dimensions. From a model calibration perspective, it could also serve *a posteriori*, to evaluate areas (in the auxiliary space) that merit further sampling efforts to improve calibration or evaluate prediction bias. Finally, further studies are required to examine the possibility of correcting map bias using the extrapolation distances.

Acknowledgements

We acknowledge the Laboratoire Interdisciplinaire des Environnements Continentaux (CNRS et l'Université de Lorraine) for supplying the ALS data and the Agence Territoriale de Mulhouse (ONF) for the field data. We thank Steen Magnussen for enlightening discussions. We thank Alain Munoz, Flavien Lamiche, and Vincet Pérez (ONF) for their help in preparing and supplying data.

Funding

ONF Département RDI is supported by the French National Research Agency (ANR) as part of the "Investissements d'Avenir" program (ANR-11-LABX-0002-01, Lab of Excellence ARBRE). Ankit Sagar received the financial support of the French PIA project "Lorraine Université d'Excellence", reference ANR-15-IDEX-04-LUE, through the project Impact DeepSurf.. Olivier Bouriaud acknowledges support from the project funded Ministry of Research, Innovation and Digitalization within Program 1 - Development of national research and development system, Subprogram 1.2 - Institutional Performance - RDI excellence funding projects, under contract no. 10PFE/2021.

Chapter III: Multisource forest inventories: A model-based approach using *k*-NN to reconcile forest attributes statistics and map products

Authors: Ankit Sagar[1, 2, 3], Cédric Vega[2, *], Olivier Bouriaud[2, 4], Christian Piedallu[3], Jean-Pierre Renaud[2, 5]

[1]Université de Lorraine, Faculté des Sciences et Technologies - Campus Aiguillettes, *Nancy, France*

[2]Laboratoire d'Inventaire Forestier, Université de Lorraine, ENSG, IGN, INRAe, *Nancy, France*

[3]UMR SILVA INRAe-AgroParisTech-Université de Lorraine, *Nancy, France*

[4]Ștefan cel Mare University of Suceava, *Suceava, Romania*

[5]Office National des Forêts, Pôle Recherche Développement Innovation, *Nancy, France*

[*]corresponding author

The article has been published in the ISPRS Journal of Photogrammetry and Remote Sensing. It is available at the following DOI: https://doi.org/10.1016/j.isprsjprs.2022.08.016.

Authors' contributions

Ankit Sagar (AS), Cédric Vega (CV) and Jean-Pierre Renaud (JPR) planned the study. AS, CV and JPR contributed to data acquisition. AS, CV and JPR developed the R-code for data processing and modelling. AS, CV, JPR and Olivier Bouriaud were responsible for interpreting the results. All authors contributed to drafting the work and have approved the submitted version.

Abstract

Forest map products are widely used and have taken benefit from progresses in the multisource forest inventory approaches, which are meant to improve the precision of forest inventory estimates at high spatial resolution. However, estimating errors of pixel-wise predictions remains difficult, and reconciling statistical outcomes with map products is still an open and important question.

We address this problem using an original approach relying on a model-based inference framework and *k*-nearest neighbours (*k*-NN) models to produce pixel-wise estimations and related quality assessment. Our approach takes advantage of the resampling properties of a model-based estimator and combines it with geometrical convex-hull models to measure respectively the precision and accuracy of pixel predictions. A measure of pixel reliability was obtained by combining precision and accuracy.

The study was carried out over a 7,694 km^2 area dominated by structurally complex broadleaved forests in centre of France. The targeted forest attributes were growing stock volume, basal area and growing stock volume increment. A total of 819 national forest inventory plots were combined with auxiliary data extracted from a forest map, Landsat 8 images, and 3D point clouds from both airborne laser scanning and digital aerial photogrammetry. *k*-NN models were built independently for both 3D data sources. Both selected models included 5 auxiliary variables, and were generated using 5 neighbours, and most similar neighbours distance measure. The models showed relative root mean square error ranging from 35.7 % (basal area, digital aerial photogrammetry) in calibration to 63.4 % (growing stock volume increment, airborne laser scanning) in the validation set. At pixel level, we found that a minimum of 86.4 % of the predictions were of high precision as their bootstrapped coefficient of variation fall below calibration's relative root mean square error. The amount of extrapolation varied from 4.3 % (digital aerial photogrammetry) to 6.3 % (airborne laser scanning). A relationship was found between extrapolation and *k*-NN distance, opening new opportunities to correct extrapolation errors. At the population level, airborne laser scanning and digital aerial photogrammetry performed similarly, offering the possibility to use digital aerial photogrammetry for monitoring purposes.

The proposed method provided consistent estimates of forest attributes and maps, and also provided spatially explicit information about pixel predictions in terms of precision, accuracy and reliability. The method therefore produced high resolution outputs, significant for either decision making or forest management purposes.

Keywords: multisource forest inventories, statistical inference, forest attribute maps, reliability assessment, LiDAR, photogrammetry.

1. Introduction

National Forest Inventories (NFIs) are crucial forest assessment programmes, providing estimates about the amount and state of the forest resources, and information forming the basis for the development of various forest management policies (Breidenbach et al., 2021). NFIs are based on a rigorous statistical framework for designing sampling and inventory procedures with corresponding estimators (Tewari and Kleinn, 2015), and can deliver precise estimates of forest attributes such as growing stock volume (GSV) and basal area (BA) at national down to regional scales (Brosofske et al., 2014; Kangas et al., 2018). Below these scales, the estimation domain is too sparsely sampled, resulting in poor estimation precision of forest attributes (Coelho and Pereira, 2011). Such a decrease in estimation precision prevents forest stakeholders from using NFI estimates to develop strategies and support decision-making processes over small functional-management territories (Vega et al., 2021). To support these activities, NFI precision has to be improved and complemented with map products providing detailed information about the amount and localization of the forest resources (Chirici et al., 2020; Rahlf et al., 2021).

Multisource National Forest Inventory (MSNFI) approaches has made it possible to answer these specific needs and also encourage wall-to-wall mapping of forest attributes at high spatial resolution (Saarela et al., 2020), through a statistical combination of NFI and auxiliary data (Tomppo et al., 2008a). The auxiliary datasets such as thematic maps (i.e. forest maps, soil maps) and remote sensing products (i.e. optical, SAR, 3D point cloud data) are selected based on their availability, correlation with the forest attributes of interest and their limited cost.

Many optical remote sensing satellites such as SPOT, Landsat, IKONOS, GeoEye-1, Quickbird, and Sentinel-2 have been tested and used in various forest inventories programmes around the world (Castillo-Santiago et al., 2010; Irulappa-Pillai-Vijayakumar et al., 2019; Puliti et al., 2021). Despite their large spatial coverage and high temporal resolution, the availability of optical imagery is often impeded by cloud cover, haze, cloud shadow, while the derived vegetation indices tends to saturate in mid biomass (~130 Mg/ha) (Zhao et al., 2016). Airborne remote sensing data from airborne laser scanning (ALS) and digital aerial photogrammetry (DAP) (Gobakken et al., 2015; Irulappa-Pillai-Vijayakumar et al., 2019) proved to be the most valuable sources of auxiliary data to characterize the forest canopy structure and estimate the most important forest attributes (Durrieu et al., 2015; White et al., 2013). Unlike ALS, DAP cannot provide forest structure information below the canopy cover, and for the computation of canopy height model, DAP relies on a digital terrain model (DTM) from an external source (St-Onge et al., 2008). After conducting analytical research on 70 peer-reviewed studies, Zolkos et al. (2013) concluded that ALS proved to be performing significantly better for forest resource estimation than any other data source. However, due to the low cost of DAP, the data are updated regularly which makes it appealing to use for forest monitoring (Rahlf et al., 2017). Hence,

the debate on which auxiliary data is the most suitable for forest resource estimation in MSNFI remains largely open.

The relationships between NFI and auxiliary data were investigated using various approaches. Numerous parametric (i.e. linear regression, Bayesian regression model, geographically weighted regression) and non-parametric (i.e. random forest, *k*-nearest neighbours or *k*-NN) methods have been implemented for downscaling NFI estimates over small management units (Barrett et al., 2016; Gregoire et al., 2016; Irulappa-Pillai-Vijayakumar et al., 2019; Tomppo et al., 2008a). These methods are already operational in the boreal region (Kangas et al., 2018), while experiences are limited in some temperate regions due to the complexity in forest composition and structure (Vega et al., 2021). Among all these methods, *k*-NN technique gained popularity in MSNFIs (Irulappa-Pillai-Vijayakumar et al., 2019; Magnussen et al., 2009). A strong argument for *k*-NN comes from its ease of implementation, its ability to predict multiple forest attributes simultaneously (Goerndt et al., 2019), and the absence of assumption regarding the distribution of predictor and response variables (Irulappa-Pillai-Vijayakumar et al., 2019).

Similarly, various inference frameworks have been used to estimate population parameters, including total, mean, and variance from plot and auxiliary data (Gregoire et al., 2016). Since NFI relies on sampling procedures, model-assisted inference has been largely used to build upon the properties of the sampling design for estimation (Saarela et al., 2015a). Small area estimation technique has been developed to downscale the estimates to small geographical domains such as municipalities and forest districts (Breidenbach and Astrup, 2012; Tomppo et al., 2008a). However, a minimum number of sample plots is required in each domain to allow estimation, thus constraining the geographical scale at which forest attributes could be reported with a requested precision (Vega et al., 2021). The model-based inference framework allows more flexibility on the sampling design and could provide estimates even in those domains that do not include any field plot (Ståhl et al., 2016). As the estimates are directly derived from the model, the emphasis is placed on the model specification to minimize bias (Longford, 2005). The downside of *k*-NN technique in this context is the absence of a well-established theoretical inference framework, although several estimators have already been proposed (McRoberts et al., 2011). Furthermore, the incapacity of k-NN to predict outside of the calibration domain (James et al., 2013) requires the development of specific approaches to account for prediction bias (Magnussen et al., 2010). With much less sampled plots than auxiliary data, MSNFIs are naturally put in a situation of imbalance that translates into frequent model extrapolation (Meyer and Pebesma, 2021). This stresses the importance of addressing model extrapolation while analysing and quantifying the reliability of the predicted forest attributes.

Models have also largely been used to produce wall-to-wall maps of forest attributes (Chirici et al., 2020; Coops et al., 2021; Nilsson et al., 2017), and error propagation methods have been proposed to assess prediction uncertainties (Blackard et al., 2008; Esteban et al., 2019; Mascaro et al., 2011).

But the reliability of pixels predictions in the context of statistical inference have rarely been appreciated (Saarela et al., 2020).

The objective of this study was to propose a method to adapt the model-based *k*-NN estimation framework of population parameters for the production of high resolution forest attribute and reliability maps at pixel level. We defined prediction reliability at pixel level in terms of precision and accuracy. Precision was derived through resampling, building upon a bootstrap model-based estimator proposed by McRoberts et al. (2022) for population parameters. Prediction accuracy was defined through a measure of extrapolation, to account for *k*-NN's inability to predict outside of its calibration domain (Magnussen et al., 2010). Extrapolation was assessed using an original convex hull approach applied to the auxiliary variable space (Conn et al., 2015; Cook, 1977). The method was evaluated for three major forest attributes, GSV, BA, and growing stock volume increment (VI) in a large territory composed of complex forest structures. The auxiliary data included a forest map, Landsat 8 images and 3D point cloud data from ALS and DAP.

2. Material

2.1. Study site

The study was carried out in the temperate forest of Sologne and Orléans, located in the French region of Centre Val De Loire (Figure 21). The area covers 7,694 km^2 which extends from 1.41° to 2.79° East Longitude and 47.1° to 48.1° North Latitude. The area is characterized by a semi-oceanic climate, with mean annual precipitation of 731 mm and a mean annual temperature of 10.9° C. Elevation ranges from 70 to 180 m and topography represents a flat terrain. The soil is predominantly made up of sand and clay, originating from the erosion of Massif Central. Because of the low permeability of these soils, the area has numerous ponds and swamps. About 53% (3,900 km^2) of the area is covered by forests. Forested areas are primarily dominated by broad-leaved stands (74%) of oaks (i.e., *Quercus petraea* Mill. and *Quercus robur* L.). Coniferous stands account for 16% of the forested area and are dominated by scots pines (*Pinus sylvestris* L.) and maritime pines (*Pinus pinaster* Ait.). The remaining forest area is covered by a mixed stand (10%) of oaks and Scots pines. The forest is characterized by different management policies influenced by forest ownership. The northern part of the study area is dominated by state-owned forests which are intensely managed. Private forests represent ~84% of the forested area.

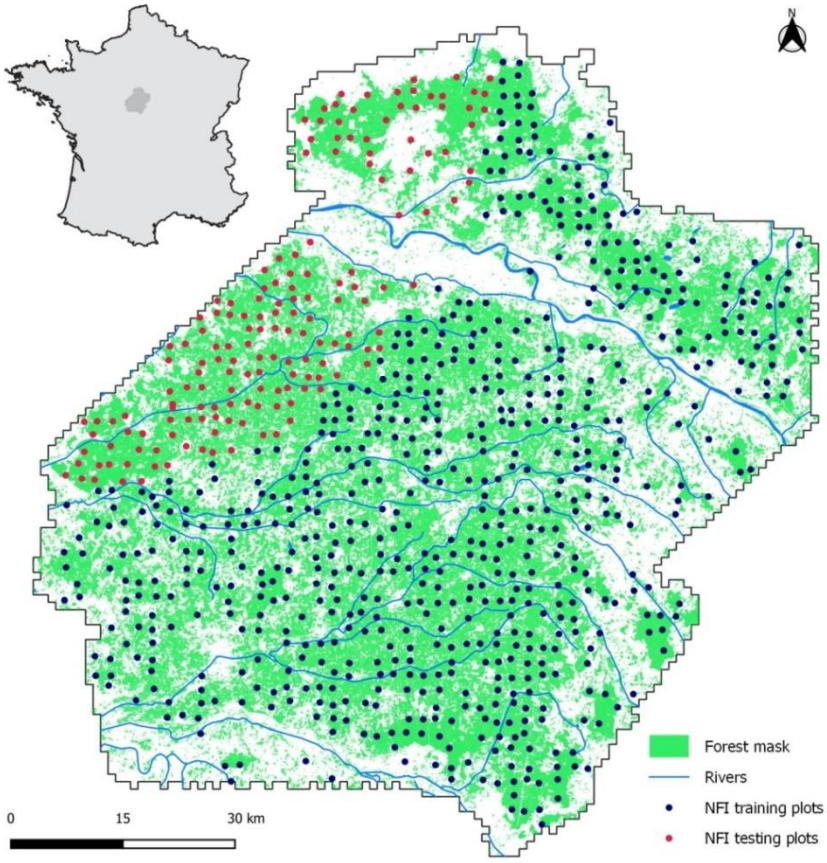

Figure 21. *Location of the study area and spatial distribution of the NFI field plots. The colour of NFI plots represents the training and testing set used for modelling (section 3.1).*

2.2. Field inventory data

A total of 819 field plots were used. The plots were surveyed on the field between 2010 and 2014 in the framework of the NFI. Such an aggregation is used to produce official statistics at national and regional level (Robert et al., 2009). The plot sample was drawn in such a way that the last annual sample (2014) corresponded to the reference year for the auxiliary data described in section 2.3.

Field information is collected on 4 concentric circular plots of radius 6, 9, 15, and 25 m. The largest concentric plot is used to describe the stand structure and composition. Tree measurements are restricted to the first three concentric plots according to the tree circumference at breast height (1.3 m). Small ([23.5 - 70.5 cm[), medium ([70.5 – 117.5 cm[), and large ([117.5 cm[) trees are measured in plots of radius 6, 9, and 15 m respectively. The information about species, vegetation state, 5-year radial increment, and circumference at breast height are collected for all the trees fulfilling the circumference constraints. Tree attributes such as stem volume and stem volume increment are computed from field measurements using NFI's species-specific allometric models. Plot position on the field is fixed using low-cost GPS, interpretation of printed aerial photographs, and/or routing and chaining. The precision of the plot centre position is evaluated at 3.67 m (±3.3 m) (Guitet, 2018).

Plot-level forest attributes are computed from the tree measurements and their inclusion probability, which is based on the tree position within the plot (Hervé et al., 2014). The study focuses on three forest attributes of importance: GSV (m^3ha^{-1}), computed as the weighted sum of the individual tree stem volume (stem diameter up to 7 cm), BA (m^2ha^{-1}), defined as the weighted sum of the tree cross-sectional area at breast height, and VI ($m^3ha^{-1}yr^{-1}$), computed as the weighted sum of the mean annual volume increment over 5 years. Summary statistics of the three forest attributes are shown in Table 5.

Table 5. *Mean and standard deviation (SD) of forest attributes, for all plots (819 plots), training (80% of the plots) and testing (20 % of the plots) sets. Training and testing sets were used for model development (section 3.1).*

Forest attribute	All plots		Training plots		Testing plots	
	Mean	SD	Mean	SD	Mean	SD
Growing stock (GSV, m^3ha^{-1})	160.7	111.3	160.0	110.0	162.9	116.7
Basal area (BA, m^2a^{-1})	21.1	11.8	21.2	11.9	20.4	11.5
Volume increment (VI, $m^3ha^{-1}yr^{-1}$)	5.7	3.9	5.7	3.9	5.3	3.8

2.3. Auxiliary data and processing

Three freely available auxiliary data were considered in this study: forest map, Landsat images, and 3D point clouds. Two sources of point cloud were used for comparison: ALS, and DAP.

The auxiliary data were processed and integrated into a grid of 30 m resolution, corresponding to the diameter of the NFI field plots. Each pixel of the grid had a surface of 900 m^2.The origin of the grid was set according to the Lambert conic projection using Lambert-93 geodetic system (EPSG: 2154). Data processing and analysis were conducted in R (Version 4.0.2) environment, using lidR (Roussel et al., 2020), yaImpute (Crookston and Finley, 2008), and geometry (Habel et al., 2019) packages.

2.3.1. Forest map

The forest map (BD-Forêt® version 2.0) is an open-source vector map, defining the geographical reference for the forest land cover and the description of forest stands. The map is produced by the National Institute of Geographic and Forest Information (IGN), through semi-automatic segmentation of near-infrared aerial images (BD ORTHO®) with a resolution of 0.5 m, followed by the photo-interpretation of the resulting segments. The map provides information about forest area and composition for the dominant species within a forest patch of at least 0.5 hectares.

The forest map was used to generate a forest mask to limit the spatial extent of the pixels within the forest land cover only. Each pixel was characterized by a dominant forest type (pure conifers, pure broadleaved, or mixed stands), which was achieved by selecting the forest type at the pixel centre (Irulappa-Pillai-Vijayakumar et al., 2019).

2.3.2. Landsat data

Four processed Landsat 8 images acquired on 8 September 2014 were used in this study. The data were acquired freely from the Theia portal *(https://theia-landsat.cnes.fr)*. The images were processed to level 2A, which includes: orthorectification, cloud and their shadow masking, and atmospheric correction (Hagolle et al., 2015). Landsat 8 Operational Land Imager images consist of nine spectral bands of 30 m spatial resolution. Along with the spectral bands, 12 spectral indices were computed: Normalized Difference Vegetation Index, Normalized Difference Moisture Index, Normalized Difference Water Index, Green Normalized Difference Vegetation Index, Soil Adjusted Vegetation Index, Specific Leaf Area Vegetation Index, Modified Soil Adjusted Vegetation Index, Enhanced Vegetation Index, Simple Ratio, Brightness, Greenness and Wetness. The details for the computation of indices were provided in Irulappa-Pillai-Vijayakumar et al. (2019).

2.3.3. Airborne laser scanning and digital aerial photogrammetry

The Airborne Laser Scanning (ALS) data were collected by IGN, between January and March 2014. The northern part of the study area (2,758 km^2) was covered using Optech ALTM 3100 EA laser scanner operated at an altitude of 1,530 m above ground level (AGL). The pulse repetition frequency was 71 Hz, and the scanning frequency was 35 Hz with a maximum scan angle of 25°. A supplementary flight was conducted to cover the southern part of the study site (4,936 km^2). The data were acquired using a Leica ALS70 sensor flying at an altitude of 1,797 m AGL. The pulse repetition frequency was 309 Hz, and the scanning frequency was 35 Hz with a maximum scan angle of 25°. The point density of both flights was 2 pts m^{-2}. The point clouds were processed using IGN processing lines using Terrasolid's Terrascan software *(https://terrasolid.com)*. The data were delivered as classified point cloud tiles of 1 km resolution. The ground classified points were used to generate a DTM at a 1 m resolution using Triangulated Irregular Network algorithm. The points above the ground level were normalized using the DTM.

The Digital Aerial Photogrammetry (DAP) data were acquired between 2013 (July 06 – July 12) and 2014 (May 18 – July 16), using the IGN CamV2 system (14,650 x 10,700 pixels of 6.8 µm each) (Souchon et al., 2010) mounted with a Zeiss lens of 125 mm focal length. The images were acquired at 6,400 m AGL with 60% overlap along track and 25% across track. The pixel resolution at ground level was 0.35 m. The oriented images were processed using IGN MicMac photogrammetric software (Rupnik et al., 2017). The dense image matching was implemented using a Per Image Matching approach. Depth maps of each image pair were generated at a pyramid level 2, merged, and then converted into a 3D point cloud. The resulting points (0.9 pts m^{-2}) were further normalized using the ALS DTM.

Multiple metrics were computed from both ALS and DAP point cloud at the grid level. These include: minimum, maximum and mean height, standard deviation, skewness, kurtosis and entropy of height distribution, percentage of returns above mean height, percentile of height distribution, and cumulative percentage of return. The above metrics were computed for all the points above 2 m. ALS metrics were computed for the first and last returns, as well as for the intensity of first returns. Additional metrics were computed for the ratio of area and canopy closure ratio (Rcc: ratio between canopy and ground cover) (Roussel et al., 2020).

3. Methods

The methods included two steps, *(i)* model selection and assessment, and *(ii)* statistical inference and mapping (Figure 22). The relationships between field attributes and the auxiliary data were investigated using non-parametric multivariate *k*-NN models (McRoberts, 2012).

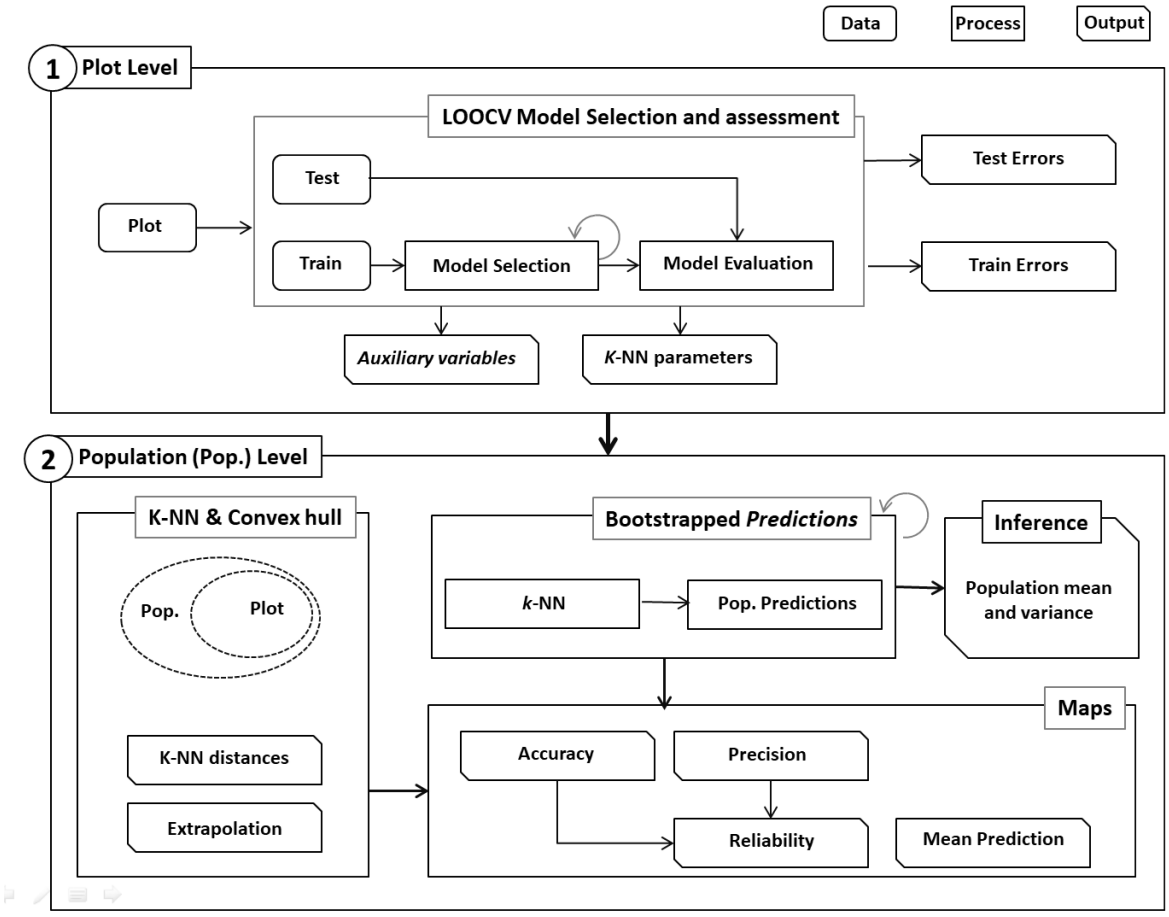

Figure 22. *Overview of the method, including (1) plot-level model selection and assessment, (2) population inference and maps.*

3.1. Model selection and assessment

Model selection and assessment was achieved using a training-testing approach. The data split was based on a geographical partitioning of the study area (Meyer and Pebesma, 2021). First, the bounding box of the field plots was computed and one of the corners was randomly selected. Then, the 20 % of the nearest plots from that corner were selected and retained as the testing set. The training set was formed with the remaining 80 % of the plots and was used for model selection and evaluation. As the number of auxiliary variables were high and could be affected by autocorrelation issues, the variables were first thinned using a variable reduction approach.

3.1.1. Variable reduction

The *k*-NN predictions are sensitive to the model dimensionality (Breidenbach et al., 2012). A model with a large number of predictor variables would increase the modelling complexity, computation time, and may degrade its performance (Bhanu and Lin, 2003). Furthermore, some auxiliary variables are auto-correlated (e.g., ALS height percentile), and may cause model overfitting problems (Moser et al., 2017).

Highly correlated auxiliary variables were circumvented through a variable reduction approach. The correlation matrix was computed between auxiliary variables and the targeted field attributes. For each field attribute, the auxiliary variables with the highest correlation were selected to initiate a vector of variables. The remaining auxiliary variables were then processed based on their correlation rank (from higher to lower). An auxiliary variable was added to the vector if its correlation with all the vector variables was lower than a threshold (0.7 units) (Dormann et al., 2013). The auxiliary variable common to all the vectors (one vector per field attribute) were then selected to initiate a vector of reduced variables and their average correlation with field attributes was computed. The remaining auxiliary variables were further ranked according to their mean correlation with the field attributes and tested for inclusion in the vector of reduced variables using the same procedure and parameters.

3.1.2. *k*-NN models

Along with the number of variables, *k*-NN model parameters include the number of neighbours, a distance metric and a distance weighting function (McRoberts, 2012). The optimal value of *k* is usually a trade-off between bias and variance (McRoberts et al., 2015a). Following previous researches, models were implemented using a *k* value of 5 (Chirici et al., 2020; Irulappa-Pillai-Vijayakumar et al., 2019). The *k*-NN were tuned for 2 distances metrics and were built using 1 up to 10 auxiliary variables selected using an iterative feature selection algorithm. For both ALS and DAP, the best model was selected from a total of 40 competing models.

Distance metrics included Euclidean (Eq.19) and most similar neighbours (Eq.20) (Crookston and Finley, 2008; Moeur and Stage, 1995). Both distances were computed in a normalized variable space by dividing their mean-centred values with their standard deviation and using an inverse distance weighting function (Eq.21):

$$d_{ij}(euc) = \sqrt{(x_i - x_j)^T (x_i - x_j)} \qquad (\textbf{\textit{Eq.19}})$$

$$d_{ij}(msn) = \sqrt{(x_i - x_j)\, \Gamma \Lambda^2 \Gamma^T (x_i - x_j)^T} \qquad (\textbf{\textit{Eq.20}})$$

$$w_{ij} = \frac{1}{1+d_{ij}} \qquad (\textbf{\textit{Eq.21}})$$

where, d_{ij} (euc) is the Euclidean distance, d_{ij} (msn) is the most similar neighbours distance, x_i is the vector of target auxiliary variables, x_j is the vector of reference auxiliary variables, Λ is the matrix of canonical correlations, Γ is the matrix of canonical vectors of auxiliary data resulting from the canonical correlation between auxiliary data and field attributes, T denotes the transpose of the matrix, and w_{ij} is the weight applied to d_{ij} to compute predictions. While d_{ij} (euc) only relies on auxiliary variables, d_{ij}(msn) also preserves the covariance structure of the field attributes.

Variable selection was performed using an iterative feature selection algorithm applied in both addition and deletion modes (Crookston and Finley, 2008). The algorithm was developed for *k*-NN models and relied on the minimization of the Root Mean Square Error (RMSE, Eq.22) of predictions. The algorithm was applied independently for each distance metric, and for each case, the best 10 variables were selected for further processing.

The nested models made of 1 up to 10 variables were evaluated using leave-one-out cross-validation. For each model, the cross-validated RMSE (Eq.22), mean error (ME, Eq.23) and total error (TE, Eq.24) (Hou et al., 2017; Vega et al., 2021) were computed for both calibration and validation sets based on the following equations:

$$\mathrm{RMSE} = \sqrt{\frac{1}{n}\sum_{i=1}^{n}(y_i - \hat{y}_i)^2} \;;\; \mathrm{rRMSE} = \frac{\mathrm{RMSE}}{\bar{y}} \times 100 \qquad (\textbf{\textit{Eq.22}})$$

$$\mathrm{ME} = \frac{1}{n}\sum_{i=1}^{n}(y_i - \hat{y}_i) \;;\quad \mathrm{rME} = \frac{\mathrm{ME}}{\bar{y}} \times 100 \qquad (\textbf{\textit{Eq.23}})$$

$$\mathrm{TE} = \sqrt{\mathrm{RMSE}^2 + \mathrm{ME}^2} \;;\; \mathrm{rTE} = \frac{\mathrm{TE}}{\bar{y}} \times 100 \qquad (\textbf{\textit{Eq.24}})$$

where y_i is the observed value, $\hat{y}_i$ is predicted value, $\bar{y}$ is the mean of observed values and n is the number of NFI plots.

The optimal model was selected for both ALS and DAP in two steps. First, models exhibiting overfitting were filtered out from the selection. Overfitting was identified using the method proposed by Valbuena et al. (2017). It consisted in computing the ratio between the square error achieved on the cross-validation dataset and the one achieved using the entire train dataset (SSR, Eq.25), and rejecting models having a ratio value above 1.1:

$$\mathrm{SSR} = \frac{1}{n}\sum_{i=1}^{n}(y_i^{cv} - \hat{y}_i) \,/\, \frac{1}{n}\sum_{i=1}^{n}(y_i^{train} - \hat{y}_i) \qquad (\textbf{\textit{Eq.25}})$$

where SSR is the overfitting index, y_i^{cv} are the cross-validated predictions and y_i^{train} are the training predictions.

From the set of remaining models, the models having a rTE within 1% of the lowest rTE were selected and the best model was defined as the one having the lowest number of predictors for model parsimony.

Finally, a *k*-NN was built using the whole train set and evaluated on the test set as an independent performance assessment. Performance measures included both RMSE and ME.

3.2. Statistical inference and mapping

Predictions at the population level were obtained using bootstrap (N = 100). The size of the bootstrap sample was set to the number of field plots. *k*-NN models were trained for each bootstrapped sample and used to predict the entire population of pixels, resulting in 100 predictions for each pixel and forest attribute.

3.2.1. Statistical inference

The population mean (Eq.26) and variance (Eq.27) from the field plots were computed using a simple expansion estimator (Magnussen et al., 2020), and were used to evaluate the *k*-NN performance at the population level:

$$\hat{\mu} = \frac{1}{n}\sum_{i=1}^{n} y_i \qquad (\textbf{\textit{Eq.26}})$$

$$\hat{V}(\hat{\mu}) = \frac{1}{n(n-1)}\sum_{i=1}^{n}(y_i - \hat{\mu})^2 \qquad (\textbf{\textit{Eq.27}})$$

where n is the number of sample plots and y_i is the plot observed value.

The bootstrapped model-based estimator was used to estimate the population parameters from *k*-NN predictions (McRoberts et al., 2022). The mean (Eq.28), bias (Eq.29), and variance (Eq.30) estimators were computed as follow:

$$\hat{\mu}_{boot} = \frac{1}{n_{boot}}\sum_{b=1}^{n_{boot}} \hat{\mu}_{boot}^{b} \qquad (\textbf{\textit{Eq.28}})$$

$$\hat{B}_{boot}(\hat{\mu}) = \hat{\mu}_{boot} - \hat{\mu} \qquad (\textbf{\textit{Eq.29}})$$

$$\hat{V}_{boot}(\hat{\mu}) = \frac{1}{n_{boot}-1}\sum_{b=1}^{n_{boot}}(\hat{\mu}_{boot}^{b} - \hat{\mu}_{boot})^2 \qquad (\textbf{\textit{Eq.30}})$$

where n_{boot} is the number of bootstrap samples, $\hat{\mu}_{boot}^{b}$ is the mean of the boot b, $\hat{\mu}_{boot}$ is the mean of the bootstrap samples.

3.2.2. Map products

The *k*-NN prediction maps were generated for each forest attribute at the grid pixel resolution (30 m) by computing the mean of the bootstrapped predictions. Along with the prediction maps, three additional maps per forest attribute were produced for the assessment of precision, accuracy and reliability.

A map of precision was generated based on the bootstrapped pixel-level predictions. The precision was assessed through the calibration-validation model rRMSEs (Eq.22) and coefficient of variation (CV_{boot}) (Eq.31) of the bootstrapped prediction at pixel level.

$$CV_{boot} = \sum_{i=1}^{n_{boot}} \left(\sqrt{\frac{(x_i - \bar{x})^2}{n_{boot}-1}} / \bar{y} \right) / n_{boot} \qquad (\textbf{\textit{Eq.31}})$$

where, n_{boot} is the number of bootstrap samples, x_i and $\overline{x}_i$ are respectively the prediction for a given sample and the prediction mean over the entire samples. For each pixel, the precision was considered high when CV_{boot} was below calibration rRMSE, intermediate when CV_{boot} was in between calibration and validation rRMSE, and low otherwise. Such a qualitative representation was preferred over a quantitative map for operational reasons.

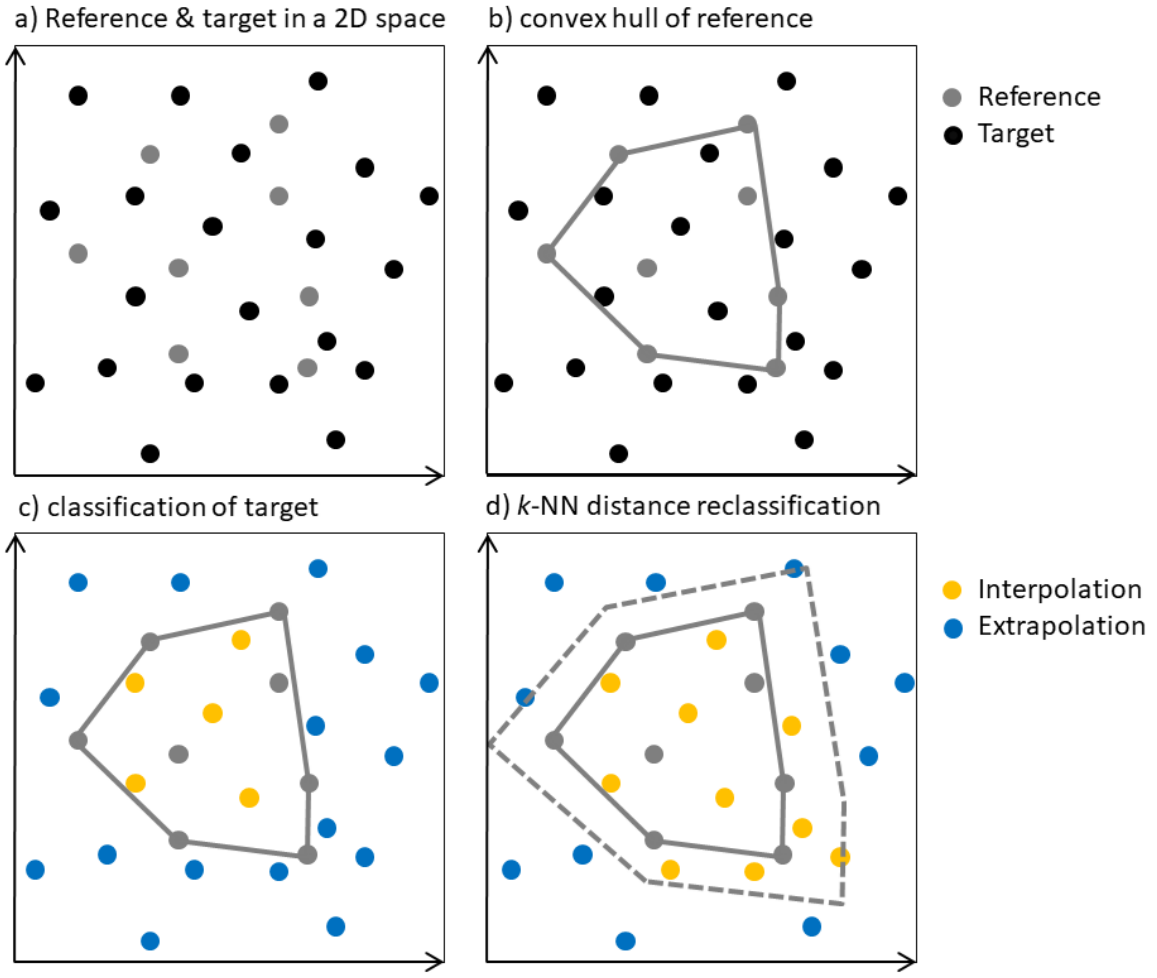

Figure 23. *Scheme of the process of identification and characterisation of extrapolation in a 2D auxiliary variable space: (a) reference (plots) and target (pixels) sets; (b) computation of the convex hull of reference; (c) classification of target into interpolation or extrapolation; (d) reclassification of extrapolated targets using an interpolation distance threshold.*

A map of accuracy was computed from the extrapolation status of the pixels. Since *k*-NN could not extrapolate, accurate predictions could only be expected from interpolated values. Extrapolation was identified in the auxiliary data space, using a convex hull approach (Figure 23) (Barber et al., 1996). The convex hull was built using the auxiliary space describing the field plots. Pixels were then classified as interpolation or extrapolation according to their position with respect to the convex hull (Figure 23.c). The impact of extrapolation on prediction accuracy is expected to be a function of the extrapolation distance. Thus, extrapolated pixels were further classified according to a distance threshold. This threshold was defined as the mean *k*-NN distance of interpolated pixels plus two times its standard deviation. Extrapolated pixels having a *k*-NN distance lower than this threshold were reclassified as interpolated. Finally, the accuracy of pixels was considered high when pixels were classified interpolated and low otherwise.

The third map relates to the reliability of the pixel predictions. From precision and accuracy maps, predictions were considered unreliable irrespective of their precision class when they were found as extrapolated. Otherwise, the reliability was set in accordance with the precision classes (Figure 24).

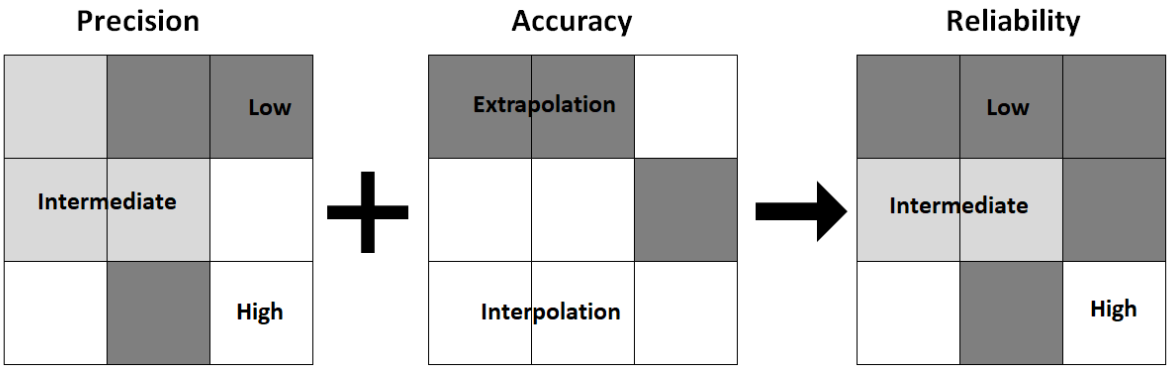

Figure 24. *Scheme of the reliability assessment for a sample of pixel's predictions based on precision and accuracy.*

4. Results

4.1. Model development and assessment

The selected *k*-NN models are presented in Table 6. For ALS, 5 variables were selected using a variable deletion algorithm and the msn distance. The selected variables are the forest type, the Landsat green band and 3 ALS metrics describing the canopy height (i.e. the 50th percentile of the height distribution, corresponding to the median height), the canopy density (i.e., the 4th cumulative percentage of return computed as the proportion of returns above the 4^{h} decile of the height distributions to the total number of returns) and canopy opening (canopy closure ratio). For DAP, the selected model also included 5 variables and was generated using the variable addition algorithm and msn distance. Like ALS, the forest type and the Landsat green band contributed to the model. The 3 remaining auxiliary variables were the short-wave infrared band 1 (SWIR1) from Landsat, and 2 point cloud metrics describing the vertical structure of the canopy (i.e. the standard deviation and the 40th percentile of height distribution).

Table 6. *Parameters of the selected k-NN models for ALS and DAP.*

Dataset	*k*-NN models		Selected variables		
	Variable selection	Distance	Forest map	3D point cloud	Landsat
ALS	Deletion	msn	Forest type	50th percentile of heights 4th cumulative percentage of returns Canopy closure ratio	Green band
DAP	Addition	msn	Forest type	Standard deviation 40th percentile of heights	Green Short-wave infrared 1

Table 7, Table 8, and Figure 25 show the performance of the model with training and testing data. For the ALS-based model, the cross-validated rRMSEs ranged from 35.9 % for BA to 50 % for VI in calibration and from 45.7 % for BA to 63.4 % for VI in validation. The rME was within 0.3 % in both calibration and validation for the three forest attributes surveyed (Table 7). The results achieved for the test set are of the same magnitude as the validation set. The test rRMSEs ranged from 46.2 % to 67.4 % for BA and VI respectively (Table 8). The lowest rME was -3 % for GSV.

For the DAP-based model, the cross-validated rRMSEs ranged from 35.7 % for BA to 48.2% for VI in calibration and from 45.0 % to 61.9% for the same attributes in validation. The rME were slightly greater than those obtained for ALS. The calibration rME ranged from -1.0 % for VI to less than 0.1 % for BA. The validation rME was of the same magnitude, with a minimum value of -0.7% for VI and a maximum of 0.5 % for BA (Table 7). The testing rRMSEs varied from 47.2 % to 64.2 %

for BA and VI respectively. The rME was negative for GSV (-2.2%) and positive for both BA and VI, with the greatest value achieved for VI (4.9%) (Table 8).

Table 7. *Cross-validation model prediction means and errors for ALS and DAP based prediction of growing stock volume (GSV, m^3ha^{-1}), basal area (BA, m^3ha^{-1}), and volume increment (VI, $m^3ha^{-1}yr^{-1}$). Numbers in parenthesis are relative errors in percent.*

Dataset	Forest attribute	Calibration			Validation		
		Prediction Mean	RMSE	ME	Prediction Mean	RMSE	ME
ALS	GSV	159.8	59.3 (37.1)	-0.1 (-0.1)	159.6	76.4 (47.8)	-0.4 (-0.2)
	BA	21.2	7.6 (35.9)	0.1 (0.3)	21.2	9.7 (45.7)	0.1 (0.3)
	VI	5.7	2.9 (50.0)	< 0.1 (0.2)	5.7	3.6 (63.4)	< 0.1 (0.1)
DAP	GSV	159.2	59 (36.9)	-0.6 (-0.4)	159.6	75.2 (47.0)	-0.3 (-0.2)
	BA	21.2	7.6 (35.7)	< 0.1 (< 0.1)	21.3	9.5 (45.0)	0.1 (0.5)
	VI	5.7	2.8 (48.2)	-0.1 (-1.0)	5.7	3.6 (61.9)	> -0.1 (-0.7)

Table 8. *Test model prediction means and errors for ALS and DAP based predictions of growing stock volume (GSV, m^3ha^{-1}), basal area (BA, m^3ha^{-1}), and volume increment (VI, $m^3ha^{-1}yr^{-1}$). Numbers in parenthesis are relative errors in percent.*

Dataset	Forest attribute	Prediction Mean	RMSE	ME
ALS	GSV	158.1	80.4 (49.3)	-4.8 (-3.0)
	BA	20.4	9.4 (46.2)	0.1 (0.3)
	VI	5.2	3.6 (67.4)	-0.1 (-2.2)
BA	GSV	159.7	79.6 (48.8)	-3.5 (-2.2)
	BA	21.0	9.6 (47.2)	0.6 (3.2)
	VI	5.6	3.4 (64.2)	0.3 (4.9)

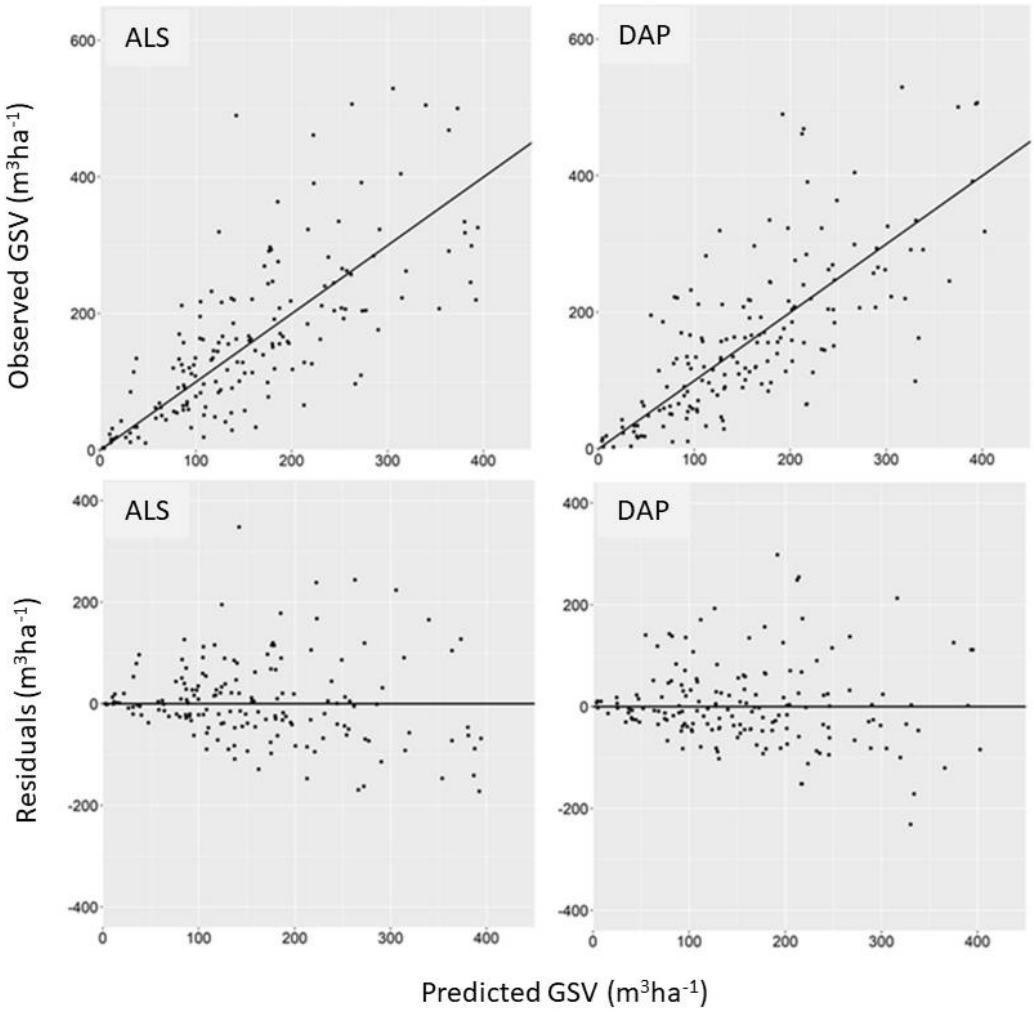

Figure 25. *Graphs of the observed versus predicted growing stock volume (GSV) and of corresponding prediction residuals over the test set for both ALS and DAP based models.*

4.2. Statistical inference and mapping

Population estimates and corresponding maps are presented in Table 9 and Figure 26 and Figure 27. The mean GSV was estimated to 161.9 m^3ha^{-1} and 160.7 m^3ha^{-1} with ALS and DAP respectively (Table 9). Corresponding variances were of 6.4 m^3ha^{-1} for ALS and 5.1 m^3ha^{-1} for DAP. Estimates for BA and VI were of the same order with both models. The largest volumes are predominantly found in public forests, localized in the northern, south-eastern and western part of the study area (Figure 26).

Table 10 showed the distribution of predictions within the three precision classes (see section 3.2.2) for the 3 surveyed forest attributes. For both models, the mean attribute estimations decreased through the precision classes, indicating that lower precisions are associated to the lower attribute values. The mean *k*-NN distances followed the inverse trend, showing the lesser values in the high precision class and the greater values in the low precision class. Overall, the high precision class

account for more than 86 % of the pixels, ranging from 89.9 % (GSV) to 97.2 % (VI) for ALS and from 86.4 % (GSV) to 95.7 (VI) pixels with DAP-based model.

Table 9. *Model-based bootstrapped population mean ($\hat{\mu}_{boot}$), variance ($\hat{V}_{boot}$), and bias ($\hat{B}_{boot}$) of predicted forest attributes with ALS and DAP based models.*

Dataset	Forest attribute	$\hat{\mu}_{boot}$	$\hat{V}_{boot}(\hat{\mu})$	$\hat{B}_{boot}(\hat{\mu})$
ALS	GSV (m^3ha^{-1})	161.9	6.4	0.2
	BA (m^3ha^{-1})	20.8	0.1	< 0.1
	VI ($m^3ha^{-1}yr^{-1}$)	5.6	< 0.1	< 0.1
DAP	GSV (m^3ha^{-1})	160.7	5.1	0.1
	BA (m^3ha^{-1})	20.7	0.1	< 0.1
	VI ($m^3ha^{-1}yr^{-1}$)	5.5	< 0.1	< 0.1

Table 11 showed the ventilation of predictions in accuracy classes. The high accuracy represented respectively 93.7 % and 95.7% of the predictions for ALS and DAP. A major difference between accuracy classes was the mean *k*-NN distance. Low accuracies, which corresponded to extrapolation, exhibited mean *k*-NN distances at least 3 times superior to the high accuracy. Mean estimates tended to be greater in the high accuracy class, indicating that extrapolation mostly affect lower attribute values. A noticeable exception from this trend was observed for GSV predicted using DAP-based model. The mean GSV in the low accuracy class was 19 m^3ha^{-1} greater than the mean GSV in the high accuracy class (i.e. 178.8 versus 159.8 m^3ha^{-1}), showing a possible saturation effect of the model toward the greatest GSV.

The reliability assessment performed through the intersection of precision and accuracy is presented in Table 12 and Figure 27. More than 86.3 % and 83.5 % of the predictions are classified as highly reliable for ALS and DAP respectively (Table 12). On the opposite, low reliability accounted for 4.7 % (VI, DAP) up to 9.5 % (GSV, DAP) of the predictions. Driven by the precision classes, the mean distance increased with decreasing reliability. That said, the low reliability class exhibited mean distances around 2 times greater than the other 2 classes. By comparison with the low precision (Table 10), the low reliability had greater prediction means. For ALS-based model, the GSV in low precision was 21.0 m^3ha^{-1} which increased up to 103.1 m^3ha^{-1} in the low reliability class. Interestingly in DAP, the large GSV found in low accuracy (178.8 m^3ha^{-1}, Table 11) decreased to 93.8 m^3ha^{-1} in the low reliability class (Table 12), indicating that a significant proportion of predictions in this class had low attribute values, and are driven by low precision. Such a result could can also be seen in Figure 27,

which indicated that low precision is predominantly affecting low attribute values while low accuracy is mostly found towards greater attribute values.

Table 10. *Mean predictions, mean k-NN distances and proportions of pixels per precision classes (H: high; I : intermediate; L: low) for both ALS and DAP-based models. The unit of the mean estimates corresponds to the unit of the forest attributes: growing stock volume (GSV, m^3ha^{-1}), basal area (BA, m^3ha^{-1}) and volume increment (VI, $m^3ha^{-1}yr^{-1}$). k-NN distances are unit less.*

Dataset	Attribute	Mean predictions			Mean distance			Pixels (%)		
		H	I	L	H	I	L	H	I	L
ALS	GSV	176.2	47.0	21.0	0.13	0.21	0.25	89.9	5.3	4.8
	BA	22.0	7.0	5.0	0.13	0.21	0.26	92.0	5.4	2.6
	VI	5.7	4.1	1.5	0.13	0.24	0.29	97.2	2.7	0.2
DAP	GSV	179.4	54.5	24.3	0.11	0.15	0.15	86.4	7.8	5.8
	BA	22.3	8.9	4.9	0.11	0.15	0.16	89.6	6.5	3.9
	VI	5.7	2.1	1.6	0.11	0.16	0.20	95.7	3.7	0.5

Table 11. *Mean predictions, mean k-NN distances and proportions of pixels per accuracy classes (H: interpolation; L: extrapolation) for both ALS and DAP-based models. The unit of the mean estimates corresponds to the unit of the forest attributes: growing stock volume (GSV, m^3ha^{-1}), basal area (BA, m^3ha^{-1}) and volume increment (VI, $m^3ha^{-1}yr^{-1}$). k-NN distances are unit less.*

Dataset	Attribute	Mean predictions		Mean distance		Pixels (%)	
		H	L	H	L	H	L
ALS	GSV	163.2	143				
	BA	21.1	15.8	0.12	0.37	93.7	6.3
	VI	5.7	4.3				
DAP	GSV	159.8	178.8				
	BA	20.8	19.9	0.10	0.37	95.7	4.3
	VI	5.6	5.5				

Table 12. *Mean predictions, mean k-NN distances and proportions of pixels per reliability classes (H: high; I : intermediate; L: low) for both ALS and DAP-based models. The unit of the mean estimates corresponds to the unit of the forest attributes: growing stock volume (GSV, m^3ha^{-1}), basal area (BA, m^3ha^{-1}) and volume increment (VI, $m^3ha^{-1}yr^{-1}$). k-NN distances are unit less.*

Dataset	Attribute	Mean predictions			Mean distance			Pixels (%)		
		H	I	L	H	I	L	H	I	L
ALS	GSV	174.0	48.8	103.1	0.12	0.17	0.31	86.3	4.3	9.4
	BA	22.0	7.6	13.6	0.12	0.17	0.34	87.9	4.2	7.9
	VI	5.7	4.0	4.2	0.12	0.19	0.37	91.7	1.9	6.4
DAP	GSV	177.2	53.7	93.8	0.1	0.12	0.24	83.5	7.0	9.5
	BA	22.2	8.8	13.2	0.1	0.13	0.26	86.4	5.8	7.7
	VI	5.7	2.0	5.1	0.1	0.13	0.35	92.0	3.3	4.7

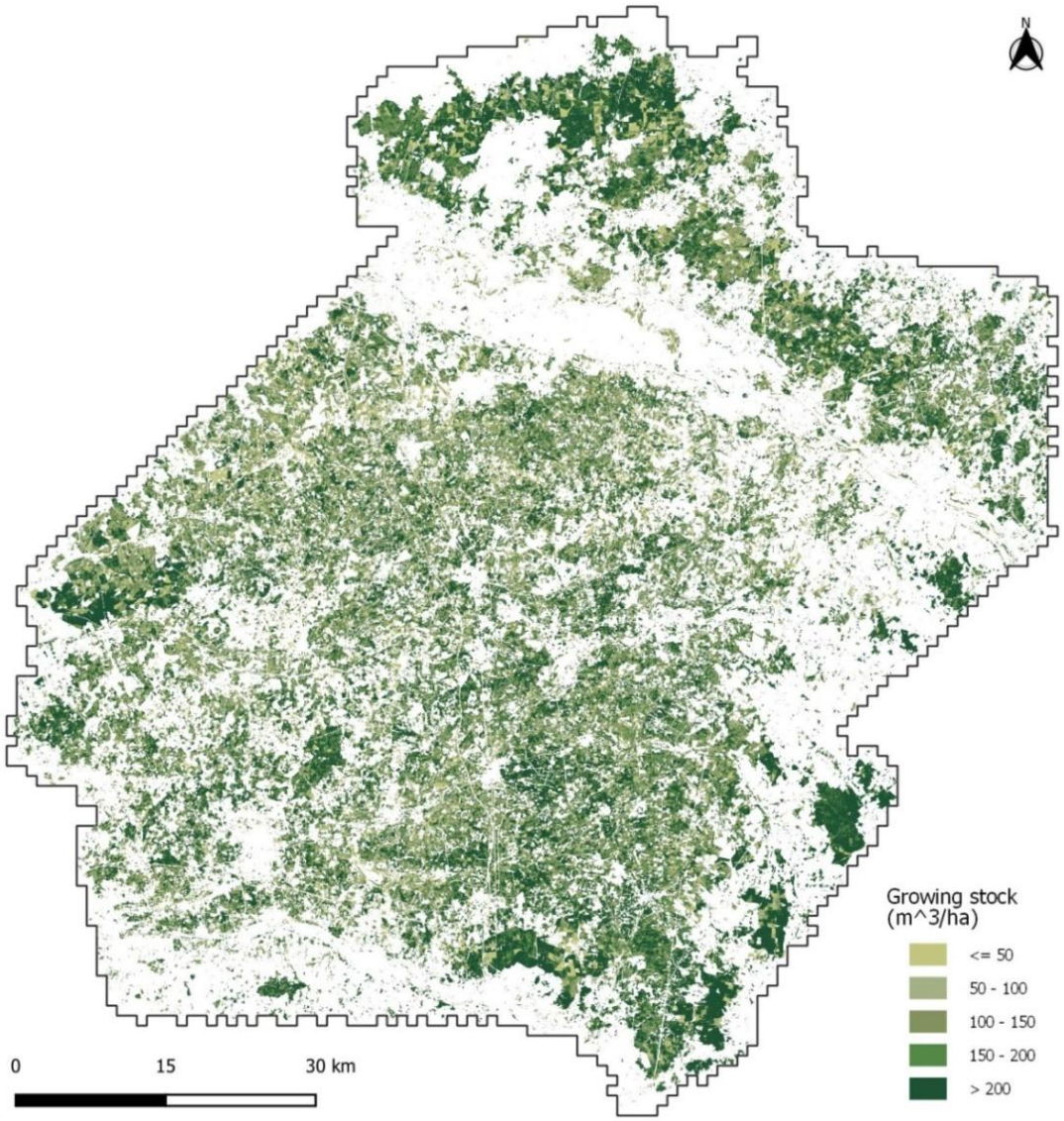

Figure 26. *Map of ALS growing stock volume predictions at 30 m spatial resolution.*

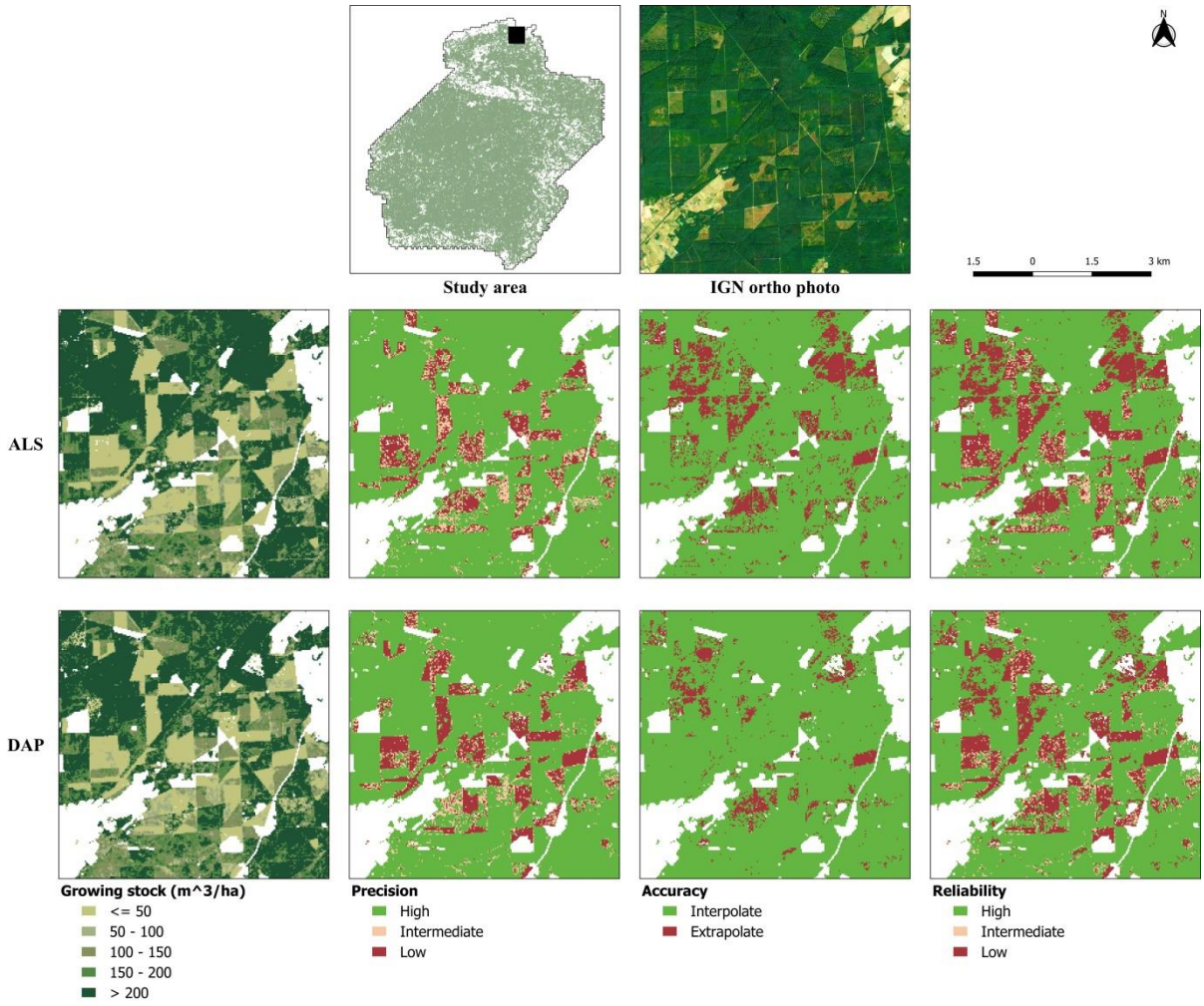

Figure 27. *Map of predicted growing stock volume, and corresponding precision, accuracy and reliability, for both ALS and DAP based models.*

5. Discussion

5.1. Model development and assessment

In this study, models based on ALS and DAP included information from the three auxiliary data sources considered. The forest type information obtained from IGN forest map is a key attribute for differentiating structural and functional traits (Irulappa-Pillai-Vijayakumar et al., 2019). Landsat 8 green band acquired between 0.53 and 0.59 µm and short-wave infrared band 1 (1.57-1.65 µm) emerged as the most influential optical remote sensing variables. Astola et al. (2019) found that Landsat 8 visible green band was ranked first for predicting GSV and BA in the boreal forest of Finland. As emphasized by Cohen and Goward (2004), the SWIR1 band provided information about the vegetation and ground humidity and could be associated here with productivity gradients. The higher number of 3D variables selected in the models is associated with the high correlation between the vertical distribution of vegetation and the major forest attributes (Næsset, 2002a). ALS data convey a higher amount of information related to the vertical distribution of the vegetation, which could explain why a higher number of ALS metrics (3 metrics) were selected compared to DAP (2 metrics) data (Filippelli et al., 2019). DAP point clouds are restricted to the outer canopy structure and could not provide information about the vertical distribution of vegetation (St-Onge et al., 2008; White et al., 2013). Similar trends in the number of auxiliary variables were also reported by Järnstedt et al. (2012).

For the estimation of forest resources, Chirici et al. (2016) and Cosenza et al. (2021) reported that *k*-NN models with 5 nearest neighbours and Euclidean distance performed better than any other *k*-NN configuration. Here, the selected models were based on the msn distance. The higher performance of msn over Euclidean could be explained by the fact that msn distance integrates information from the field attributes. That said, this could make *k*-NN models less flexible to predict field attributes which were not considered during calibration. From investigating over 260 studies, Chirici et al. (2016), reported an average rRMSE of 37 % (±32 %) for growing stock volume, biomass and carbon stock. With test errors ranging from 46 % (ALS, BA) to 67 % (ALS, VI), our results are in the upper range of results reported by Chirici et al. (2016). The large errors achieved here could be explained by the model selection method, which emphasize on model parsimony (Pestov, 2013), and reduction of overfitting (Valbuena et al., 2017). Indeed, numerous studies included a large number of auxiliary variables in their models (Beaudoin et al., 2014; Nurminen et al., 2013), which tends to reduce the variance at the expense of a possible risk of model overfitting and bias. Part of our error could also be explained by positioning precision of the field plots (Fadili et al., 2019), as well as the complexity of the forest structure studied, with mixture of conifers and hardwood stands and various management strategies from coppice stand to even-aged ones, and uneven-aged stands resulting from the transition from coppice to even-aged stands (Jarret, 2004). Regarding field attributes, the larger errors achieved for VI with respect to both GSV and BA could be explained by the nature of the attribute. VI is

computed from volume and the 5 year radial increment, thus including a temporal dimension that is not well captured with the auxiliary data used. As shown in Irulappa-Pillai-Vijayakumar et al. (2019), the estimation of such flux-related attribute could be improved by taking into account auxiliary data from various points in time.

5.2. Statistical inference and mapping

In line with the model's performances, the population estimates from both ALS and DAP models were of the same range. This result is in agreement with previous studies, which also indicated that the performance of DAP and ALS based predictions of forest attributes are similar (Bohlin et al., 2012; Gobakken et al., 2015; Järnstedt et al., 2012; Nurminen et al., 2013). This highlights the capability of DAP to compete with ALS in the estimation of major forest attributes. The large spatial coverage of aerial surveys and their high renewal rates in many countries makes DAP a serious competitor to ALS when a high resolution DTM is available (St-Onge et al., 2008). The availability of time series of aerial photographs opens up the possibility to further improve the variance of estimates of forest attributes related to fluxes such as VI (Irulappa-Pillai-Vijayakumar et al., 2019) and could also be an integral part of a forest monitoring systems (Ginzler et al., 2019).

Nevertheless, the inflated variance observed for the GSV predicted with ALS was unexpected and questioned the quality of the model at population level. A possible explanation could be found in the *k*-NN distances and amount of extrapolation. The ALS model showed larger mean *k*-NN distances than it's DAP counterpart (Table 12). Also, mean *k*-NN distances are inflating faster with decreasing reliability (i.e.. from high to low) with ALS than with DAP (Table 12). This inflation in distances suggested that the choice of neighbours during the resampling process was more variable with ALS, thus contributing to an increased variance at the population level. This phenomenon was accentuated by the higher proportion of extrapolation with ALS (Table 11). A possible reason for this result may be associated to the nature of the data. As ALS is more sensitive to the inner-crown canopy structure (Filippelli et al., 2019), one might consider that the variability brought in the auxiliary variable space could have introduced uncertainty in the neighbourhood selection during the resampling, contributing to an increase variance at the population level. The results of the inverted models, generated by applying the auxiliary variables selected with one model to the other, and provided in Table A1 and Table A2, showed that predictions with ALS remained more variables, corroborating this hypothesis.

The high-resolution maps complement the bootstrap model-based estimates, by providing information about the localisation of the forest resources as well as their reliability. These maps can be anticipated to be increasingly relevant for future forest management and planning. The *k*-NN predictions were found to be imprecise in young stands and along forest transitions (Figure 27), which are not measured in the French NFI. Indeed, with a minimum circumference at breast height of 23.5 cm, forest stands below 10 m height are very poorly described. Extrapolation was also found in those

areas. More importantly, with the use of the convex hull approach, we observed that an even higher proportion of the pixels were extrapolated in highly stocked stands. This highlights a possible saturation of the model towards the upper values of the targeted forest attributes. It underlines the need to further study the magnitude of such a bias and the possibilities to correct it. Interestingly, the mean distance to the closest neighbours is significantly different for interpolation and extrapolation, suggesting that the extrapolation distance could serve as a metric to correct extrapolation bias in *k*-NN models (Magnussen et al., 2010).

A limitation of our results comes from the binary assessment of the extrapolation. We used the entire calibration domain to identify the extrapolated pixels, resulting in a binary map. A more robust but time-consuming approach would be to assess extrapolation both at the plot level and population level by taking advantage of the bootstrap properties. Computing extrapolation for each bootstrap sample would provide a continuous evaluation of extrapolation (i.e. varying from 0 = no extrapolation; to the number of bootstrap samples = full extrapolation). Such information could be useful in complement the *k*-NN distances to analyse the relationship between extrapolation and errors at plot level (Meyer and Pebesma, 2021), to identify outliers at both plot and population level (Cook, 1977) and develop appropriate bias-correction methods.

6. Conclusion

This research is a step ahead to connect prediction and reliability maps within an inferential framework. The approach relies on bootstrapped predictions to infer population parameters in a model-based framework and provide high-resolution maps of forest attributes with reliability assessment. The approach was developed for *k*-NN models, owing to their capabilities to predict multiple forest attributes in a single model. To account for the incapacity of *k*-NN to extrapolate, we further adapted the convex hull approach to measure the accuracy of prediction. Bootstrapped predictions with precision and accuracy were combined to provide a measure of prediction reliability at the unit level (grid cell or pixel). The high-resolution prediction maps will assist forest managers in the localisation of forest resources, and subsequently, the reliability maps (extrapolation and precision) will allow for judgments about whether the predicted forest attributes map is accurate enough for decision making.

Acknowledgements

This work was supported by the French PIA project “Lorraine Université d’Excellence”, reference ANR-15-IDEX-04-LUE, through the project Impact DeepSurf and the Labex ARBRE (ANR-11-LABX-0002-01). The authors deeply thank David Sterratt and C Bradford Barber for their help with the convex-hull computation with the Quickhull algorithm and the R Geometry package. We also greatly thank Jean-Romain Roussel for his support with R lidR package.

7. Appendix A. Inverted model outputs

Table A1. *Test model prediction means and errors for inverted ALS and DAP based predictions of growing stock volume (GSV, m^3ha^{-1}), basal area (BA, m^3ha^{-1}), and volume increment (VI, $m^3ha^{-1}yr^{-1}$). Numbers in parenthesis are relative errors in percent. Inverted models were built using auxiliary data selected for ALS to DAP and conversely.*

Dataset	Forest attribute	Prediction Mean	RMSE	ME
ALS	GSV	163.8	84.4 (51.8)	0.8 (0.5)
	BA	21.3	10.1 (49.4)	0.9 (4.6)
	VI	5.7	3.7 (69.2)	0.4 (7.2)
BA	GSV	163.8	80.5 (49.4)	0.6 (0.4)
	BA	21.4	9.7 (47.4)	1 (4.8)
	VI	5.7	3.7 (69.4)	0.4 (8.4)

Table A2. *Model-based bootstrapped population mean ($\hat{\mu}_{boot}$), variance ($\hat{V}_{boot}$), bias ($\hat{B}_{boot}$), of predicted forest attributes with inverted ALS and DAP based models. Inverted models were built using auxiliary data selected for ALS to DAP and conversely.*

Dataset	Forest attribute	$\hat{\mu}_{boot}$	$\hat{V}_{boot}(\hat{\mu})$	$\hat{B}_{boot}(\hat{\mu})$
ALS	GSV (m^3ha^{-1})	162.3	7.2	0.6
	BA (m^3ha^{-1})	20.9	0.1	0.1
	VI ($m^3ha^{-1}yr^{-1}$)	5.6	< 0.0	< 0.0
DAP	GSV (m^3ha^{-1})	161.8	5.3	-0.1
	BA (m^3ha^{-1})	20.8	0.1	< 0.0
	VI ($m^3ha^{-1}yr^{-1}$)	5.5	< 0.0	< 0.0

Chapter IV: Forest resource predictive maps: a bridge for small area estimation of forest disturbance areas

Authors: Ankit Sagar[1, 2, 3], Cédric Vega[2, *], Olivier Bouriaud[2, 4], Jean-Pierre Renaud[2, 5]

[1]Université de Lorraine, Faculté des Sciences et Technologies - Campus Aiguillettes, *Nancy, France*

[2]ENSG, IGN, INRAe, Laboratoire d'Inventaire Forestier, *Nancy, France*

[3]UMR SILVA INRAe-AgroParisTech-Université de Lorraine, *Nancy, France*

[4]Ștefan cel Mare University of Suceava, *Suceava, Romania*

[5]Office National des Forêts, Pôle Recherche Développement Innovation, *Nancy, France*

[*]corresponding author

The article is the author's version of the submitted manuscript.

Authors' contributions

Cédric Vega (CV), Ankit Sagar (AS) and Jean-Pierre Renaud (JPR) planned the study. AS, CV and JPR contributed to data acquisition. AS, CV and JPR developed the R-code for data processing and modelling. CV designed the grid weighting scheme and Olivier Bouriaud (OB) provided the estimators. CV, JPR, AS and OB were responsible for interpreting the results. All authors contributed to drafting the work and have approved the submitted version.

Abstract

Forests are increasingly under the pressure from climate change. In Europe, recurrent droughts are weakening species and promote biotic disturbances. Since 2017, the North-Eastern part of France is experiencing severe bark beetle outbreaks affecting spruce and fir. While remote sensing data have made it possible to asses and monitor the spatial evolution of outbreaks, the assessment of associated resource is still lacking. Here we propose to use a small area estimation procedure that combine independently generated bark beetle outbreak and forest resource maps, to evaluate the amount of forest resource in outbreak areas. The forest resource map was generated for 2021 using NFI plots and auxiliary data from lidar and Sentinel 2 data, and a k nearest neighbour model. The bark-beetle maps were generated using times series of Sentinel 2 data from 2018 to 2022. The period 2018-2020 was used to control outliers in the modelling phase. The period 2021-2022 supported the small area estimation process to assess the total amount and relative errors in impacted growing stock volume and basal area. As a secondary objective, we evaluated the performance of the general forest map as opposed to a specific resource map developed for spruce and fir. Overall, 1139 ha of the forest area was affected in 2021-2022, corresponding to 494,213 m^3 (general model) and 505,401 m^3 (specific models) of growing stock volume. Associated errors ranged from 2.2 % (general model) to 2.6 % (specific model). The mean volume of outbreaks was found to be 67 m^3 above the mean volume of spruce and fir over the study area showing that mature stands are more sensitive to infestation. The regular renewal of 3D models through photogrammetric means could allow renewing the forest map every 3 years in France opening possibilities to monitor the dynamic of the resource impacted by various disturbances.

Keywords: multisource forest inventories, statistical inference, forest attribute maps, forest disturbances, insect outbreak, LiDAR.

1. Introduction

Multisource National Forest Inventory (MSNFI) is a convenient technique to gain precision and improve National Forest Inventory (NFI) estimates of forest resources (e.g. population mean, total) in those areas which have few to no field inventory plots (Tuominen et al., 2020). The technique relies on a statistical combination of NFI data with spatially continuous auxiliary data (e.g. thematic maps, remote sensing data) (Tomppo et al., 2008b), and can also provide wall-to-wall maps of forest resources to complement population estimates (Esteban et al., 2019; Saarela et al., 2020; Sagar et al., 2022). These maps provide detailed forest resource information at a spatial resolution that approximates the field plot area, and are particularly useful for sustainable forest management and other forest-related applications, including harvest monitoring, habitat modelling, or evaluating the impacts of climate change (D'Amico et al., 2021; Hauglin et al., 2021).

With ongoing climate changes, the frequency of forest disturbance events, such as windstorms, fires, droughts, and insect outbreaks, is increasing worldwide (Canelles et al., 2021). These events are important drivers of local and global change in forest ecosystems, as they disrupt their composition, structure and functioning, and alter the forest resource availability (Seidl et al., 2017). In order to inform decision-making in the aftermath or during such events, forest mangers require precise estimates of impacted forest attributes, preferably in the form of maps that pinpoint the location and quantity of impacted resources (Bright et al., 2013; Renaud et al., 2017).

While methods are available to identify and map the spread of forest disturbance areas (Abdullah et al., 2019; Lausch et al., 2013; Myroniuk et al., 2020), techniques for estimating the impacted forest resources are rarely explored. In order to do so, map intersection of a MSNFI forest resource map with one of forest disturbances provides a means of estimating the amount of impacted forest resources. However, estimation in disturbance areas is not a straightforward task, because these areas are of varying shapes, sizes and are spatially disjoint (Seidl et al., 2017). Usually in such areas, the NFI samples size is inadequate or even absent, resulting in estimates which lack the precision required to support decision-making processes (Vega et al., 2021). Small area estimation (SAE) techniques in such areas can cover these problems.

SAE techniques have gained popularity in forest inventory applications due to their ability to provide precise estimates of forest resource at higher spatial resolutions (Gaines and Affleck, 2021; Stanke et al., 2021). The technique has been mainly used in improving the precision of estimates at administrative (Breidenbach et al., 2010; Vega et al., 2021) or management (Hill et al., 2018) units, but marginally been used in SAE of forest fires (Gaines and Affleck, 2021), and forest land removal (Coulston et al., 2021). The precision improvement is achieved by "*borrowing strength*" of NFI and auxiliary data from other similar areas to increase the effective sample size (Dettmann et al., 2022). This "*borrowing*" process is arranged by a statistical model to obtain a measure of estimation precision (Frescino et al., 2022; Jiang and Rao, 2020).

The choice of the statistical model or estimation framework depends on the characteristics of the disturbance areas and the availability of field plots within those areas. In the case of large patches of disturbances, such as those resulting from large fires or extensive windstorms, the amount of NFI plots available may be sufficient for design-based estimators (Gaines and Affleck, 2021) or even model-assisted estimators (Bell et al., 2022; McConville et al., 2020). Conversely, disturbances occurring at smaller scales or exhibiting heterogeneous spatial patterns, such as those resulting from insect outbreaks (Bright et al., 2012; Li et al., 2021), may require different estimation approaches due to an insufficient amount of NFI plots. In such small areas, model-based estimators can produce estimates of substantial quality even in the absence of NFI plots (Frescino et al., 2022). While estimating for forest land removal in South-Eastern US, Coulston et al. (2021) have reported higher estimation precision obtained with model-based estimator than with direct design-based estimators. Moreover, Saarela et al. (2020) and Sagar et al. (2021) showed that model-based estimators can be used for mapping forest attributes of interest and produce a corresponding map of prediction reliability. The reliability map comes handy to detect modelling issues when disturbance event is continuous over space and time.

The objective of this research was to develop a model-based SAE approach for estimating forest resources impacted by forest disturbance events. The proposed approach relies on the combination of MSNFI forest resource maps with independently generated disturbance map. The specific focus of this study is on the ongoing bark beetle outbreak occurring in the Vosges forest (Hlásny et al., 2021; Piedallu et al., 2023). The approach aimed to evaluate two major forest attributes, namely growing stock volume (GSV) and basal area (BA), using auxiliary data from forest maps, 3D point cloud data from airborne laser scanning (ALS), and metrics from Sentinel-2 remote sensing images. Since the bark beetle primarily attacks coniferous species, a secondary objective of this research was to compare the performance of a general model based on all NFI plots to a specific model based only on spruce and fir dominated field plots.

2. Materials

2.1. Study site

The study was carried out in the Vosges mountainous forest, located in the North-East region of Grand Est, France (Figure 28). The area covers 3,612 km^2 which extends from 6.57° to 7.50° East longitude and 48.01° to 48.89° North latitude. The terrain of the area is predominantly mountainous, with elevations ranging from 200 to 1424 m and slopes mostly exceeding 30° (Giacona et al., 2018). The area is characterized by temperate oceanic climate (Minářová et al., 2018) with mean annual temperature between 6° and 11° C, and mean annual precipitation between 500 and 2000 mm. About 64% (2,305 km^2) of the study area is covered with forests. Forested areas are dominated by coniferous stands (51%) mainly of fir and spruce (i.e., *Abies alba* and *Picea abies)* found at higher altitudes. Pure broadleaved stands on the low altitude account for 22% of the forest area and are dominated by beech and oak *(Fagus sylvatica* and *Quercus petraea)*. The remaining forest area is covered by a mixed stand (27%) of coniferous and broadleaved.

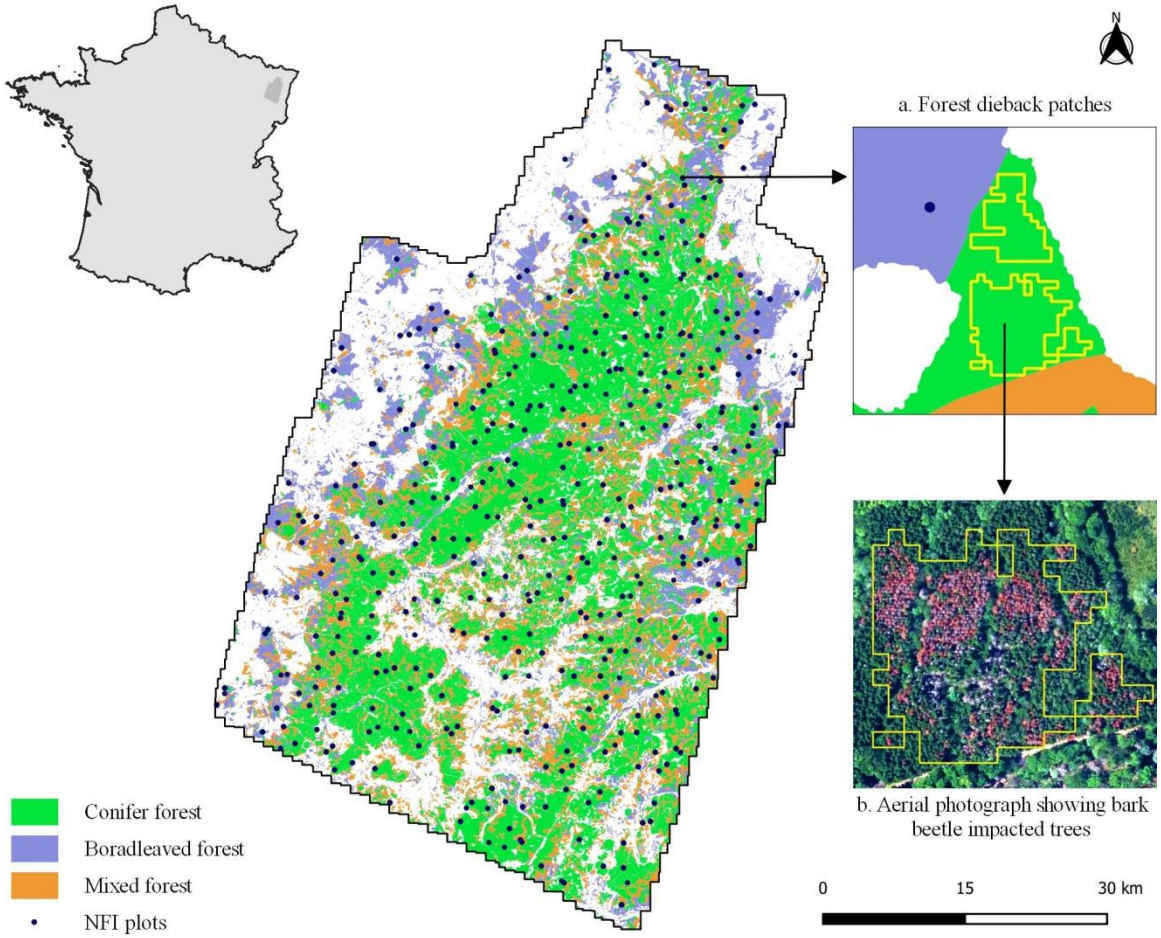

Figure 28. *Location of the study site and spatial distribution of the NFI plots inside the forest types. Subfigures (a and b) are showing a part of bark beetle-impacted forest outbreak patches.*

2.2. NFI data

The study area includes 430 NFI field plots from the aggregation of five annual samples acquired between 2016 and 2020. This 5-year time interval aligns with the standard practice of the French NFI for generating official statistics, which is also followed by many other NFIs (Robert et al., 2009).

Field information is collected within four concentric circular plots of radii 6, 9, 15, and 25 m. Tree measurements are conducted within the first three concentric plots. Trees are categorized based on their circumference at breast height (CBH at 1.3 m). Small trees with a circumference in the range of [23.5–70.5 cm [are measured on the 6 m radius plot, medium-sized trees with a circumference in the range of [70.5–117.5 cm [are measured on the 9 m radius plot, and large trees with a circumference equal to or greater than 117.5 cm are measured on the 15 m radius plot. Additionally, tree measurements also include information on species and state (dead or alive). Tree height and diameter increment during the last five years are collected for a sub-sample of trees. Tree attributes such as stem volume up to 7 cm in diameter and stem volume increment are computed from field measurements using NFI's species-specific allometric models. Detailed information regarding data collection and processing can be found in Hervé (2016) and Hervé et al. (2014).

For this study, two forest attributes were considered: growing stock volume (GSV, m^3ha^{-1}) and basal area (BA, m^2ha^{-1}). The plot statistics are presented in Table 13.

Table 13. *Number of NFI plots (N), mean and standard deviation (SD) of GSV (m^3ha^{-1}) and BA (m^2ha^{-1}) for training and testing set in general and specific model. Training and testing sets are described in section 3.3.*

Model	Forest attribute	All plots			Training plots			Testing plots		
		N	Mean	SD	N	Mean	SD	N	Mean	SD
General	GSV	430	308.5	208.3	344	317.1	211.2	86	274.1	193.4
	BA		30.7	15.2		31.4	15.3		27.9	14.5
Specific	GSV	176	369.2	215.7	141	360.6	209.0	35	403.8	240.6
	BA		34.9	14.7		35.0	14.3		34.6	16.5

2.3. MFI data

Bark-beetle related sanitary logging information was obtained from management forest inventory (MFI) data conducted by the National Forest Office (ONF) and used for independent validation purpose. The data consists in an extraction from ONF databases logging operations (ONF, Regis Bindner, pers. com.), which account for harvesting following disturbances and are

predominately, related to bark-beetle in the Vosges area. In Table 14, stand volumes are aggregated by ONF districts and harvested volumes are distinguished between normal, and salvage loggings. Note that estimates of salvage loggings are expected to overestimate the true sanitary volume, as damaged stands are often completely harvested even if only a proportion of the stand is impacted. Over the study area, the estimates from 4 ONF districts (that include 159 forests) are summarised in Table 14.

Table 14. *Harvested volumes of fir and spruce in 2021 for the 4 ONF district of the area of interest. The type of harvests was also recorded (regular cuts or salvage for sanitary reasons).*

ONF District	Number of forests	Harvested volume (m^3)	
		Total	Salvage
8665	20	16 220	5 437
8670	81	123 600	44 214
8683	32	32 484	31 860
8692	26	83 817	69 112

2.4. Auxiliary data

Along with the NFI data, four freely available auxiliary data were also used in this study. These data include: (*i*) a forest map, (*ii*) ALS data, (*iii*) Sentinel-2 optical data, and (*iv)* bark beetle outbreak maps. The timeline of these dataset is presented in Figure 29.

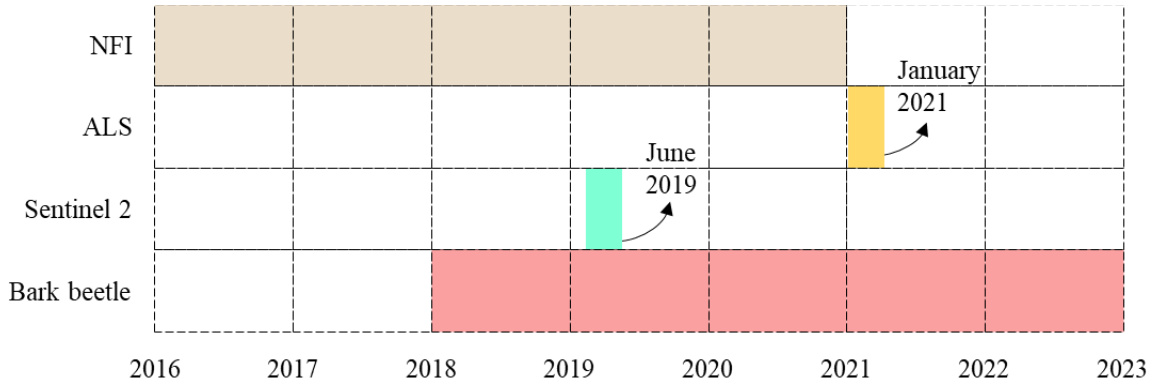

Figure 29. *A timeline showing the various datasets used in the study. The distinct colors on the timeline correspond to their respective acquisition year or date.*

2.4.1. Forest map

The forest map (BD-Forêt® version 2.0) is a freely available vector map provided by the National Institute of Geographic and Forest Information (IGN, *https://geoservices.ign.fr/*, last consulted June

03, 2023). The map provides geographical location, quantitative (area), and qualitative (composition, 32 classes) description of forest stands of at least 0.5 hectares.

2.4.2. ALS data

The airborne laser scanning (ALS) data was acquired by IGN in January 2021 using a Leica ALS70 laser scanner. The scanner operated at an altitude of 1,797 m above ground level (AGL), with a pulse repetition frequency of 309 Hz and a scanning frequency of 35 Hz. The maximum scan angle was 25°, and the point density was 8.3 pts. m^{-2}. The preliminary processing of the lidar point cloud was done at IGN using Terrasolid's Terrascan software (*www.terrasolid.com*) and delivered as a 1 × 1 km tile.

Ground classified points were used to generate a 1 m resolution digital terrain model (DTM) through inverse distance weighted interpolation. The elevation of the points above the ground was converted into height by subtracting the corresponding values from the DTM. Subsequently, the normalized point cloud data was used to generate a 1 m canopy height model (CHM) by selecting the maximum point height per pixel. In cases where pixels did not have values, interpolation was performed by averaging the values of the eight neighbouring pixels (Vega et al., 2016).

2.4.3. Sentinel-2 data

Two images from Sentinel-2 satellite acquired on 29 June 2019 were used in this study. The images were obtained from the Theia portal (*www.theia-land.fr*) and were processed to level 2A products. This processing level included orthorectification, atmospheric correction, and cloud detection with a shadow mask (Hagolle et al., 2015). The data included spectral bands with spatial resolutions of 10 m (blue, green, red), 20 m VNIR (visible and near infrared; 4 bands), 10 m VNIR (1 band), and 20 m SWIR (short wave infrared; 2 bands).

2.4.4. Forest outbreak map

Bark-beetle outbreak maps were generated from 2018 to 2022 using the ForDead method (Dutrieux et al., 2020) and obtained from the Theia platform (*www.theia-land.fr*), for the stands dominated by spruce and fir according to BD Forêt®. The method uses time series of CR_{SWIR} (Continuum Removal $_{SWIR}$; Figure 30) vegetation indices to detect vegetation anomalies. CRswir relies on a convex-hull fit and accounts for the differences between SWIR1 and SWIR 2 bands with respect to the NIRa band, providing information about water stress.

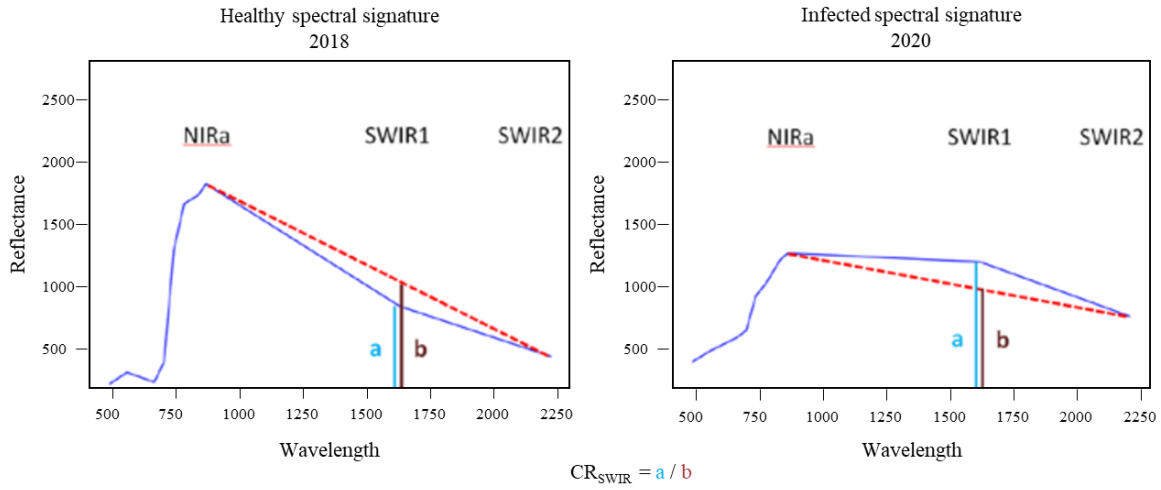

Figure 30. *Illustration of the calculation of the CR_{SWIR} index on a spectral profile corresponding to a "healthy" stand and an "impacted" stand profile (adapted from Dutrieux et al. 2020).*

Within the spruce and fir stands mask, bare ground and clouds are identified to filter out non-vegetation pixels. Then, a harmonic model is fitted to 2 years of Sentinel-2 data collected prior to the bark-beetle event, and anomalies are detected by comparing the actual vegetation index with the predicted index from the harmonic model (Dutrieux et al. 2020). These anomalies are accumulated over the year and classified into four classes. Class 1 and 2 consist of pixels with one or two successive anomalies detected, respectively. Class 3 includes pixels affected by at least three consecutive anomalies and is considered as outbreak cells. Lastly, class 4 consists of pixels where anomalies have been detected before being identified as bare ground, indicating sanitary logging. It should be noted that anomalies can be reversed (i.e., from outbreak to a healthy state). For example, it could be the case if three successive anomalies are detected at the beginning of the time series, followed by three successive non-detections. More detailed information about the method could be find in Dutrieux et al. (2020). The source code of the method is available at the following address: *https://fordead.gitlab.io/fordead_package/* (last consulted, May 21, 2023).

3. Methods

3.1. NFI data filtering

NFI data were collected up to 4 years before the ALS data acquisition (i.e. 2016 - 2020). To ensure that none of the NFI data were affected by bark-beetle outbreaks between the field and the ALS acquisition, the NFI plot positions were intersected with the ForDead Maps from 2018 to 2020. NFI plots falling within the outbreak areas were discarded from the analysis to maintain consistency between the field data and auxiliary data used for generating the resource maps.

3.2. Feature-level Auxiliary data fusion

Auxiliary data processing was performed at a spatial resolution of 30 m to match with the diameter of the NFI plots. A computation grid with a 30 m resolution was set according to the Lambert conic projection using Lambert-93 geodetic system (EPSG: 2154). The origin of the grid was defined as the origin of the coordinate system, and the extent of the grid fixed according to the bounding box of the area of interest. Auxiliary variables/features derived from the auxiliary data were fused within this grid for modelling purposes. The following sub-section provides a detailed description of the auxiliary data processing.

BD Forêt® was used to classify each grid cell into forest or non-forest. Cells whose centre was located within the boundaries of BD Forêt® polygons were classified as forest, otherwise non-forest. Non-forest cells and cells partially inside the BD Forêt® were discarded from the computation domain. Furthermore, a forest type (conifer, hardwood, or mixed) was affected for each cell using the corresponding polygon's attributes (Irulappa-Pillai-Vijayakumar et al., 2019).

Two types of features were extracted from the ALS data: point-based and raster-based. Point-based features were computed for each grid cell using the first return points above 5 meters height above ground. These features included: minimum, maximum, and mean height, along with the standard deviation, skewness, kurtosis, and entropy of the height distribution. Additionally, the percentage of returns above the mean height, the percentile of the height distribution, and the cumulative percentage of return were also computed (Roussel et al., 2020).

On the other hand, given that the study area represents a mountainous region, a set of raster-based topographic features was derived using the DTM. These features included the mean and standard deviation of altitude and slope of the terrain. Another set of raster-based features was computed using the CHM, which included: Rumple index, gap area, gap ratio, total inner volume, total outer volume, canopy inner volume, canopy outer volume, gap inner volume, and gap outer volume (Vega et al., 2016). Computational details are provided in Table A3.

All spectral bands with a spatial resolution greater than 10 m were resampled to a resolution of 10 m. The resampled images were then mosaicked and aggregated to a 30 m resolution. Along with 10 spectral bands, 17 vegetation indices were computed as auxiliary variables (Sonobe et al., 2018). These indices included: Atmospherically resistant vegetation index, advanced vegetation index, canopy chlorophyll content index, chlorophyll index green, disease-water stress index, enhanced vegetation index, green normalized difference vegetation index, modified chlorophyll absorption in reflectance index, modified soil adjusted vegetation index, moisture stress index, normalized difference moisture index, normalized difference red-edge, normalized difference vegetation index, normalized difference water index, pigment specific simple ratio, simple ratio and visible atmospherically resistant index green. Computational details are provided in Table A4.

For the bark-beetle analysis, the period following the ALS acquisition was selected for estimating the amount of forest resource impacted by bark-beetle infestation (i.e., 2021 and 2022). The estimation domain was defined as the area formed by ForDead's pixels of classes 3 and 4. A computation grid cell was classified as disturbed if it contained at least one outbreak pixel. Furthermore, for each cell, the proportion of the surface impacted was computed using an area-weighted approach (Eq.32) (Hill et al., 2021):

$$prop_{outbreak} = \frac{\text{area}_{outbreak}}{\text{area}_{grid}} \quad \textbf{(Eq.32)}$$

where, $prop_{outbreak}$ is the proportion of outbreak area in the grid cell, $\text{area}_{outbreak}$ is the total outbreak area in one grid cell and area_{grid} is the area of one grid cell.

Note that the same set of features was extracted for the cells centred on each NFI plot for the model development process.

3.3. Model selection

The workflow of model selection and assessment is presented Figure 31.

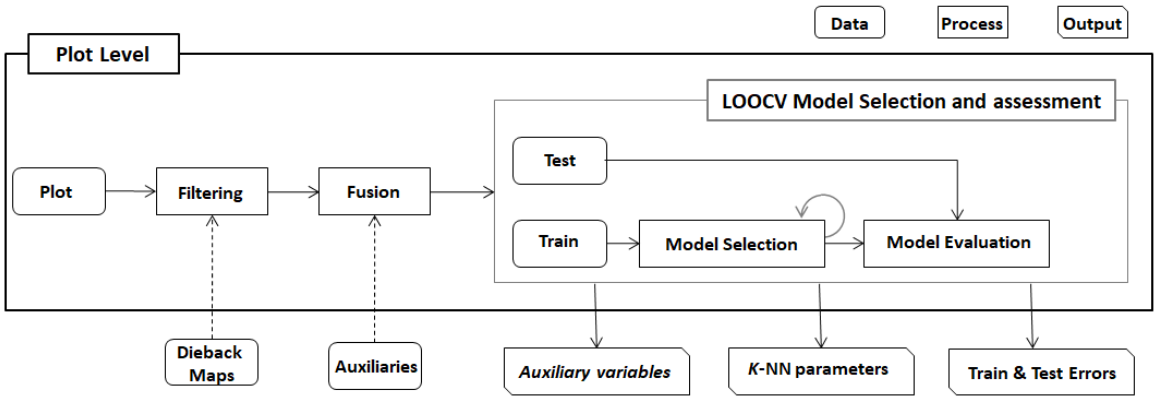

Figure 31. *Workflow of the plot-level model selection.*

The relationship between NFI forests attributes and auxiliary data was investigated using a non-parametric *k*-nearest neighbour (kNN) model. Such models are widely used in MSNFI because they do not rely on assumptions regarding the distribution of the variables, can predict multiple forest attributes at once, and preserve the covariance structure of the variables (Kim and Tomppo, 2006). Also kNN model relies on a limited set on parameters:(number of neighbours (k), distance metric, weighting function, set of auxiliary variables) making them attractive for modelling purposes (McRoberts, 2012).

Following previous studies, the models were trained using k = 5 (Chirici et al., 2016; Irulappa-Pillai-Vijayakumar et al., 2019; Sagar et al., 2022), and two distance metrics were considered : Most Similar Neighbours (Eq.33) and Euclidean (Eq.34) (Crookston and Finley, 2008), along with an inverse distance weighting function (Eq.35) (Altman, 1992):

$$d_{ij}(msn) = \sqrt{(x_i - x_j)\,\Gamma\Lambda^2\Gamma^T(x_i - x_j)^T} \qquad \textbf{(Eq.33)}$$

$$d_{ij}(euc) = \sqrt{(x_i - x_j)^T\,(x_i - x_j)} \qquad \textbf{(Eq.34)}$$

$$w_{ij} = \frac{1}{1+d_{ij}} \qquad \textbf{(Eq.35)}$$

where, $d_{ij}(msn)$ and $d_{ij}(euc)$ are most similar neighbour and Euclidean distances, x_i and x_j are the vector of target and reference auxiliary variables, Λ is a matrix of canonical correlation, Γ is a matrix of canonical vectors of auxiliary data, T is the transpose of the matrix, and w_{ij} is the weighted distance.

Auxiliary variables were selected using an iterative feature selection algorithm applied in addition and deletion mode (Crookston and Finley, 2008). For each distance metric and variable selection approach, the best models made of 1 up to 7 variables were selected. Such a limit was set because kNN models are sensitive to the dimensionality of auxiliary variables which may lead to model overfitting problems (Breidenbach et al., 2012). Prior to variable selection, the set of auxiliary variables was filtered to avoid multicollinearity. The filtering process relied on the correlation matrix between the response variables and the auxiliary variables. The auxiliary data were ranked in descending order with respect to their correlation with the response variables. A vector of candidate auxiliary variables was initiated by selecting the auxiliary variable having the highest correlation with the response variables. The remaining auxiliary variables were iteratively tested again the vector in descending order and included in the vector if their correlation with the auxiliary variables contributing to it was lower than a threshold fixed here to 0.7.

Among the 28 models generated (2 distance x 2 selection approaches x 7 sets of auxiliary data) for both the general and specific models, the best model was selected and evaluated using a train-test

approach. The NFI data were spitted into train and test sets using a geographical partitioning (Meyer and Pebesma, 2021). The bounding box of the coordinates of the NFI plots was first generated, and one of its corners randomly selected. Then, 20 % of the closest plots from the selected corner were kept as an independent testing set and the remaining 80 % of the plots as a training set. The same corner was used for generating the training-testing sets for both the general and specific models. The training set was used for model development and selection, and the testing set was used to validate the model against independent, external data (Karasiak et al., 2022).

Model selection and assessment was performed on the training set using a leave one out cross-validation (LOOCV) method. Performance metrics included the calibration and the validation relative root mean square error (RMSE%, Eq.36), the relative mean error (ME%, Eq.37), the relative total error (TE%, Eq.38), and a measure of overfitting (OFI, Eq.39, Valbuena et al., 2017):

$$\mathrm{RMSE} = \sqrt{\frac{1}{\mathrm{n}}\sum_{\mathrm{i}=1}^{\mathrm{n}}(\mathrm{y}_i - \hat{\mathrm{y}}_i)^2}\ ;\ \ \mathrm{RMSE\%} = \frac{\mathrm{RMSE}}{\bar{\mathrm{y}}} \times 100 \qquad \textbf{(Eq.36)}$$

$$\mathrm{ME} = \frac{1}{\mathrm{n}}\sum_{\mathrm{i}=1}^{\mathrm{n}}(\mathrm{y}_i - \hat{\mathrm{y}}_i)\,;\qquad \mathrm{ME\%} = \frac{\mathrm{ME}}{\bar{\mathrm{y}}} \times 100 \qquad \textbf{(Eq.37)}$$

$$\mathrm{TE} = \sqrt{\mathrm{RMSE}^2 + \mathrm{ME}^2}\ ;\ \ \mathrm{TE\%} = \frac{\mathrm{TE}}{\bar{\mathrm{y}}} \times 100 \qquad \textbf{(Eq.38)}$$

$$\mathrm{OFI} = \frac{1}{\mathrm{n}}\sum_{\mathrm{i}=1}^{\mathrm{n}}(\mathrm{y}_i^{cv} - \hat{\mathrm{y}}_i) \,/\, \frac{1}{\mathrm{n}}\sum_{\mathrm{i}=1}^{\mathrm{n}}(\mathrm{y}_i^{train} - \hat{\mathrm{y}}_i) \qquad \textbf{(Eq.39)}$$

where $\mathrm{y_i}$ is the observed value, $\hat{\mathrm{y}}_\mathrm{i}$ is predicted value, $\bar{\mathrm{y}}$ is the mean of observed values, n is the number of NFI plots, OFI is the overfitting index, y_i^{cv} are the cross-validated predictions and y_i^{train} are the training predictions.

The best general and specific models were selected in a two stage process. First, the models having an OFI greater than 1.1 (Valbuena et al., 2017) were considered as overfitted and were filtered out. Then, the models with TE% within 1% of the minimum TE% were selected, of which the more parsimonious model (Pestov, 2013), i.e. having the least number of auxiliary variables, was considered as the best model.

Finally, the resulting models were calibrated again using the entire training set and applied to the test set to evaluate their performance on external data.

3.4. Model propagation

Forest resource and reliability maps were generated for the 2 selected models using bootstrap (Figure 32). For each bootstrap sample (N = 100), the NFI plots were randomly selected with replacement. The NFI sample was then used to train the two kNN models and to predict the grid cells.

The final prediction for each forest attribute over the entire study site was computed by taking the mean of bootstrapped predictions and produce predictive raster maps at 30 m spatial resolution.

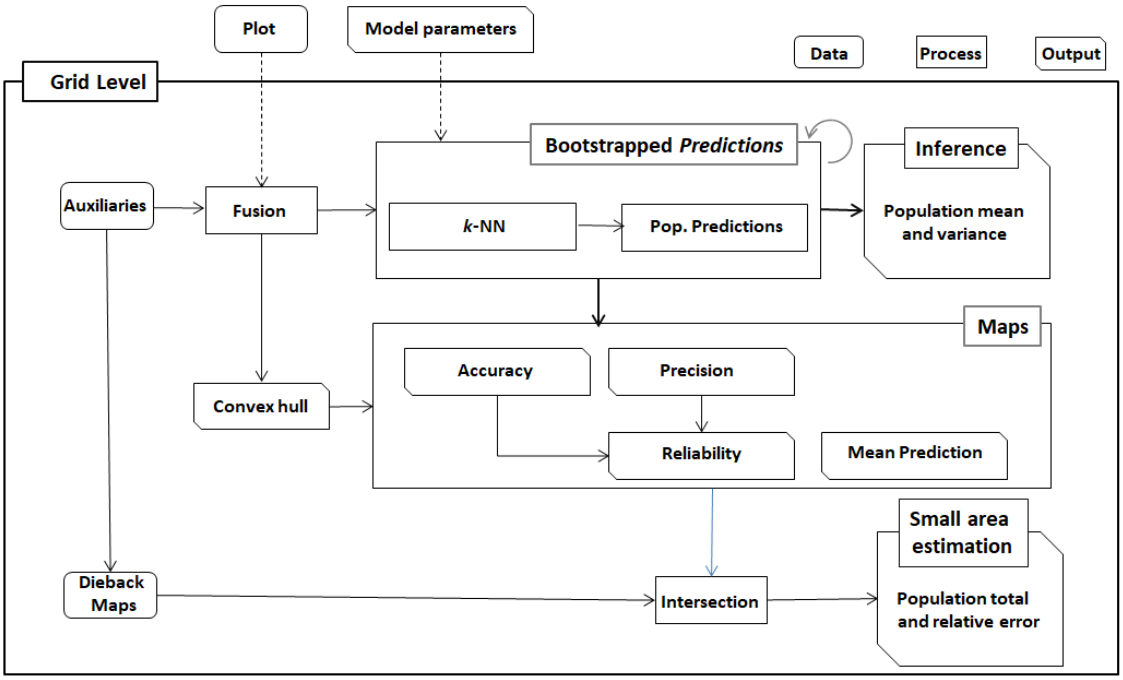

Figure 32. *Workflow of the grid-level model propagation and estimation framework.*

Reliability maps were generated following Sagar et al. (2022) using classes of precision and accuracy. Precision classes (low, intermediate, high) were derived from the kNN model's calibration–validation RMSE% and coefficient of variation of the bootstrapped prediction at pixel level. Precision was considered low if the coefficient of variation of the grid cell – level bootstrapped predictions was greater than the validation RMSE%. On the contrary, precision was considered high if the coefficient of variation of the grid cell – level bootstrapped predictions was lower than the calibration RMSE%. Values between the two RMSE% were considered of intermediate precision. Accuracy was defined through a measure of extrapolation (Renaud et al., 2022). It consisted first in generating the convex hull of the auxiliary data used in the models at plot level, and then, to test if the auxiliary data describing each cell of the computation grid were included or not in the convex hull. Cells outside of the convex hull were considered in extrapolation and were classified as of low accuracy. On the opposite, cells inside the convex hull were considered as having a high accuracy. Finally the reliability classes were computed by intersecting precision and accuracy, and assigning the most unfavourable quality class to each cell.

3.5. Statistical inference

For both the general and specific model, population parameters (mean, variance and relative error) were derived from the kNN predictions using a bootstrapped model-based estimator proposed by McRoberts et al. (2022) (Figure 32):

$$\hat{\mu}_{boot} = \frac{1}{n_{boot}} \sum_{b=1}^{n_{boot}} \hat{\mu}_{boot}^{b} \quad \textbf{(Eq.40)}$$

$$\hat{V}_{boot}(\hat{\mu}) = \frac{1}{n_{boot}-1} \sum_{b=1}^{n_{boot}} (\hat{\mu}_{boot}^{b} - \hat{\mu}_{boot})^2 \quad \textbf{(Eq.41)}$$

$$RE(\hat{\bar{\mu}}_{boot}) = \frac{\sqrt{\hat{V}_{boot}(\hat{\mu})}}{\hat{\mu}_{boot}} \times 100 \quad \textbf{(Eq.42)}$$

where n_{boot} is the number of bootstrap samples, $\hat{\mu}_{boot}^{b}$ is the mean of the boot b, $\hat{\mu}_{boot}$ is the mean of the bootstrap samples.

The estimation of the amount of resource impacted by bark-beetle was achieved by sub-setting the grid cells using the outbreak map. The amount of resource predicted was converted from per hectare values to per cell values, and weighted using the proportion of grid cell affected. From these weighted values, estimates of total, variance of total and relative errors were estimated as follow:

$$\hat{\bar{t}}_{boot} = \frac{1}{n_{boot}} \sum_{b=1}^{n_{boot}} \sum_{i=1}^{N} y_i \quad \textbf{(Eq.43)}$$

$$\hat{V}_{boot}(\hat{\bar{t}}_{boot}) = \frac{1}{n_{boot}-1} \sum_{b=1}^{n_{boot}} (\hat{t}_{boot}^{b} - \hat{\bar{t}}_{boot})^2 \quad \textbf{(Eq.44)}$$

$$RE(\hat{\bar{t}}_{boot}) = \frac{\sqrt{\hat{V}_{boot}(\hat{\bar{t}}_{boot})}}{\hat{\bar{t}}_{boot}} \times 100 \quad \textbf{(Eq.45)}$$

Where, y_i is the predicted value, N is the number of outbreak sample, n_{boot} is number of bootstrap samples, $\hat{t}_{boot}$ is the total of the bootstrap samples.

4. Results

Since the beginning of the bark-beetle crises in the North-Est of France in 2018, the computation grid included 2838 ha of ForDead classes 3 and 4. This represented 3.0 % of the surface of spruce and fir dominated forests according to the BD-forêt (Table 15). For the period 2021-2022, the total reached 1139 ha, corresponding to 1.2 % of the surveyed conifer areas.

Table 15. *Forest surfaces detected by the ForDead method in class 3, 4 and total of both. Values are given in hectare. Number of parenthesis corresponded to percent to the total area.*

Period	ForDead classes		
	3	4	Total
2018-2022	925.9 (1.0)	1912.6 (2.0)	2838.4 (3.0)
2021	52 (0.1)	224 (0.2)	277 (0.3)
2022	642 (0.7)	219 (0.2)	861 (0.9)
2021-2022	697 (0.7)	442 (0.5)	1139 (1.2)

The kNN models used for estimating the amount of resources impacted are presented in Table 16. The two selected models were built with Euclidean distance and variables selected using a variable addition approach. The general model of forest resources included 4 auxiliary variables, of which 3 derived from the lidar data (i.e. Total inner canopy volume, Gap area, 2nd cumulative percentage of returns) and one from Sentinel (i.e. mean of near infrared values). The model cross-validated RMSE% ranged from 28.4 % (calibration) to 41.7 % (test) for GSV and from 26.8% (calibration) to 42% (test) for BA (Table 17). The mean error was within the 1 % range in both calibration and validation for both variables, but exhibited greater and negative values with the independent test set, reaching -5.9% for GSV (Table 17). Model residuals computed for the independent test set (Figure 33) did not show significant departure from normality, but exhibit a slight underestimation of GSV above 600 m^3 ha^{-1}. The specific model included only two auxiliary variables extracted from the lidar data: the total inner canopy volume and the gap area. These two variables were also included in the general model. The model cross-validated RMSE% varied from 25.1 % (calibration) to 33.1 % (test) for GSV and from 22.9% (calibration) to 30.8 % (test) for BA (Table 17). Corresponding mean errors varied from -1.1 % (GSV, calibration) to 1.7 % (GSV, test), and model residuals showed a random distribution (Figure 33).

Table 16. *kNN parameters for the general and specific selected models.*

Model	kNN parameter		Selected auxiliary variables
	Feature selection	Distance	
General	Addition	Euclidean	Total inner canopy volume Gap area 2nd cumulative percentage of returns Near infrared band
Specific	Addition	Euclidean	Total inner canopy volume Gap Area

Table 17. *Model prediction mean, training (calibration-validation) and testing relative errors of growing stock volume (GSV, m^3ha^{-1}) and basal area (BA, m^2ha^{-1}) for the general and specific models.*

Model	Forest attribute	Calibration			Validation			Test		
		Prediction Mean	RMSE%	ME%	Prediction Mean	RMSE%	ME%	Prediction Mean	RMSE%	ME%
General	GSV	318.5	28.4	0.4	317.1	37.7	0.1	257.8	41.7	-5.9
	BA	31.6	26.8	0.7	31.7	36.0	0.8	27.5	42.0	-1.8
Specific	GSV	356.6	25.1	-1.1	356.5	32.8	-1.1	410.8	33.1	1.7
	BA	35.0	22.9	0.3	35.1	30.1	0.4	36.7	30.8	1.5

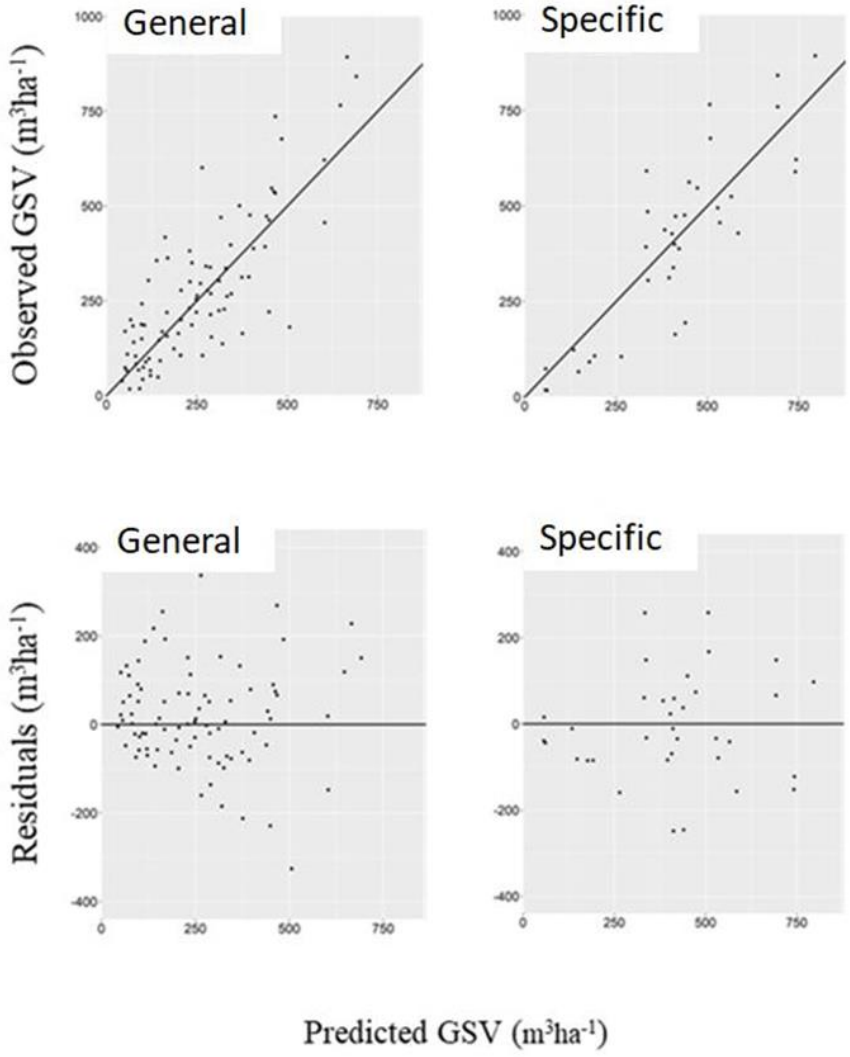

Figure 33. *Observation and residuals versus prediction of growing stock volume (GSV) over the test set for both general and specific models.*

Table 18 provided estimates of the forest resource for the entire region of interest, and the subset of spruce and fir forest. Overall, the mean GSV was estimated to 312.28 $m^3.ha^{-1}$ and with an error of 1.78 %. The mean BA was estimate to 30.75 $m^2.ha^{-1}$, with a relative error of 1.65 %. The estimations of sub-population corresponding to spruce and fir with the general model were 366.37 $m^3.ha^{-1}$ for GSV and 34.22 $m^2.ha^{-1}$ for BA. Relative errors established to 1.92 % for GSV and 1.76 % for BA. With the specific model, GSV was estimated to 376.76 $m^2.ha^{-1}$ with a relative error of 2.36 %. For BA, the mean value was 34.37 $m^2.ha^{-1}$, with a 2.09 % error.

Table 18. *Population mean and relative error for growing stock volume (GSV, m^3ha^{-1}) and basal area (BA, m^2ha^{-1}) achieved using the two model.*

Model	Forest type	Forest attribute	$\hat{\mu}_{boot}$	$RE(\hat{\mu}_{boot})(\%)$
General	All	GSV	312.28	1.78
		BA	30.75	1.65
	Conifer	GSV	366.37	1.92
		BA	34.22	1.76
Specific	Conifer	GSV	376.79	2.36
		BA	34.37	2.09

The amount of volume impacted by bark-beetles with the two models in presented Table 19, and an illustration of the underlying prediction maps is presented Figure 34. In 2021, the GSV of outbreak areas (classes 3-4), which represented a surface of 277 ha, is estimated at 117,658 m^3 and 120,901 m^3 with the general and specific models respectively. These estimates are supported by respectively 75.9 % and 79.6 % of reliable predictions. Corresponding total BA were respectively 10,189 m^2 and 10,039 m^2. In 2022, the 861 ha of outbreaks accounted for 376,555 m^3 and 384,500 m^3 of GSV for the general and specific model respectively. The percentages of reliable pixel were of the same magnitude, ranging from 77.1 % (GSV, general model) to 82.6 % (GSV, specific model).

Table 19. *Total growing stock volume (GSV) and basal area (BA) estimated in confirmed outbreak areas (class 3-4), along with corresponding means and percentage of reliable pixels Number in parenthesis are relative errors.*

Model	Year	Estimation totals		Means		High reliability (%)	
		GSV (m^3)	BA (m^2)	GSV ($m^3.ha^{-1}$)	BA ($m^2.ha^{-1}$)	GSV	BA
General	2021	117,658 (2.2)	10,189 (2.1)	424.8	36.8	75.9	77.6
	2022	376,555 (2.2)	32,246 (2.2)	437.3	37.5	78.2	79.5
Specific	2021	120,901 (2.5)	10,039 (2.3)	436.5	36.2	79.6	78.6
	2022	384,500 (2.6)	31,566 (2.3)	446.6	36.7	82.6	81.3

Overall, the distribution of outbreak cells with respect to ground elevation showed a skewed distribution toward the lower elevations. In both 2021 and 2022, the maximum frequency was achieved around 450 m. In terms of GSV, higher frequencies were found for GSV classes under 450 $m^3.ha^{-1}$ (Figure 36), but relative values showed a slight trend toward increasing proportion of outbreaks with increasing GSV values. Indeed, the total GSV impacted, represented from 433 to 443 $m^3.ha^{-1}$ with respect to the model, which indicated that mature stands were more susceptible to bark-beetle outbreaks than younger ones in the area. With the exception of a few points in 2022, our estimates almost always underestimated ONF reported salvage volumes (Figure 37).

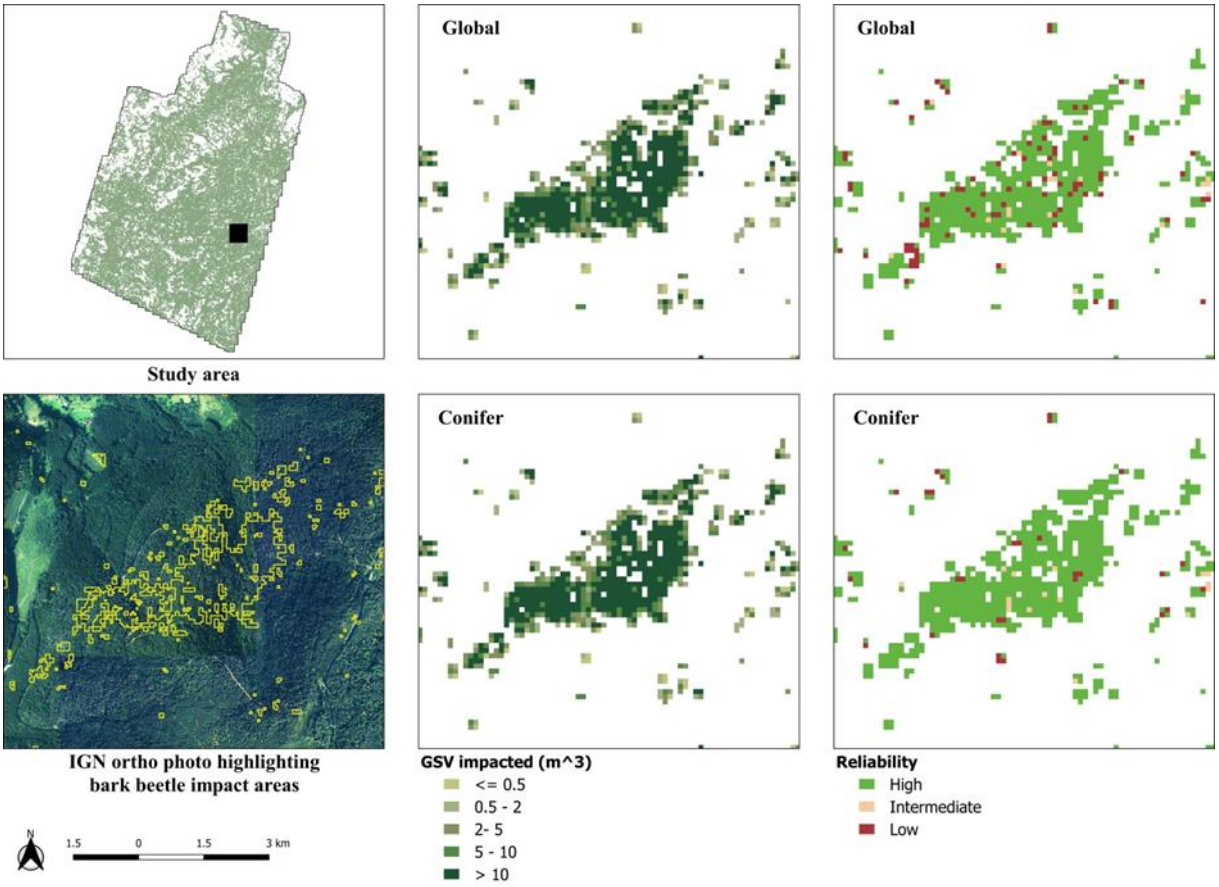

Figure 34. *Maps of bark beetle impacted growing stock volume and corresponding reliability for both global and conifer model.*

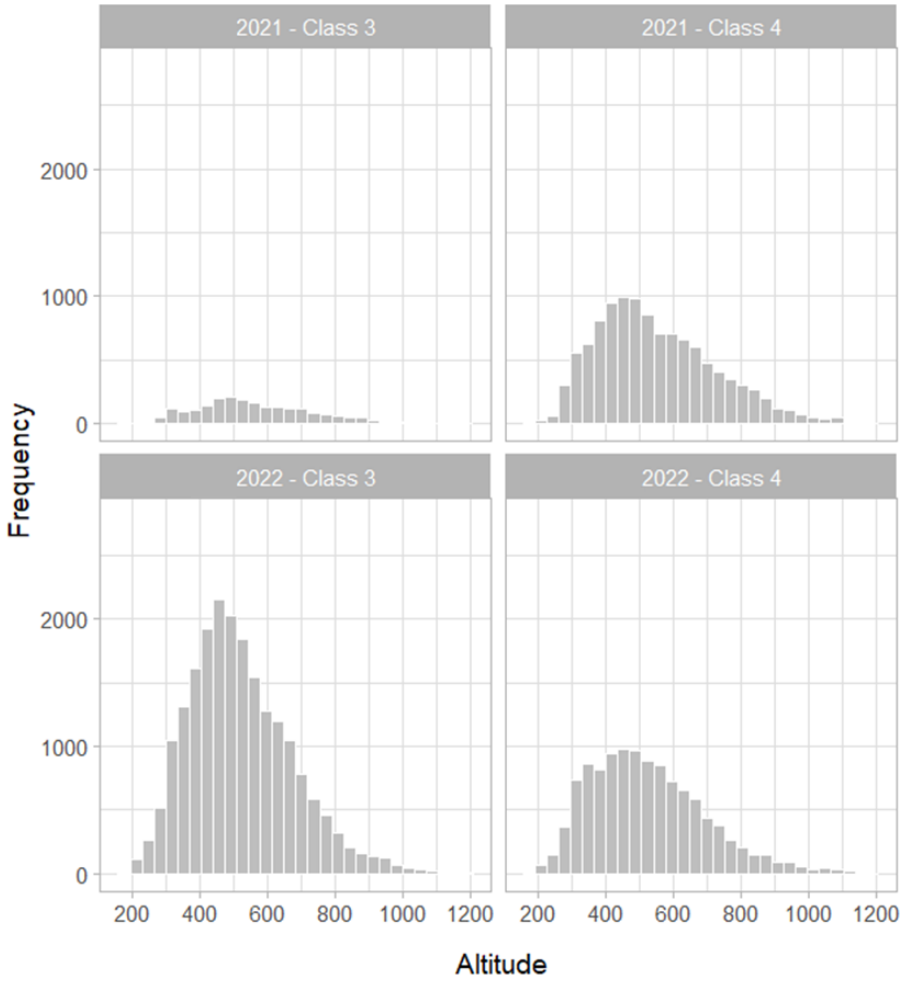

Figure 35. *Frequency of outbreak cells according to altitude classes.*

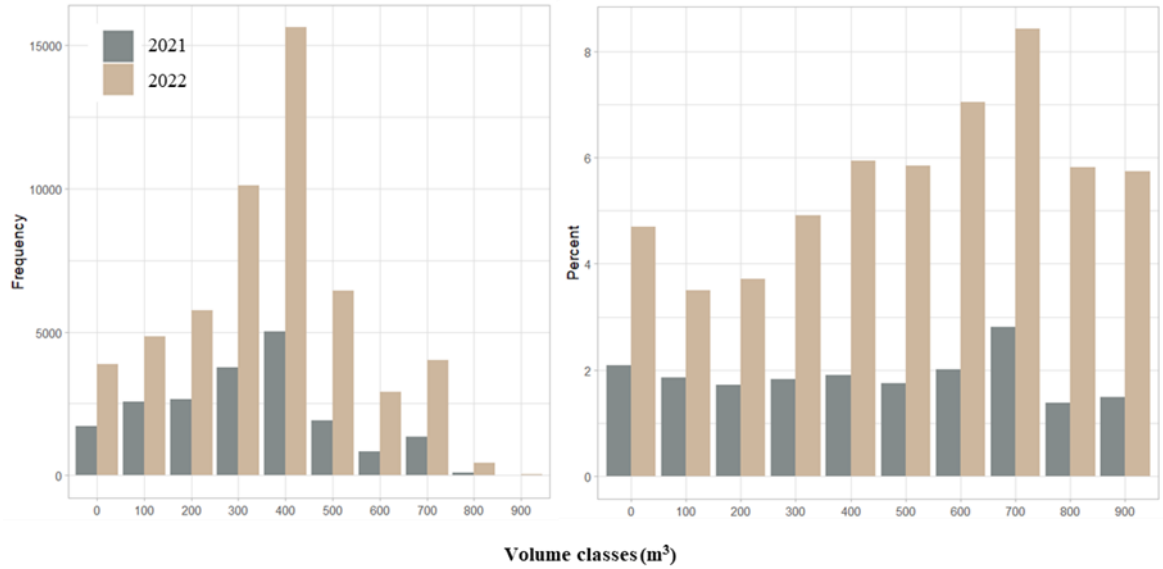

Figure 36. *Frequency and proportions of outbreak growing stock volume (GSV) by 50 m^3 GSV classes*

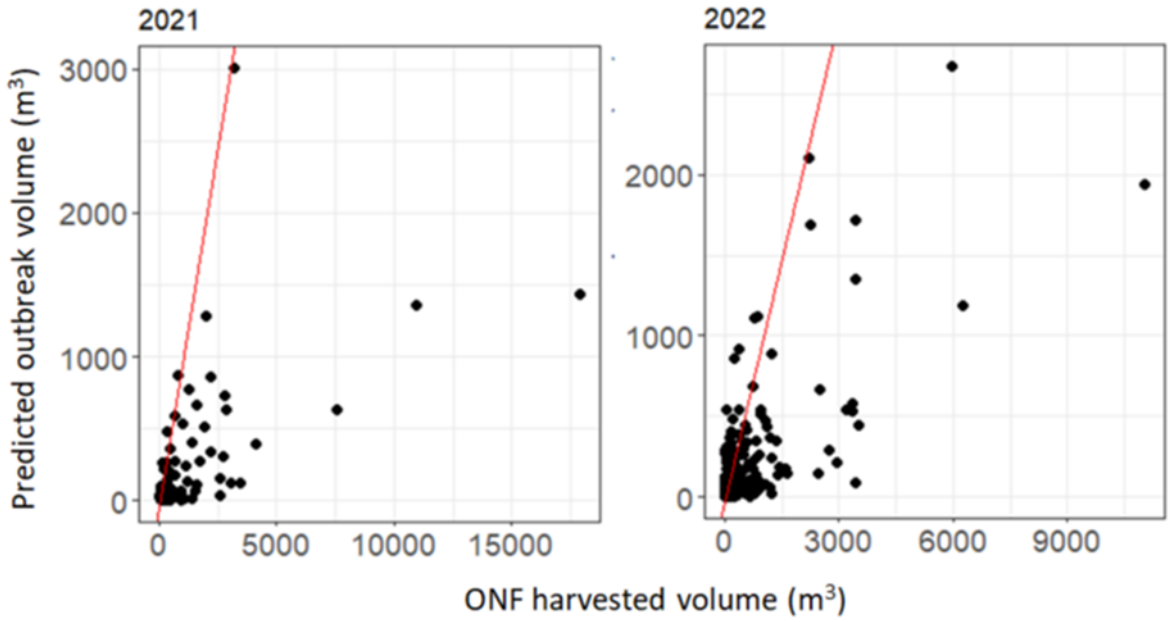

Figure 37. *Predicted outbreak growing stock volume (GSV) against ONF sanitary harvests aggregated by forest units.*

5. Discussion

Our results showed that resource maps generated for other purposes than small area estimation could be efficiently combined with polygons of bark-beetle outbreaks to estimate the amount of resource impacted. With a mean value per ha of 366.4 m^3 for GSV, the general model predicted a lower amount of resource than the specific model (376.8 $m^{3}.ha^{-1}$), and exhibit slightly lower relative errors, for both parameters. However, pixel level predictions exhibited an overall lower reliability compared to the specific model. Various reasons could explain this result. On the one side, the lower amount of field plots in the specific model might generate a higher variability in bootstrap predictions than for the general model. Also, by including the variability of all the forest plots, the general model might borrow additional strength from mixed forest stands that could be similar to conifer ones in term of composition and structure (Ghosh and Rao, 1994). On the other side, the larger variability in field data might increase the amount of extrapolation in the general model, thus decreasing its reliability (Sagar et al., 2022). Overall, our results indicated that a general model of resource could efficiently be used to derive small area estimates in a specific part of the domain. It is thus possible to compute predictions in a more effective way if resource maps are produced regularly.

While lidar is often considered as the most effective source of 3D data to model forest attributes, the capabilities to renew the information is still limited with this data source. Despite technological improvements allowing to cover larger areas at continuously lower costs, lidar data remain still costly to be renewed regularly (Barrett et al., 2016). That said, when a lidar DTM exist, photogrammetric measurements can be used to renew the forest information layer (Price et al., 2020), borrow strength of times-series estimates to assess flux variables (Irulappa-Pillai-Vijayakumar et al., 2019), or quantify forest changes (Renaud et al., 2017) .In many countries, aerial photographs with photogrammetric capabilities (i.e. with enough overlap between images along and across tracks), are regularly acquired for surveying purposes. In France, for example, such covers are renewed every 3 years at department level. Such an acquisition frequency could be sufficient to estimate the amount of resources in disturbed areas, with a maximal time difference of two years. Estimations could be more difficult to derive for small areas distributed over different departments which could have been surveyed in different years. For larger scale disturbances, design-based estimation could be sufficient, as the number of NFI point increases. But if the estimation precision is not sufficient or if specialized estimates are required, data from spaceborne sensors such as GEDI in combination with optical and/or radar data, could support estimation (Duncanson et al., 2022; Lang et al., 2022; Potapov et al., 2021).

The estimation domains used to support the estimation were derived from vegetation anomaly detection of ForDead, which is based on times series analysis of Sentinel 2 data. Spatially, the detected outbreaks were predominantly localized in the lower altitude of the study area, which is in accordance with the ecology of bark beetle populations (Luo et al., 2022; Seidl et al., 2007), and the results reported by Piedallu et al. (2023) over the same area. Our results further suggested that the mature

stands are more impacted than the younger ones (Figure 36, right). This can be explained by the fact that the development of bark beetle populations is associated to the presence of dead trees which are mainly found in the mature stands. That said, Müller et al. (2022), suggested that during drought period young stands might become more sensitive to bark beetle attacks, as can be also observed through the frequencies distribution of Figure 36.

The amount of outbreak surface detected (1.2 % of the total resource, Table 15) is limited with respect to the intensity of the crisis in the Grand-Est region of France. Saintonge et al. (2022) reported that around 30 % of the surface of spruce and fir has been impacted by bark-beetle during the period 2017-2022. Part of this result could be explained by the definition of the computation domain. ForDead anomalies were computed only spruce and fir dominated forests according to the BD forêt®. From the NFI data, such a spatial restriction discarded around 25.4 % of the GSV of spruce and fir, which are located within mixed stands or stand not identified within the BD forêt® as pure spruce and fir stands. Another explanation comes from the spatial variability of outbreaks at the regional level. Outbreaks are dominated in lowland area and are of lower intensity in the mountainous area, due to elevation. The low amount of surface detected in 2021 (Table 15) could be explained by unfavourable climatic conditions to bark-beetle development, with cooler temperatures. Also, summer 2021 was characterized by higher-than-normal cloud coverage, making it more difficult to detect vegetation anomalies. Indeed, an underestimation of surface is expected for that year within the BD forêt® mask, which will affect estimated totals. Despite this issue, the estimated totals are consistent with the MFI reported volumes (Figure 37). The large underestimations obtained for some forests illustrate a gap between the outbreak detection and management of epidemics. In many circumstances, entire stands will be harvested even if a small proportion of the stand is affected by outbreaks. On the opposite, the overestimations achieved for some forest in 2022 could be attributed to an increase in bark-beetle activity at the end of 2022 (Saintonge et al., 2022).

A key issue with remote sensing-based outbreak detection is limiting the impact of cloud covers. This can be done through the use of sensor insensitive to atmospheric conditions. While Huo et al. (2021) reported that radar signal did not significantly contribute to the detection of outbreaks, Hollaus and Vreugdenhil (2019) stated that times-series of radar data could enable detecting bark beetle impacts, thus providing more time-consistent surface estimates. Alternative approaches could be to use time for space spatial interpolation to interpolate missing date (He et al., 2022). But these kinds of approaches could be of limited efficiency in the framework of change detection. Another promising approach would be to use high temporal frequency height models from Gedi data (Boucher et al., 2020) to support both surface detection and estimation of the corresponding resource. In particular, the combination of Gedi's 3D measurement together with the high spatio-temporal frequency of Sentinel 1 data could both reduce the amount of missing information and solve radar data detection problems.

In the same way, linking estimations from remote sensing detection with to the outputs of the MFI will require a better integration of detection approaches associated with capabilities to specify the nature of detection. This can be achieved be associating contextual information during the classification process (Zheng et al., 2022), for example in order associate clear cut in the surrounding of vegetation anomalies to an ensemble of sanitary loggings. With the growing impact of climate change on forest health, the remote sensing based approach will also face the challenge of detecting and classifying changes in order to support decision-making.

Accounting for uncertainty of detected surfaces is a key issue that has a direct impact on affected resource estimates (Lark et al., 2022; Olofsson et al., 2020), and will be addressed in future work. A possible solution could be to rely on photointerpretation of aerial photographs, using a specific sampling design, targeted to conifers and mixed stands. Such an evaluation is possible because the bark-beetle crises started in 2017 and is still on-going. As aerial images are also renewed every 3 years in France, such a photointerpretation would help the analysis of omission and commission errors in ForDead detection and to compute the variance of the detected surface. This would then be taken into account to estimate the variance associated to the forest attributes estimations. Another alternative would be to rely of NFI data at a larger scale. As the bark-beetle crisis impacted more than 100,000 ha of forest in the North-Eastern part of France, the intersection of ForDead map with the NFI data might provide enough data to directly evaluate the uncertainty in the impacted surface for the whole period.

6. Conclusion

We demonstrated here how forest resource maps could be combined to independent disturbance maps to produce small area estimation of impacted resources by a bark beetle outbreak. With the rapid development of times-series of remote sensing data, including 3D data, these approaches will benefit from improved capabilities to produce information over large areas, at both high spatial and temporal resolution. Challenges remain with the use of 3D remote sensing data, with possible solutions from spaceborne data such as Gedi. Similarly, the detection of and qualification of disturbances under cloud cover still remain difficult with optical data, but the current development of radar times-series and times for space approaches might overcome this difficulty in the short term. Finally, estimating uncertainties associated with outbreak detection will certainly contribute to provide more robust estimates of forest attributes impacted by bark beetles.

Acknowledgements

This work was supported by the French PIA project “Lorraine Université d’Excellence”, reference ANR-15-IDEX-04-LUE, through the project Impact DeepSurf and the Labex ARBRE (ANR-11-LABX-0002-01).

7. Appendix A.

Table A3. *Canopy height model (CHM) metrics. P represents a pixel height of the CHM, and s its spatial resolution.* p_{Max} *represents the maximum height of the portion of the CHM considered, and i and j represents line and column indices of p.* CHM_a *and* CHM_{pa} *represented respectively the area and the projected area of the CHM* (Véga et al., 2016).

Metric name	Formulae
total inner volume	$TIV = \sum_{p>0} p \times s^2$
total outer volume	$TOV = \sum_{p>0} (p_{Max} \times s^2) - TIV$
canopy inner volume	$CIV = \sum_{p>Th} p \times s^2$
canopy outer volume	$COV = \sum_{p>Th} (p_{Max} \times s^2) - ICV$
Gap Area	$GA = \sum_{p<Th} s^2$
gap inner volume	$GIV = \sum_{p<Th} p \times s^2$
r gap outer volume	$GOV = (p_{Max} \times GA) - IGV$
Rumple area	RA = CHM_a / CHM_{pa}
	$CHM_{pa} = \sum_{p>Th} s^2$
	$CHM_a = \sum_{p>Th} \left\| \frac{\overrightarrow{p_{i,j}p_{i+1,j}} \wedge \overrightarrow{p_{i,j}p_{i,j+1}}}{2} + \frac{\overrightarrow{p_{i+1,j+1}p_{i,j+1}} \wedge \overrightarrow{p_{i+1,j+1}p_{i+1,j}}}{2} \right\| \times s^2$

Table A4. *Vegetation indices calculated from Sentinel-2 data* (Sonobe et al., 2018; *www.custom-scripts.sentinel-hub.com*). *"b" refers to band number.*

Vegetation indices	Formula
Atmospherically resistant vegetation index	$\frac{b8 - b4 - 1 * (b4 - b2)}{b8 + b4 - 1 * (b4 - b2)}$
Advanced vegetation index	$\sqrt[3]{b8 * (1 - b4) * (b8 - b4)}$
Canopy chlorophyll content index	$\frac{(b8 - b5) / (b8 + b5)}{(b8 - b4) / (b8 + b4)}$
Chlorophyll index green	$\frac{b8}{b3} - 1$
Disease-water stress index	$\frac{b3}{b4}$
Enhanced vegetation index	$\frac{2.5 * (b8 - b4)}{(b8 + 6.0 * b4 - 7.5 * b2) + 1.0}$
Green normalized difference vegetation index	$\frac{b8 - b3}{b8 + b3}$
Modified Chlorophyll Absorption in Reflectance Index	$(b5 - b4) - 0.2 * (b5 - b3) * \frac{b5}{b4}$
Modified soil adjusted vegetation index	$\frac{2.0 * b8 + 1.0 - \sqrt{(2.0 * b8 + 1.0)^2 - 8.0 * (b8 - b4)}}{2}$
Moisture stress index	$\frac{b11}{b8}$
Normalized difference 820/1600 normalized difference moisture index	$\frac{b8 - b11}{b8 + b11}$
Normalized Difference NIR/Red-edge Normalized Difference Red-Edge	$\frac{b8 - b5}{b8 + b5}$
Normalized difference vegetation index	$\frac{b8 - b4}{b8 + b4}$
Normalized difference water index	$\frac{b3 - b8}{b3 + b8}$
Pigment specific simple ratio	$\frac{b7}{b4}$
Simple ratio	$\frac{b8}{b4}$
Visible atmospherically resistant index green	$\frac{b3 - b4}{b3 + b4 - b2}$

Discussion, Perspectives and Conclusion

1. Discussion and perspectives

1.1. Small area estimation

In this thesis, estimating forest attributes in small domains has taken an important part. SAE studies were conducted using either a model-assisted (Chapter I) or a model-based inference framework (Chapter IV). The selection of the inference framework was driven by the objectives of the studies (Gregoire, 1998).

In Chapter I, the estimation of forest attributes focused on administrative units, specifically municipalities. Model-assisted framework was used to leverage on the properties of the NFI sampling design (unbiasedness), and to remain in close agreement with NFI outputs. A multi-scale downscaling approach was used to improve the estimation precision in small municipalities that have too few NFI plots. And also, to prevent any possibility of estimation failure in municipalities that have no plots at all. In Norway, Breidenbach and Astrup (2012) were unable to provide estimates for 20% of the municipalities. In contrast, our study faced even greater issues, as we were unable to estimate in 57% of the municipalities. This substantial difference can be attributed to the fact that the administrative boundaries of municipalities in France were generally smaller in size. By using the multi-scale approach, when we set the error threshold to 10%, we were able to provide estimate in 20 groups of municipalities with an average error of 7.5%. When using a higher error threshold of 50%, we were able to provide estimates at a finer scale (80 groups of municipalities), although with an increased average error of 15.1%. Nonetheless, this error rate remained considerably lower than the 27.3% reported by Breidenbach and Astrup (2012) for estimating in NFI-available municipalities only. These findings support our approach, as it effectively mitigates large variations in error caused by the estimation domain and associated sample size within those domains. The users can strike a balance between precision and spatial scale by using this approach.

It is noteworthy that this downscaling approach is not limited to specific administrative boundaries and can be extended to estimate forest attributes in any desired estimation domains or groups of domains that are of interest to the end user. For example, domains representing various forest aggregation levels (e.g., forest stands, forest districts) could be utilized. Moreover, the approach can also be applied to various kinds of polygon structures. One example of such structure could involve aggregating Voronoi polygons centered on NFI plots. This way of aggregation would result in a better distribution of NFI plots in the BSP tree structure, and facilitate the generation of a more complex BSP tree structure (i.e. higher number of smaller estimation domains). However, this would come at the expense of losing estimation at administrative units which are crucial for decision-making and management purposes. Some of these solutions (i.e. administrative layers, NFI Voronoi structure) have been included in a Shiny application (R software, accessible at *http://46.18.194.16/IFM*) developed by the DAFOR (*"Département d'analyse des forêts et des haies"*, IGN). The application serves as a demonstrator of MSNFI approaches for end-users. Users can select a specific domain,

forest attribute of interest and define a maximum error threshold for estimations. Subsequently, an iterative map is generated, which can be exported (Figure 38).

An interesting aspect with multi-scale approach may lies in its capacity to provide estimates for ventilated parameters (e.g., forest attributes by species, diameter class, or a combination of both) in an optimal manner. While not tested in this study, one might hypothesize that ventilation may have an impact on the precision levels of the estimates, depending on factors such as the forest's characteristics, the sample size, and the chosen level of aggregation (best possible domains according to the ventilation). Aggregating data into fixed domains (i.e. cantons, municipalities) could be constraining as it will degrade the precision for ventilated parameters. Given the scale flexibility, the BSP can accommodate the precision issues. Investigating such aspects further would contribute to a comprehensive understanding of the multi-scale approach's capabilities and limitations in precisely estimating ventilated parameters.

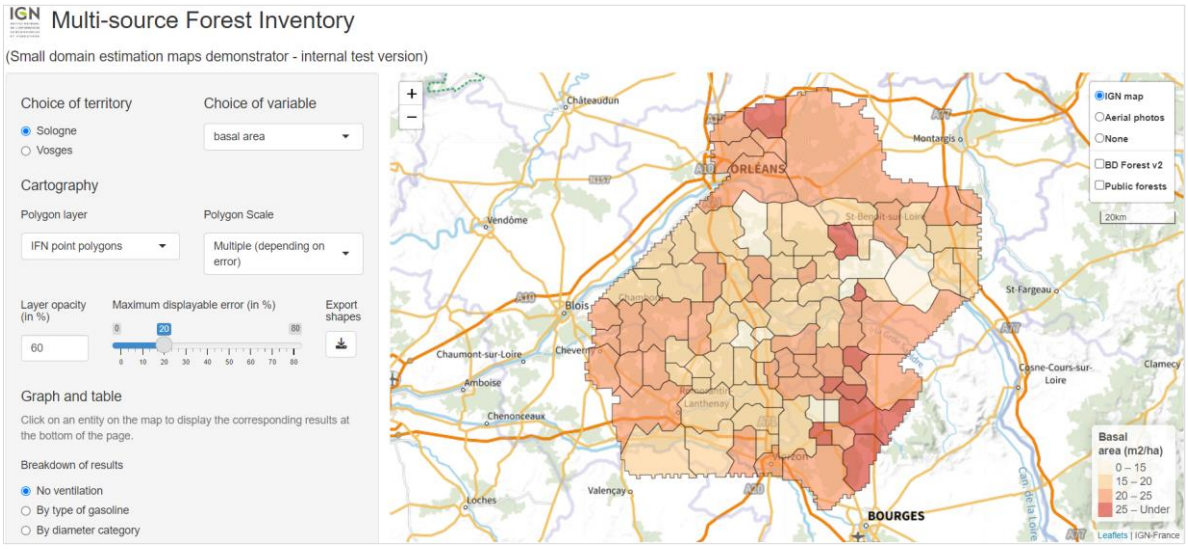

Figure 38. *A screen capture of the Shiny application, that incorporates the downscaling approach across the Sologne and Vosges forest (accessible at http://46.18.194.16/IFM).*

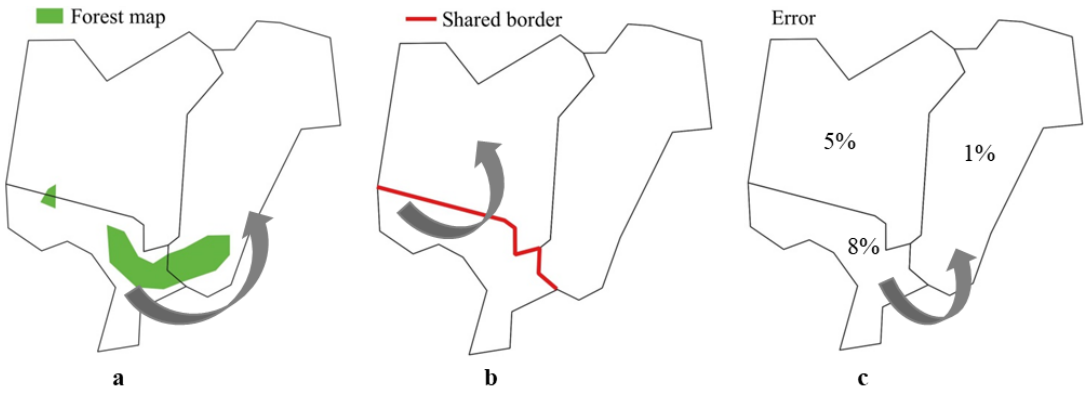

Figure 39. *An illustration of proposed polygon aggregation approach. (a) Aggregation based on amount of shared forest; (b) Aggregation based on length of shared border; (c) Aggregation based on obtained error%.*

From a methodological standpoint, our study indicates that the structure of the BSP tree is influenced by the forest attributes of interest. The higher the correlation between the auxiliary data and forest attributes, the higher the complexity of the BSP tree. This complexity was higher for state variables (GSV and BA) compared to flux variables (VI). Irulappa-Pillai-Vijayakumar et al. (2019) showed that the correlation of flux variables could be improved by using 3D data from different points in time, thereby increasing the performance of BSP tree for such variables. Furthermore, we acknowledge that the BSP method, owing to its binary splitting nature, imposes significant constraints on the division process (see Figure 10 in Chapter I). If a branch of the division tree fails to meet the error term requirement, the parent aggregation becomes fixed, even if the other branch could have generated more division. A possible way to improve the method would be to shift from a top-down to a bottom-up aggregation approach, by considering each municipality as an individual data points and gradually aggregating them based on certain criteria, creating larger entities (Gómez et al., 2009). This could involve aggregating municipalities (Figure 39) based on the spatial distribution of forests (municipalities with largest forest cover could be grouped together), the length of shared borders (grouping municipalities with longer shared borders together), or the estimation error (grouping municipalities with smaller errors alongside those with larger errors). On the other hand, the estimates produced at municipality or a group of municipality level may pose limitations, when specific municipalities require estimates without aggregation. A potential solution could involve a mixed approach that combines both model-assisted and model-based frameworks. In cases involving large forest municipalities, a sufficient number of plots are typically available for model-assisted estimations. For municipalities with limited economic interest in forests, using model-based methods can produce precise estimates.

A different approach of SAE was followed in Chapter IV, where a model-based framework was used. Such a framework is well suited for SAE in domains which are heterogeneous in terms of sampling and could not satisfy aggregation for model-assisted estimation. This was particularly the case in our Chapter regarding estimation of forest resources impacted by bark beetles, where the outbreak area was associated with the absence of field plots.

When it comes to disturbances, a key aspect relates to defining the estimation domains, which often requires external information such as satellite images to obtain a spatial delineation. In our study, the domains of impacted area were obtained using the ForDead method (Dutrieux et al., 2020, 2021), which relies on times-series analysis of Sentinel-2 data. However, over our study area in 2021, cloud cover posed limitations on detection and impacted the anomaly detection capabilities of the ForDead method. Consequently, detected areas contained uncertainties with expected impacts on estimation totals. While this detection issues was outside our objectives, we acknowledge that estimating in domains that are not error-free presents challenges. Future work would require to takes into account potential map errors in the resource estimation approach, thus improving the quality of the domains delineation.

Given the widespread impact of the bark beetle crisis across the entire North-East of France, one potential approach to incorporate map error criteria would involve assessing ForDead methods' omission and commission errors using aerial images (Fernandez-Carrillo et al., 2020; Meddens et al., 2013). The intersection with field plots could also benefit from the error estimation for this large-scale detection. To that end, mortality criteria from NFI plots would have to be contrasted to the bark-beetle attacks, in order to refine area estimations. Another option could involve the use of cloud-penetrating data, such as radar, which could complement the ForDead detection indicators. While Huo et al. (2021) reported that radar signal did not significantly contribute to the detection of outbreaks, Hollaus and Vreugdenhil (2019) stated that radar times-series data could enable detecting bark beetle impacts, thus providing more time-consistent surface estimates. Additionally, the change detection should also be connected with other forest health issues, as the ongoing climate changes can impact a wider range of tree species, and not only spruce and fir (Seidl et al., 2017). In such conditions, time-series analysis becomes crucial to confirm the problem and specify its origin. Back propagation of estimation (i.e., validating detection year *"n"* with year *"n+1"* year) is also a solution to avoid false detection. The analysis should also differ for conifers and hardwoods. In most cases, the loss of leaves could be reversed for hardwoods (a physiological response to stress), whereas it is more frequently linked to mortality in conifers (Aoki et al., 2018). Furthermore, incorporating expert-based knowledge could aid in the analysis of detections.

ForDead method has been specifically developed for the spruce and fir species. Some of these species found in mixed stands, as well as pure stands with surfaces lower than 2 ha (following the BD Foret definition used in ForDead) were not considered by this method. These stands can account up to 30% of the total resources (Saintonge et al., 2022). Additionally, it is important to consider that the estimation domain could also include clear cuts that may have been carried out due to the bark-beetle infestation. For instance, in cases where a full stand is clear cut while only a portion is affected by the infestation, there can be qualification issues and a potential mismatch between the clear-cut volumes and the estimated impacted volumes.

From a modelling perspective, both the general and specific models demonstrated similar performance, indicating that there is no need to develop a specific model and that the available general resources map is sufficient. This finding aligns with the results reported by Bouvier et al. (2015) in France, who found that specific models performed closely to general models, with a slight improvement ranging from 2% to 5% of the former's. Furthermore, the reliability of pixels within the bark-beetle affected areas was found to be similar to those outside the infestation zones, indicating that predictions from supporting auxiliary data were not impacted by the presence of the bark-beetle and can be used for estimation. However, it is important to consider the expected increase in bark-beetle outbreaks in the future, which may introduce discrepancies in the auxiliary data, particularly the optical data, even when there are no visually apparent signs of infestation.

In our general model, only one optical band was selected, while in the specific model, no band was selected at all. This suggests that relying solely on 3D data could be sufficient to predict resources in bark-beetle impacted areas, thus avoiding potential sensitivity of optical data to early, yet undetected infestation. However, it is worth noting that the timing of data acquisition can also influence 3D data. For instance, defoliation mostly occurs during summer months (Pollastrini et al., 2019), and collecting 3D data during this period may introduce variability in the overall structure of the point cloud data.

1.2. Forest resource mapping

Small area estimations rely on high resolution prediction maps which are of interest to support either decision making or management activities. However, as pointed out by Kangas et al. (2023) and McRoberts (2011), those maps, which are derived from models, inherently carry a considerable risk of unreliability. Without a means to identify unreliable predictions these maps are merely *"pretty pictures"* and can lead to sub-optimal decisions. Another closely topic concerned to this aspect is model transferability (Meyer and Pebesma, 2021). The concern is how a model developed within a specific calibration domain can be applied to a larger population that may extend beyond the calibration space or to different domains. Following this, Chapter II and Chapter III aimed to develop an index of prediction's reliability based on the use of convex hulls.

We defined a model's calibration domain as the convex hull of its calibration space and identify whether predicted pixels were located inside or outside this domain (i.e., interpolated or extrapolated). Furthermore, we found in Chapter II that predictions' bias tended to increase with extrapolation distance. This finding led to the development of a reliability index based on extrapolation distance (Chapter III). This index was found to be interesting, since parametric models often exhibit inaccuracies when operating outside their calibration domains (Kangas et al., 2016). Similarly, non-parametric models like kNN or random forest models are also known for their inability to extrapolate beyond their calibration domains (James et al., 2013; Magnussen et al., 2010).

Interestingly, we found in Chapter II that a larger sampling effort was required to minimize extrapolation, in contrast to the reduction in prediction error (rRMSE). This finding underlined the importance of the sampling effort and the need for the calibration domain to cover as much as possible the parameter space of the population, in order to avoid extrapolation. In this perspective, one possible solution to reduce extrapolation could either involve increasing the NFI sampling effort which could be costly, or incorporating supplementary plots from other sources, such as MFIs, although this may be feasible only for a limited number of management units. Another interesting solution could be to explore more advanced sampling methods, such as the cube method (Grafström et al., 2014). This method is specifically designed to improve the spread of probabilistic samples within the space of some auxiliary variables and can be utilized to sample from the space of dependent variables used in model construction. But such approaches could be difficult to implement in the

framework of NFIs, as the sampling design cannot be change easily because of the need to maintain a sampling stability over time.

Finally, the reliability index can also be used during the variable selection phase of a model. Typically, models are selected on the basis of minimizing their errors, such as RMSEs. From our finding, it could be interesting to add considerations about the level of extrapolation at the variable selection stage. Thus, among few competitive models, in terms of RMSEs, one could select the one which extrapolates the least. Additionally, certain variables may be affected by environmental stresses, such as the infra-red band of satellite images. It is therefore possible that the use of the convex hull could help to identify such variables that are sensitive to stresses occurring outside the calibration domain.

Apart from this, a limitation of convex hull approach was encountered during the model development process. It was observed that the convex hull computation time was exponential with the number of auxiliary variables used in the model. Specifically, when dealing with multidimensional convex hulls involving eight or more variables, the computational demands were substantial at population level. While in our studies, where the area of interest was described effectively by a maximum of five variables (as seen in Chapter III and Chapter IV), the convex hull approach proved to be practical. However, in cases where a larger number of auxiliary variables are necessary to accurately define the characteristics of the area of interest, the convex hull method may become impractical. In light of this, a possible solution for future studies would be to explore alternative approaches such as the isolation forest (Lesouple et al., 2021). This machine learning algorithm, based on binary trees, was specifically designed to identify anomalies within large datasets and offers faster computation (Lesouple et al., 2021; Liu et al., 2008). Its effectiveness to detect pixels out of the calibration domain could be tested in further studies.

An illustration of the reliability maps produced in Chapter III is presented in Figure 40. These reliability maps serve to inform the end-users about the usefulness and the reliance on the corresponding prediction maps.

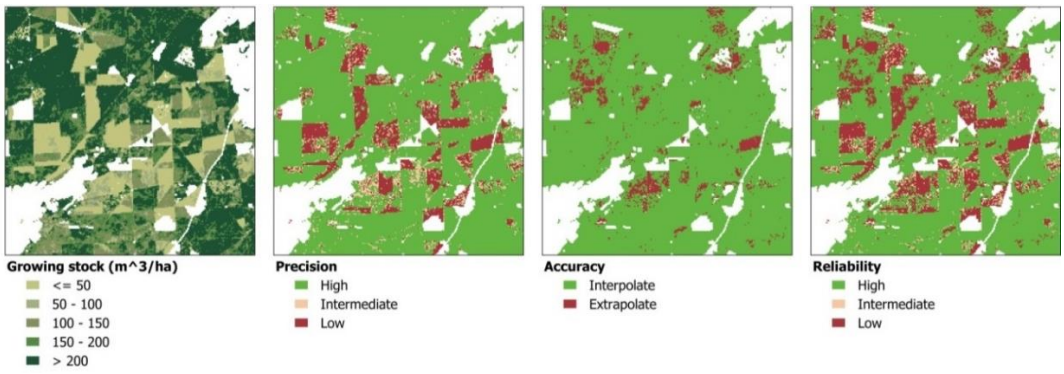

Figure 40. *Maps of predicted GSV, and corresponding precision, accuracy and reliability, for ALS based models.*

The maps we produced in Chapter III and Chapter IV, showed that stands with low values of growing stocks for example, exhibited low reliability, coinciding with lower model precision (Figure 40). These lower attribute values correspond to young stands and stands along forest transitions, which are not measured by the French NFI. Interestingly, we also observed that a higher proportion of the pixels were extrapolated in highly stocked stands. This result highlights a possible saturation of the model towards the upper values of the targeted forest attributes, suggesting that auxiliary data were not able to capture the full variability of the field data. Similar saturation issues were also reported in previous studies (Chirici et al., 2020; Saarela et al., 2015b). A potential solution could be to include new auxiliary data that are more relevant to forest characteristics and can better capture the variability in forest structure and composition. In order to better capture the forest canopy and sub-canopy structure, high-density ALS (HD ALS) data could be explored. However, the acquisition of such data may pose challenges due to their associated costs and limitations on data renewal. Interestingly, our research in Chapter III indicated that 3D point cloud data obtained from both DAP (47% rRMSE) and ALS (47.8% rRMSE) performed similarly. This finding is consistent with previous studies (Bohlin et al., 2012; Gobakken et al., 2015; Nurminen et al., 2013). While HD ALS may offer a slight improvement in estimation accuracy, the cost-effective DAP data could serve as a viable alternative if a high-resolution digital terrain model (DTM) is available (St-Onge et al., 2008). It is worth noting that the regular renewal of DAP data (~ 3 years) in many counties (Rahlf et al., 2017), presents an appealing solution for mitigating the saturation effect by providing time-series of growth-related information. This enable its utilization for various monitoring purposes, fertility analysis, and disturbance detection (Gobakken et al., 2015; Irulappa-Pillai-Vijayakumar et al., 2019; Véga and St-Onge, 2009).

Due to certain limitations in data acquisition for DAP or even ALS, there are concerns about their applicability in covering a large-scale landscape or in situations where forest disturbance regime is widespread. In such cases, an alternative to conventional DAP or ALS data could involve utilizing remote sensing data from spaceborne platforms. For instance, the integration of 3D data from GEDI sensor could provide valuable insights on forest canopy structure. Although this sensor provides discontinuous footprints rather than continuous data (Guerra-Hernández and Pascual, 2021), its data has been combined with other spatially continuous remote sensing data to generate continuous forest resource maps (Lang et al., 2022; Potapov et al., 2021). Alternatively, spaceborne radar sensors, such as Sentinel 1 or ALOS PALSAR, have also been investigated to compute forest structural properties and estimate several forest attributes of interest (Duncanson et al., 2020; Hajnsek et al., 2009; Silva et al., 2021). The data from these sensors are cost-effective and have good temporal resolution. However, it should be noted that the inclusion of radar data in forest inventory applications is still rare due to the complexity involved in processing radar data, and estimates obtained in complex canopies and mountainous areas are found to be less accurate (Boyd and Danson, 2005; Duncanson et al., 2020).

Additionally, preliminary tests were conducted on the Vosges study site (Chapter IV) using auxiliary variables related to climate (temperature, precipitation, solar radiation) and soil characteristics (soil acidity, water logging, soil water holding capacity) (Piedallu et al., 2016, 2013). It was hypothesized that the topographic conditions of the mountainous area would exhibit strong correlations with forest composition and structure, making these variables potentially influential to develop GSV models. However, these variables did not rank first as our best model but consistently appeared within the top 5 models. This was mainly because these variables were masked by highly correlated 3D variables. Nevertheless, the inclusion of these variables would be interesting in those areas where the most important auxiliary data, particularly 3D data are not available.

In terms of kNN model performance, the results obtained in both studies (Chapter III and Chapter IV) were consistent with the range reported in other studies (Chirici et al., 2016). However, we observed an improvement of 23% in the performance of the kNN model in Chapter IV compared to the model developed in Chapter III. This improvement can be attributed to the fact that we included new ALS-CHM variables in this study that were missing in the previous Chapter III. These variables are found to be highly correlated with the major forest attributes of interest (Véga et al., 2016). Further improvement in model performance may be achieved by using other approaches, such as the non-parametric Random Forest (RF) model. While estimating forest resources in Boreal forest of Canada, Penner et al. (2013) reported that performance of RF models were 33% superior to kNN. This superiority of RF performance can be attributed to its ability to combine multiple decision trees for more accurate predictions, eliminating the reliance on the number of nearest neighbors and the distance metric as in kNN. Another alternative approach to produce maps would be to utilize deep learning algorithms, such as convolutional neural networks (CNN) or recurrent neural network (RNN), which are gaining popularity over conventional machine learning methods. These algorithms have the capability to learn complex patterns and features from large datasets, enabling them to capture complex relationships between the NFI and auxiliary data. Several studies have emphasized on the modelling performance enhancements achieved by using neural network algorithms (Astola et al., 2021; Lahssini et al., 2022; Zhang et al., 2019). However, it is important to note that deep learning algorithms require high computational resources and large amounts of training data. Moreover, they are often considered black box models, lacking interpretability and confidence intervals. The challenge of understanding the reasoning behind predictions made by deep learning models limits their practical applicability in domains where interpretability is crucial (Chakraborty et al., 2017), such as decision-making in forestry management.

2. Conclusion

The increasing demand for forest resource information at the smallest possible domains has encouraged the rigorous implementation of MSNFI approaches in estimation and mapping forest attributes. This thesis has focused on addressing the challenges associated with MSNFI approaches in estimating forest attributes across various estimation domains, utilizing either model-assisted or model-based inference frameworks.

Although few general recommendations have been provided regarding the most suitable inference framework for specific estimation domains, the selection of an appropriate framework should be based on both the properties of the sampling design and the pursuing objectives. Design-based inference is well-suited for larger geographical areas (e.g., national up to regional scales) where a sufficient number of NFI plots are available. On the other hand, model-assisted inference is particularly effective for SAE at the sub-regional level, assuming an adequate number of NFI plots are available in each estimation domain to facilitate estimation. This framework is capable of generating unbiased estimates even when the relationship between the target forest attributes and the auxiliary variables is weak. In cases where there are too few to even no NFI plots available in the area of interest, the model-based framework becomes the only viable option. Given a well-specified model, this framework can generate estimates that are as good as model-assisted estimators.

The MSNFI approaches proposed in this thesis are capable to generate estimates using either model-assisted or model based approach depending on the nature and the size of the domain. The method proposed to evaluate pixel reliability provides a high flexibility, allowing using the same modelling approach with different estimation framework.

The proposed algorithm developed in Chapter I constitutes an appealing approach for flexible estimation domains and user controlled precision. Additionally, the approach developed in Chapter III and applied in Chapter IV provides high-resolution prediction maps that assist forest managers in localizing forest resources and estimating the bark beetle impacted resources. Furthermore, the reliability maps, which are developed from the combination of accuracy (Chapter II and Chapter III) and precision maps (Chapter III), will allow for judgments about whether the predicted forest attributes map is reliable enough for decision making.

While the research presented in this thesis has primarily focused on state variables and for aggregated quantities, further development are necessary to address estimation problems related to flux variables and ventilated data (e.g., diameter size, species). The estimation of flux variables poses particular challenges as they require temporal integration. Possible improvement for such variables is expected, thanks to the development of times series of remote sensing databases, as well as the increasing availability of 3D models derived from ALS and DAP. Such times-series might provide auxiliary data correlated with fluxes, enabling significant precision gain for small domains.

References

Abdullah, H., Skidmore, A.K., Darvishzadeh, R., Heurich, M., 2019. Sentinel-2 accurately maps green-attack stage of European spruce bark beetle (Ips typographus, L.) compared with Landsat-8. Remote Sensing in Ecology and Conservation 5, 87–106. https://doi.org/10.1002/rse2.93.

Achard, F., 2009. Vital Forest Graphics. UNEP/GRID-Ardenal/UNFF, Ardenal, Norway.

Altman, N.S., 1992. An Introduction to Kernel and Nearest-Neighbor Nonparametric Regression. The American Statistician 46, 175. https://doi.org/10.2307/2685209.

Andersen, H.E., Barrett, T., Winterberger, K., Strunk, J., Temesgen, H., 2009. Estimating forest biomass on the western lowlands of the Kenai Peninsula of Alaska using airborne lidar and field plot data in a model-assisted sampling design, in: Proceedings of the IUFRO Division 4 Conference: Extending Forest Inventory and Monitoring over Space and Time. pp. 19–22.

Aoki, C.F., Cook, M., Dunn, J., Finley, D., Fleming, L., Yoo, R., Ayres, M.P., 2018. Old pests in new places: Effects of stand structure and forest type on susceptibility to a bark beetle on the edge of its native range. Forest Ecology and Management 419–420, 206–219. https://doi.org/10.1016/j.foreco.2018.03.009.

Arroyo-Rodríguez, V., Fahrig, L., Tabarelli, M., Watling, J.I., Tischendorf, L., Benchimol, M., Cazetta, E., Faria, D., Leal, I.R., Melo, F.P.L., Morante-Filho, J.C., Santos, B.A., Arasa-Gisbert, R., Arce-Peña, N., Cervantes-López, M.J., Cudney-Valenzuela, S., Galán-Acedo, C., San-José, M., Vieira, I.C.G., Slik, J.W.F., Nowakowski, A.J., Tscharntke, T., 2020. Designing optimal human-modified landscapes for forest biodiversity conservation. Ecology letters 23, 1404–1420. https://doi.org/10.1111/ele.13535.

Asner, G.P., Mascaro, J., Muller-Landau, H.C., Vieilledent, G., Vaudry, R., Rasamoelina, M., Hall, J.S., van Breugel, M., 2012. A universal airborne LiDAR approach for tropical forest carbon mapping. Oecologia 168, 1147–1160. https://doi.org/10.1007/s00442-011-2165-z.

Astola, H., Häme, T., Sirro, L., Molinier, M., Kilpi, J., 2019. Comparison of Sentinel-2 and Landsat 8 imagery for forest variable prediction in boreal region. Remote Sensing of Environment 223, 257–273. https://doi.org/10.1016/j.rse.2019.01.019.

Astola, H., Seitsonen, L., Halme, E., Molinier, M., Lönnqvist, A., 2021. Deep Neural Networks with Transfer Learning for Forest Variable Estimation Using Sentinel-2 Imagery in Boreal Forest. Remote Sensing 13, 2392. https://doi.org/10.3390/rs13122392.

Astrup, R., Rahlf, J., Bjørkelo, K., Debella-Gilo, M., Gjertsen, A.-K., Breidenbach, J., 2019. Forest information at multiple scales: development, evaluation and application of the Norwegian forest

resources map SR16. Scandinavian Journal of Forest Research 34, 484–496. https://doi.org/10.1080/02827581.2019.1588989.

Baccini, A., Laporte, N., Goetz, S.J., Sun, M., Dong, H., 2008. A first map of tropical Africa's above-ground biomass derived from satellite imagery. Environmental Research Letters 3, 045011. https://doi.org/10.1088/1748-9326/3/4/045011.

Baffetta, F., Fattorini, L., Franceschi, S., Corona, P., 2009. Design-based approach to k-nearest neighbours technique for coupling field and remotely sensed data in forest surveys. Remote Sensing of Environment 113, 463–475. https://doi.org/10.1016/j.rse.2008.06.014.

Baig, M.H.A., Zhang, L., Shuai, T., Tong, Q., 2014. Derivation of a tasselled cap transformation based on Landsat 8 at-satellite reflectance. Remote Sensing Letters 5, 423–431. https://doi.org/10.1080/2150704X.2014.915434.

Barati, S., Rayegani, B., Saati, M., Sharifi, A., Nasri, M., 2011. Comparison the accuracies of different spectral indices for estimation of vegetation cover fraction in sparse vegetated areas. The Egyptian Journal of Remote Sensing and Space Science 14, 49–56. https://doi.org/10.1016/j.ejrs.2011.06.001.

Barber, C.B., Dobkin, D.P., Huhdanpaa, H., 1996. The quickhull algorithm for convex hulls. ACM Transactions on Mathematical Software (TOMS) 22, 469–483. https://doi.org/10.1145/235815.235821.

Barbier, E.B., Burgess, J.C., Grainger, A., 2010. The forest transition: Towards a more comprehensive theoretical framework. Land Use Policy 27, 98–107. https://doi.org/10.1016/j.landusepol.2009.02.001.

Barrett, F., McRoberts, R.E., Tomppo, E., Cienciala, E., Waser, L.T., 2016. A questionnaire-based review of the operational use of remotely sensed data by national forest inventories. Remote Sensing of Environment 174, 279–289. https://doi.org/10.1016/j.rse.2015.08.029.

Beaudoin, A., Bernier, P.Y., Guindon, L., Villemaire, P., Guo, X.J., Stinson, G., Bergeron, T., Magnussen, S., Hall, R.J., 2014. Mapping attributes of Canada's forests at moderate resolution through kNN and MODIS imagery. Canadian Journal of Forest Research 44, 521–532. https://doi.org/10.1139/cjfr-2013-0401.

Bell, D.M., Wilson, B.T., Werstak, C.E., Oswalt, C.M., Perry, C.H., 2022. Examining k-Nearest Neighbor Small Area Estimation Across Scales Using National Forest Inventory Data. Frontiers in Forests and Global Change 5:763422. https://doi.org/10.3389/ffgc.2022.763422.

Bhanu, B., Lin, Y., 2003. Genetic algorithm based feature selection for target detection in SAR images. Image and Vision Computing 21, 591–608. https://doi.org/10.1016/S0262-8856(03)00057-X

Binelli, E.K., Gholz, H.L., Duryea, M.L., 2008. Plant succession and disturbances in the urban forest ecosystem. University of Florida, IFAS Extension, Gainesville 1–23.

Blackard, J.A., Finco, M.V., Helmer, E.H., Holden, G.R., Hoppus, M.L., Jacobs, D.M., Lister, A.J., Moisen, G.G., Nelson, M.D., Riemann, R., 2008. Mapping U.S. forest biomass using nationwide forest inventory data and moderate resolution information. Remote Sensing of Environment 112, 1658–1677. https://doi.org/10.1016/j.rse.2007.08.021.

Bohlin, J., Wallerman, J., Fransson, J.E.S., 2012. Forest variable estimation using photogrammetric matching of digital aerial images in combination with a high-resolution DEM. Scandinavian Journal of Forest Research 27 (7), 692–699. https://doi.org/10.1080/02827581.2012.686625.

Botkin, D.B., Simpson, L.G., 1990. Biomass of the North American Boreal Forest: A Step toward Accurate Global Measures. Biogeochemistry 9, 161–174.

Boucher, P., Hancock, S., Orwig, D., Duncanson, L., Armston, J., Tang, H., Krause, K., Cook, B., Paynter, I., Li, Z., Elmes, A., Schaaf, C., 2020. Detecting Change in Forest Structure with Simulated GEDI Lidar Waveforms: A Case Study of the Hemlock Woolly Adelgid (HWA; Adelges tsugae) Infestation. Remote Sensing 12, 1304. https://doi.org/10.3390/rs12081304.

Bouchet, P.J., Miller, D.L., Roberts, J.J., Mannocci, L., Harris, C.M., Thomas, L., 2020. dsmextra: Extrapolation assessment tools for density surface models. Methods in Ecology and Evolution 11, 1464–1469. https://doi.org/10.1111/2041-210X.13469.

Boudreau, J., Nelson, R., Margolis, H., Beaudoin, A., Guindon, L., Kimes, D., 2008. Regional aboveground forest biomass using airborne and spaceborne LiDAR in Québec. Remote Sensing of Environment 112, 3876–3890. https://doi.org/10.1016/j.rse.2008.06.003.

Bouvier, M., Durrieu, S., Fournier, R.A., Renaud, J.-P., 2015. Generalizing predictive models of forest inventory attributes using an area-based approach with airborne LiDAR data. Remote Sensing of Environment 156, 322–334. https://doi.org/10.1016/j.rse.2014.10.004.

Bouvier, M., Durrieu, S., Fournier, R.A., Saint-Geours, N., Guyon, D., Grau, E., De Boissieu, F., 2019. Influence of Sampling Design Parameters on Biomass Predictions Derived from Airborne LiDAR Data. Canadian Journal of Remote Sensing 45, 650–672. https://doi.org/10.1080/07038992.2019.1669013.

Boyd, D.S., Danson, F.M., 2005. Satellite remote sensing of forest resources: three decades of research development. Progress in Physical Geography: Earth and Environment 29, 1–26. https://doi.org/10.1191/0309133305pp432ra.

Brassel, R., Lischke, H., 2001. Swiss National Forest Inventory: Methods and Models of the Second Assessment. Swiss Federal Research Institute WSL, Birmensdorf, CH.

Breidenbach, J., Astrup, R., 2012. Small area estimation of forest attributes in the Norwegian National Forest Inventory. European Journal of Forest Research 131, 1255–1267. https://doi.org/10.1007/s10342-012-0596-7.

Breidenbach, J., Magnussen, S., Rahlf, J., Astrup, R., 2018. Unit-level and area-level small area estimation under heteroscedasticity using digital aerial photogrammetry data. Remote Sensing of Environment 212, 199–211. https://doi.org/10.1016/j.rse.2018.04.028.

Breidenbach, J., McRoberts, R.E., Alberdi, I., Antón-Fernández, C., Tomppo, E., 2021. A century of national forest inventories – informing past, present and future decisions. Forest Ecosystems 8, 36. https://doi.org/10.1186/s40663-021-00315-x.

Breidenbach, J., Næsset, E., Gobakken, T., 2012. Improving k-nearest neighbor predictions in forest inventories by combining high and low density airborne laser scanning data. Remote Sensing of Environment 117, 358–365. https://doi.org/10.1016/j.rse.2011.10.010.

Breidenbach, J., Nothdurft, A., Kändler, G., 2010. Comparison of nearest neighbour approaches for small area estimation of tree species-specific forest inventory attributes in central Europe using airborne laser scanner data. European Journal of Forest Research 129, 833–846. https://doi.org/10.1007/s10342-010-0384-1.

Breidt, F.J., Opsomer, J.D., 2017. Model-Assisted Survey Estimation with Modern Prediction Techniques. Statistical Science 32. https://doi.org/10.1214/16-STS589.

Breiman, L., 2001. Random Forests. Machine Learning 45, 5–32. https://doi.org/10.1023/A:1010933404324.

Bright, B.C., Hicke, J.A., Hudak, A.T., 2012. Estimating aboveground carbon stocks of a forest affected by mountain pine beetle in Idaho using lidar and multispectral imagery. Remote Sensing of Environment 124, 270–281. https://doi.org/10.1016/j.rse.2012.05.016.

Bright, B.C., Hudak, A.T., McGaughey, R., Andersen, H.-E., Negrón, J., 2013. Predicting live and dead tree basal area of bark beetle affected forests from discrete-return lidar. Canadian Journal of Remote Sensing 39, S99–S111. https://doi.org/10.5589/m13-027.

Brooks, D.G., Carroll, S.S., Verdini, W.A., 1988. Characterizing the Domain of a Regression Model. The American Statistician 42, 187–190. https://doi.org/10.1080/00031305.1988.10475559.

Brosofske, K.D., Froese, R.E., Falkowski, M.J., Banskota, A., 2014. A Review of Methods for Mapping and Prediction of Inventory Attributes for Operational Forest Management. Forest Science 60, 733–756. https://doi.org/10.5849/forsci.12-134.

Brus, R., Pötzelsberger, E., Lapin, K., Brundu, G., Orazio, C., Straigyte, L., Hasenauer, H., 2019. Extent, distribution and origin of non-native forest tree species in Europe. Scandinavian Journal of Forest Research 34, 533–544. https://doi.org/10.1080/02827581.2019.1676464.

Canelles, Q., Aquilué, N., James, P.M.A., Lawler, J., Brotons, L., 2021. Global review on interactions between insect pests and other forest disturbances. Landscape Ecology 36, 945–972. https://doi.org/10.1007/s10980-021-01209-7.

Castillo-Santiago, M.A., Ricker, M., de Jong, B.H.J., 2010. Estimation of tropical forest structure from SPOT-5 satellite images. International Journal of Remote Sensing 31, 2767–2782. https://doi.org/10.1080/01431160903095460.

Chakraborty, S., Tomsett, R., Raghavendra, R., Harborne, D., Alzantot, M., Cerutti, F., Srivastava, M., Preece, A., Julier, S., Rao, R.M., Kelley, T.D., Braines, D., Sensoy, M., Willis, C.J., Gurram, P., 2017. Interpretability of deep learning models: A survey of results. Presented at the 2017 IEEE SmartWorld, Ubiquitous Intelligence & Computing, Advanced & Trusted Computed, Scalable Computing & Communications, Cloud & Big Data Computing, Internet of People and Smart City Innovation (SmartWorld/SCALCOM/UIC/ATC/CBDCom/IOP/SCI), IEEE, San Francisco, CA, pp. 1–6. https://doi.org/10.1109/UIC-ATC.2017.8397411.

Chambers, J.Q., Higuchi, N., Tribuzy, E.S., Trumbore, S.E., 2001. Carbon sink for a century. Nature 410, 429–429. https://doi.org/10.1038/35068624.

Chen, Q., McRoberts, R.E., Wang, C., Radtke, P.J., 2016. Forest aboveground biomass mapping and estimation across multiple spatial scales using model-based inference. Remote Sensing of Environment 184, 350–360. https://doi.org/10.1016/j.rse.2016.07.023.

Chirici, G., Barbati, A., Corona, P., Marchetti, M., Travaglini, D., Maselli, F., Bertini, R., 2008. Non-parametric and parametric methods using satellite images for estimating growing stock volume in alpine and Mediterranean forest ecosystems. Remote Sensing of Environment 112, 2686–2700. https://doi.org/10.1016/j.rse.2008.01.002.

Chirici, G., Corona, P., Marchetti, M., Mastronardi, A., Maselli, F., Bottai, L., Travaglini, D., 2012. K-NN FOREST: a software for the non-parametric prediction and mapping of environmental variables by the k-Nearest Neighbors algorithm. European Journal of Remote Sensing 45, 433–442. https://doi.org/10.5721/EuJRS20124536.

Chirici, G., Giannetti, F., McRoberts, R.E., Travaglini, D., Pecchi, M., Maselli, F., Chiesi, M., Corona, P., 2020. Wall-to-wall spatial prediction of growing stock volume based on Italian National Forest Inventory plots and remotely sensed data. International Journal of Applied Earth Observation and Geoinformation 84, 101959. https://doi.org/10.1016/j.jag.2019.101959.

Chirici, G., Mura, M., McInerney, D., Py, N., Tomppo, E.O., Waser, L.T., Travaglini, D., McRoberts, R.E., 2016. A meta-analysis and review of the literature on the k-Nearest Neighbors technique for forestry applications that use remotely sensed data. Remote Sensing of Environment 176, 282–294. https://doi.org/10.1016/j.rse.2016.02.001.

Chojnacky, D.C., Wynne, R.H., Blinn, C.E., 2006. Mapping forest inventory and analysis data attributes within the framework of double sampling for stratification design, in: McRoberts, R.E., Reams, G.A., Van Deusen, P.C., McWilliams, W.H. (Eds.), Proceedings of the Eighth Annual Forest Inventory and Analysis Symposium; Monterey, CA. Gen. Tech. Report WO-79. Washington, DC: U.S. Department of Agriculture, Forest Service, 2009.

Christensen, N.L., 2014. An historical perspective on forest succession and its relevance to ecosystem restoration and conservation practice in North America. Forest Ecology and Management 330, 312–322. https://doi.org/10.1016/j.foreco.2014.07.026.

Christianson, D.S., Kaufman, C.G., 2016. Effects of sample design and landscape features on a measure of environmental heterogeneity. Methods in Ecology and Evolution 7, 770–782. https://doi.org/10.1111/2041-210X.12539.

Clark, D.B., Castro, C.S., Alvarado, L.D.A., Read, J.M., 2004. Quantifying mortality of tropical rain forest trees using high-spatial-resolution satellite data. Ecology Letters 7, 52–59. https://doi.org/10.1046/j.1461-0248.2003.00547.x.

Coelho, P.S., Pereira, L.N., 2011. A spatial unit level model for small area estimation. Revstat Statistical Journal 9, 155–180.

Cohen, W.B., Goward, S.N., 2004. Landsat's Role in Ecological Applications of Remote Sensing. BioScience 54, 535. https://doi.org/10.1641/0006-3568(2004)054[0535:LRIEAO]2.0.CO;2.

Cohen, W.B., Kushla, J.D., Ripple, W.J., Garman, S.L., 1996. An introduction to digital methods in remote sensing of forested ecosystems: Focus on the Pacific Northwest, USA. Environmental Management 20, 421–435. https://doi.org/10.1007/BF01203849.

Cohen, W.B., Maiersperger, T.K., Spies, T.A., Oetter, D.R., 2001. Modelling forest cover attributes as continuous variables in a regional context with Thematic Mapper data. International Journal of Remote Sensing 22, 2279–2310. https://doi.org/10.1080/01431160121472.

Colwell, R.N., 1964. Aerial photography – a valuable sensor for the scientist. American Scientist 52, 16–49.

Conn, P.B., Johnson, D.S., Boveng, P.L., 2015. On Extrapolating Past the Range of Observed Data When Making Statistical Predictions in Ecology. PLOS ONE 10, e0141416. https://doi.org/10.1371/journal.pone.0141416.

Cook, R.D., 1977. Detection of Influential Observation in Linear Regression. Technometrics 19, 15–18. https://doi.org/10.1080/00401706.1977.10489493.

Coops, N.C., Tompalski, P., Goodbody, T.R.H., Queinnec, M., Luther, J.E., Bolton, D.K., White, J.C., Wulder, M.A., van Lier, O.R., Hermosilla, T., 2021. Modelling lidar-derived estimates of forest attributes over space and time: A review of approaches and future trends. Remote Sensing of Environment 260, 112477. https://doi.org/10.1016/j.rse.2021.112477.

Corona, P., Fattorini, L., Franceschi, S., Scrinzi, G., Torresan, C., 2014. Estimation of standing wood volume in forest compartments by exploiting airborne laser scanning information: model-based, design-based, and hybrid perspectives. Canadian Journal of Forest Research 44, 1303–1311. https://doi.org/10.1139/cjfr-2014-0203.

Cosenza, D.N., Korhonen, L., Maltamo, M., Packalen, P., Strunk, J.L., Næsset, E., Gobakken, T., Soares, P., Tomé, M., 2021. Comparison of linear regression, k-nearest neighbour and random forest methods in airborne laser-scanning-based prediction of growing stock. Forestry 94, 311–323. https://doi.org/10.1093/forestry/cpaa034.

Coulston, J.W., Green, P.C., Radtke, P.J., Prisley, S.P., Brooks, E.B., Thomas, V.A., Wynne, R.H., Burkhart, H.E., 2021. Enhancing the precision of broad-scale forestland removals estimates with small area estimation techniques. Forestry 94, 427–441. https://doi.org/10.1093/forestry/cpaa045.

Crookston, N.L., Finley, A.O., 2008. yaImpute: An R Package for kNN Imputation. Journal of Statistical Software 23. https://doi.org/10.18637/jss.v023.i10.

D'Amico, G., Vangi, E., Francini, S., Giannetti, F., Nicolaci, A., Travaglini, D., Massai, L., Giambastiani, Y., Terranova, C., Chirici, G., 2021. Are we ready for a National Forest Information System? State of the art of forest maps and airborne laser scanning data availability in Italy. iForest 14, 144–154. https://doi.org/10.3832/ifor3648-014.

Danson, F.M., 1987. Preliminary evaluation of the relationships between SPOT-1 HRV data and forest stand parameters. International Journal of Remote Sensing 8, 1571–1575. https://doi.org/10.1080/01431168708954798.

Datta, G.S., Rao, C.R., 2009. Model-Based Approach to Small Area Estimation, in: Pfeffermann, Rao (Eds.), Handbook of Statistics 29B, Sample Surveys: Inference and Analysis. Elsevier, Amsterdam, pp. 251–288. https://doi.org/10.1016/S0169-7161(09)00232-6.

Denardou, A., Hervé, J.C., Dupouey, J.L., Bir, J., Audinot, T., Bontemps, J.D., 2017. L'expansion séculaire des forêts françaises est dominée par l'accroissement du stock sur pied et ne sature pas dans le temps. Revue Forestière Française 69, 319–339.

Deo, R.K., Froese, R.E., Falkowski, M.J., 2011. Geospatial Forest Inventory Models for Michigan. Final report submitted to Michigan Economic Development Corporation. Michigan Technological University, Houghton MI. 24 pp.

Dettmann, G.T., Radtke, P.J., Coulston, J.W., Green, P.C., Wilson, B.T., Moisen, G.G., 2022. Review and Synthesis of Estimation Strategies to Meet Small Area Needs in Forest Inventory. Frontiers in Forests and Global Change 5. http://dx.doi.org/10.3389/ffgc.2022.813569.

Dormann, C.F., Elith, J., Bacher, S., Buchmann, C., Carl, G., Carré, G., Marquéz, J.R.G., Gruber, B., Lafourcade, B., Leitão, P.J., Münkemüller, T., McClean, C., Osborne, P.E., Reineking, B., Schröder, B., Skidmore, A.K., Zurell, D., Lautenbach, S., 2013. Collinearity: a review of methods to deal with it and a simulation study evaluating their performance. Ecography 36, 27–46. https://doi.org/10.1111/j.1600-0587.2012.07348.x.

Drake, J.B., Dubayah, R.O., Clark, D.B., Knox, R.G., Blair, J.B., Hofton, M.A., Chazdon, R.L., Weishampel, J.F., Prince, S., 2002. Estimation of tropical forest structural characteristics using large-footprint lidar. Remote Sensing of Environment 79, 305–319. https://doi.org/10.1016/S0034-4257(01)00281-4.

Duncanson, L., Kellner, J.R., Armston, J., Dubayah, R., Minor, D.M., Hancock, S., Healey, S.P., Patterson, P.L., Saarela, S., Marselis, S., Silva, C.E., Bruening, J., Goetz, S.J., Tang, H., Hofton, M., Blair, B., Luthcke, S., Fatoyinbo, L., Abernethy, K., Alonso, A., Andersen, H.-E., Aplin, P., Baker, T.R., Barbier, N., Bastin, J.F., Biber, P., Boeckx, P., Bogaert, J., Boschetti, L., Boucher, P.B., Boyd, D.S., Burslem, D.F.R.P., Calvo-Rodriguez, S., Chave, J., Chazdon, R.L., Clark, D.B., Clark, D.A., Cohen, W.B., Coomes, D.A., Corona, P., Cushman, K.C., Cutler, M.E.J., Dalling, J.W., Dalponte, M., Dash, J., de-Miguel, S., Deng, S., Ellis, P.W., Erasmus, B., Fekety, P.A., Fernandez-Landa, A., Ferraz, A., Fischer, R., Fisher, A.G., García-Abril, A., Gobakken, T., Hacker, J.M., Heurich, M., Hill, R.A., Hopkinson, C., Huang, H., Hubbell, S.P., Hudak, A.T., Huth, A., Imbach, B., Jeffery, K.J., Katoh, M., Kearsley, E., Kenfack, D., Kljun, N., Knapp, N., Král, K., Krůček, M., Labrière, N., Lewis, S.L., Longo, M., Lucas, R.M., Main, R., Manzanera, J.A., Martínez, R.V., Mathieu, R., Memiaghe, H., Meyer, V., Mendoza, A.M., Monerris, A., Montesano, P., Morsdorf, F., Næsset, E., Naidoo, L., Nilus, R., O'Brien, M., Orwig, D.A., Papathanassiou, K., Parker, G., Philipson, C., Phillips, O.L., Pisek, J., Poulsen, J.R., Pretzsch, H., Rüdiger, C., Saatchi, S., Sanchez-Azofeifa, A., Sanchez-Lopez, N.,

Scholes, R., Silva, C.A., Simard, M., Skidmore, A., Stereńczak, K., Tanase, M., Torresan, C., Valbuena, R., Verbeeck, H., Vrska, T., Wessels, K., White, J.C., White, L.J.T., Zahabu, E., Zgraggen, C., 2022. Aboveground biomass density models for NASA's Global Ecosystem Dynamics Investigation (GEDI) lidar mission. Remote Sensing of Environment 270, 112845. https://doi.org/10.1016/j.rse.2021.112845.

Duncanson, L., Neuenschwander, A., Hancock, S., Thomas, N., Fatoyinbo, T., Simard, M., Silva, C.A., Armston, J., Luthcke, S.B., Hofton, M., Kellner, J.R., Dubayah, R., 2020. Biomass estimation from simulated GEDI, ICESat-2 and NISAR across environmental gradients in Sonoma County, California. Remote Sensing of Environment 242, 111779. https://doi.org/10.1016/j.rse.2020.111779.

Durrieu, S., Vega, C., Bouvier, M., Gosselin, F., Renaud, J.-P., Saint-André, L., 2015. Optical remote sensing of tree and stand heights, in: Land Resources Monitoring, Modeling, and Mapping with Remote Sensing, Remote Sensing Handbook. CRC Press, pp. 449–485.

Dutrieux, R., Férét, J.-B., Ose, K., 2020. Mise au point d'une méthode reproductible pour le suivi généralisé des dégâts de scolytes par télédétection satellitaire. Rendez-Vous Tech. ONF Les 37–44.

Dutrieux, R., Feret, J.-B., Ose, K., De Boissieu, F., 2021. Package Fordead. https://doi.org/10.15454/4TEO6H.

Eastman, J.R., Fulk, M., 1993. Long sequence time series evaluation using standardized principal components. Photogrammetric Engineering and Remote Sensing 59, 1307–1312.

Ebert, T., Belz, J., Nelles, O., 2014. Interpolation and extrapolation: Comparison of definitions and survey of algorithms for convex and concave hulls. Presented at the 2014 IEEE Symposium on Computational Intelligence and Data Mining (CIDM), IEEE, Orlando, FL, USA, pp. 310–314. https://doi.org/10.1109/CIDM.2014.7008683.

Efron, B., Tibshirani, R.J., 1994. An Introduction to the Bootstrap. Boca Raton, FL: Chapman and Hall/CRC. https://doi.org/10.1201/9780429246593.

Ekström, M., Nilsson, M., 2021. A Comparison of Model-Assisted Estimators, With and Without Data-Driven Transformations of Auxiliary Variables, With Application to Forest Inventory. Frontiers in Forests and Global Change 4, 764495. https://doi.org/10.3389/ffgc.2021.764495.

Ene, L.T., Næsset, E., Gobakken, T., Gregoire, T.G., Ståhl, G., Nelson, R., 2012. Assessing the accuracy of regional LiDAR-based biomass estimation using a simulation approach. Remote Sensing of Environment 123, 579–592. https://doi.org/10.1016/j.rse.2012.04.017.

Ene, L.T., Næsset, E., Gobakken, T., Mauya, E.W., Bollandsås, O.M., Gregoire, T.G., Ståhl, G., Zahabu, E., 2016. Large-scale estimation of aboveground biomass in miombo woodlands using

airborne laser scanning and national forest inventory data. Remote Sensing of Environment 186, 626–636. https://doi.org/10.1016/j.rse.2016.09.006.

Esteban, J., McRoberts, R., Fernández-Landa, A., Tomé, J., Næsset, E., 2019. Estimating Forest Volume and Biomass and Their Changes Using Random Forests and Remotely Sensed Data. Remote Sensing 11, 1944. https://doi.org/10.3390/rs11161944.

Fadili, M., Renaud, J.-P., Bock, J., Vega, C., 2019. RegisTree: a registration algorithm to enhance forest inventory plot georeferencing. Annals of Forest Science 76, 30. https://doi.org/10.1007/s13595-019-0814-2.

Fan, J., 2000. Prospects of Nonparametric Modeling. Journal of the American Statistical Association 95, 1296–1300. https://doi.org/10.1080/01621459.2000.10474334.

FAO, 2020. Global Forest Resources Assessment 2020. UN Food and Agriculture Organization, Rome. https://doi.org/10.4060/ca9825en.

FAO, 2010. Global Forest Resources Assessment 2010. FAO Forestry Paper No. 163. UN Food and Agriculture Organization, Rome.

Fattorini, L., Marcheselli, M., Pisani, C., 2006. A three-phase sampling strategy for large-scale multiresource forest inventories. Journal of Agricultural, Biological, and Environmental Statistics 11, 296–316. https://doi.org/10.1198/108571106X130548.

Fernandez-Carrillo, A., Patočka, Z., Dobrovolný, L., Franco-Nieto, A., Revilla-Romero, B., 2020. Monitoring Bark Beetle Forest Damage in Central Europe. A Remote Sensing Approach Validated with Field Data. Remote Sensing 12, 3634. https://doi.org/10.3390/rs12213634.

Filippelli, S.K., Lefsky, M.A., Rocca, M.E., 2019. Comparison and integration of lidar and photogrammetric point clouds for mapping pre-fire forest structure. Remote Sensing of Environment 224, 154–166. https://doi.org/10.1016/j.rse.2019.01.029.

Finegan, B., 1984. Forest succession. Nature 312, 109–114. https://doi.org/10.1038/312109a0.

Forest Europe, 2020. State of Europe's Forest 2020. Ministerial Conference on the Protection of Forests in Europe, Forest Europe Liaison Unit Bratislava.

Fortin, M., 2020. Updating plots to improve the precision of small-area estimates: the example of the Lorraine region, France. Canadian Journal of Forest Research 50, 648–658. https://doi.org/10.1139/cjfr-2019-0405.

Fortin, M., Manso, R., Schneider, R., 2018. Parametric bootstrap estimators for hybrid inference in forest inventories. Forestry 91, 354–365. https://doi.org/10.1093/forestry/cpx048.

Frank, B., Mauro, F., Temesgen, H., 2020. Model-Based Estimation of Forest Inventory Attributes Using Lidar: A Comparison of the Area-Based and Semi-Individual Tree Crown Approaches. Remote Sensing 12, 2525. https://doi.org/10.3390/rs12162525.

Franklin, S.E., 2001. Remote sensing for sustainable forest management. Boca Raton, FL: Lewis.

Fraser, R.H., Fernandes, R., Latifovic, R., 2003. Multi-temporal Mapping of Burned Forest over Canada Using Satellite-based Change Metrics. Geocarto International 18, 37–47. https://doi.org/10.1080/10106040308542271.

Frazer, G.W., Magnussen, S., Wulder, M.A., Niemann, K.O., 2011. Simulated impact of sample plot size and co-registration error on the accuracy and uncertainty of LiDAR-derived estimates of forest stand biomass. Remote Sensing of Environment 115, 636–649. https://doi.org/10.1016/j.rse.2010.10.008.

Frelich, L., 2016. Forest dynamics. F1000Research 5, 183. https://doi.org/10.12688/f1000research.7412.1.

Frescino, T.S., McConville, K.S., White, G.W., Toney, J.C., Moisen, G.G., 2022. Small Area Estimates for National Applications: A Database to Dashboard Strategy Using FIESTA. Frontiers in Forests and Global Change 5. https://doi.org/10.3389/ffgc.2022.779446.

Fridman, J., Holm, S., Nilsson, M., Nilsson, P., Ringvall, A., Ståhl, G., 2014. Adapting National Forest Inventories to changing requirements – the case of the Swedish National Forest Inventory at the turn of the 20th century. Silva Fennica 48. https://doi.org/10.14214/sf.1095.

Fridman, J., Westerlund, B., 2016. Sweden, in: Vidal, C., Alberdi, I.A., Hernández Mateo, L., Redmond, J.J. (Eds.), National Forest Inventories - Assessment of Wood Availability and Use. Springer, Cham, pp. 769–782. https://doi.org/10.1007/978-3-319-44015-6_42.

Gabler, K., Schadauer, K., 2007. Some approaches and designs of sample-based National Forest Inventories. Austrian Journal of Forest Science 124, 105–133.

Gagliasso, D., Hummel, S., Temesgen, H., 2014. A Comparison of Selected Parametric and Non-Parametric Imputation Methods for Estimating Forest Biomass and Basal Area. Open Journal of Forestry 04, 42–48. https://doi.org/10.4236/ojf.2014.41008.

Gaines, G.C., Affleck, D.L.R., 2021. Small Area Estimation of Postfire Tree Density Using Continuous Forest Inventory Data. Frontiers in Forests and Global Change 4, 761509. https://doi.org/10.3389/ffgc.2021.761509.

Ghosh, M., Rao, J.N.K., 1994. Small Area Estimation: An Appraisal. Statistical Science 9. https://doi.org/10.1214/ss/1177010647.

Giacona, F., Eckert, N., Mainieri, R., Martin, B., Corona, C., Lopez-Saez, J., Monnet, J.-M., Naaim, M., Stoffel, M., 2018. Avalanche activity and socio-environmental changes leave strong footprints in forested landscapes: a case study in the Vosges medium-high mountain range. Annals of Glaciology 59, 111–133. https://doi.org/10.1017/aog.2018.26.

Gillis, M.D., 2001. Canada's National Forest Inventory (Responding to Current Information Needs). Environmental Monitoring and Assessment 67, 121–129. https://doi.org/10.1023/A:1006405820244.

Ginzler, C., Price, B., Bösch, R., Fischer, C., Hobi, M.L., Psomas, A., Rehush, N., Wang, Z., Waser, L.T., 2019. Area-Wide Products, in: Fischer, C., Traub, B. (Eds.), Swiss National Forest Inventory – Methods and Models of the Fourth Assessment, Managing Forest Ecosystems. Springer International Publishing, Cham, pp. 125–142. https://doi.org/10.1007/978-3-030-19293-8_7.

Gjertsen, A.K., Tomppo, E., Tomter, S., 1999. National Forest Inventory in Norway: using sample plots, digital maps, and satellite images. Presented at the IEEE 1999 International Geoscience and Remote Sensing Symposium, IEEE, Hamburg, Germany, pp. 729–731. https://doi.org/10.1109/IGARSS.1999.774421.

Gobakken, T., Bollandsås, O.M., Næsset, E., 2015. Comparing biophysical forest characteristics estimated from photogrammetric matching of aerial images and airborne laser scanning data. Scandinavian Journal of Forest Research 30, 73–86. https://doi.org/10.1080/02827581.2014.961954.

Gobakken, T., Næsset, E., Nelson, R., Bollandsås, O.M., Gregoire, T.G., Ståhl, G., Holm, S., Ørka, H.O., Astrup, R., 2012. Estimating biomass in Hedmark County, Norway using national forest inventory field plots and airborne laser scanning. Remote Sensing of Environment 123, 443–456. https://doi.org/10.1016/j.rse.2012.01.025.

Goerndt, M.E., Monleon, V.J., Temesgen, H., 2011. A comparison of small-area estimation techniques to estimate selected stand attributes using LiDAR-derived auxiliary variables. Canadian Journal of Forest Research 41, 1189–1201. https://doi.org/10.1139/x11-033.

Goerndt, M.E., Wilson, B.T., Aguilar, F.X., 2019. Comparison of small area estimation methods applied to biopower feedstock supply in the Northern U.S. region. Biomass Bioenergy 121, 64–77. https://doi.org/10.1016/j.biombioe.2018.12.008.

Gómez, L., Haesevoets, S., Kuijpers, B., Vaisman, A.A., 2009. Spatial aggregation: Data model and implementation. Information Systems 34, 551–576. https://doi.org/10.1016/j.is.2009.03.002.

Grafström, A., Saarela, S., Ene, L.T., 2014. Efficient sampling strategies for forest inventories by spreading the sample in auxiliary space. Canadian Journal of Forest Research 44, 1156–1164. https://doi.org/10.1139/cjfr-2014-0202.

Graubardand, B.I., Korn, E.L., 2002. Inference for Superpopulation Parameters Using Sample Surveys. Statistical Science 17, 73–96. https://doi.org/10.1214/ss/1023798999.

Gregoire, T.G., 1998. Design-based and model-based inference in survey sampling: appreciating the difference. Canadian Journal of Forest Research 28, 1429–1447. https://doi.org/10.1139/x98-166.

Gregoire, T.G., Næsset, E., McRoberts, R.E., Ståhl, G., Andersen, H.-E., Gobakken, T., Ene, L., Nelson, R., 2016. Statistical rigor in LiDAR-assisted estimation of aboveground forest biomass. Remote Sensing of Environment 173, 98–108. https://doi.org/10.1016/j.rse.2015.11.012.

Gregoire, T.G., Ståhl, G., Næsset, E., Gobakken, T., Nelson, R., Holm, S., 2011. Model-assisted estimation of biomass in a LiDAR sample survey in Hedmark County, Norway. Canadian Journal of Forest Research 41, 83–95. https://doi.org/10.1139/X10-195.

Guerra-Hernández, J., Pascual, A., 2021. Using GEDI lidar data and airborne laser scanning to assess height growth dynamics in fast-growing species: a showcase in Spain. Forest Ecosystems 8, 14. https://doi.org/10.1186/s40663-021-00291-2.

Guitet, S., 2018. Analyses du contrôle national : Premières visites. Inventaire Forestier National, 153 p.

Guldin, R.W., 2021. A Systematic Review of Small Domain Estimation Research in Forestry During the Twenty-First Century From Outside the United States. Frontiers in Forests and Global Change 4, 695929. https://doi.org/10.3389/ffgc.2021.695929.

Haakana, H., Heikkinen, J., Katila, M., Kangas, A., 2020. Precision of exogenous post-stratification in small-area estimation based on a continuous national forest inventory. Canadian Journal of Forest Research 50, 359–370. https://doi.org/10.1139/cjfr-2019-0139.

Haakana, H., Heikkinen, J., Katila, M., Kangas, A., 2019. Efficiency of post-stratification for a large-scale forest inventory—case Finnish NFI. Annals of Forest Science 76, 9. https://doi.org/10.1007/s13595-018-0795-6.

Habel, K., Grasman, R., Gramacy, R.B., Mozharovskyi, P., Sterratt, D.C., 2019. Geometry: Mesh Generation and Surface Tessellation.

Hagolle, O., Huc, M., Villa Pascual, D., Dedieu, G., 2015. A Multi-Temporal and Multi-Spectral Method to Estimate Aerosol Optical Thickness over Land, for the Atmospheric Correction of FormoSat-2, LandSat, VENμS and Sentinel-2 Images. Remote Sensing 7, 2668–2691. https://doi.org/10.3390/rs70302668.

Hajnsek, I., Kugler, F., Lee, S.-K., Papathanassiou, K.P., 2009. Tropical-Forest-Parameter Estimation by Means of Pol-InSAR: The INDREX-II Campaign. IEEE Transactions on Geoscience and Remote Sensing 47, 481–493. https://doi.org/10.1109/TGRS.2008.2009437.

Hansen, M.C., DeFries, R.S., 2004. Detecting Long-term Global Forest Change Using Continuous Fields of Tree-Cover Maps from 8-km Advanced Very High Resolution Radiometer (AVHRR) Data for the Years 1982–99. Ecosystems 7, 695–716. https://doi.org/10.1007/s10021-004-0243-3.

Hansen, M.C., Stehman, S.V., Potapov, P.V., Loveland, T.R., Townshend, J.R.G., DeFries, R.S., Pittman, K.W., Arunarwati, B., Stolle, F., Steininger, M.K., Carroll, M., DiMiceli, C., 2008. Humid tropical forest clearing from 2000 to 2005 quantified by using multitemporal and multiresolution remotely sensed data. Proceedings of the National Academy of Sciences 105, 9439–9444. https://doi.org/10.1073/pnas.0804042105.

Hansen, M.H., Madow, W.G., Tepping, B.J., 1983. An Evaluation of Model-Dependent and Probability-Sampling Inferences in Sample Surveys. Journal of the American Statistical Association 78, 776–793. https://doi.org/10.1080/01621459.1983.10477018.

Hauglin, M., Rahlf, J., Schumacher, J., Astrup, R., Breidenbach, J., 2021. Large scale mapping of forest attributes using heterogeneous sets of airborne laser scanning and National Forest Inventory data. Forest Ecosystems 8, 65. https://doi.org/10.1186/s40663-021-00338-4.

Hawbaker, T.J., Keuler, N.S., Lesak, A.A., Gobakken, T., Contrucci, K., Radeloff, V.C., 2009. Improved estimates of forest vegetation structure and biomass with a LiDAR-optimized sampling design. Journal of Geophysical Research: Biogeosciences 114, n/a-n/a. https://doi.org/10.1029/2008JG000870.

Hayes, D.J., Cohen, W.B., Sader, S.A., Irwin, D.E., 2008. Estimating proportional change in forest cover as a continuous variable from multi-year MODIS data. Remote Sensing of Environment 112, 735–749. https://doi.org/10.1016/j.rse.2007.06.003.

He, H., Yan, J., Wang, L., Liang, D., Peng, J., Li, C., 2022. Bayesian Temporal Tensor Factorization-Based Interpolation for Time-Series Remote Sensing Data With Large-Area Missing Observations. IEEE Transactions on Geoscience and Remote Sensing 60, 1–13. https://doi.org/10.1109/TGRS.2022.3140436.

Helmer, E.H., Ruzycki, T.S., Wunderle, J.M., Vogesser, S., Ruefenacht, B., Kwit, C., Brandeis, T.J., Ewert, D.N., 2010. Mapping tropical dry forest height, foliage height profiles and disturbance type and age with a time series of cloud-cleared Landsat and ALI image mosaics to characterize avian habitat. Remote Sensing of Environment 114, 2457–2473. https://doi.org/10.1016/j.rse.2010.05.021.

Hervé, J.-C., 2016. France, in: Vidal, C., Alberdi, I.A., Hernández Mateo, L., Redmond, J.J. (Eds.), National Forest Inventories - Assessment of Wood Availability and Use. Springer, Cham, pp. 385–404. https://doi.org/10.1007/978-3-319-44015-6_20.

Hervé, J.-C., Wurpillot, S., Vidal, C., Roman-Amat, B., 2014. L'inventaire des ressources forestières en France : un nouveau regard sur de nouvelles forêts. Revue Forestière Française 247–260. https://doi.org/10.4267/2042/56055.

Hijmans, R.J., 2021. terra: Spatial Data Analysis. R package version 1.2-10. https://CRAN.R-project.org/package=terra.

Hill, A., Breschan, J., Mandallaz, D., 2014. Accuracy Assessment of Timber Volume Maps Using Forest Inventory Data and LiDAR Canopy Height Models. Forests 5, 2253–2275. https://doi.org/10.3390/f5092253.

Hill, A., Mandallaz, D., Langshausen, J., 2018. A Double-Sampling Extension of the German National Forest Inventory for Design-Based Small Area Estimation on Forest District Levels. Remote Sensing 10, 1052. https://doi.org/10.3390/rs10071052.

Hill, A., Massey, A., Mandallaz, D., 2021. The R Package forestinventory: Design-Based Global and Small Area Estimations for Multiphase Forest Inventories. Journal of Statistical Software 97. https://doi.org/10.18637/jss.v097.i04.

Hlásny, T., König, L., Krokene, P., Lindner, M., Montagné-Huck, C., Müller, J., Qin, H., Raffa, K.F., Schelhaas, M.-J., Svoboda, M., Viiri, H., Seidl, R., 2021. Bark Beetle Outbreaks in Europe: State of Knowledge and Ways Forward for Management. Current Forestry Reports 7, 138–165. https://doi.org/10.1007/s40725-021-00142-x.

Hollaus, M., Vreugdenhil, M., 2019. Radar Satellite Imagery for Detecting Bark Beetle Outbreaks in Forests. Current Forestry Reports 5, 240–250. https://doi.org/10.1007/s40725-019-00098-z.

Hollaus, M., Wagner, W., Maier, B., Schadauer, K., 2007. Airborne Laser Scanning of Forest Stem Volume in a Mountainous Environment. Sensors 7, 1559–1577. https://doi.org/10.3390/s7081559.

Horvitz, D.G., Thompson, D.J., 1952. A Generalization of Sampling Without Replacement from a Finite Universe. Journal of the American Statistical Association 47, 663–685. https://doi.org/10.1080/01621459.1952.10483446.

Hou, Z., Xu, Q., McRoberts, R.E., Greenberg, J.A., Liu, J., Heiskanen, J., Pitkänen, S., Packalen, P., 2017. Effects of temporally external auxiliary data on model-based inference. Remote Sensing of Environment 198, 150–159. https://doi.org/10.1016/j.rse.2017.06.013.

Hsu, Y.-H., Chen, Y., Yang, T.-R., Kershaw, J.A., Ducey, M.J., 2020. Sample strategies for bias correction of regional LiDAR-assisted forest inventory Estimates on small woodlots. Annals of Forest Science 77, 75. https://doi.org/10.1007/s13595-020-00976-8.

Hudak, A.T., Crookston, N.L., Evans, J.S., Falkowski, M.J., Smith, A.M.S., Gessler, P.E., Morgan, P., 2006. Regression modeling and mapping of coniferous forest basal area and tree density from discrete-return lidar and multispectral satellite data. Canadian Journal of Remote Sensing 32, 126–138. https://doi.org/10.5589/m06-007.

Huo, L., Persson, H.J., Lindberg, E., 2021. Early detection of forest stress from European spruce bark beetle attack, and a new vegetation index: Normalized distance red & SWIR (NDRS). Remote Sensing of Environment 255, 112240. https://doi.org/10.1016/j.rse.2020.112240.

Irulappa-Pillai-Vijayakumar, D.B., Renaud, J.-P., Morneau, F., McRoberts, R.E., Vega, C., 2019. Increasing Precision for French Forest Inventory Estimates using the k-NN Technique with Optical and Photogrammetric Data and Model-Assisted Estimators. Remote Sensing 11, 991. https://doi.org/10.3390/rs11080991.

James, G., Witten, D., Hastie, T., Tibshirani, R., 2013. An Introduction to Statistical Learning, Springer Texts in Statistics. Springer New York, New York, NY. https://doi.org/10.1007/978-1-4614-7138-7.

Järnstedt, J., Pekkarinen, A., Tuominen, S., Ginzler, C., Holopainen, M., Viitala, R., 2012. Forest variable estimation using a high-resolution digital surface model. ISPRS Journal of Photogrammetry and Remote Sensing 74, 78–84. https://doi.org/10.1016/j.isprsjprs.2012.08.006.

Jarret, P., 2004. Guide des sylvicultures : Chênaie atlantique. Office National des Forêts; Lavoisier.

Jensen, J.R., 2007. Remote Sensing of the Environment: an Earth Resource Perspective, 2nd ed. Prentice Hall, Upper Saddle River, NJ, USA.

Jentsch, A., Beierkuhnlein, C., 2008. Research frontiers in climate change: Effects of extreme meteorological events on ecosystems. Comptes Rendus Geoscience 340, 621–628. https://doi.org/10.1016/j.crte.2008.07.002.

Jiang, J., Rao, J.S., 2020. Robust Small Area Estimation: An Overview. Annual Review of Statistics and Its Application 7, 337–360. https://doi.org/10.1146/annurev-statistics-031219-041212.

Jin, S., Sader, S.A., 2005. MODIS time-series imagery for forest disturbance detection and quantification of patch size effects. Remote Sensing of Environment 99, 462–470. https://doi.org/10.1016/j.rse.2005.09.017.

Kangas, A., Astrup, R., Breidenbach, J., Fridman, J., Gobakken, T., Korhonen, K.T., Maltamo, M., Nilsson, M., Nord-Larsen, T., Næsset, E., Olsson, H., 2018. Remote sensing and forest inventories in Nordic countries – roadmap for the future. Scandinavian Journal of Forest Research 33, 397–412. https://doi.org/10.1080/02827581.2017.1416666.

Kangas, A., Maltamo, M. (Eds.), 2006. Forest Inventory: Methodology and Applications, Managing Forest Ecosystems. Springer Netherlands. https://doi.org/10.1007/1-4020-4381-3.

Kangas, A., Myllymäki, M., Gobakken, T., Næsset, E., 2016. Model-assisted forest inventory with parametric, semiparametric, and nonparametric models. Canadian Journal of Forest Research 46, 855–868. https://doi.org/10.1139/cjfr-2015-0504.

Kangas, A., Myllymäki, M., Mehtätalo, L., 2023. Understanding uncertainty in forest resources maps. Silva Fennica. https://doi.org/10.14214/sf.22026.

Kangas, A., Räty, M., Korhonen, K.T., Vauhkonen, J., Packalen, T., 2019. Catering Information Needs from Global to Local Scales—Potential and Challenges with National Forest Inventories. Forests 10. https://doi.org/10.3390/f10090800.

Karasiak, N., Dejoux, J.-F., Monteil, C., Sheeren, D., 2022. Spatial dependence between training and test sets: another pitfall of classification accuracy assessment in remote sensing. Mach. Learn. 111, 2715–2740. https://doi.org/10.1007/s10994-021-05972-1.

Kim, H.-J., Tomppo, E., 2006. Model-based prediction error uncertainty estimation for k-nn method. Remote Sensing of Environment 104, 257–263. https://doi.org/10.1016/j.rse.2006.04.009.

Knaub, J., 2017. Comparison of Model-Based to Design-Based Ratio Estimators, in: Proceedings of the Joint Statistical Meetings 2017 Survey Research Methods Section Baltimore, Maryland, July 29 - August 3, 2017.

Koch, B., 2015. Remote Sensing supporting national forest inventories NFA, in: Food and Agriculture Organization of the United Nations, Knowledge Reference for National Forest Assessments. Rome: Food and Agriculture Organization of the United Nations, pp. 77–92.

Koivuniemi, J., Korhonen, K.T., 2006. Inventory by Compartments, in: Kangas, A., Maltamo, M. (Eds.), Managing Forest Ecosystems. Kluwer Academic Publishers, Dordrecht, pp. 271–278. https://doi.org/10.1007/1-4020-4381-3_16.

Korhonen, K.T., 2016. Finland, in: Vidal, C., Alberdi, I.A., Hernández Mateo, L., Redmond, J.J. (Eds.), National Forest Inventories - Assessment of Wood Availability and Use. Springer, Cham, pp. 369–384. https://doi.org/10.1007/978-3-319-44015-6_19.

Koukal, T., Suppan, F., Schneider, W., 2007. The impact of relative radiometric calibration on the accuracy of kNN-predictions of forest attributes. Remote Sensing of Environment 110, 431–437. https://doi.org/10.1016/j.rse.2006.08.016.

Lahssini, K., Dayal, K.R., Durrieu, S., Monnet, J.-M., 2022. Joint Use of Airborne LiDAR Metrics and Topography Information to Estimate Forest Parameters via Neural Networks. Presented at the 2022 IEEE 21st Mediterranean Electrotechnical Conference (MELECON), Palermo, Italy, pp. 442–447. https://doi.org/10.1109/MELECON53508.2022.9843039.

Lambin, E.F., Strahlers, A.H., 1994. Change-vector analysis in multitemporal space: A tool to detect and categorize land-cover change processes using high temporal-resolution satellite data. Remote Sensing of Environment 48, 231–244. https://doi.org/10.1016/0034-4257(94)90144-9

Lang, N., Kalischek, N., Armston, J., Schindler, K., Dubayah, R., Wegner, J.D., 2022. Global canopy height regression and uncertainty estimation from GEDI LIDAR waveforms with deep ensembles. Remote Sensing of Environment 268, 112760. https://doi.org/10.1016/j.rse.2021.112760.

Langner, A., Miettinen, J., Siegert, F., 2007. Land cover change 2002–2005 in Borneo and the role of fire derived from MODIS imagery. Global Change Biology 13, 2329–2340. https://doi.org/10.1111/j.1365-2486.2007.01442.x.

Lark, R.M., Chagumaira, C., Milne, A.E., 2022. Decisions, uncertainty and spatial information. Spatial Statistics 50, 100619. https://doi.org/10.1016/j.spasta.2022.100619.

Lausch, A., Heurich, M., Gordalla, D., Dobner, H.-J., Gwillym-Margianto, S., Salbach, C., 2013. Forecasting potential bark beetle outbreaks based on spruce forest vitality using hyperspectral remote-sensing techniques at different scales. Forest Ecology and Management 308, 76–89. https://doi.org/10.1016/j.foreco.2013.07.043.

Lehtonen, R., Sarndal, C.E., Veijanen, A., 2003. The effect of model choice in estimation for domains, including small domains. Survey Methodology, Statistique Canada 29, 33-44.

LeMaire, G., Marsden, C., Nouvellon, Y., Grinand, C., Hakamada, R., Stape, J.-L., Laclau, J.-P., 2011. MODIS NDVI time-series allow the monitoring of Eucalyptus plantation biomass. Remote Sensing of Environment 115, 2613–2625. https://doi.org/10.1016/j.rse.2011.05.017.

Lesouple, J., Baudoin, C., Spigai, M., Tourneret, J.-Y., 2021. Generalized isolation forest for anomaly detection. Pattern Recognition Letters 149, 109–119. https://doi.org/10.1016/j.patrec.2021.05.022.

Lewis, S.L., Brando, P.M., Phillips, O.L., van der Heijden, G.M.F., Nepstad, D., 2011. The 2010 Amazon Drought. Science 331, 554–554. https://doi.org/10.1126/science.1200807.

Li, Y., Wu, Z., Xu, X., Fan, H., Tong, X., Liu, J., 2021. Forest disturbances and the attribution derived from yearly Landsat time series over 1990–2020 in the Hengduan Mountains Region of Southwest China. Forest Ecosystems 8, 73. https://doi.org/10.1186/s40663-021-00352-6.

Liu, F.T., Ting, K.M., Zhou, Z.-H., 2008. Isolation Forest. Presented at the 2008 Eighth IEEE International Conference on Data Mining (ICDM), IEEE, Pisa, Italy, pp. 413–422. https://doi.org/10.1109/ICDM.2008.17.

Lohr, S.L., 1999. Sampling: Design and Analysis. Duxbury Press, Pacific Grove, CA.

Longford, N.T., 2005. Editorial: Model selection and efficiency-is "Which model ...?" the right question? Journal of the Royal Statistical Society: Series A (Statistics in Society) 168, 469–472. https://doi.org/10.1111/j.1467-985X.2005.00366.x.

Lowe, D.G., 2004. Distinctive Image Features from Scale-Invariant Keypoints. International Journal of Computer Vision 60, 91–110. https://doi.org/10.1023/B:VISI.0000029664.99615.94.

Lund, H.G., 2018. Definitions of Forest, Deforestation, Afforestation, and Reforestation. [Online] Gainesville, VA: Forest Information Services. Misc. pagination: Note, this paper has been continuously updated since 1998. https://doi.org/10.13140/RG.2.2.14093.03042.

Luo, F., Meng, L.-Z., Wang, J., Liu, Y.-H., 2022. The patterns of co-occurrence variation are explained by the low dependence of bark beetles (Coleoptera: Scolytinae and Platypodinae) on hosts along altitude gradients. Frontiers in Zoology 19, 10. https://doi.org/10.1186/s12983-022-00455-y.

Magnussen, S., 2015. Arguments for a model-dependent inference? Forestry 88, 317–325. https://doi.org/10.1093/forestry/cpv002.

Magnussen, S., Breidenbach, J., 2017. Model-dependent forest stand-level inference with and without estimates of stand-effects. Forestry 90, 675–685. https://doi.org/10.1093/forestry/cpx023.

Magnussen, S., Frazer, G., Penner, M., 2016. Alternative mean-squared error estimators for synthetic estimators of domain means. Journal of Applied Statistics 43, 2550–2573. https://doi.org/10.1080/02664763.2016.1142942.

Magnussen, S., Mandallaz, D., Breidenbach, J., Lanz, A., Ginzler, C., 2014. National forest inventories in the service of small area estimation of stem volume. Canadian Journal of Forest Research 44, 1079–1090. https://doi.org/10.1139/cjfr-2013-0448.

Magnussen, S., Mauro, F., Breidenbach, J., Lanz, A., Kändler, G., 2017. Area-level analysis of forest inventory variables. European Journal of Forest Research 136, 839–855. https://doi.org/10.1007/s10342-017-1074-z.

Magnussen, S., McRoberts, R.E., Breidenbach, J., Nord-Larsen, T., Ståhl, G., Fehrmann, L., Schnell, S., 2020. Comparison of estimators of variance for forest inventories with systematic sampling - results from artificial populations. Forest Ecosystems 7, 17. https://doi.org/10.1186/s40663-020-00223-6.

Magnussen, S., McRoberts, R.E., Tomppo, E.O., 2009. Model-based mean square error estimators for k-nearest neighbour predictions and applications using remotely sensed data for forest inventories. Remote Sensing of Environment 113, 476–488. https://doi.org/10.1016/j.rse.2008.04.018.

Magnussen, S., Næsset, E., Gobakken, T., Frazer, G., 2012. A fine-scale model for area-based predictions of tree-size-related attributes derived from LiDAR canopy heights. Scandinavian Journal of Forest Research 27, 312–322. https://doi.org/10.1080/02827581.2011.624116.

Magnussen, S., Nord-Larsen, T., Riis-Nielsen, T., 2018. Lidar supported estimators of wood volume and aboveground biomass from the Danish national forest inventory (2012–2016). Remote Sensing of Environment 211, 146–153. https://doi.org/10.1016/j.rse.2018.04.015.

Magnussen, S., Tomppo, E., McRoberts, R.E., 2010. A model-assisted k-nearest neighbour approach to remove extrapolation bias. Scandinavian Journal of Forest Research 25, 174–184. https://doi.org/10.1080/02827581003667348.

Mäkisara, K., Katila, M., Peräsaari, J., 2022. The Multi-Source National Forest Inventory of Finland — methods and results 2017 and 2019. Natural Resources and Bioeconomy Studies. Natural Resources Institute Finland, Helsinki.

Maltamo, M., Bollandsas, O.M., Naesset, E., Gobakken, T., Packalen, P., 2011. Different plot selection strategies for field training data in ALS-assisted forest inventory. Forestry 84, 23–31. https://doi.org/10.1093/forestry/cpq039.

Maltamo, M., Packalen, P., Kangas, A., 2021. From comprehensive field inventories to remotely sensed wall-to-wall stand attribute data — a brief history of management inventories in the Nordic countries. Canadian Journal of Remote Sensing 51, 257–266. https://doi.org/10.1139/cjfr-2020-0322.

Maltamo, M., Packalén, P., Suvanto, A., Korhonen, K.T., Mehtätalo, L., Hyvönen, P., 2009. Combining ALS and NFI training data for forest management planning: a case study in Kuortane, Western Finland. European Journal of Forest Research 128, 305–317. https://doi.org/10.1007/s10342-009-0266-6.

Mandallaz, D., 2013. Design-based properties of some small-area estimators in forest inventory with two-phase sampling. Canadian Journal of Forest Research 43, 441–449. https://doi.org/10.1139/cjfr-2012-0381.

Mascaro, J., Detto, M., Asner, G.P., Muller-Landau, H.C., 2011. Evaluating uncertainty in mapping forest carbon with airborne LiDAR. Remote Sensing of Environment 115, 3770–3774. https://doi.org/10.1016/j.rse.2011.07.019.

Maselli, F., Chirici, G., Bottai, L., Corona, P., Marchetti, M., 2005. Estimation of Mediterranean forest attributes by the application of k-NN procedures to multitemporal Landsat ETM+ images. International Journal of Remote Sensing 26, 3781–3796. https://doi.org/10.1080/01431160500166433.

Matérn, B., 1960. Spatial variation : Stachastic models and their application to some problems in forest surveys and other sampling investigations. Meddelanden fran Statens Skogsforskningsinstitud 49.

Mather, A.S., Fairbairn, J., Needle, C.L., 1999. The course and drivers of the forest transition: The case of France. Journal of Rural Studies 15, 65–90. https://doi.org/10.1016/S0743-0167(98)00023-0.

Mauro, F., Monleon, V.J., Temesgen, H., Ford, K.R., 2017. Analysis of area level and unit level models for small area estimation in forest inventories assisted with LiDAR auxiliary information. PLOS ONE 12, e0189401. https://doi.org/10.1371/journal.pone.0189401.

McConville, K.S., Moisen, G.G., Frescino, T.S., 2020. A Tutorial on Model-Assisted Estimation with Application to Forest Inventory. Forests 11, 244. https://doi.org/10.3390/f11020244.

McInerney, D., Barrett, F., McRoberts, R.E., Tomppo, E., 2018. Enhancing the Irish NFI using k-nearest neighbors and a genetic algorithm. Canadian Journal of Forest Research 48, 1482–1494. https://doi.org/10.1139/cjfr-2018-0011.

McInerney, D.O., Nieuwenhuis, M., 2009. A comparative analysis of kNN and decision tree methods for the Irish National Forest Inventory. International Journal of Remote Sensing 30, 4937–4955. https://doi.org/10.1080/01431160903022936.

McRoberts, R.E., 2012. Estimating forest attribute parameters for small areas using nearest neighbors techniques. Forest Ecology and Management 272, 3–12. https://doi.org/10.1016/j.foreco.2011.06.039.

McRoberts, R.E., 2011. Satellite image-based maps: Scientific inference or pretty pictures? Remote Sensing of Environment 115, 715–724. https://doi.org/10.1016/j.rse.2010.10.013.

McRoberts, R.E., 2010. Probability- and model-based approaches to inference for proportion forest using satellite imagery as ancillary data. Remote Sensing of Environment 114, 1017–1025. https://doi.org/10.1016/j.rse.2009.12.013.

McRoberts, R.E., 2009. A two-step nearest neighbors algorithm using satellite imagery for predicting forest structure within species composition classes. Remote Sensing of Environment 113, 532–545. https://doi.org/10.1016/j.rse.2008.10.001.

McRoberts, R.E., Chen, Q., Domke, G.M., Ståhl, G., Saarela, S., Westfall, J.A., 2016. Hybrid estimators for mean aboveground carbon per unit area. Forest Ecology and Management 378, 44–56. https://doi.org/10.1016/j.foreco.2016.07.007.

McRoberts, R.E., Chen, Q., Walters, B.F., 2017. Multivariate inference for forest inventories using auxiliary airborne laser scanning data. Forest Ecology and Management 401, 295–303. https://doi.org/10.1016/j.foreco.2017.07.017.

McRoberts, R.E., Cohen, W.B., Næsset, E., Stehman, S.V., Tomppo, E.O., 2010a. Using remotely sensed data to construct and assess forest attribute maps and related spatial products. Scandinavian Journal of Forest Research 25, 340–367. https://doi.org/10.1080/02827581.2010.497496.

McRoberts, R.E., Holden, G.R., Nelson, M.D., Liknes, G.C., Gormanson, D.D., 2005. Using satellite imagery as ancillary data for increasing the precision of estimates for the Forest Inventory and Analysis program of the USDA Forest Service. Canadian Journal of Forest Research 35, 2968–2980. https://doi.org/10.1139/x05-222.

McRoberts, R.E., Magnussen, S., Tomppo, E.O., Chirici, G., 2011. Parametric, bootstrap, and jackknife variance estimators for the k-Nearest Neighbors technique with illustrations using forest inventory and satellite image data. Remote Sensing of Environment 115, 3165–3174. https://doi.org/10.1016/j.rse.2011.07.002.

McRoberts, R.E., Næsset, E., Gobakken, T., 2015a. Optimizing the k-Nearest Neighbors technique for estimating forest aboveground biomass using airborne laser scanning data. Remote Sensing of Environment 163, 13–22. https://doi.org/10.1016/j.rse.2015.02.026.

McRoberts, R.E., Naesset, E., Gobakken, T., 2013. Accuracy and Precision for Remote Sensing Applications of Nonlinear Model-Based Inference. IEEE Journal of Selected Topics in Applied Earth Observations and Remote Sensing 6, 27–34. https://doi.org/10.1109/JSTARS.2012.2227299.

McRoberts, R.E., Næsset, E., Gobakken, T., Bollandsås, O.M., 2015b. Indirect and direct estimation of forest biomass change using forest inventory and airborne laser scanning data. Remote Sensing of Environment 164, 36–42. https://doi.org/10.1016/j.rse.2015.02.018.

McRoberts, R.E., Næsset, E., Hou, Z., Ståhl, G., Saarela, S., Esteban, J., Travaglini, D., Mohammadi, J., Chirici, G., 2023. How many bootstrap replications are necessary for estimating remote sensing-assisted, model-based standard errors? Remote Sensing of Environment 288, 113455. https://doi.org/10.1016/j.rse.2023.113455.

McRoberts, R.E., Næsset, E., Saatchi, S., Quegan, S., 2022. Statistically rigorous, model-based inferences from maps. Remote Sensing of Environment 279, 113028. https://doi.org/10.1016/j.rse.2022.113028.

McRoberts, R.E., Tomppo, E., 2007. Remote sensing support for national forest inventories. Remote Sensing of Environment 110, 412–419. https://doi.org/10.1016/j.rse.2006.09.034.

McRoberts, R.E., Tomppo, E.O., Finley, A.O., Heikkinen, J., 2007. Estimating areal means and variances of forest attributes using the k-Nearest Neighbors technique and satellite imagery. Remote Sensing of Environment 111, 466–480. https://doi.org/10.1016/j.rse.2007.04.002.

McRoberts, R.E., Tomppo, E.O., Næsset, E., 2010b. Advances and emerging issues in national forest inventories. Scandinavian Journal of Forest Research 25, 368–381. https://doi.org/10.1080/02827581.2010.496739.

McRoberts, R.E., Wendt, D.G., Nelson, M.D., Hansen, M.H., 2002. Using a land cover classification based on satellite imagery to improve the precision of forest inventory area estimates. Remote Sensing of Environment 81, 36–44. https://doi.org/10.1016/S0034-4257(01)00330-3.

Meddens, A.J.H., Hicke, J.A., Vierling, L.A., Hudak, A.T., 2013. Evaluating methods to detect bark beetle-caused tree mortality using single-date and multi-date Landsat imagery. Remote Sensing of Environment 132, 49–58. https://doi.org/10.1016/j.rse.2013.01.002.

Mesgaran, M.B., Cousens, R.D., Webber, B.L., 2014. Here be dragons: a tool for quantifying novelty due to covariate range and correlation change when projecting species distribution models. Diversity and Distributions 20, 1147–1159. https://doi.org/10.1111/ddi.12209.

Meyer, H., Pebesma, E., 2021. Predicting into unknown space? Estimating the area of applicability of spatial prediction models. Methods in Ecology and Evolution 12, 1620–1633. https://doi.org/10.1111/2041-210X.13650.

Minářová, J., Müller, M., Clappier, A., Kašpar, M., 2018. Comparison of extreme precipitation characteristics between the Ore Mountains and the Vosges Mountains (Europe). Theoretical and Applied Climatology 133, 1249–1268. https://doi.org/10.1007/s00704-017-2247-x.

Moeur, M., Stage, A., 1995. Most Similar Neighbor: An Improved Sampling Inference Procedure for Natural Resource Planning. Forest Science 41, 337–359.

Moisen, G.G., Blackard, J.A., Finco, M., 2004. Small area estimation in forests affected by wildfire in the Interior West, in: Greer, Jerry Dean (Ed.), Remote Sensing for Field Users; Proceedings of the Tenth Forest Service Remote Sensing Applications Conference, April 5–9, Salt Lake City.

Morin, D., Planells, M., Guyon, D., Villard, L., Mermoz, S., Bouvet, A., Thevenon, H., Dejoux, J.-F., Le Toan, T., Dedieu, G., 2019. Estimation and Mapping of Forest Structure Parameters from Open Access Satellite Images: Development of a Generic Method with a Study Case on Coniferous Plantation. Remote Sensing 11, 1275. https://doi.org/10.3390/rs11111275.

Moser, P., Vibrans, A.C., McRoberts, R.E., Næsset, E., Gobakken, T., Chirici, G., Mura, M., Marchetti, M., 2017. Methods for variable selection in LiDAR-assisted forest inventories. Forestry 90, 112–124. https://doi.org/10.1093/forestry/cpw041.

Müller, M., Olsson, P.-O., Eklundh, L., Jamali, S., Ardö, J., 2022. Features predisposing forest to bark beetle outbreaks and their dynamics during drought. Forest Ecology and Management 523, 120480. https://doi.org/10.1016/j.foreco.2022.120480.

Muukkonen, P., Heiskanen, J., 2005. Estimating biomass for boreal forests using ASTER satellite data combined with standwise forest inventory data. Remote Sensing of Environment 99, 434–447. https://doi.org/10.1016/j.rse.2005.09.011.

Myers, N., 1996. The world's forests: problems and potentials. Environmental Conservation 23, 156–168. https://doi.org/10.1017/S0376892900038546.

Myroniuk, V., Bilous, A., Khan, Y., Terentiev, A., Kravets, P., Kovalevskyi, S., See, L., 2020. Tracking Rates of Forest Disturbance and Associated Carbon Loss in Areas of Illegal Amber Mining in Ukraine Using Landsat Time Series. Remote Sensing 12, 2235. https://doi.org/10.3390/rs12142235.

Næsset, E., 2007. Airborne laser scanning as a method in operational forest inventory: Status of accuracy assessments accomplished in Scandinavia. Scandinavian Journal of Forest Research 22, 433–442. https://doi.org/10.1080/02827580701672147.

Næsset, E., 2004. Practical large-scale forest stand inventory using a small-footprint airborne scanning laser. Scandinavian Journal of Forest Research 19, 164–179. https://doi.org/10.1080/02827580310019257.

Næsset, E., 2002a. Determination of Mean Tree Height of Forest Stands by Digital Photogrammetry. Scandinavian Journal of Forest Research 17, 446–459. https://doi.org/10.1080/028275802320435469.

Næsset, E., 2002b. Predicting forest stand characteristics with airborne scanning laser using a practical two-stage procedure and field data. Remote Sensing of Environment 80, 88–99. https://doi.org/10.1016/S0034-4257(01)00290-5.

Næsset, E., Gobakken, T., Bollandsås, O.M., Gregoire, T.G., Nelson, R., Ståhl, G., 2013. Comparison of precision of biomass estimates in regional field sample surveys and airborne LiDAR-assisted surveys in Hedmark County, Norway. Remote Sensing of Environment 130, 108–120. https://doi.org/10.1016/j.rse.2012.11.010.

Næsset, E., Gobakken, T., Solberg, S., Gregoire, T.G., Nelson, R., Ståhl, G., Weydahl, D., 2011. Model-assisted regional forest biomass estimation using LiDAR and InSAR as auxiliary data: A case

study from a boreal forest area. Remote Sensing of Environment 115, 3599–3614. https://doi.org/10.1016/j.rse.2011.08.021.

Neyman, J., 1934. On the Two Different Aspects of the Representative Method: The Method of Stratified Sampling and the Method of Purposive Selection. Journal of the Royal Statistical Society 97, 558. https://doi.org/10.2307/2342192.

Nilson, T., Peterson, U., 1994. Age dependence of forest reflectance: Analysis of main driving factors. Remote Sensing of Environment 48, 319–331. https://doi.org/10.1016/0034-4257(94)90006-X.

Nilsson, M., 1997. Estimation of forest variables using satellite image data and airborne Lidar. Acta Universitatis Agriculturae Sueciae Silvestria.

Nilsson, M., Nordkvist, K., Jonzén, J., Lindgren, N., Axensten, P., Wallerman, J., Egberth, M., Larsson, S., Nilsson, L., Eriksson, J., Olsson, H., 2017. A nationwide forest attribute map of Sweden predicted using airborne laser scanning data and field data from the National Forest Inventory. Remote Sensing of Environment 194, 447–454. https://doi.org/10.1016/j.rse.2016.10.022.

Ni-Meister, W., Lee, S., Strahler, A.H., Woodcock, C.E., Schaaf, C., Yao, T., Ranson, K.J., Sun, G., Blair, J.B., 2010. Assessing general relationships between aboveground biomass and vegetation structure parameters for improved carbon estimate from lidar remote sensing. Journal of Geophysical Research: Biogeosciences 115, n/a-n/a. https://doi.org/10.1029/2009JG000936.

Nurminen, K., Karjalainen, M., Yu, X., Hyyppä, J., Honkavaara, E., 2013. Performance of dense digital surface models based on image matching in the estimation of plot-level forest variables. ISPRS Journal of Photogrammetry and Remote Sensing 83, 104–115. https://doi.org/10.1016/j.isprsjprs.2013.06.005.

Nyyssönen, A., 1955. On the estimation of the growing stock from aerial photographs. Communicationes Instituti Forestalis Fenniae 46, 1–57.

Olofsson, P., Arévalo, P., Espejo, A.B., Green, C., Lindquist, E., McRoberts, R.E., Sanz, M.J., 2020. Mitigating the effects of omission errors on area and area change estimates. Remote Sensing of Environment 236, 111492. https://doi.org/10.1016/j.rse.2019.111492.

Opsomer, J.D., Breidt, F.J., Moisen, G.G., Kauermann, G., 2007. Model-Assisted Estimation of Forest Resources With Generalized Additive Models. Journal of the American Statistical Association 102, 400–409. https://doi.org/10.1198/016214506000001491.

Packalén, P., Mehtätalo, L., Maltamo, M., 2011. ALS-based estimation of plot volume and site index in a eucalyptus plantation with a nonlinear mixed-effect model that accounts for the clone effect. Annals of Forest Science 68, 1085. https://doi.org/10.1007/s13595-011-0124-9.

Penner, M., Pitt, D.G., Woods, M.E., 2013. Parametric vs. nonparametric LiDAR models for operational forest inventory in boreal Ontario. Canadian Journal of Remote Sensing 39, 426–443. https://doi.org/10.5589/m13-049.

Persson, H.J., Ståhl, G., 2020. Characterizing Uncertainty in Forest Remote Sensing Studies. Remote Sensing 12, 505. https://doi.org/10.3390/rs12030505.

Pesonen, A., Leino, O., Maltamo, M., Kangas, A., 2009. Comparison of field sampling methods for assessing coarse woody debris and use of airborne laser scanning as auxiliary information. Forest Ecology and Management 257, 1532–1541. https://doi.org/10.1016/j.foreco.2009.01.009.

Pestov, V., 2013. Is the k -NN classifier in high dimensions affected by the curse of dimensionality? Computers & Mathematics with Applications 65, 1427–1437. https://doi.org/10.1016/j.camwa.2012.09.011.

Petit, R.J., Hampe, A., 2006. Some Evolutionary Consequences of Being a Tree. Annual Review of Ecology, Evolution, and Systematics 37, 187–214. https://doi.org/10.1146/annurev.ecolsys.37.091305.110215.

Piedallu, C., Dallery, D., Bresson, C., Legay, M., Gégout, J.-C., Pierrat, R., 2023. Spatial vulnerability assessment of silver fir and Norway spruce dieback driven by climate warming. Landscape Ecology 38, 341–361. https://doi.org/10.1007/s10980-022-01570-1.

Piedallu, C., Gégout, J.-C., Lebourgeois, F., Seynave, I., 2016. Soil aeration, water deficit, nitrogen availability, acidity and temperature all contribute to shaping tree species distribution in temperate forests. Journal of Vegetation Science 27, 387–399. https://doi.org/10.1111/jvs.12370.

Piedallu, C., Gégout, J.-C., Perez, V., Lebourgeois, F., 2013. Soil water balance performs better than climatic water variables in tree species distribution modelling: Soil water balance improves tree species distribution models. Global Ecology and Biogeography 22, 470–482. https://doi.org/10.1111/geb.12012.

Pollastrini, M., Puletti, N., Selvi, F., Iacopetti, G., Bussotti, F., 2019. Widespread Crown Defoliation After a Drought and Heat Wave in the Forests of Tuscany (Central Italy) and Their Recovery—A Case Study From Summer 2017. Frontiers in Forests and Global Change 2, 74. https://doi.org/10.3389/ffgc.2019.00074.

Poso, S., Häme, T., Paananen, R., 1984. A method for estimating the stand characteristics of a forest compartment using satellite imagery. Silva Fennica 18. https://doi.org/10.14214/sf.a15398.

Potapov, P., Li, X., Hernandez-Serna, A., Tyukavina, A., Hansen, M.C., Kommareddy, A., Pickens, A., Turubanova, S., Tang, H., Silva, C.E., Armston, J., Dubayah, R., Blair, J.B., Hofton, M., 2021.

Mapping global forest canopy height through integration of GEDI and Landsat data. Remote Sensing of Environment 253, 112165. https://doi.org/10.1016/j.rse.2020.112165.

Price, B., Waser, L.T., Wang, Z., Marty, M., Ginzler, C., Zellweger, F., 2020. Predicting biomass dynamics at the national extent from digital aerial photogrammetry. International Journal of Applied Earth Observation and Geoinformation 90, 102116. https://doi.org/10.1016/j.jag.2020.102116.

Puliti, S., Breidenbach, J., Schumacher, J., Hauglin, M., Klingenberg, T.F., Astrup, R., 2021. Above-ground biomass change estimation using national forest inventory data with Sentinel-2 and Landsat. Remote Sensing of Environment 265, 112644. https://doi.org/10.1016/j.rse.2021.112644.

Pulkkinen, M., Ginzler, C., Traub, B., Lanz, A., 2018. Stereo-imagery-based post-stratification by regression-tree modelling in Swiss National Forest Inventory. Remote Sensing of Environment 213, 182–194. https://doi.org/10.1016/j.rse.2018.04.052.

Queinnec, M., Tompalski, P., Bolton, D.K., Coops, N.C., 2021. FOSTER—An R package for forest structure extrapolation. PLoS One 16, e0244846. https://doi.org/10.1371/journal.pone.0244846.

Rahlf, J., Breidenbach, J., Solberg, S., Næsset, E., Astrup, R., 2017. Digital aerial photogrammetry can efficiently support large-area forest inventories in Norway. Forestry 90, 710–718. https://doi.org/10.1093/forestry/cpx027.

Rahlf, J., Hauglin, M., Astrup, R., Breidenbach, J., 2021. Timber volume estimation based on airborne laser scanning — comparing the use of national forest inventory and forest management inventory data. Annals of Forest Science 78, 49. https://doi.org/10.1007/s13595-021-01061-4.

Ramage, M.H., Burridge, H., Busse-Wicher, M., Fereday, G., Reynolds, T., Shah, D.U., Wu, G., Yu, L., Fleming, P., Densley-Tingley, D., Allwood, J., Dupree, P., Linden, P.F., Scherman, O., 2017. The wood from the trees: The use of timber in construction. Renewable and Sustainable Energy Reviews 68, 333–359. https://doi.org/10.1016/j.rser.2016.09.107.

Rao, J.N.K., Molina, I., 2015. Small area estimation, 2nd ed. John Wiley & Sons, Hoboken, New Jersey.

Reese, H., Nilsson, M., Sandström, P., Olsson, H., 2002. Applications using estimates of forest parameters derived from satellite and forest inventory data. Computers and Electronics in Agriculture 37, 37–55. https://doi.org/10.1016/S0168-1699(02)00118-7.

Remondino, F., Spera, M.G., Nocerino, E., Menna, F., Nex, F., 2014. State of the art in high density image matching. The Photogrammetric Record 29, 144–166. https://doi.org/10.1111/phor.12063.

Renaud, J.P., Sagar, A., Barbillon, P., Bouriaud, O., Deleuze, C., Vega, C., 2022. Characterizing the calibration domain of remote sensing models using convex hulls. Int. J. Appl. Earth Obs. Geoinformation 112, 102939. https://doi.org/10.1016/j.jag.2022.102939.

Renaud, J.-P., Vega, C., Durrieu, S., Lisein, J., Magnussen, S., Lejeune, P., Fournier, M., 2017. Stand-level wind damage can be assessed using diachronic photogrammetric canopy height models. Annals of Forest Science 74, 74. https://doi.org/10.1007/s13595-017-0669-3.

Reutebuch, S.E., Andersen, H.-E., McGaughey, R.J., 2005. Light Detection and Ranging (LIDAR): An Emerging Tool for Multiple Resource Inventory. Journal of Forestry 103, 286–292. https://doi.org/10.1093/jof/103.6.286.

Robert, N., Vidal, C., Colin, A., Hervé, J.-C., Hamza, N., Cluzeau, C., 2010. France, in: Tomppo, E., Gschwantner, T., Lawrence, M., McRoberts, R.E. (Eds.), National Forest Inventories: Pathways for Common Reporting. Springer, Netherlands, pp. 207–221.

Robert, N., Vidal, C., Colin, A., Hervé, J.-C., Hamza, N., Cluzeau, C., 2009. Developement of France's national forest inventory, in: Tomppo, E., Gschwantner, T., Lawrence, M., McRoberts, R.E. (Eds.), National Forest Inventories – Pathways for Common Reporting. Springer International Publishing, Cham, pp. 207–221.

Rodrigues, A.R., Marques, S., Botequim, B., Marto, M., Borges, J.G., 2021. Forest management for optimizing soil protection: a landscape-level approach. Forest Ecosystems 8, 50. https://doi.org/10.1186/s40663-021-00324-w.

Romme, W.H., Boyce, M.S., Gresswell, R., Merrill, E.H., Minshall, G.W., Whitlock, C., Turner, M.G., 2011. Twenty Years After the 1988 Yellowstone Fires: Lessons About Disturbance and Ecosystems. Ecosystems 14, 1196–1215. https://doi.org/10.1007/s10021-011-9470-6.

Roussel, J.-R., Auty, D., 2021. Airborne LiDAR Data Manipulation and Visualization for Forestry Applications. R package version 3.1.1. https://cran.r-project.org/package=lidR.

Roussel, J.-R., Auty, D., Coops, N.C., Tompalski, P., Goodbody, T.R.H., Meador, A.S., Bourdon, J.-F., de Boissieu, F., Achim, A., 2020. lidR: An R package for analysis of Airborne Laser Scanning (ALS) data. Remote Sensing of Environment 251, 112061. https://doi.org/10.1016/j.rse.2020.112061.

Rupnik, E., Daakir, M., Pierrot Deseilligny, M., 2017. MicMac – a free, open-source solution for photogrammetry. Open Geospatial Data, Software and Standards 2, 14. https://doi.org/10.1186/s40965-017-0027-2.

Saarela, S., Grafström, A., Ståhl, G., Kangas, A., Holopainen, M., Tuominen, S., Nordkvist, K., Hyyppä, J., 2015a. Model-assisted estimation of growing stock volume using different combinations

of LiDAR and Landsat data as auxiliary information. Remote Sensing of Environment 158, 431–440. https://doi.org/10.1016/j.rse.2014.11.020.

Saarela, S., Holm, S., Healey, S., Andersen, H.-E., Petersson, H., Prentius, W., Patterson, P., Næsset, E., Gregoire, T., Ståhl, G., 2018. Generalized Hierarchical Model-Based Estimation for Aboveground Biomass Assessment Using GEDI and Landsat Data. Remote Sensing 10, 1832. https://doi.org/10.3390/rs10111832.

Saarela, S., Schnell, S., Grafström, A., Tuominen, S., Nordkvist, K., Hyyppä, J., Kangas, A., Ståhl, G., 2015b. Effects of sample size and model form on the accuracy of model-based estimators of growing stock volume. Canadian Journal of Forest Research 45, 1524–1534. https://doi.org/10.1139/cjfr-2015-0077.

Saarela, S., Wästlund, A., Holmström, E., Mensah, A.A., Holm, S., Nilsson, M., Fridman, J., Ståhl, G., 2020. Mapping aboveground biomass and its prediction uncertainty using LiDAR and field data, accounting for tree-level allometric and LiDAR model errors. Forest Ecosystems 7, 43. https://doi.org/10.1186/s40663-020-00245-0.

Sagar, A., Vega, C., Bouriaud, O., Piedallu, C., Renaud, J.-P., 2022. Multisource forest inventories: A model-based approach using k-NN to reconcile forest attributes statistics and map products. ISPRS Journal of Photogrammetry and Remote Sensing 192, 175–188. https://doi.org/10.1016/j.isprsjprs.2022.08.016.

Sagar, A., Véga, C., Piédallu, C., Bouriaud, O., Renaud, J.-P., 2021. High Resolution Mapping of Forest Resources and Prediction Uncertainty using Multisource Inventory Approach. In Proceedings of the SilviLaser Conference 2021, pp. 219-221. https://doi.org/10.34726/wim.1986.

Saintonge, F.X., Gillette, M., Belouard, T., 2022. Crise scolytes sur épicéea: bilan 2022. Departement santé des forêts, DGAL/SDSPV, 5p. https://agriculture.gouv.fr/.

Santoro, A., Venturi, M., Bertani, R., Agnoletti, M., 2020. A Review of the Role of Forests and Agroforestry Systems in the FAO Globally Important Agricultural Heritage Systems (GIAHS) Programme. Forests 11, 860. https://doi.org/10.3390/f11080860.

Särndal, C.-E., Swensson, B., Wretman, J., 1992. Model assisted survey sampling. New York: Springer-Verlag.

Särndal, C.E., Thomsen, I., Hoem, J.M., Barndor-Nielsen, O., Dalenius, T., 1978. Design-Based and Model-Based Inference in Survey Sampling. Scandinavian Journal of Statistics 5, 27–52.

Schelhaas, M.-J., Nabuurs, G.-J., Schuck, A., 2003. Natural disturbances in the European forests in the 19th and 20th centuries. Global Change Biology 9, 1620–1633. https://doi.org/10.1046/j.1365-2486.2003.00684.x.

Segura, D., Jiménez, D., Iglesias, J., Sola, A., Chinchero, M., Casanoves, F., Chacón, M., Cifuentes, M., Torres, R., 2016. Ecuador, in: Vidal, C., Alberdi, I.A., Hernández Mateo, L., Redmond, J.J. (Eds.), National Forest Inventories - Assessment of Wood Availability and Use. Springer, Cham, pp. 347–367. https://doi.org/10.1007/978-3-319-44015-6_18.

Seidl, R., Baier, P., Rammer, W., Schopf, A., Lexer, M.J., 2007. Modelling tree mortality by bark beetle infestation in Norway spruce forests. Ecological Modelling 206, 383–399. https://doi.org/10.1016/j.ecolmodel.2007.04.002.

Seidl, R., Thom, D., Kautz, M., Martin-Benito, D., Peltoniemi, M., Vacchiano, G., Wild, J., Ascoli, D., Petr, M., Honkaniemi, J., Lexer, M.J., Trotsiuk, V., Mairota, P., Svoboda, M., Fabrika, M., Nagel, T.A., Reyer, C.P.O., 2017. Forest disturbances under climate change. Nature Climate Change 7, 395–402. https://doi.org/10.1038/nclimate3303.

Senf, C., Seidl, R., 2020. Mapping the forest disturbance regimes of Europe. Nature Sustainability 4, 63–70. https://doi.org/10.1038/s41893-020-00609-y.

Sheil, D., Bongers, F., 2020. Interpreting forest diversity-productivity relationships: volume values, disturbance histories and alternative inferences. Forest Ecosystems 7, 6. https://doi.org/10.1186/s40663-020-0215-x.

Silva, C.A., Duncanson, L., Hancock, S., Neuenschwander, A., Thomas, N., Hofton, M., Fatoyinbo, L., Simard, M., Marshak, C.Z., Armston, J., Lutchke, S., Dubayah, R., 2021. Fusing simulated GEDI, ICESat-2 and NISAR data for regional aboveground biomass mapping. Remote Sensing of Environment 253, 112234. https://doi.org/10.1016/j.rse.2020.112234.

Sonobe, R., Yamaya, Y., Tani, H., Wang, X., Kobayashi, N., Mochizuki, K., 2018. Crop classification from Sentinel-2-derived vegetation indices using ensemble learning. Journal of Applied Remote Sensing 12, 1. https://doi.org/10.1117/1.JRS.12.026019.

Souchon, J.-P., Thom, C., Meynard, C., Martin, O., Pierrot-Deseilligny, M., 2010. The IGN CAMv2 System. The Photogrammetric Record 25, 402–421. https://doi.org/10.1111/j.1477-9730.2010.00601.x.

Stage, A.R., Crookston, N.L., 2007. Partitioning Error Components for Accuracy-Assessment of Near-Neighbor Methods of Imputation. Forest Science 53, 62–72. https://doi.org/10.1093/forestscience/53.1.62.

Ståhl, G., Saarela, S., Schnell, S., Holm, S., Breidenbach, J., Healey, S.P., Patterson, P.L., Magnussen, S., Næsset, E., McRoberts, R.E., Gregoire, T.G., 2016. Use of models in large-area forest surveys: comparing model-assisted, model-based and hybrid estimation. Forest Ecosystems 3, 5. https://doi.org/10.1186/s40663-016-0064-9.

Stanke, H., Finley, A.O., Domke, G.M., 2021. Simplifying small area estimation with rFIA: a demonstration of tools and techniques. arXiv. https://arxiv.org/abs/2109.03863.

Stevens, D.L., 1997. Variable Density Grid-Based Sampling Designs For Continuous Spatial Populations. Environmetrics 8, 167–195. https://doi.org/10.1002/(SICI)1099-095X(199705)8:3<167::AID-ENV239>3.0.CO;2-D.

Stevens, D.L., Olsen, A.R., 2004. Spatially Balanced Sampling of Natural Resources. Journal of the American Statistical Association 99, 262–278. https://doi.org/10.1198/016214504000000250.

Stinson, G., Magnussen, S., Boudewyn, P., Eichel, F., Russo, G., Cranny, M., Song, A., 2016. Canada, in: Vidal, C., Alberdi, I.A., Hernández Mateo, L., Redmond, J.J. (Eds.), National Forest Inventories - Assessment of Wood Availability and Use. Springer, Cham, pp. 233–247. https://doi.org/10.1007/978-3-319-44015-6_12.

St-Onge, B., Vega, C., Fournier, R.A., Hu, Y., 2008. Mapping canopy height using a combination of digital stereo-photogrammetry and lidar. International Journal of Remote Sensing 29, 3343–3364. https://doi.org/10.1080/01431160701469040.

Tewari, V.P., Kleinn, C., 2015. Considerations on capacity building for national forest assessments in developing countries – with a case study of India. International Forestry Review 17, 244–254. https://doi.org/10.1505/146554815815500633.

Tomppo, E., 2006. The Finnish Multi-source National Forest Inventory - Small Area Estimation and Map Production, in: Kangas, A., Maltamo, M. (Eds.), Forest Inventory, Managing Forest Ecosystems. Springer, Dordrecht, pp. 195–224. https://doi.org/10.1007/1-4020-4381-3_12.

Tomppo, E., 1990. Satellite Image-Based National Forest Inventory of Finland. The Photogrammetric Journal of Finland 12, 115–120.

Tomppo, E., 1988. Standwise forest variate estimation by means of satellite images, Satellite imageries for forest inventory and monitoring: experiences, methods, perspectives: proc. from the IUFRO Subject Group 4.02.05 meeting in Finland, Aug. 29 – Sept. 2, 1988: research notes No. 21. University of Helsinki, Dept. of forest mensuration and management. Helsinki, 103-111.

Tomppo, E., Goulding, C., Katila, M., 1999. Adapting Finnish Multi-Source Forest Inventory Techniques to the New Zealand Preharvest Inventory. Scandinavian Journal of Forest Research 14, 182–192. https://doi.org/10.1080/02827589950152917.

Tomppo, E., Gschwantner, T., Lawrence, M., McRoberts, R.E. (Eds.), 2010. National Forest Inventories: Pathways for Common Reporting. Springer, Heidelberg. https://doi.org/10.1007/978-90-481-3233-1.

Tomppo, E., Haakana, M., Katila, M., Peräsaari, J., 2008a. Multi-Source National Forest Inventory: Methods and Applications. Springer, Netherlands.

Tomppo, E., Halme, M., 2004. Using coarse scale forest variables as ancillary information and weighting of variables in k-NN estimation: a genetic algorithm approach. Remote Sensing of Environment 92, 1–20. https://doi.org/10.1016/j.rse.2004.04.003.

Tomppo, E., Korhonen, K., Heikkinen, J., Yli-Kojola, H., 2001. Multi-source inventory of the forests of the Hebei Forestry Bureau, Heilongjiang, China. Silva Fennica 35. https://doi.org/10.14214/sf.587.

Tomppo, E., Olsson, H., Ståhl, G., Nilsson, M., Hagner, O., Katila, M., 2008b. Combining national forest inventory field plots and remote sensing data for forest databases. Remote Sensing of Environment 112, 1982–1999. https://doi.org/10.1016/j.rse.2007.03.032.

Tomter, S.M., 2016. Norway, in: Vidal, C., Alberdi, I.A., Hernández Mateo, L., Redmond, J.J. (Eds.), National Forest Inventories - Assessment of Wood Availability and Use. Springer, Cham, pp. 601–619. https://doi.org/10.1007/978-3-319-44015-6_32.

Tuominen, S., Balazs, A., Kangas, A., 2020. Comparison of photogrammetric canopy models from archived and made-to-order aerial imagery in forest inventory. Silva Fennica 54, 1–18. https://doi.org/10.14214/sf.10291.

UNCCD, 2022. Drought in Numbers 2022-Restoration to Readiness and Resilience. United Nations.

Valbuena, R., Hernando, A., Manzanera, J.A., Görgens, E.B., Almeida, D.R.A., Mauro, F., García-Abril, A., Coomes, D.A., 2017. Enhancing of accuracy assessment for forest above-ground biomass estimates obtained from remote sensing via hypothesis testing and overfitting evaluation. Ecological Modelling 366, 15–26. https://doi.org/10.1016/j.ecolmodel.2017.10.009.

van Aardt, J., Wynne, R.H., Oderwald, R.G., 2006. Forest Volume and Biomass Estimation Using Small-Footprint Lidar-Distributional Parameters on a Per-Segment Basis. Forest Science 52, 636–649. https://doi.org/10.1093/forestscience/52.6.636.

Vandendijck, Y., Faes, C., Kirby, R.S., Lawson, A., Hens, N., 2016. Model-based inference for small area estimation with sampling weights. Spatial Statistics 18, 455–473. https://doi.org/10.1016/j.spasta.2016.09.004.

Véga, C., Renaud, J.-P., Durrieu, S., Bouvier, M., 2016. On the interest of penetration depth, canopy area and volume metrics to improve Lidar-based models of forest parameters. Remote Sensing of Environment 175, 32–42. https://doi.org/10.1016/j.rse.2015.12.039.

Vega, C., Renaud, J.-P., Sagar, A., Bouriaud, O., 2021. A new small area estimation algorithm to balance between statistical precision and scale. International Journal of Applied Earth Observation and Geoinformation 97, 102303. https://doi.org/10.1016/j.jag.2021.102303.

Véga, C., St-Onge, B., 2009. Mapping site index and age by linking a time series of canopy height models with growth curves. Forest Ecology and Management 257, 951–959. https://doi.org/10.1016/j.foreco.2008.10.029.

Vega, C., St-onge, B., 2008. Height growth reconstruction of a boreal forest canopy over a period of 58 years using a combination of photogrammetric and lidar models. Remote Sensing of Environment 112, 1784–1794. https://doi.org/10.1016/j.rse.2007.09.002.

Véga, C., Vepakomma, U., Morel, J., Bader, J.-L., Rajashekar, G., Jha, C., Ferêt, J., Proisy, C., Pélissier, R., Dadhwal, V., 2015. Aboveground-Biomass Estimation of a Complex Tropical Forest in India Using Lidar. Remote Sensing 7, 10607–10625. https://doi.org/10.3390/rs70810607.

Ver Planck, N.R., Finley, A.O., Kershaw, J.A., Weiskittel, A.R., Kress, M.C., 2018. Hierarchical Bayesian models for small area estimation of forest variables using LiDAR. Remote Sensing of Environment 204, 287–295. https://doi.org/10.1016/j.rse.2017.10.024.

Vibrans, A.C., McRoberts, R.E., Moser, P., Nicoletti, A.L., 2013. Using satellite image-based maps and ground inventory data to estimate the area of the remaining Atlantic forest in the Brazilian state of Santa Catarina. Remote Sensing of Environment 130, 87–95. https://doi.org/10.1016/j.rse.2012.10.023.

Vidal, C., Alberdi, I., Redmond, J., Vestman, M., Lanz, A., Schadauer, K., 2016a. The role of European National Forest Inventories for international forestry reporting. Annals of Forest Science 73, 793–806. https://doi.org/10.1007/s13595-016-0545-6.

Vidal, C., Alberdi, I.A., Hernández Mateo, L., Redmond, J.J. (Eds.), 2016b. National Forest Inventories - Assessment of Wood Availability and Use. Springer, Cham. https://doi.org/10.1007/978-3-319-44015-6.

Vidal, C., Belouard, T., Herve, J.-C., Robert, N., Wolsack, J., 2007. A new flexible forest inventory in France, in: McRoberts, R.E., Reams, G.A., Van Deusen, P.C., McWilliams, W.H. (Eds.), Proceedings of the 7th Annual Forest Inventory and Analysis Symposium. General Technical Report WO-77, USDA Forest Service, Portland 3-6 Oct 2005, pp. 67–73.

Vose, J.M., Clark, J.S., Luce, C.H., Patel-Weynand, T., 2016. Effects of drought on forests and rangelands in the United States: a comprehensive science synthesis. Gen. Tech. Report WO-93b. U.S. Department of Agriculture, Forest Service, Washington Office, Washington, D.C. https://doi.org/10.2737/WO-GTR-93b.

Weng, Q., Fu, P., Gao, F., 2014. Generating daily land surface temperature at Landsat resolution by fusing Landsat and MODIS data. Remote Sensing of Environment 145, 55–67. https://doi.org/10.1016/j.rse.2014.02.003.

White, J., Wulder, M., Vastaranta, M., Coops, N., Pitt, D., Woods, M., 2013. The Utility of Image-Based Point Clouds for Forest Inventory: A Comparison with Airborne Laser Scanning. Forests 4, 518–536. https://doi.org/10.3390/f4030518.

White, J.C., Tompalski, P., Vastaranta, M., Wulder, M.A., Saarinen, S., Stepper, C., Coops, N.C., 2017. A model development and application guide for generating an enhanced forest inventory using airborne laser scanning data and an area-based approach. In: CWFC Information Report FI-X-018, Canadian Forest Service. Pacific Forestry Centre, Victoria, BC, Canada, p. 38.

Wojcik, O.C., Olson, S.D., Nguyen, P.-H.V., McConville, K.S., Moisen, G.G., Frescino, T.S., 2022. GREGORY: A Modified Generalized Regression Estimator Approach to Estimating Forest Attributes in the Interior Western US. Frontiers in Forests and Global Change 4, 763414. https://doi.org/10.3389/ffgc.2021.763414.

Woods, M., Pitt, D., Penner, M., Lim, K., Nesbitt, D., Etheridge, D., Treitz, P., 2011. Operational implementation of a LiDAR inventory in Boreal Ontario. The Forestry Chronicle 87, 512–528. https://doi.org/10.5558/tfc2011-050.

Wulder, M., 1998. Optical remote-sensing techniques for the assessment of forest inventory and biophysical parameters. Progress in Physical Geography: Earth and Environment 22, 449–476. https://doi.org/10.1177/030913339802200402.

Yamamoto, S.-I., 2000. Forest Gap Dynamics and Tree Regeneration. Journal of Forest Research 5, 223–229. https://doi.org/10.1007/BF02767114.

Zeng, W., Tomppo, E., Healey, S.P., Gadow, K.V., 2015. The national forest inventory in China: history - results - international context. Forest Ecosystems 2, 23. https://doi.org/10.1186/s40663-015-0047-2.

Zhang, L., Shao, Z., Liu, J., Cheng, Q., 2019. Deep Learning Based Retrieval of Forest Aboveground Biomass from Combined LiDAR and Landsat 8 Data. Remote Sensing 11, 1459. https://doi.org/10.3390/rs11121459.

Zhao, P., Lu, D., Wang, G., Wu, C., Huang, Y., Yu, S., 2016. Examining Spectral Reflectance Saturation in Landsat Imagery and Corresponding Solutions to Improve Forest Aboveground Biomass Estimation. Remote Sensing 8, 469. https://doi.org/10.3390/rs8060469.

Zheng, Z., Zhong, Y., Tian, S., Ma, A., Zhang, L., 2022. ChangeMask: Deep multi-task encoder-transformer-decoder architecture for semantic change detection. ISPRS Journal of Photogrammetry and Remote Sensing 183, 228–239. https://doi.org/10.1016/j.isprsjprs.2021.10.015.

Zolkos, S.G., Goetz, S.J., Dubayah, R., 2013. A meta-analysis of terrestrial aboveground biomass estimation using lidar remote sensing. Remote Sensing of Environment 128, 289–298. https://doi.org/10.1016/j.rse.2012.10.017.